Vol. 298, No. 1, November 20, 1994

ISSN 0003-2670

ANALYTICA CHIMICA ACTA

An international journal devoted to all branches of analytical chemistry

ELSEVIER

ANALYTICA CHIMICA ACTA

Scope. *Analytica Chimica Acta* publishes original papers, rapid publication letters and reviews dealing with every aspect of modern analytical chemistry. Reviews are normally written by invitation of the editors, who welcome suggestions for subjects. Letters can be published within **four months** of submission. For information on the Letters section, see inside back cover.

Submission of Papers

Americas

Prof. Harry L. Pardue
Department of Chemistry
1393 BRWN Bldg, Purdue University
West Lafayette, IN 47907–1393
USA

Tel:(+1-317) 494 5320
Fax:(+1-317) 496 1200

Computer Techniques

Prof. J.T. Clerc
Universität Bern
Pharmazeutisches Institut
Baltzerstrasse 5, CH-3012 Bern
Switzerland

Tel:(+41-31) 6314191
Fax:(+41-31) 6314198

Prof. Sarah C. Rutan
Department of Chemistry
Virginia Commonwealth University
P.O. Box 2006
Richmond, VA 23284-2006
USA
Tel:(+1-804) 367 7517
Fax:(+1-804) 367 8599

Other Papers

Prof. Alan Townshend
Department of Chemistry
The University
Hull HU6 7RX
Great Britain

Tel:(+44-482) 465027
Fax:(+44-482) 466410

Prof. Willem E. van der Linden
Laboratory for Chemical Analysis
Department of Chemical Technology
Twente University of Technology
P.O. Box 217, 7500 AE Enschede
The Netherlands
Tel:(+31-53) 892629
Fax:(+31-53) 356024

Prof. Paul Worsfold
Dept. of Environmental Sciences
University of Plymouth
Plymouth PL4 8AA
Great Britain

Tel:(+44-752) 233006
Fax:(+44-752) 233009

Submission of an article is understood to imply that the article is original and unpublished and is not being considered for publication elsewhere. *Anal. Chim. Acta* accepts papers in English only. There are no page charges. Manuscripts should conform in layout and style to the papers published in this issue. See inside back cover for "Information for Authors".

Publication. *Analytica Chimica Acta* appears in 18 volumes in 1995 (Vols. 297–314). *Vibrational Spectroscopy* appears in 2 volumes in 1995 (Vols. 8 and 9). Subscriptions are accepted on a prepaid basis only, unless different terms have been previously agreed upon. It is possible to order a combined subscription (*Anal. Chim. Acta* **and** *Vib. Spectrosc.*).
Our p.p.h. (postage, packing and handling) charge includes surface delivery of all issues, except to subscribers in the U.S.A., Canada, Australia, New Zealand, China, India, Israel, South Africa, Malaysia, Thailand, Singapore, South Korea, Taiwan, Pakistan, Hong Kong, Brazil, Argentina and Mexico, who receive all issues by air delivery (S.A.L.–Surface Air Lifted) at no extra cost. For Japan, air delivery requires 25% additional charge of the normal postage and handling charge; for all other countries airmail and S.A.L. charges are available upon request.

Subscription orders. Subscription prices are available upon request from the publisher. Subscription orders can be entered only by calendar year and should be sent to: Elsevier Science B.V., Journals Department, P.O. Box 211, 1000 AE Amsterdam, The Netherlands. Tel: (+31-20) 5803 642, Telex: 18582, Telefax: (+31-20) 5803598, to which requests for sample copies can also be sent. Claims for issues not received should be made within six months of publication of the issues. If not they cannot be honoured free of charge. Readers in the U.S.A. and Canada can contact the following address: Elsevier Science Inc., Journal Information Center, 655 Avenue of the Americas, New York, NY 10010, U.S.A. Tel: (+1-212) 633 3750, Telefax: (+1-212) 633 3990, for further information, or a free sample copy of this or any other Elsevier Science journal.
Advertisements. Advertisement rates are available from the publisher on request.

US mailing notice – Analytica Chimica Acta (ISSN 0003-2670) is published 3 times a month (total 54 issues) by Elsevier Science B.V. (Molenwerf 1, Postbus 211, 1000 AE Amsterdam). Annual subscription price in the USA US$ 3677.75 (valid in North, Central and South America), including air speed delivery. Second class postage paid at Jamaica, NY 11431. *USA Postmasters*: Send address changes to Anal. Chim. Acta, Publications Expediting, Inc., 200 Meacham Av., Elmont, NY 11003. Airfreight and mailing in the USA by Publication Expediting.

ANALYTICA CHIMICA ACTA

An international journal devoted to all branches of analytical chemistry

(Full texts are incorporated in CJELSEVIER, a file in the Chemical Journals Online database available on STN International; Abstracted, indexed in: Aluminum Abstracts; Anal. Abstr.; Biol. Abstr.; BIOSIS; Chem. Abstr.; Curr. Contents Phys. Chem. Earth Sci.; Engineered Materials Abstracts; Excerpta Medica; Index Med.; Life Sci.; Mass Spectrom. Bull.; Material Business Alerts; Metals Abstracts; Sci. Citation Index)

VOL. 298 NO. 1 CONTENTS NOVEMBER 20, 1994

(Continued overleaf)

Contents (continued)

ANALYTICA CHIMICA ACTA
VOL. 298 (1994)

ANALYTICA CHIMICA ACTA

An international journal devoted to all branches of analytical chemistry
Revue internationale consacrée à tous les domaines de la chimie analytique
Internationale Zeitschrift für alle Gebiete der analytischen Chemie

Anal. Chim. Acta, Vol. 298 (1994)

ELSEVIER

Amsterdam – Lausanne – New York – Oxford – Shannon – Tokyo

0003-2670/94/$07.00

ELSEVIER

Analytica Chimica Acta 298 (1994) 1–10

ANALYTICA CHIMICA ACTA

A fixed film bioassay for the detection of micropollutants toxic to anaerobic sludges [1]

Bruno R. Erasin, Anthony P.F. Turner *, Andrew D. Wheatley [2]

Cranfield Biotechnology Centre, Cranfield University, Cranfield, Bedford MK43 0AL, UK

Received 8 September 1993; revised manuscript received 23 May 1994

Abstract

Micropollutants in waste water streams can be a serious problem for the anaerobic digestion process. A short-term acute bioassay system is described for testing the effects of new and potentially toxic compounds on anaerobic digestion processes. Change in methanogenic activity was used as the monitored process parameter and the performance of intoxicated inocula was compared to activity prior to adding test compounds and to the activity of a parallel control assay. The performance of the bioassay was tested with chlorinated solvents and heavy metals. Trichloroethane caused a 50% reduction in methanogenic activity at 7 mg/l assay. The performance of suspended and fixed biomass assays were compared; the suspended growth was found to be five times more sensitive to trichloroethane. There was no clear inhibition with the heavy metals even at the highest concentration used (up to 750 mg Cu/l). The duration of assay was found to be an important parameter in the evaluation of anaerobic toxicity.

Keywords: Fixed film bioassay; Micropollutants; Toxicity; Waters

1. Introduction

In the past decade, the controlled treatment and stabilization of wastes by anaerobic digestion has increased rapidly. The treatment of industrial effluents is of particular interest because of low running costs compared to the alternatives [1]. The effects of heavy metals and chlorinated hydrocarbons on the performance of municipal anaerobic sludge digesters has been widely researched over the past 15 years and their adverse affects on the process are well known [2–6].

Several anaerobic toxicity assay procedures and methodologies have accordingly been developed [7–9] to test the treatability of industrial effluents by the anaerobic processes. Changes in methanogenic activity have been quantified either externally [10,11], with a gas pressure lock syringe [12–15], manometrically [5,16] or with a pressure transducer [17–19]. On-line analysis of dissolved methane and hydrogen was carried out using a membrane mass spectrometry [20,21]. Other major performance effects associated with anaerobic toxicity found in these studies included accumulation of volatile fatty acids, reduction in chemical oxygen demand removal, decreases in alkalinity and changes in the redox potential. Recently, it was suggested that trace gases such as hydrogen and carbon monoxide are useful parameters to indicate anaerobic

* Corresponding author.

[1] Presented at *Euroanalysis VIII*, session New Methods and Strategies in Environmental Analysis. The majority of papers for this session was presented in *Anal. Chim. Acta*, Vol. 291, No.3. .

[2] Present address: Department of Civil Engineering, Loughborough University of Technology, Loughborough, Leics., LE11 3TU, UK.

SSDI 0003-2670(94)00254-J

toxicity when used in conjunction with other parameters [14,22].

The literature shows a wide range of concentrations necessary to cause a 50% reduction in the measured parameters depending on whether studies were carried out under batch or continuous flow conditions and whether suspended, granulated or attached biomass was used. Differences are also reported from pure and mixed cultures, and between acclimatized or non-acclimatized sludge. Further variability has been noted with the duration of the assay [6,12], biomass concentration [5,6,23,24] and soluble sulphide concentration [3,23]. Acclimatization to toxic compounds has also been shown in several studies [12,25]. Results are also presented in the literature which show the different groups of bacteria in the anaerobic consortia vary in their reaction to possible toxins [5,6,14,22,26–28]. Typically for example the slow growing methanogens are the most susceptible but in a recent study using a multi-substrate it was reported that acetogenesis is more severely inhibited than aceticlastic methanogenesis by some heavy metals [29] and chlorophenols [30].

The results of short term anaerobic treatability tests are therefore difficult to interpret even when using standard methods. For example, the reported concentration of nickel causing 50% inhibition ranges from 10 mg/l to 15,000 mg/l [4,23,24,26].

Ideally, the waste water treatment industry requires a toxicity assay which can use the treatment plants own anaerobic digester sludge, can use real industrial effluent samples, is comparable with other tests and give a rapid result, i.e. in hours. Some batch bioassay methods already exist for toxicity testing using diluted or undiluted industrial effluents [30] and municipal digester sludge as inocula source [31].

There are several commercially available toxicity tests using aerobic organisms which are recommended to assess toxicity of waste water streams or industrial effluents [32–38]. These produce results within a short period (3 min to 18 h).

In this study therefore an attempt was made to develop a short-term, acute toxicity assay for anaerobic sludges. The inocula were immobilized in a reactor with a support matrix to give a rapid response and allow testing of large volumes of dilute samples. The effects of toxicants on the methanogenic activity was monitored by the reduction of methane production.

2. Experimental

2.1. Biocell and inocula

A biocell was developed which consisted of a pyrex glass column (275×42 mm i.d.) (Soham Scientific, Ely, UK). The top of the column was stoppered with a rubber bung and sealed at the bottom with a glass plate held in place with silicone (Dow Corning, 781, Acetoxy). In the top rubber bung 3 glass tubes (5 mm i.d.) were inserted, the first passing through the bioreactor to 30 mm above the bottom glass plate. This was used for introducing the sludge inocula and the liquid. The second tube was inserted to 50 mm below the liquid level of the reactor and was for removal of liquid samples. The third was level with the rubber bung and was for escaping effluent and generated biogas. The separation of the liquid and biogas took place outside the reactor using a Y-shaped polypropylene tubing connector attached to two neoprene pipes one for the biogas and the other for liquid outflow. Hoffman clips were used to close and open these tubes as required. Biogas was collected over water in a 150 ml graduated glass column, standing in a plastic tray. One hundred reticulated polyurethane foam cubes 10×10×10 mm (FILTREN, Declon, Corby) with a density of 20–24 kg m^{-3} and a pore count of 200–240 per linear mm and a specific surface area of 500 m^2 m^{-3} were used to construct the reactor column. These were placed randomly into the bioreactor, but were separated into 5 distinct sections by plastic retaining rings giving 25 to each compartment (Fig. 1). The total empty volume of the reactor was 400 ml and the actual liquid volume was approximately 360 ml after the addition of the support matrix. The bioreactor was mixed by a magnetic stirrer and follower (diameter 35 mm).

2.2. Inocula source and preliminary treatment

The sludge inocula was collected from a municipal sewage digester at Bedford, UK, using an air tight 5 l plastic container. The anaerobic sludge was filtered through a 1.5 mm pore vacuum assisted sieve to remove coarse debris whilst continually sparging with oxygen free nitrogen. The inoculum was transferred to a 10 l anaerobic reactor run in a constant temperature room (35°C). The anaerobic sludge biomass was settled in the vessel and the liquid fraction discarded and replaced

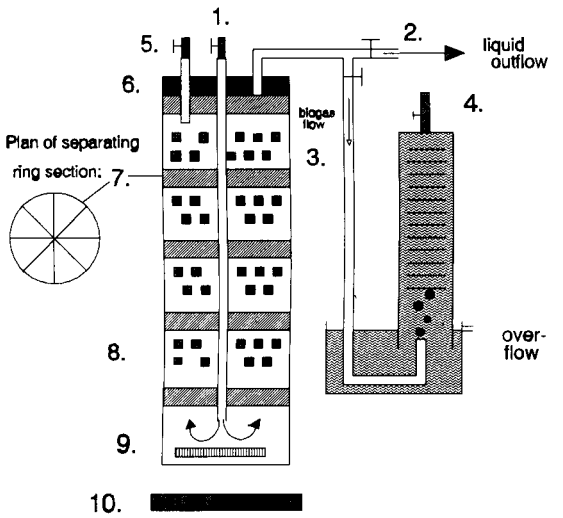

Fig. 1. Schematic diagram of the sequential batch bioassay and the biogas collection device.

with a mineral media solution (Composition after [17]) and stirred for 5 min. This step was repeated in order to replace any dissolved compounds from the sludge liquor. After this second washing then a feed substrate was added consisting of glucose, acetate, propionate and butyrate giving final concentration of 500, 300, 100 and 400 mg/l of reactor, respectively.

2.3. Preparation of anaerobic sequential batch bioassay (ASBA)

An anaerobic sludge inoculum of 100 ml which was collected, prepared and fed the previous day (described above) was anaerobically transferred at a flow rate of 10 ml/min into the bioreactor which had beforehand been filled with a mineral solution. During displacement of this liquid the anaerobic sludge was pushed upward and entrapped within the support matrix. To enhance uniform distribution of the inoculum the bioreactor was stirred continuously. The biomass concentration of the inocula was 11.53 g/l mixed liquor suspended solids (MLSS) and 8.5 g/l mixed liquor volatile suspended solids (MLVSS) within the reactor. After sludge introduction a small volume of oxygen free nitrogen was sparged through the sampling tubing in order to remove residual liquid in the outflow tubing which was then closed and the biogas tubing opened. The bioreactor was then fed with 5 ml of a concentrated feed substrate (described below) followed by 10 ml of nitrogen gas to insure dispersal of the substrate into the reactor.

2.4. Mode of sequential batch bioassay

During non-toxicity periods

At various intervals, 200 ml of the reactor liquid phase was displaced (flow rate of 10 ml min^{-1}) with an equivalent volume of fresh mineral salt solution, pH 7.0 also containing 0.001 mg l^{-1} resazurin, using a multi-channel peristaltic pump. Resazurin was used as an indicator of the redox potential. (i.e. colour changes at -40 mV). Then 5 ml of a stock solution of a composite substrate was injected into the reactor which resulted in final concentration of 700 mg l^{-1} acetate, 150 mg l^{-1} propionate and 350 mg l^{-1} butyrate in the reactor liquid. These were added as sodium salts. The biogas collection tubing was thereafter sparged with oxygen free N_2 to remove residual methane from previous runs.

During toxicity periods

When toxic chemicals were assayed then these were added at various concentrations to the 200 ml mineral media solution and compared to control assays with just the mineral solution. The feed substrate was the same in all tests.

After assaying of toxicants

The reactor liquid was displaced by 750 ml of fresh mineral media after each assay both in the test and control bioreactors in order to remove some of the residues. Feed substrate was then added as before.

2.5. Activity of ASBA inocula

The bioassays were run for 3 to 5 days as a sequential batch bioassay using non-toxic mineral solutions between each test in order to obtain a reproducible methane production rate from each inocula and to 'acclimitize' the anaerobic digester sludge to the hydraulic regime. From the composite feed substrate added to the reactor, theoretically 107.9 ml methane are expected to be generated, when completely utilized. This was calculated by the following method: 1 g of acetate generates, when completely oxidized, 415 ml of methane at 35°C; the oxidization of 1 mole of propionate generates 1 mole of acetate and 1 mole of buty-

rate generates 2 moles of acetate. Thus the feed substrate added to the bioreactor consisting of acetate, propionate and butyrate are equal to 0.26 g of acetate equivalents.

When the cumulative methane production reached an apparent 'steady state' i.e. the total methane production after each cycle approximated the theoretical methane production, then the bioreactors were judged to be ready for assaying toxicants.

2.6. Toxicity evaluation

The degree of inhibition of the inocula was calculated as percentage of the cumulative methane production over 6, 12 and 24 h and compared to active controls and also compared to the activity prior to addition of the toxin.

$$100 - [\text{ml } CH_4 \text{ (toxicassay)} / \text{ml } CH_4 \text{ (controls)} \times 100] = \%\text{inhibition}$$

2.7. Analysis of parameters

The methane content of the biogas was analyzed using gas chromatography (Pye Unicam, series 304) equipped with a flame ionization detector and a Porapack Q column. Temperatures of the oven, injector and detector were 120°C, 200°C and 200°C, respectively. Helium was used as carrier gas at a flow rate of 30 ml min^{-1}. One ml of biogas sample was used for analysis. The peak heights were used to calculate the % methane in the biogas, using a external standard calibration curve, and performed by an interconnected Minichrom data analyzer (VG Data systems, Altrincham).

Analysis of heavy metals was performed using an atomic absorption spectrophotometer (Perkin Elmer 2380). Samples were acidified and solubilized with concentrated nitric acid according to standard methods. [39].

Mixed liquor suspended solids (MLSS) and volatile solids (VS) were quantified after standard procedures and expressed as mg/l and g/l respectively [39].

2.8. Chemicals

Chloroform, and 1,1,1-trichloroethane (TCE) were of spectroscopic grade, the chromium added as sodium dichromate and copper as copper(II) chloride dihydrate (Fisons).

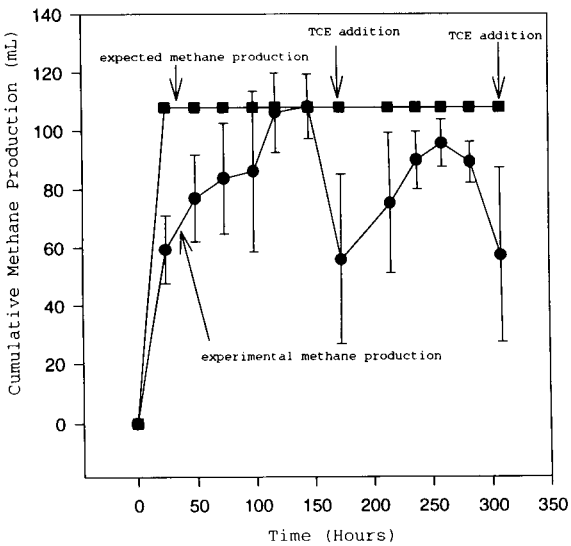

Fig. 2. Cumulative methane production (●) of 8 sequential batch bioassays over a 314 h assay period during which 13 feed substrate additions were made. Error bars indicate the standard deviation of the mean of 8 assays. The expected cumulative methane production (■) from the amount of substrate added is also shown. Trichloroethane was added at the times indicated.

3. Results

3.1. Start-up and performance of the ASBA

During the initial start-up the bioassay inocula required 100 to 120 h before producing the theoretical volume of methane from the amount of feed substrate added (Fig. 2). In particular in the first 70 h the rate of methane production was only 50 to 70% of that of the expected. The results of a 314 h assay period are shown in Fig. 2. Two doses of toxicants were added as indicated by the arrows. Transfer of the anaerobic sludge to the new environment of the bioassay might have contributed to the requirement for a long stabilization and establishment period. Loss of inocula during sequential cycles could also have contributed to the lower than expected methane production. The loss of biomass has been evaluated after each liquid displacement, shown in Fig. 3, and calculated as the percentage of the residue inocula. During each liquid displacement between 2.5 to 4% of the biomass is lost due to washout,

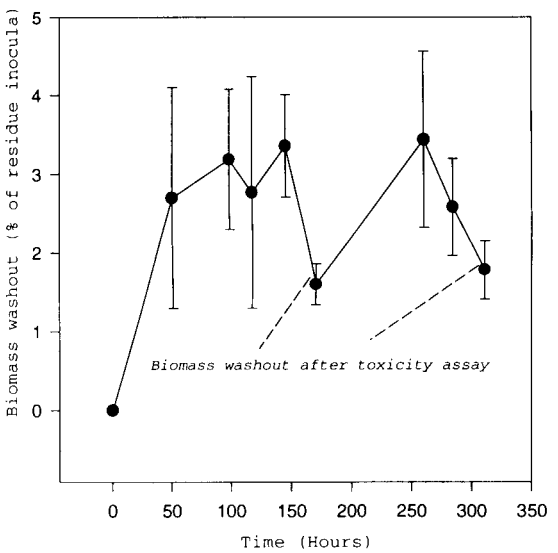

Fig. 3. Biomass washout of 8 bioassays using fresh non-acclimatized municipal digester sludge inocula over a 314 h period during which reactor liquid was replaced at the time interval shown. At 170 and 311 hours reactor liquid was replaced 3 times with fresh non-toxic liquid. Biomass washout was calculated as % biomass loss of the residual inocula concentration (●). Error bars are the standard deviation of the mean of 8 assays.

this corresponds to a sludge retention time of 25 to 40 days. During the 314 h assay period with 8 liquid displacement cycles the accumulative loss of biomass could have been from 14 to 25% of the original inocula concentration.

3.2. Response of bioassays to trichloroethane (TCE)

After 150 h of stabilization trichloroethane was added to the toxicity assays to obtain final concentrations in the bioreactor of 2.5, 5.0 and 10.0 mg/l. Fig. 4 shows the rate of methane production from the bioassays prior the addition of the toxicant, during toxicity evaluation and thereafter. The rate of methane production is initially slow, increases steadily and then decreases due to substrate depletion. After introduction of TCE to the bioassays and a non-toxic solution to the controls, the rate of methane production is reduced in proportion to the concentration of TCE. During the 24 h toxicity assay the initially strongly inhibited assays showed some recovery in the rate of methane production at the lower concentrations of added TCE. After displacement of the reactor liquid (3 times) with a non-toxic solution and addition of further feed substrates the rate of methane production was still affected compared to the controls. Total recovery of the bioassays to similar methane production rates before additions of toxin required 20 to 80 h.

3.3. Acclimatization to toxicant

In order to investigate whether the inocula became acclimatized to a toxicant, the assay was repeated after 113 h. The same units and tests were carried out as before. Similar trends in the rate of methane production were observed (Fig. 5). Table 1 compares the cumulative methane production of the assays before toxicant addition with the cumulative methane production during toxicity evaluation. The standard deviation and coefficient of variance values of the first and second run are shown. The % inhibition of the methane production due to TCE is compared with the parallel controls and the activity prior to the addition of the toxin.

The cumulative methane production in all assays during the first run was close the theoretical methane yield and had acceptable sample variations for the heterogeneous inocula used. The variation of the methane production during toxicity evaluation were greater, par-

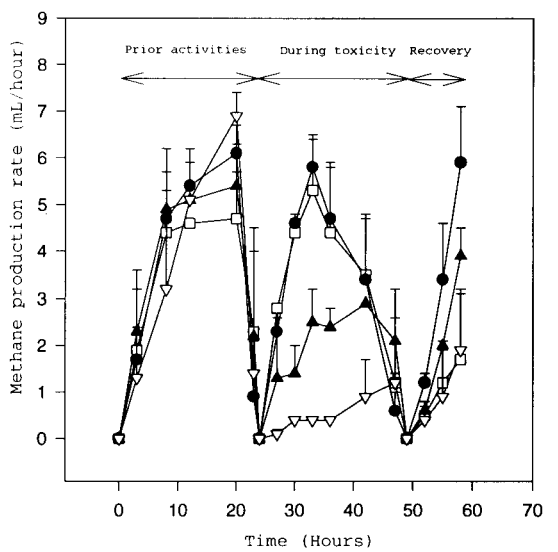

Fig. 4. Hourly rate of methane production at various intervals prior to trichloroethane toxicity evaluation, during assaying trichloroethane and after toxicity assay. Exposing bioassays the first time to trichloroethane. Controls (□) have received a non-toxic solution and three concentration ranges of trichloroethane were tested including 2.5 mg/l (●), 5.0 mg/l (▲) and 10 mg/l (▼). All assays are in duplicate and the standard deviations are shown as error bars.

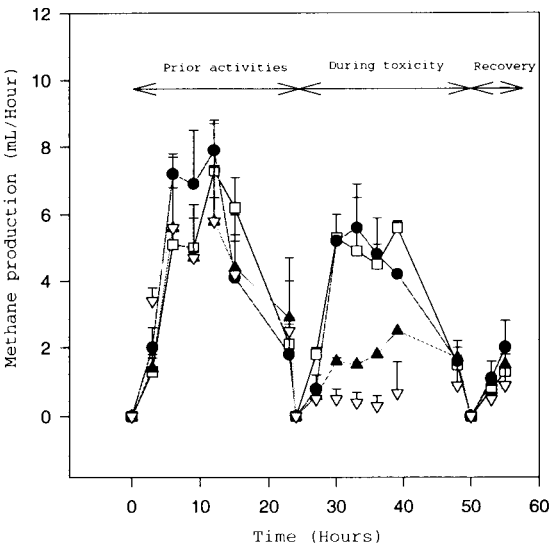

Fig. 5. Second test run showing hourly rate of methane production at various intervals prior to trichloroethane toxicity evaluation, during assaying trichloroethane and after toxicity assay. Exposing the same bioassays the second time to trichloroethane. Controls (□) have received a non-toxic solution and three concentration ranges of trichloroethane were tested including 2.5 mg/l (●), 5.0 mg/l (▲) and 10 mg/l (▼). All assays are in duplicate and the standard deviations are shown as error bars.

ticularly at the highest concentrations used. Further research will be required to improve the reproducibility. During the second run, carried out 113 h later, the cumulative methane production was only 83% of the theoretical methane yield, this indicates a gradual decline of inocula activity over its 300 h working life.

The methanogenic inhibition was plotted against the 3 TCE concentrations used during the assays (Fig. 6). A regression analysis was performed on the data and an r value of 0.96 was obtained. Both the parallel controls and the activity prior to the bioassays were used to calculate % inhibition. Both base values indicate similar trends in the overall inhibition pattern. A 50% inhibition is caused by 7.0 mg/l TCE when compared to the control and 5.25 mg/l when compared to the prior activity. The second exposure to TCE, Fig. 7, shows a similar trend in inhibition. A 50% methanogenic inhibition is caused by 6.0 mg/l of TCE compared to the control and 5.5 mg/l when compared to the prior activity. The toxicity assays using TCE were conducted over a total of a 24 h exposure period but the % inhibition of the cumulative methane production has also been calculated over a 6 and 12 h experimental period. These are shown in Fig. 8. It indicates that the shorter the assay duration then the greater the degree of inhibition of the methanogenic activity. A concentration dependent recovery of the assays can be noted over a 24 h period.

In earlier experiments reported in [40] chloroform toxicity was also evaluated but with a different inocula source and a shorter assay duration of 6 h. Three concentration ranges were tested. It was found that chloroform at final concentrations in the bioassay of 0.27, 0.53 and 1.30 mg/l inhibited the methane production by 3%, 28% and 88% after a 6 h assay period. Regression analysis of the data gave an 50% methanogenic inhibition estimate of 0.9 mg/l with an r^2 value of 0.81.

3.4. Response of sequential bioassay inocula to heavy metals

Several heavy metals were evaluated in experiments reported in [40] using a similar assay method but with different inocula sources, including chromium and copper. In the case of chromium for example methanogenic activity was inhibited by 50% in 6 h after exposure by using 33.6 mg/l chromium but recovered completely within 24 h. In the present study copper was not found to be inhibitory even at the highest concentration used (750 mg/l) over the 24 h assay period. Analysis of the effluent solution during introduction of the toxic solution showed that over 60% of the chromium toxicant and 90 to 95% of the copper remained in the reactor. Dismantling the reactor and subsequent analysis of the sludge showed that 55 to 60% of the initial added copper was associated with the anaerobic sludge.

4. Discussion

The results showed that a period of stabilization and establishment was required by the inocula before full activity was achieved using the anaerobic sequential batch bioassay (ASBA). The development of this type of assay assumed that during the sequential cycles the biomass concentration and the methanogenic activity was not affected. The results have shown however that there was a decline in the theoretical methanogenic activity during extended assay periods and that after 10 days' activity was 75 to 86% of that of the initial inocula. These findings demonstrate a distinct disadvan-

Table 1
Cumulative methane production of assays before toxicant addition and during toxicity evaluation, both during the first and second run. Sample standard deviation and coefficient of variance are shown. The % inhibition of the methane production is compared with the parallel controls and the activity prior to the addition of TCE

Trichloro-ethane	Methane production prior to toxi. test (ml/day)	S.D., $n=2$	C.V. (%)	Methane production during toxi. test (ml/day)	S.D., $n=2$	C.V. (%)	Methanogenic activity	
							Compared to active controls (% inhibition)	Compared to prior activity (% inhibition)
First run								
Control	97.5	±11.9	±12.2	78.5	±8.5	±10.8		
2.5 mg/l	113.2	±14.8	±13.1	75.5	±15.8	±20.9	4	33
5.0 mg/l	110.1	±5.8	±5.3	52.8	±15.1	±28.6	33	52
10 mg/l	112.1	±12.8	±11.4	16.2	±14.6	±90.1	79	85
Second run								
Control	97.5	±11.9	±12.2	82.7	±0.2	±0.2		
2.5 mg/l	94.6	±6	±6.3	73.9	±7.2	±9.7	11	22
5.0 mg/l	87.5	±9.5	±10.9	40.9	±1.2	±2.9	51	53
10 mg/l	89.0	±8.1	±9.1	15.5	±16.8	±108.4	81	83

S.D. = Standard deviation of the mean.
C.V. = Coefficient of variance.
During the first run all 8 assays had a cumulative methane production over 24 h of 108.2 ml CH_4 with a standard deviation of ±11.2 ml CH_4, corresponding to a C.V. of ±10.4 %.
During the second run all 8 assays had a cumulative methane production over 24 h of 89.1 ml CH_4 with a standard deviation of ±7.0 ml CH_4 and a C.V. of ±7.8 %.

tage of the method. However, considering the heterogeneous nature of anaerobic sludge and the hydraulic stresses exerted, the fact that reproducible results near to the theoretical methanogenic yields were obtained is encouraging. The loss of the inocula ranged from 2.5 to 4% per reactor per liquid displacement, corresponding to a sludge retention time of about 25 to 67 days. The aceticlastic methanogens and acetogenic bacteria have long doubling times of about 5 to 10 days [41] so that growth of these bacteria during a typical cycle described here will be small. Taking into account the loss of biomass and reduction in methanogenic activity of the bioassays during the assay periods it is suggested that when the methanogenic activity is below 70% of the theoretical then the test unit should be discarded. A useful working period of the sequential batch bioassay was between 15 to 20 days. Further research on using the assay system with a continuous feed and of the impact of long term inactive storage of the inocula is recommended.

The response of the bioassay to TCE toxicity showed reproducible results at specific concentrations when observing the cumulative methane production over 6, 12 and 24 h. In case of the hourly methane production rates there was a large spread of the data at the same toxicity concentrations. The test is not therefore as useful for quick and instant toxicity results. The nature of the heterogeneous anaerobic sludge and the small volumes of the methane produced during these short time intervals would have contributed to these variations. The degree of methanogenic inhibition was much stronger at 6 and 12 h than it was after 24 h when recovery had begun to occur. The duration of the assay is therefore a very important parameter in order to consider sensitivity threshold levels of a toxic solution.

The results have shown, in the case of TCE, that comparisons with parallel control and activity prior to the introduction of toxin give similar results. Recovery of the bioassay inocula to similar methanogenic activities to that prior to the introduction of a toxin took about 20 to 80 h. The recovery to this prior 'baseline' activity was dependent on the concentration of the toxin and the duration of the toxicity assay.

The response of the bioassay inocula does not correlate well with comparable work in the literature using suspended mixed anaerobic sludge. The current work

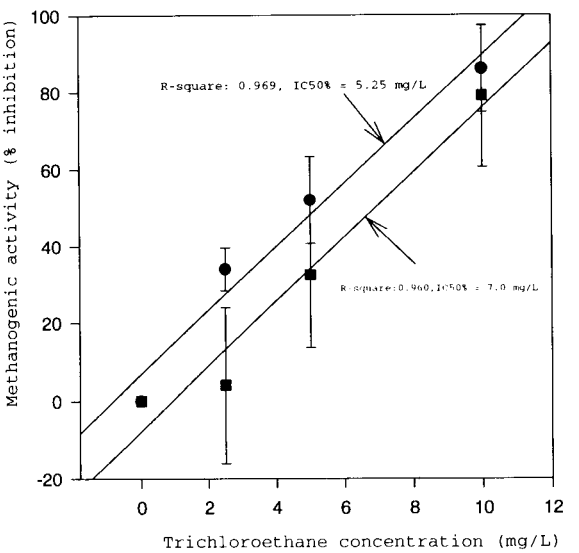

Fig. 6. Plot of trichloroethane concentration evaluated against percentage inhibition of cumulative methane production over 24 h, during the first exposure to trichloroethane. Error bars show the standard deviation of two bioassays receiving the same toxicity concentrations. The control methanogenic activities (■) of two bioassays were used in combination with the methanogenic activities prior to assaying trichloroethane (●) to calculate % inhibition. *R*-square values from regression analysis are shown and the estimated IC 50% concentrations stated.

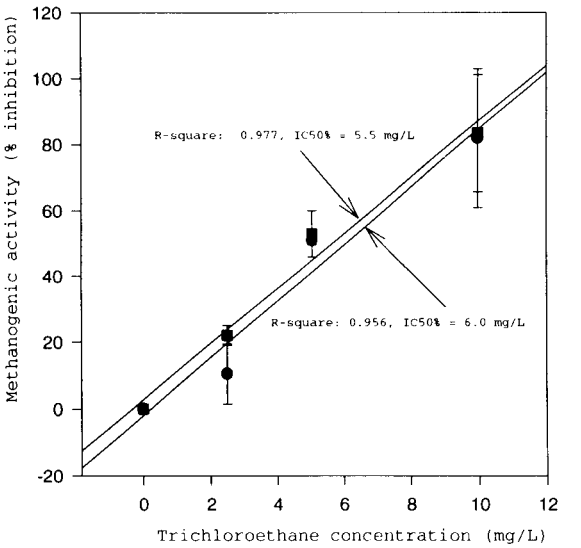

Fig. 7. Plot of trichloroethane concentration evaluated against percentage inhibition of cumulative methane production over 24 h, during the second time exposure to trichloroethane. Error bars show the standard deviation of two bioassays receiving the same toxicity concentrations. Both the control methanogenic activities (■) and also the methanogenic activities prior to assaying trichloroethane (●) were used to calculate % inhibition. *R*-square values from regression analysis are shown and the estimated IC 50% concentrations stated.

showed that much higher toxic compound concentrations (i.e. 5 to 10 times greater) were required using the anaerobic sequence batch assay in order to obtain a 50% inhibition of methanogenic activity. In particular the heavy metals tested gave no reproducible inhibition. For example, in the case of copper 5 times the concentration (i.e 750 mg/l) reported to cause complete inhibition of methanogenesis to an anaerobic suspended mixed assay [3] produced no clear reduction in the ASBA. This was despite the fact that about 55 to 60% of the copper was shown to be associated with the anaerobic biomass. These findings concur with other work which reports that attached biofilm reactors are less severely affected by toxicants than completely mixed reactors [4,42].

There is extensive information on two commercial bioassay systems for monitoring waste water streams. These are based on aerobic bacteria but may also be useful to protect anaerobic sludge digesters from toxic events. One of these is Microtox toxicity assay [33] in which bioluminescence is reduced following exposure to toxicants. The second is the RODTOX toxicity assay

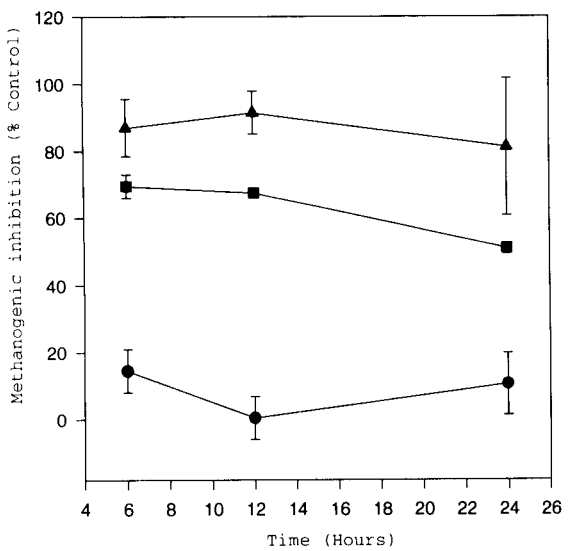

Fig. 8. Concentration dependent inhibition of trichloroethane at a concentration of 2.5 mg/l (●), 5.0 mg/l (■) and 10.0 mg/l (▲) on cumulative methane production over a 24 h assay period. Calculated over a 6, 12 and 24 h periods and expressed as % inhibition of control activity. Each test is the mean value of two bioassays and error bars indicate the standard deviation.

Table 2
List of toxicants and inhibitory concentration (IC 50%) in RODTOX assay, Microtox assay, Anaerobic Sequence Batch Assay and literature values

Toxicant	RODTOX IC50, 15 min ($mg\ l^{-1}$)	Microtox EC50, 15 min ($mg\ l^{-1}$)	Anaerobic sequential batch bioassay IC50%, 24 h			Anaerobic toxicity values, $mg\ l^{-1}$, IC50%
			$mg\ l^{-1}$	C.V. (%)	r^2	
Cr^{6+}	–[d]	26.9 [44]	≫ 55	±11	0.81	28 [29]–160 [15]
Cu^{2+}	12.8 [43]	3.5 [44]	≫ 750	–[d]	0.69	75 [22]–175 3]
Chloroform	4000 [43]	677 [45]	0.9 [a]	±5	0.81	0.3 [14]–0.91 [15]
Trichloroethane	–[d]	110 [46]	6.25 [b]	±11	0.96	0.84 [47]
Trichloroethane	–[d]	110 [46]	5.75 [c]	±0.4	0.95	0.84 [47]

[a] Inhibition values refer to 6 h toxicity assay.
[b] First time of TCE toxicity assay.
[c] Second time of TCE toxicity assay using same assays.
[d] No data available.

[38], which uses a heterogenous mixture of aerobic activated sludge bacteria and measures the changes in oxygen consumption following contact with toxicants. Table 2 compares the performance of the ASBA reported on here with RODTOX and Microtox with several micropollutants. Literature values of other anaerobic toxicity assays are also given. It is indicative from this table that the threshold toxicity levels causing a 50% reduction in methanogenic activity show similar trends for the chlorinated solvents when ASBA and literature data is compared. The aerobic Microtox and the RODTOX assay exhibit different toxicity values to heavy metals and chlorinated solvents compared to those reported for anaerobic cultures. An extensive laboratory study has been conducted by another group [15] comparing the response of several classes of micropollutants to established anaerobic toxicity assays and with those from the Microtox assay and found that the correlation coefficient for inorganic chemicals and organics was 0.3 and 0.49, respectively.

Even though the anaerobic sequential batch bioassay described in this paper does not reflect the same concentration thresholds as suspended biomass batch assays it does show similar trends of toxicity. Furthermore, there is scope to improve the usefulness and reliability of the ASBA. For example, biomass losses could be reduced and the unit run more continuously to promote biomass growth. It may also be a better model for toxicity to anaerobic fixed film reactors.

Several recent research reports indicate that mixtures of toxic chemicals exert a stronger degree of inhibition on anaerobic sludges than single compounds [29,47–50]. This information increases the urgency of the need to establish reproducible anaerobic toxicity assays for industrial effluents and waste water streams.

Acknowledgements

This work was funded by the Science and Engineering Research Council (Grant No. 91310342).

References

[1] J. Coombs, in A.D. Wheatley (Ed.), Anaerobic Digestion: A Waste Treatment Technology, Critical Reports on Applied Chemistry, Vol. 31, Elsevier Applied Science, Amsterdam, 1990, p. 1.
[2] J.D. Swanwick, D.G. Shurben and S. Jackson, Water Pollut. Control, 68 (1969) 639.
[3] F.E. Mosey and D.A. Hughes, Water Pollut. Control, 74 (1975) 18.
[4] G.F. Parkin, R.E. Speece, C.H.J. Yang and W.M. Kocher, J. Water Pollut. Control Fed., 55 (1983) 44.
[5] L.D. Johnson and J.C. Young, J. Water Pollut. Control Fed., 55 (1983) 1441.

[6] G.B. Patel, B.J. Agnew and C.J. Dicaire, Appl. Environ. Microbiol., 57 (1991) 2969.
[7] R.E. Hungate, in J.R. Norris and D.W. Ribbons (Eds.), Methods of Microbiology, Vol. 3B, Academic Press, New York, 1969, p. 117.
[8] T.L. Miller and M.J. Wolin, Appl. Microbiol., 27 (1974) 985.
[9] W.F. Owen, D.C. Stuckey, J.B. Healy, L.Y. Young and P.L. McCarty, Water Res., 13 (1979) 485.
[10] D. Valke and W. Verstrate, J. Water Pollut. Control Fed., 55 (1983) 1191.
[11] J.C. Young and H.H. Tabak, Water Environ. Res., 65 (1993) 34.
[12] D.C. Stuckey, W.F. Owen, P.L. McCarty and G.F. Parkin, J. Water Pollut. Control Fed., 52 (1980) 720.
[13] J. Dolfing and W.G.B.M. Bloemen, J. Microbiol. Methods, 4 (1985) 1.
[14] R.F. Hickey, J. Vanderwellen and M.S. Switzenbaum, Water Res., 21 (1987) 1417.
[15] D.S. Atkinson and M.S. Switzenbaum, in R.J. Scholze Jr., Biotechnology for Degradation of Toxic Chemicals in Hazardous Waste, Noyes Data Co., New Jersey, 1988, p. 622.
[16] A. James, C.A. Chernicharo and C.M.M. Campos, Water Res., 24 (1990) 813.
[17] D.R. Shelton and J.M. Tiedje, Appl. Environ. Microbiol., 47 (1984) 850.
[18] P.J. Reynolds, F. Concannon and E. Colleran, in G. Crassi (Ed.), Energy from Biomass, 4th EEC Conference, Elsevier, Amsterdam, 1987, p. 285.
[19] A. Cohen, in Proceedings of the 6th International Symposium on Anaerobic Digestion, Pergamon, Oxford, 1991, p. 7.
[20] R.I. Scott, T.N. Williams, T.N. Whitmore and D. Lloyd, Eur. J. Appl. Microbiol. Biotechnol., 18 (1983) 236.
[21] J. Benstead, D.B. Archer and D. Lloyd, Biotechnol. Techniques, 7 (1993) 31.
[22] R.F. Hickey, J. Vanderwielen and M.S. Switzenbaum, Water Res., 23 (1989) 207.
[23] S. Bhattacharya and G.E. Parkin, in R.J. Scholze Jr. (Ed.), Biotechnology for Degradation of Toxic Chemicals in Hazardous Waste, Noyes Data Co., New Jersey, 1988, p. 89.
[24] K.F. Jarrell, M. Saulnier and A. Ley, Can. J. Microbiol., 33 (1987) 551.
[25] W.L. Chou, R.E. Speece, R.H. Siddiqi and K. McKeon, Prog. Water Tech., 10 (1978) 545.
[26] B.K. Ahring and P. Westerman, Eur. J. Appl. Microbiol. Biotechnol., 17 (1983) 365.
[27] E. Colleran, F. Concannon, T. Golden, F. Geoghegan, B. Crumlish, E. Killilea, M. Henry and J. Coates, in Proceedings of the 6th International Symposium on Anaerobic Digestion, Pergamon, Oxford, 1991, p. 12.
[28] D.G. Capone, D.D. Reese and R.P. Kiene, Appl. Environ. Microbiol., 45 (1983) 1586.
[29] C-Y. Lin, Water Res., 26 (1992) 177.
[30] W-M. Wu, R.F. Hickey, L. Bhatnagar, M.K. Jain and J.G. Zeikus, in 44th Purdue Industrial Waste Conference Proceedings, Lewis Publishers, Chelsea, MI, 1990, p. 225.
[31] Standing Committee of Analysts, UK Dept. of the Environment, in Amenability of Sewage Sludge to Anaerobic Digestion 1977, H.M.S.O., London, 1978.
[32] P. Solyom, Prog. Water Tech., 9 (1977) 193.
[33] A.A. Bulich and D.L. Isenberg, Adv. Instrum., 35 (1980) 35.
[34] M. Kohne, F.W. Siepmann and D.A. te Heesen, Korrespondenz Abwasser, 33 (1986) 787.
[35] Y. Levi, C. Henriet, J.P. Countant, M. Lucas and G. Leger, Water Supply, 7 (1989) 25.
[36] J.E. Taraldsen and T.J. Norberg-King, Environ. Toxicol. Chem., 9 (1990) 761.
[37] P. Vanrolleghem, D. Dries and W. Verstraete, in Proc. 5th European Congress on Biotechnology, Copenhagen, 1990, p. 161.
[38] E.E. Herricks, B.E. Rittmann, C.P.L. Grady Jr., D. Pascoe, L. Somlyody, E. Fleit, J. Olah, M. van der Gaag, C. van de Guchte, W. Verstraete, D. Dries and D. Schowanek, Water Sci. Technol., 23 (1991) 271.
[39] APHA-AWWA-WPCF, in Standard Methods for the Examination of Water and Wastewater, APHA, Washington, DC, 17th edn., 1989.
[40] B.R. Erasin, A.P.F. Turner and A.D. Wheatley, Poster presented at the 7th International Symposium on Anaerobic Digestion, Cape Town, RSA Litho, 1994, p. 6.
[41] F.E. Mosey and X.A. Fernandes, Water Sci. Technol.. 21 (1989) 187.
[42] J.A. Oleszkiewicz and V.K. Sharma, Biol. Wastes, 31 (1990) 45.
[43] Z. Kong, P.A. Vanrollenghem and W. Verstraete, Biosensors and Bioelectronics 8 (1993) 49.
[44] A.A. Qureshi, R.N. Coleman and J.H. Paran, in D. Liu, B.J. Dutka (Eds.), Toxicity Screening Procedures Using Bacterial Systems, Marcel Dekker, New York, 1984, p. 1.
[45] A.A. Queshi, K.W. Flood, S.R. Thomson, S.M. Janhurst, C.S. Inniss and D.A. Rokosh, in J.G. Person, R.B. Foster and W.E. Bishop (Eds.), Aquatic Toxicology and Hazard Assessment: Fith Conference, Am. Soc. Testing and Materials, Spec. Techn. Publ. 737, 1982, p. 179.
[46] D.J.W. Blum and R.E. Speece, JWPCF, 63 (1991) 198.
[47] J.D. Swanwick and M. Foulkes, Water Pollut. Control, 70 (1971) 58.
[48] I.J. Kugelman and K.K. Chin, Adv. Chem. Ser., 105 (1970) 55.
[49] R. Sierra-Alvarez and G. Lettinga, Appl. Microbiol. Biotechnol., 34 (1991) 544.
[50] P. Renard, C. Bouillon, H. Naveau and E.-J. Nyns, Biotechnol. Lett., 15 (i1993) 195.

ELSEVIER

Analytica Chimica Acta 298 (1994) 11–18

ANALYTICA CHIMICA ACTA

Dual enzyme labels for simultaneous heterogeneous enzyme-linked competitive binding assays

Jeanette M. Buckwalter, Xuan Guo, Mark E. Meyerhoff *

Department of Chemistry, University of Michigan, Ann Arbor, MI 48109-1055, USA

Received 7 December 1993; revised manuscript received 2 June 1994

Abstract

The use of two enzyme labels in a dual analyte simultaneous heterogeneous enzyme-linked competitive binding assay is examined. Reaction conditions for monitoring glucose-6-phosphate dehydrogenase (G6PDH) and β-galactosidase (β-gal) activities are found which enable the independent measurement of each enzyme activity in the presence of the other. The two enzymes are used as labels in the development of a model simultaneous heterogeneous competitive binding assay for detecting the biotin and vitamin B_{12} content of vitamin tablets. The simultaneous assay is shown to exhibit analytical dose-response characteristics comparable to those of the single analyte assays. The potential use of the G6PDH/β-gal enzyme pair for devising other dual analyte competitive and non-competitive binding assays is discussed.

Keywords: Enzymatic methods; Simultaneous detection; Enzyme-linked binding assays; Vitamins; Glucose-6-phosphate dehydrogenase; β-Galactosidase

1. Introduction

Since their introduction in 1971, enzyme immunoassays have become important analytical tools for the determination of biomolecules at trace levels [1,2]. Enzymes are attractive as labels for binding assays because of their ease in handling and innate signal amplification qualities [3]. It has also been shown that naturally occurring binding proteins may be used in place of selective antibodies in such methods. This is especially useful when the analyte to be assayed is an endogenous molecule to which raising antibodies is difficult, e.g., vitamins [4–6].

Recently, interest has focused on developing binding assays that can analyze more than one analyte at a time in the same assay mixture. Indeed, many clinically important species are commonly determined in pairs, e.g., folate/vitamin B_{12}, TSH/free T_4, etc. [3,7,8], where quantitative data for both species is required for diagnostic purposes. The advantages of performing simultaneous analyses are a decreased reagent and sample volume requirement and an enhanced analytical efficiency which can lead to a decrease in assay cost. Simultaneous heterogeneous binding assays (solid-phase assays) have been carried out previously using dual radioisotope and fluorophore labels [9–11]. There have also been attempts to adapt enzyme-labeled assays to a simultaneous format; however, these previous assays were based on sequential rather than simultaneous enzyme reactions (i.e., the second enzyme was assayed after measuring the first) [3,12]. To date, there has been no published report describing a system in which a truly simultaneous assay for two analytes is performed by monitoring the rate of two enzyme reac-

* Corresponding author.

SSDI 0003-2670(94)00262-K

tions concurrently in the same sample mixture. This may be due to the difficulty in choosing compatible enzymes and reaction conditions in which the substrates or products can be quantitated accurately and simultaneously in the same solution.

The initial purpose of this work was to screen a number of potential enzyme pairs for use in truly simultaneous enzyme-linked binding assays. The criteria used for these evaluations included [3,13–15]: (a) the purity and specific activity of the enzymes; (b) their stability; (c) the ease of preparing the required conjugates of each enzyme; (d) the ability to resolve products/substrates spectrophotometrically for simultaneous kinetic assays; (e) similar pH optima for the two enzymes; and (f) reaction conditions required for one enzyme (e.g., given cofactors, metal ions, etc.) do not greatly affect the activity of the second enzyme. Of the various enzyme pairs examined, glucose-6-phosphate dehydrogenase (G6PDH) and β-galactosidase (β-gal) were found to be suitable for use in a simultaneous heterogeneous assay format. In this paper, the optimized reaction conditions for dual enzyme measurements is reported. In addition, a model simultaneous enzyme-linked competitive binding assay for the detection of vitamin B_{12} and biotin is demonstrated using G6PDH and β-gal as the enzyme labels.

2. Experimental

2.1. Apparatus and reagents

Enzyme activities were measured with a Gilford-Stasar-III spectrophotometer equipped with a vacuum-operated sampling system and temperature-controlled cuvette (maintained at 25°C). This spectrophotometer was connected to a Syva CP-5000 EMIT clinical processor for automatically setting the reading intervals and recording the absorbance values. A Perkin-Elmer Lambda Array 3840 UV–visible spectrophotometer operated by a Model 7300 professional computer was used for measuring the changes in absorbance at two wavelengths during the simultaneous assays. An IEC Centra-7R refrigerated centrifuge (4°C) was used for all centrifugation steps.

Glucose-6-phosphate dehydrogenase (G6PDH) from *L. mesenteroides*, β-galactosidase (β-gal) from *E. coli*, glucose-6-phosphate (G6P), β-nicotinamide adenine dinucleotide (NAD), *o*-nitrophenyl galactopyranoside (ONPG), biotinylated β-galactosidase (β-gal-biotin), avidin from egg white, porcine non-intrinsic factor (R-protein), vitamin B_{12}, biotin, *N*-hydroxysuccinimide, 3,3′-diethylaminopropyl carbodiimide, dithiothreitol (DTT), as well as other chemicals were purchased from Sigma (St. Louis, MO). The vitamin tablets, multivitamin/multimineral and B-100, were commercially available from Kroger (Cincinnati, OH).

The optimal dual assay buffer consisted of 0.05 M tris(hydroxymethyl)aminomethane–hydrochloric acid (Tris–HCl), pH 7.8, containing 0.10 M NaCl, 0.002 M $MgCl_2$, 0.1% (w/v) gelatin, and 0.01% (w/v) NaN_3. All substrate, standard solutions, and dilutions were prepared in assay buffer. All incubations were performed at room temperature.

Independent liquid chromatographic (LC) determinations of the B_{12} and biotin content of the given vitamin preparations were carried out using a Waters 600E solvent delivery system (Marlborough, MA), a Waters 486 tunable absorbance detector, and a Hewlett Packard 3396 Series II integrator. A reversed-phase C_{18} column (15 × 4.6 mm i.d.) from Supelco (Bellefonte, PA) was employed for both assays.

2.2. Simultaneous analysis of β-gal and G6PDH

To determine the influence of the G6PDH reaction on β-gal activity, the linearity of β-gal activity was measured in the presence of G6P/NAD and the G6PDH reaction running simultaneously. In a final volume of 1 ml, 25–250 mU of β-gal, 1.7 mM ONPG, 0.5 mM G6P, 3.2 mM NAD, and 55 mU G6PDH or assay buffer were mixed together. The β-gal activity was determined by measuring the rate of absorbance change at 415 nm over a 4 min period.

To determine the linearity of G6PDH activity in the presence of ONPG and the β-gal reaction, 2.2–22 mU of G6PDH, 0.5 mM G6P, 3.2 mM NAD, 1.7 mM ONPG, and 0.625 U of β-gal or assay buffer were mixed together and brought to a final volume of 1 ml. The G6PDH activity was determined by measuring the rate of absorbance change at 347 nm over a 4 min period.

2.3. Preparation of conjugates

Carboxylated vitamin B_{12} was prepared according to the method suggested by Armitage et al. [16]. The monocarboxylic derivatives were isolated using ion-exchange chromatography [17]. Further purification to isolate the e-monocarboxyl derivative was not necessary since R-protein does not differentiate among the three monocarboxylic isomers of vitamin B_{12} [18–20].

G6PDH–vitamin B_{12} conjugates were prepared using a modified *N*-hydroxysuccinimide method as described previously in the literature [21–23]. A G6PDH–vitamin B_{12} conjugate useful for the proposed simultaneous assay system was prepared containing an average of 1.0 vitamin B_{12} molecules per enzyme as determined by analysis of the absorbance spectra [21]. This enzyme conjugate possessed 55% of its original catalytic activity after conjugation.

The β-gal-biotin conjugate was prepared by Sigma via the reaction of 3-(*N*-maleimido-propionyl) biocytin with β-gal. This is a thiol-specific biotinylating reagent which incorporates a long spacer group required for efficient avidin/biotin binding [24,25]. According to Sigma, there are 3.5 biotin molecules attached per enzyme.

2.4. Preparation of solid phase R-protein and avidin

Solid phase R-protein was prepared by reacting 2000 U of R-protein with 360 mg of CNBr-activated Sepharose 4B according to the method suggested by the manufacturer of the Sepharose [26]. The protein and solid phase were mixed for 2 h at room temperature in an end-over-end mixer. The excess active sites were blocked by adding 1 M glycine and mixing overnight at 4°C. Non-specifically adsorbed protein was removed by alternately washing with 0.10 M $NaHCO_3$, 0.50 M NaCl, pH 8.3 and 0.10 M sodium acetate–acetic acid, 0.50 M NaCl, pH 4.0. The particles were stored in assay buffer at a 1:20 (packed bead v/v) dilution. Solid phase avidin was prepared by reacting 13.2 U of avidin with 1000 mg of CNBr-activated Sepharose 4B using this same procedure.

2.5. Preparation of vitamin tablets

Ten vitamin tablets were ground and the amount equivalent to one tablet was dissolved in 50 ml deionized water in a 50 ml polypropylene centrifuge tube. The solution was vigorously shaken for 30 min at room temperature. The suspension was then centrifuged at 3200 rpm for 15 min. The supernatant was saved and the solid was again washed with 50 ml deionized water and 50 ml 0.04 M NaOH with centrifugation between washes and subsequent pooling of the supernatant solutions. The solution was brought to a final volume of 200 ml with deionized water containing 0.01% (w/v) NaN_3 to prevent bacterial growth, and was stored at 4°C in the dark.

To prepare spiked samples for recovery studies, 44.5 μl of 0.10 mM vitamin B_{12} and 123 μl of 1.0 mM biotin standards or 133 μl of 0.10 mM vitamin B_{12} and 368 μl of 1.0 mM biotin standards were added to the vitamin powder. The samples were then treated as described above.

The determinations of biotin and vitamin B_{12} in the two vitamin tablet preparations by LC were carried out by adapting the methods reported previously by Crivelli et al. [33] and Dalbacke [37], respectively.

2.6. Single analyte assays

For single vitamin B_{12} assays, 50 μl of R-protein particles, 50 μl of 0.672 M DTT, 100 μl of vitamin B_{12} standard or unknown, and 500 μl of assay buffer were added to conical polypropylene culture tubes previously coated overnight with a 1% gelatin solution. The solutions were incubated for 30 min with mixing. Next, 100 μl of 2.0×10^{-8} M G6PDH–vitamin B_{12} conjugate and 200 μl of assay buffer were added, and the solutions were incubated for 60 min. The solid phase was then washed three times with 2 ml of assay buffer to remove any unbound analyte or conjugate. Finally, 100 μl of 0.010 M G6P and 0.063 M NAD solution and 800 μl of assay buffer were added and allowed to mix for 60 min. The solutions were centrifuged and the absorbance of the supernatant was determined at 347 nm.

For single biotin assays, 50 μl of avidin solid phase, 50 μl of 0.672 M DTT, 100 μl of biotin standard or unknown, and 550 μl of assay buffer were incubated for 30 min with mixing. Then, 50 μl of 4.63×10^{-9} M β-gal-biotin and 200 μl of assay buffer were added, the solutions were mixed for 60 min, and the particles were washed three times with 2 ml of assay buffer. The particles were suspended in 100 μl of 0.034 M ONPG solution and 800 μl of assay buffer, and the solution

was again incubated for 60 min. The particles were removed, and the absorbance of the solution was measured at 415 nm.

2.7. Simultaneous vitamin B_{12} and biotin assay

Fifty μl of R-protein particles, 50 μl of avidin particles, 50 μl of 0.672 M DTT, 100 μl of vitamin B_{12} standard or unknown, 100 μl of biotin standard or assay buffer, and 500 μl of assay buffer were added. After incubating for 30 min, 50 μl of 4.63×10^{-9} M β-gal-biotin and 4.00×10^{-8} M G6PDH–vitamin B_{12} solution along with 100 μl of assay buffer were added, and the solutions were incubated for another 60 min. After the particles were washed three times with 2 ml aliquots of assay buffer, 100 μl of 0.010 M G6P, 0.063 M NAD, and 0.034 M ONPG solution and 800 μl of assay buffer were added. The solutions were mixed for 60 min, the solid phase was removed, and the absorbances of the solutions were determined at 347 and 415 nm via the diode array spectrophotometer. Alternately, similar results should be obtainable by sequential measurements of the supernatant at these same two wavelengths using a conventional UV–visible spectrophotometer.

3. Results and discussion

The enzymes G6PDH and β-gal were chosen for use as the labeling enzymes because they meet most of the requirements envisioned for the development of a successful simultaneous enzyme-linked binding assay system (see Introduction). β-Gal catalyses the conversion of ONPG to *o*-nitrophenol (ONP), while G6PDH converts NAD and G6P to NADH and 6-phosphogluconate. These substrates/products were chosen because they can be resolved spectrophotometrically. The wavelengths for measuring the enzymatic activities were determined based on the absorption spectra of the substrates and products. *o*-Nitrophenol production was monitored at 415 nm because no other species present absorbs at this wavelength. However, as shown in Fig. 1, ONPG and ONP as well as NADH absorb in the region around 340 nm which is the usual wavelength for monitoring NADH. Fortunately, at 347 nm there is an isosbestic point in the absorbance spectra relating to the conversion of ONPG to ONP. Thus, NADH can be monitored at 347 nm independent of the concentrations

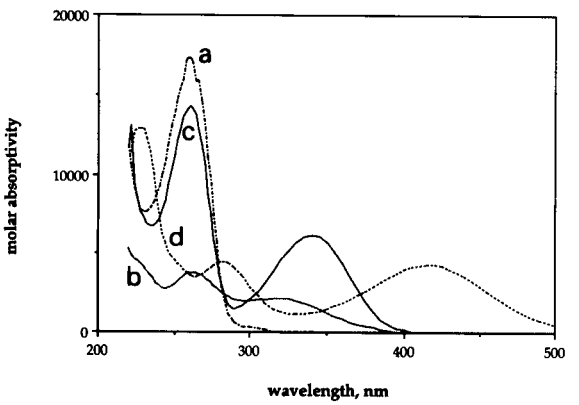

Fig. 1. Absorbance spectra of the substrates and products of the G6PDH and β-gal enzymatic reactions: (a) NAD, (b) NADH, (c) ONPG, and (d) ONP.

of ONPG or ONP within a reaction mixture with only a 4% loss in signal for NADH detection (i.e., $\varepsilon_{347\,nm}=5891$ and $\varepsilon_{340\,nm}=6106$).

Both enzyme reactions were studied individually, and the reaction conditions were optimized for maximum enzyme activity when the reactions are run simultaneously. It is known that the presence of magnesium ions has little effect on the activity of G6PDH from *L. mesenteroides* [27] yet is required for optimal β-gal activity [28]. This was verified here by studies in which Mg^{2+} concentrations varied between 0–5 mM resulted in no significant change in G6PDH activity; therefore, 2 mM Mg^{2+} was used for all subsequent enzyme assays. This level corresponds to the concentration of Mg^{2+} recommended for maximizing β-gal activity [28].

DTT is a common additive in β-gal activity assays since it acts as an acceptor alcohol thereby increasing the β-gal activity [28]. However, other reagents such as Tris–HCl can also act as activators of β-gal via the same mechanism [28]. Thus, little additional activation of the β-gal activity occurs when DTT is added to the Tris-HCl-based buffer (data not shown). Consequently, no DTT was added to the buffer in subsequent enzymatic determinations. However, as described below for vitamin assays, DTT is required in the buffer used during the initial sample/reagent incubation step of the single biotin and dual biotin/B_{12} binding assay to prevent aggregation of the β-gal-biotin conjugate.

For a simultaneous enzyme-linked binding assay to be successful, conditions must be found in which the

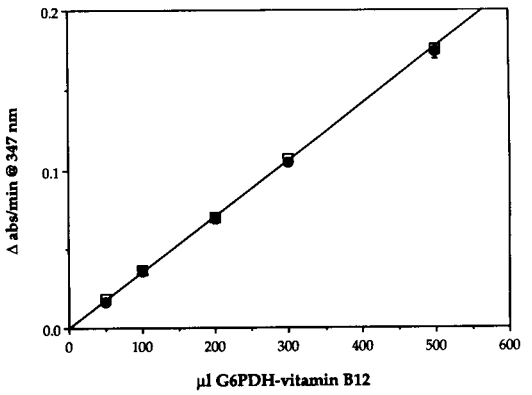

Fig. 2. Linearity of G6PDH activity for different amounts of 2.0×10^{-9} M G6PDH–vitamin B_{12} conjugate in the presence of 100 μl of 0.034 M ONPG alone (●) and ONPG with 50 μl of 4.63×10^{-9} M β-gal-biotin conjugate (□). Data points are average of triplicate determinations with ± S.D.

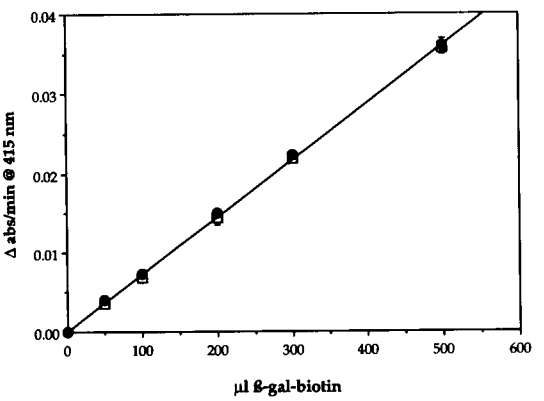

Fig. 3. Linearity of β-gal activity for different amounts of 4.63×10^{-10} M β-gal-biotin conjugate in the presence of 100 μl of 0.010 M G6P and 0.063 M NAD (●) and G6P/NAD with 50 μl of 2.0×10^{-8} M G6PDH–vitamin B_{12} conjugate (□). Data points are average of triplicate determinations with ± S.D.

second enzyme-linked assay does not significantly affect the first. To determine the influence of a second enzyme reaction occurring simultaneously, the activity of β-gal and G6PDH were examined individually in the presence of all substrates as well as the other enzymatic reaction in the Tris–HCl, pH 7.8 assay buffer. It was found that both enzyme activities when present in the same mixture do not differ significantly from the activities when examined individually. This was confirmed by comparing the mean values for absorbance changes that occur over the range of 2.2–22 mU/ml of G6PDH in the presence and absence of 625 mU/ml of β-gal and 25–250 mU/ml of β-gal in the presence and absence of 55 mU/ml of G6PDH. Use of the F test for each enzyme concentration, as well as a comparison of the slopes of the ΔA/min values vs. enzyme activities added indicated that there is no statistical difference in the measured enzyme activities with and without the second enzyme reaction running simultaneously (at the 95% confidence level) [29].

Based on these preliminary studies, a model assay for measuring biotin and vitamin B_{12} was studied to demonstrate the dual simultaneous assay concept. The required β-gal-biotin and G6PDH–vitamin B_{12} conjugates were prepared as described in the Experimental section. The enzyme conjugate activities were examined as above to determine whether conjugation of the enzymes results in reactions that are no longer independent of each other. As found for the native enzymes, the conjugated enzyme activities do not differ significantly when examined in the presence of all substrates or with the second enzyme reaction running simultaneously (see Figs. 2 and 3). In addition, the kinetic parameters of the enzyme conjugates were examined in detail and compared with the native enzymes. As Table 1 shows, there is very little change in these parameters; this was expected since there was only slight modification of the enzymes caused by the attachment

Table 1
Kinetic constants of β-gal-biotin and G6PDH–vitamin B_{12} compared to the native enzymes

Enzyme	substrate	K_M (μmol/l)	k_{cat} (min^{-1})	k_{cat}/K_M ($M^{-1}\,min^{-1}$)
β-gal	ONPG	155	1.07×10^4	7.71×10^7
β-gal-biotin	ONPG	151	9.39×10^3	6.22×10^7
G6PDH	G6P	239	3.22×10^4	1.59×10^8
	NAD	333	3.53×10^4	1.29×10^8
G6PDH– vitamin B_{12}	G6P	271	1.48×10^4	5.44×10^7
	NAD	345	1.66×10^4	4.67×10^7

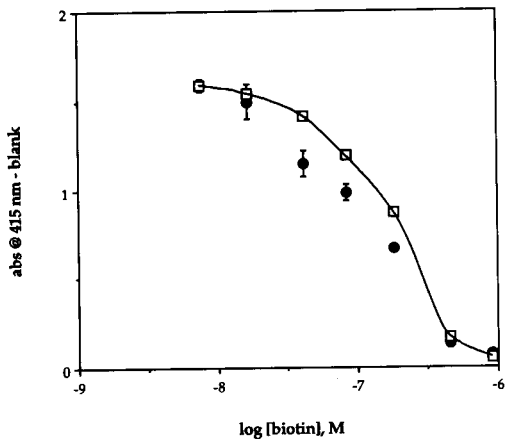

Fig. 4. Biotin dose–response curve in the absence (●) and presence (□) of 50 μl of 0.672 M DTT.

of biotin and B_{12} onto the respective enzymes (i.e., low ligand to enzyme ratios).

Detection limits for the simultaneous analysis of biotin and vitamin B_{12} were not fully optimized here; they were set for the convenient determination of these compounds in vitamin tablets. The sequential incubation times employed (30 min for binding beads with sample/standard and 60 min with conjugates) were based on findings by Tsalta et al. [30] who used a G6PDH–vitamin B_{12} conjugate and Sepharose-bound R-protein to devise a solid-phase B_{12} enzyme-linked binding assay. Indeed, preliminary studies indicated that the kinetics of the G6PDH–vitamin B_{12} conjugate binding to immobilized R-protein was slower than the reaction of β-gal-biotin with immobilized avidin. This might be expected based on the known higher affinity of the avidin/biotin reaction compared with the R-protein/vitamin B_{12} interaction (binding constants of 1.3×10^{15} M^{-1} and 2.0×10^{11} M^{-1}, respectively [31,32]).

During initial efforts to utilize the single biotin assay to determine biotin in vitamin preparations, it appeared that there was poor recovery of the biotin from the vitamin tablets. However, analysis of these same solutions by LC [33] revealed that biotin was present nearly in the same amount claimed by the manufacturers. Further studies demonstrated that the vitamin tablets were causing an apparent shift in the dose–response curve by increasing the amount of β-gal-biotin conjugate bound to the solid phase, resulting in a shift of the dose–response curve to lower apparent biotin concentrations. It is known that β-gal can form aggregates on standing in solution due to oxidation of free sulfhydryl groups to form intermolecular disulfide bonds. These aggregates can be dissociated by adding DTT or other reducing agents [27,34–36]. The vitamin tablets contain antioxidants (e.g., BHA and BHT) while the biotin standards do not. Thus, the presence of these antioxidants in the sample can dissociate the β-gal-biotin aggregates. By eliminating aggregation and thereby decreasing the size of the conjugate, more β-gal-biotin conjugate can bind to the solid phase (see Fig. 4). Thus, DTT was added to all solutions during the initial incubation period (but not during enzymatic determinations) to reduce this effect. DTT was found to have minimal effect on the G6PDH–vitamin B_{12} conjugate under these conditions.

Typical dose–response curves obtained in the single and simultaneous formats for vitamin B_{12} and biotin assays are shown in Figs. 5 and 6, respectively. There is no change in the curve shape or detection range when the assays are performed in the single vs. simultaneous format. This confirms that there is no interference between the two sets of assay reagents. This is to be expected since both binding proteins are analyte-specific and both vitamins are structurally quite different.

The selectivity of the vitamin B_{12}/biotin assay is comparable in both the single and simultaneous formats as demonstrated by the determination of the vitamin content in two different vitamin tablet formulations

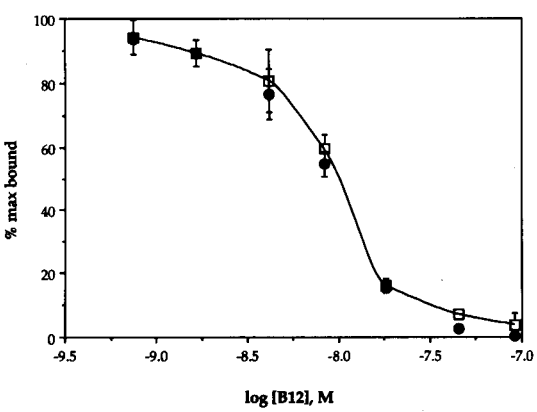

Fig. 5. Typical dose–response curve for vitamin B_{12} detection using the G6PDH–vitamin B_{12} conjugate (2.0×10^{-8} M in 50 μl aliquot) with the R-protein solid phase (50 μl of 1:20 (packed bead v/v)) in the single (●) and simultaneous (□) assay formats. Data points are the average of triplicate determinations with ± S.D.

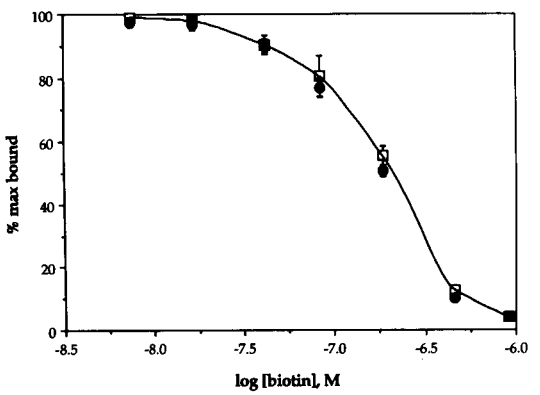

Fig. 6. Typical dose–response curve for biotin detection using the β-gal-biotin conjugate (4.63×10^{-9} M in 50 μl aliquot) with the avidin solid phase (50 μl of 1:20 (packed bead v/v)) in the single (●) and simultaneous (□) assay formats. Data points are the average of triplicate determinations with ± S.D.

(see Table 2). These results indicated that even when vitamin B_{12} and biotin are present at different concentrations, they can be measured with reasonable accuracy by the dual enzyme simultaneous binding assay. Indeed, biotin and B_{12} levels obtained for the same two preparations via LC methods [33,37] are in good agreement with the values determined by both the single and simultaneous enzyme-linked binding assay methods (see Table 2). Recovery studies for vitamin B_{12} and biotin were also performed by spiking vitamin tablets with different amounts of the vitamins to be analyzed. As shown in Table 3, the added vitamins can be recovered with acceptable accuracy given the low levels added. It should be noted that for all tablet measurements, the analytical determinations were made using graphical estimations from the non-linear dose–response curves. More accurate analysis could likely be accomplished by fitting the dose–response curve data to an appropriate equation describing such competitive binding curves.

Table 3
Recovery study for determining biotin and vitamin B_{12} in multivitamin tablet using single and simultaneous assay format

Vitamin	Added, μg	Found [a]	
		Single	Simultaneous
Biotin	30	35 ± 7	25 ± 2
	90	94 ± 6	77 ± 8
Vitamin B_{12}	6.0	7.8 ± 1.1	5.0 ± 0.7
	18	17 ± 3	18 ± 1

[a] Average of triplicate determinations.

In summary, we have shown that the activities of β-gal and G6PDH can be measured accurately in a simultaneous format without interference from the second enzymatic reaction. In the case where two binding proteins are analyte-specific, it is possible to assay both analytes simultaneously using β-gal and G6PDH as dual labeling enzymes. This simultaneous enzyme-linked binding assay offers the potential to determine the concentrations of two analytes occurring in a single reaction mixture. While applied here for the model analytes vitamin B_{12} and biotin, this same dual enzyme system could be used for the simultaneous detection of drugs using anti-drug antibodies, or in sandwich-type enzyme immunoassays for simultaneous measurements of two proteins (using Ab-enzyme conjugates). In addition, it may be possible to extend this concept to the development of more rapid simultaneous homogeneous enzyme-linked assays. Such work is currently in progress in this laboratory.

Table 2
Analysis of vitamin tablets for biotin and vitamin B_{12} using both single and simultaneous assay formats

Analyte	Sample	Claimed, μg/tablet	Claimed, single	Found [a], simultaneous	Found, LC [b]
Biotin	Multivitamin	30	31 ± 3	25 ± 4	25.8 ± 1.5
	B-Complex	100	111 ± 31	115 ± 13	85.8 ± 8.6
Vitamin B_{12}	Multivitamin	6	6.4 ± 0.8	5.7 ± 0.4	6.5 ± 0.2
	B-Complex	100	103 ± 15	109 ± 13	93.8 ± 3.9

[a] Average of triplicate determinations.
[b] Using methods reported in Refs. [33] and [37].

Acknowledgements

We gratefully acknowledge the National Science Foundation for supporting this work (CHE 9119728).

References

[1] E. Engvall and P. Perlmann, Immunochemistry, 8 (1971) 871.
[2] B.K. VanWeemen and A.H.W.M. Schuurs, FEBS Lett., 15 (1971) 232.
[3] A. Johannsson, C.P. Price and D.J. Newman (Eds.), in Principles and Practice of Immunoassay, Stockton Press, New York, 1991, p. 265.
[4] L.G. Bachas, C.D. Tsalta and M.E. Meyerhoff, BioTechniques, 4 (1986) 42.
[5] G.S. Cha and M.E. Meyerhoff, Anal. Biochem., 168 (1988) 216.
[6] S. Daunert, L.G. Bachas and M.E. Meyerhoff, Anal. Chim. Acta, 208 (1988) 43.
[7] L.J. Kricka, Clin. Chem., 38 (1992) 327.
[8] R. Ekins and F. Chu, Clin. Chem., 39 (1993) 369.
[9] S. Gutcho and L. Mansbach, Clin. Chem., 23 (1977) 1609.
[10] W.R. Whigham and L. Sudarsanan, Clin. Chem., 23 (1977) 1778.
[11] S.E. Kakabakos, T.K. Christopoulos and E.P. Diamandis, Clin. Chem., 38 (1992) 338.
[12] C. Blake, M.N. Al-Bassam, B.J. Gould, V. Marks, J.W. Bridges and C. Riley, Clin. Chem., 28 (1982) 1469.
[13] A.H.W.M. Schuurs and B.K. VanWeemen, Clin. Chim. Acta, 81 (1977) 1.
[14] G.B. Wisdom, Clin. Chem., 22 (1976) 1243.
[15] M.J. O'Sullivan, Anal. Proc. (London), 18 (1981) 104.
[16] J.B. Armitage, J.R. Cannon, A.W. Johnson, L.F.J. Parker, E.L. Smith, W.H. Stafford and A.R. Todd, J. Chem. Soc., 75 (1953) 3849.
[17] D.L. Anton, H.P.C. Hogenkamp, T.E. Walker and N.A. Matwiyoff, J. Am. Chem. Soc., 102 (1980) 2215.
[18] R. Grasbeck, in B. Zagalak and W. Friedrich (Eds.), Vitamin B_{12}, Walter de Gruyter, New York, 1979, p. 743.
[19] J.F. Kolhouse, H. Kondo, N.C. Allen, E. Poddell and R.H. Allen, N. Engl. J. Med. 299 (1978) 785.
[20] J.F. Kolhouse and R.H. Allen, J. Clin. Invest., 60 (1977) 1381.
[21] C.D. Tsalta and M.E. Meyerhoff, Anal. Chem., 59 (1987) 837.
[22] G.W. Anderson, J.E. Zimmerman and F.M. Callahan, J. Am. Chem. Soc., 86 (1964) 1839.
[23] M.C. Carter and M.E. Meyerhoff, J. Immunol. Methods, 81 (1985) 245.
[24] E.A. Bayer, M.G. Zalis and M. Wilchek, Anal. Biochem., 149 (1985) 529.
[25] O. Livnah, E.A. Bayer, M. Wilchek and J.L. Sussman, Proc. Natl. Acad. Sci. USA, 90 (1993) 5076.
[26] Affinity Chromatography, Principles and Methods, Pharmacia Fine Chemicals, Piscataway, NJ, 1979.
[27] C. Olive and H.R. Levy, Methods Enzymol., 41 (1975) 196.
[28] K. Wallenfels and R. Weil, in P.D. Boyer (Ed.), The Enzymes, Vol. 7, Academic Press, New York, 1972, p. 617.
[29] M. Hamburg, Basic Statistics: A Modern Approach, Harcourt Brace Jovanovich, Chicago, 1979.
[30] C.D. Tsalta, S.A. Rosario, G.S. Cha, L.G. Bachas and M.E. Meyerhoff, Mikrochim. Acta, 1 (1989) 65.
[31] N.M. Green, Adv. Protein Chem., 29 (1975) 85.
[32] E. Hippe and H. Olesen, Biochim. Biophys. Acta, 243 (1971) 83.
[33] S.L. Crivelli, P.F. Quirk, D.J. Steible and S.P. Assenza, Pharm. Res., 4 (1987) 261.
[34] H. Sund and K. Weber, Biochem. Z., 337 (1963) 24.
[35] K. Wallenfels, M.L. Zarnitz, G. Laule, H. Bender and M. Keser, Biochem. Z., 331 (1959) 459.
[36] S.R. Rohlfing and I.P. Crawford, J. Bacteriol., 91 (1966) 1085.
[37] J. Dalbacke and I. Dahlquist, J. Chromatogr., 541 (1991) 383.

ELSEVIER

Analytica Chimica Acta 298 (1994) 19–26

ANALYTICA CHIMICA ACTA

Simultaneous determination of catalysts based on the differences in the characteristic rate spectra of catalytic kinetics

Zhong-liang Zhu *, Zhi-cheng Gu, Rong-mei Chen, Chuan-qiang Han, Bing-liang Lu

Department of Chemistry, Tongji University, Shanghai, 200092, China

Received 29 December 1993; revised manuscript received 2 May 1994

Abstract

When a catalyst catalyses an indicator reaction, the reaction rate is a certain function of the concentration of each reactant and product. The plot of rate against the concentration of a reactant or product is called the characteristic rate spectrum (CRS) when the concentration of the catalyst is fixed. The CRS data are obtained from time-dependent concentrations of the reactant or the product by using the method of Savitzky and Golay and the method of linear interpolation. Based on the difference in CRS, a method for the simultaneous determination of catalysts in a single kinetic run is proposed. The concentration of each catalyst is calculated by principal component regression. As an example, Ru and Os were determined based on their catalytic effects on the indicator reaction between Ce(IV) and As(III). Factors that affect the accuracy and precision were studied by using the method of cross-validation.

Keywords: Catalytic methods; Kinetic methods; Catalysts; Characteristic rate spectrum; Principle component regression; Osmium; Ruthenium

1. Introduction

Differences in kinetic behaviour have been used extensively for the simultaneous determination of two or more components in mixtures. Many differential kinetic methods have been proposed for the analysis of mixtures of closely related species without prior separation [1]; however, most of these methods are based on uncatalysed reactions. To date, only a few catalysed reactions have been applied to the differential kinetic determination of two or more components in a mixture [2–5], and most of them have relied on two or more kinetic runs under the optimum reaction conditions.

The simultaneous determination of catalysts in a single kinetic run has seldom been discussed. Based in their different catalytic behaviours, a method for determination of Br^- and I^- was proposed [6]. A method for the determination of catalysts based on the difference in rates of inhibition was developed by Fitzpatrick and Pardue [7]. Recently, we proposed a method for the simultaneous determination of catalysts that is based on the difference in the apparent orders of the indicator reaction catalysed by each catalyst [8].

Principal component regression (PCR) [9] is an efficient multivariate regression method. It has

* Corresponding author.

SSDI 0003-2670(94)00244-G

been widely used in data processing of multicomponent analyses, including pseudo-first-order non-catalytic kinetic analysis [10]. This study was done to develop a method for the simultaneous determination of catalysts in a single kinetic run based on the difference in the characteristic rate spectrum of each catalyst. After suitable data processing, PCR is applied to calculate the concentration of each catalyst.

2. Mathematical description

Consider two catalysts C_1 and C_2 that catalyse the following indicator reaction:

$$r_1R_1 + r_2R_2 \xrightarrow{C_1,C_2} p_1P_1 + p_2P_2 \quad (1)$$

where R_1 and R_2 are reactants and P_1 and P_2 are products. It is assumed that the process of the reaction is monitored by the concentration of R_1 and that the rate is proportional to each catalyst. When only one catalyst exists, the rate equation can be represented by

$$v_i = -dR_1/dt = f_i(R_{1,t}, R_{2,t}, P_{1,t}, P_{2,t})C_i + v_0 \quad (2)$$

where v_0 is the rate of the uncatalysed reaction and $R_{1,t}$, $R_{2,t}$, $P_{1,t}$, $P_{2,t}$ are the time-dependent concentrations of each reactant or product, C_i is the concentration of the ith catalyst and $f_i(R_{1,t}, R_{2,t}, P_{1,t}, P_{2,t})$ is a function of the rate and each reactant and product when C_i acts as a catalyst. If the initial concentrations of each reactant and product are known, according to the stoichiometric relationships, $R_{2,t}$, $P_{1,t}$ and $P_{2,t}$ can be expressed by $R_{1,t}$ and the initial concentration, i.e., only one concentration of reactant or product is independent. In this case, Eq. 2 can be simplified to

$$v_i = -dR_1/dt = f_i(R_{1,t})C_i + v_0 \quad (2a)$$

It can be seen from Eq. 2a that the reaction rate is a function only of the reaction process (here presented by $R_{1,t}$).

In this paper, the plot of v, the rate when the conditions and the concentrations of C_i (C_i) are fixed, against $R_{1,t}$ is called the characteristic rate spectrum (CRS) of C_i, and $f_i(R_{1,t})$ is called the characteristic catalytic kinetic function (CCKF). It is assumed that both catalysts behave independently, so that the rates are additive, and when they co-exist the rates can be represented by

$$v = dR_1/dt = f_1(R_{1,t})C_1 + f_2(R_{1,t})C_2 + v_0 \quad (3)$$

Obviously, it is possible to determine two catalysts simultaneously through a single kinetic run when their CCKFs are different. In this paper, based on the catalytic effects on the reaction between Ce(IV) and As(III), Ru and Os were determined to test the method outlined above.

3. Data processing

This paper concentrates on decolorization kinetic processes. According to Eq. 1, it is assumed that at the specified wavelength the concentration of R_1 can be measured by spectrophotometry and can be simply described by the absorbance (A). It is also assumed that at the same wavelength the reactant R_2 and the products P_1 and P_2 all have no absorption. However, the time-dependent concentration of R_2 can be expressed as

$$R_{2,t} = R_{2,0} - (r_2/r_1)(R_{1,0} - R_{1,t}) \quad (4)$$

For the sake of simplification, we assume $r_1 = r_2 = 1$ and consider $R_{1,t} = A/\epsilon b$, and the concentration of R_2 can be described by the absorbance of R_1. Thus,

$$B = \epsilon b R_{2,t} = B_0 - A_0 + A \quad (4a)$$

where B indicates the converted absorbance of R_2, A_0 and B_0 are the initial absorbance of R_1 and the converted absorbance of R_2, respectively, and ϵ and b are the molar absorptivity of R_1 and the length of the cuvette, respectively. The reaction rate is simply described by $v = -dA/dt$, with the units absorbance s^{-1}. Data processing is illustrated by simulated data as follows.

It is assumed that the CCKFs, when C_1 and C_2 catalyse a decolorization reaction and when these is no catalyst, are

$$f_1(A) = k_{11}AB = k_{11}A(A + k_{12})$$
$$f_2(A) = k_{21}B = k_{21}(A + k_{22}) \quad (5)$$
$$f_0(A) = k_0A$$

Table 1
Parameters used to generate simulated data

Parameter	Value
k_0	5.0×10^{-4}
k_{11}	1.6×10^{4}
k_{22}	9.0×10^{3}
$k_{12}=k_{21}$	0.50
Initial absorbance, A_0	1.00
Time interval, Δt	10 s

where k_{11} and k_{21} are the rate constants of the catalytic reaction, k_{12} and k_{22} are the initial concentration differences between R_2 and R_1 (here $k_{12}=k_{22}=B_0-A_0$) and k_0 is the rate constant of the uncatalysed reaction. When both catalysts are present, the kinetic equation is

$$-\mathrm{d}A/\mathrm{d}t = k_{11}A(k_{12}+A)C_1 + k_{21}(A+k_{22})C_2 + k_0A \quad (6)$$

Generally the uncatalysed reaction always takes place whether the catalyst is present or not, so Eq. 6 also includes the rate of the uncatalysed reaction.

Simulated data are obtained by using integrated Eq. 6 and the parameters shown in Table 1. In Table 1, the constant k_{11} is calculated under the conditions $C_1=1\times10^{-7}$ and $C_2=0$ mol l^{-1} and the extent of reaction of R_1 is 70% when the reaction time is $t=600$ s. Similarly, the constant of k_{21} is calculated for $C_1=0$ and $C_2=1\times10^{-7}$ mol l^{-1}. The constant k_0 is calculated under the condition that the extent of reaction of R_1 is 25% when $t=600$ s and without any catalyst. In fact, for analysis of real samples, rate constants are never used in the data processing for determining the concentration, so no rate constants need be known.

The response curve is shown in Fig. 1. Rate data $(-\mathrm{d}A/\mathrm{d}t)$ are calculated from the A–t relationship by using the method of Savitzky and Golay [11]. Fig. 2 shows the rate–time relationship. Curve 3 presents the reaction rate when both catalysts are present. Obviously at a certain moment the rate is not equal to the sum of v_0, (v_1-v_0) and (v_2-v_0). After changing the abscissa from time to absorbance, the CRS can be obtained. By using the method of linear interpolation, the original CRS can be converted into the CRS of a specified absorbance (generally, the intervals of absorbance are equal), as shown in Fig. 3. It is obvious that $v_3=v_0+(v_1-v_0)+(v_2-v_0)$. This means that the contributions of catalysts to the rate are additive. The method of PCR is suitable for solving such a problem and for determining the concentrations of C_1 and C_2.

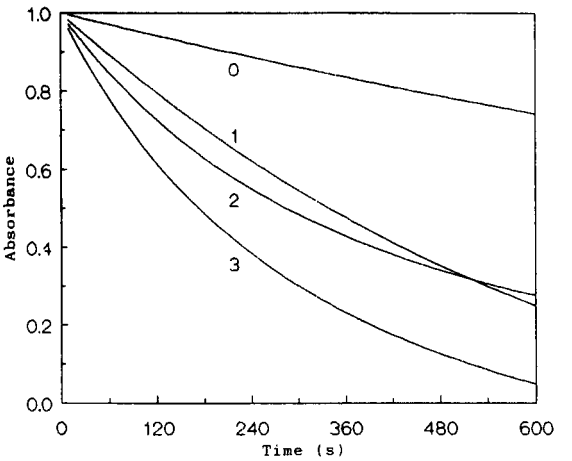

Fig. 1. Absorbance–time curves. (0) Blank; (1) $C_1=1.0\times10^{-7}$ M; (2) $C_2=1.0\times10^{-7}$ M; (3) $C_1=1.0\times10^{-7}$ M and $C_2=1.0\times10^{-7}$ M.

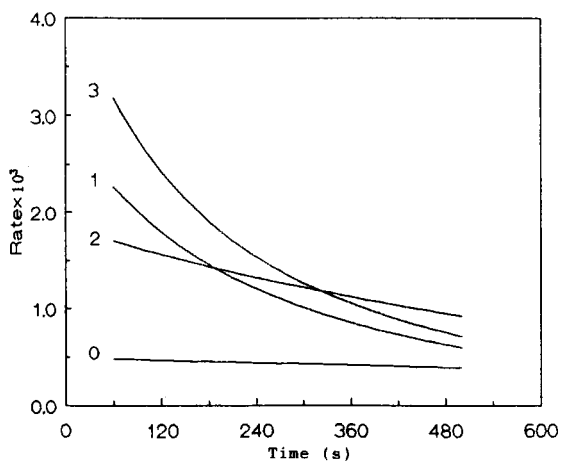

Fig. 2. Rate–time curves. (0) Blank; (1) $C_1=1.0\times10^{-7}$ M; (2) $C_2=1.0\times10^{-7}$ M; (3) $C_1=1.0\times10^{-7}$ M and $C_2=1.0\times10^{-7}$ M.

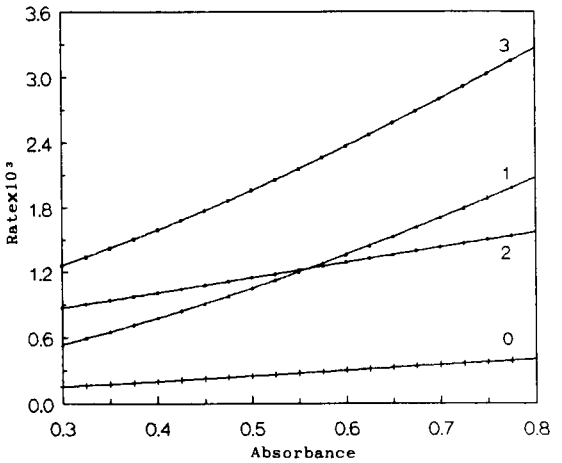

Fig. 3. Characteristic rate spectrum. (0) Blank; (1) $C_1 = 1.0 \times 10^{-7}$ M; (2) $C_2 = 1.0 \times 10^{-7}$ M; (3) $C_1 = 1.0 \times 10^{-7}$ M and $C_2 = 1.0 \times 10^{-7}$ M.

4. Experimental

4.1. Apparatus

An F7230 spectrophotometer equipped with a thermostat and an IBM microcomputer was used.

4.2. Reagents

All the chemicals used were of analytical-reagent grade and sub-boiling distilled water was used.

As(III) solution. Prepare a 0.020 M As(III)–2 M H_2SO_4 solution by dissolving As_2O_3 in 1 M NaOH and adding a suitable amount of H_2SO_4.

Ce(IV) solution. Prepare a 0.039 M Ce(IV)–2 M H_2SO_4 solution by dissolving $(NH_4)_4Ce(SO_4)_4 \cdot 2H_2O$ in 2 M H_2SO_4.

Stock standard Ru solution. Prepare this solution by dissolving $RuO_2 \cdot H_2O$ and discarding the part that is not dissolved, then standardizing by spectrophotometry. Dilute this stock standard solution as required before use.

Stock standard Os solution. Prepare this solution by dissolving OsO_4 in water and standardizing by spectrophotometry. Dilute this stock standard solution as required before use.

4.3. Procedures

Ce(IV) solution was mixed with sample solution containing Ru and Os (solution A). All solutions were placed in a thermostat at the required temperature until the temperature remained stable. A 1.0-ml aliquot of solution A was transferred into a cuvette and 2.0 ml of As(III)–H_2SO_4 solution were rapidly added. The absorbance changes with time against water were recorded synchronously at time intervals of 10 s and the total reaction time was 600 s, so the number of sampling points was 60. By using the method of Savitzky and Golay and the method of linear interpolation, these data could be converted into CRS with equal intervals of absorbance.

4.4. Experimental conditions

Ru and Os were determined under two sets of conditions in a single kinetic run. Table 2 gives the conditions.

Table 2
Determination conditions

Parameter	Conditions I	Conditions II
Wavelength (nm)	418	412
Temperature (°C)	28.0	26.0
Initial Ce(IV) concentration (M)	2.59×10^{-3}	1.9×10^{-3}
Initial As(III) concentration (M)	1.23×10^{-3}	4.0×10^{-2}
Ru catalyst concentration (10^{-8} M)	1.2–6.8	0.67–6.0
Os catalyst concentration (10^{-8} M)	1.0–5.7	0.13–1.2

5. Results and discussion

5.1. Dependence of CRS on initial concentration ratio of reactants

The kinetic behaviour of the Ru- and Os-catalysed reaction between Ce(IV) and As(III) has been studied in detail [3,8,12]. It was found that under conditions I (Table 2), the initial concen-

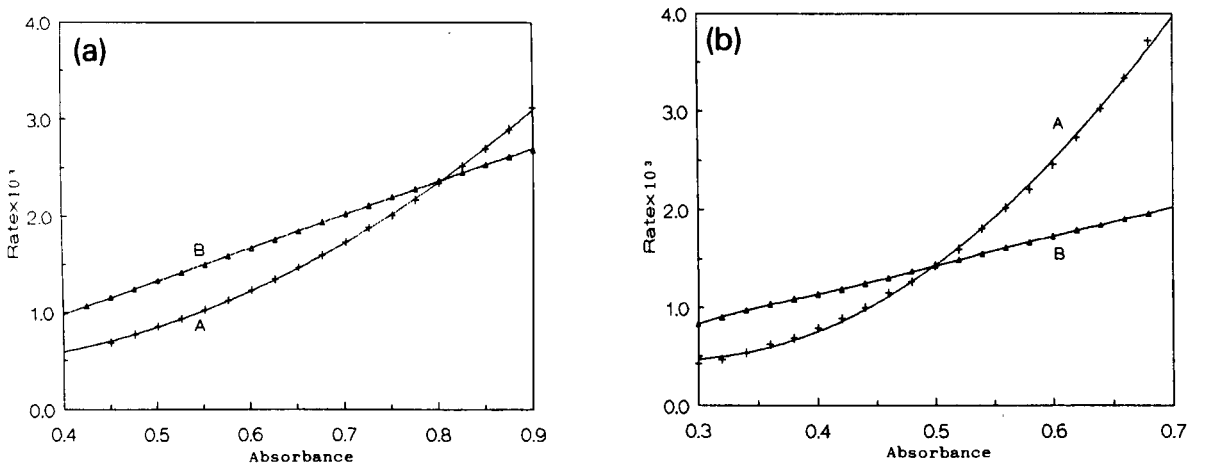

Fig. 4. (a) CRS of Ru and Os under conditions I (see Table 2). (A) [Ru] = 8.0×10^{-8} M; (B) [Os] = 6.7×10^{-8} M. (b) CRS of Ru and Os under conditions II. (A) [Ru] = 6.7×10^{-8} M; (B) [Os] = 1.3×10^{-8} M.

trations of As(III) and Ce(IV) are close to the stoichiometric ratio, and the catalytic activity of Os is dependent on [As(III)] but almost independent of [Ce(IV)]. The catalytic activity of Ru is dependent on [Ce[IV]] and is almost independent of [As(III)]. Under conditions II, however, the initial concentration of As(III) is greatly in excess, so [As(III)] is almost constant during the reaction process. The catalytic activities of both Ru and Os decrease with decrease in [Ce(IV)], particularly that of the former. The CRS of both catalysts under the two sets of conditions are shown in Fig. 4. The difference between the CRS of Ru and Os under conditions II is significant and the catalytic activity of Os is also far higher than that of Ru. The difference between the catalytic activities of Ru and Os under conditions I is comparatively small. Obviously, for two-component determination, the relative error for the minor component is large. Hence conditions I are suitable when [Ru]/[Os] in the sample approaches 1, whereas conditions II are suitable

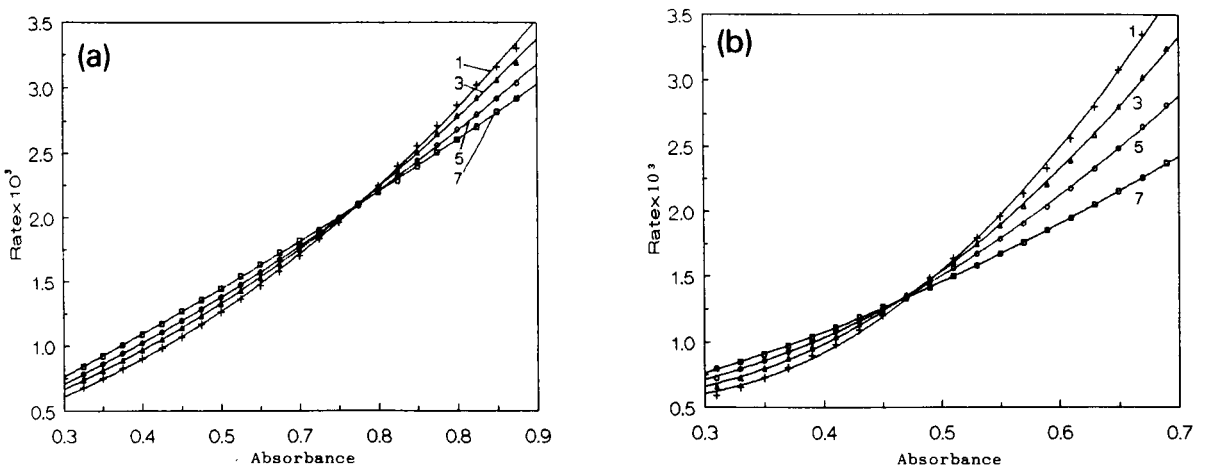

Fig. 5. CRS of different mixtures of Ru and Os, (a) under conditions I and (b) under conditions II. The numbers on the curves correspond to those in Table 3.

Table 3
Concentrations of standard solution

No.	Conditions I [a]		Conditions II [a]	
	[Ru] (10^{-8} M)	[Os] (10^{-8} M)	[Ru] (10^{-8} M)	[Os] (10^{-8} M)
1	6.40	1.53	5.33	2.67
2	5.60	2.00	4.67	4.00
3	4.80	2.67	4.00	5.33
4	4.00	3.33	3.33	6.67
5	3.20	4.00	2.67	8.00
6	2.40	4.67	2.00	9.33
7	1.60	5.33	1.33	10.7

[a] See Table 2.

when [Ru] > [Os]. In other words, sample mixtures with different concentration ratios are analysed under different conditions.

5.2. Factors that affect accuracy and precision

Two sets of catalyst mixtures were prepared with the concentrations shown in Table 3 and measured under conditions I and II. The CRS of different mixtures after data processing is shown in Fig. 5. The method of cross-validation (leave one out) was used to determine the number of principal components, range of absorbance, number of absorbance and number of smoothing points. The results are given in Table 4. A detailed discussion of the data processing conditions is given below.

Number of principal components

Fig. 6 shows a plot of the PRESS (prediction residual sum of squares) against the number of components(n_c). As $n_c = 2$ or 3 gives a minimum PRESS valve, $n_c = 3$ is specified in this paper.

Table 4
Parameters used in data processing

Parameter	I	II
Range of absorbance	0.90–0.45	0.68–0.32
Interval of absorbance	0.05	0.04
Number of absorbance	10	10
Number of smoothing points	15	15
Number of principal components	3	3

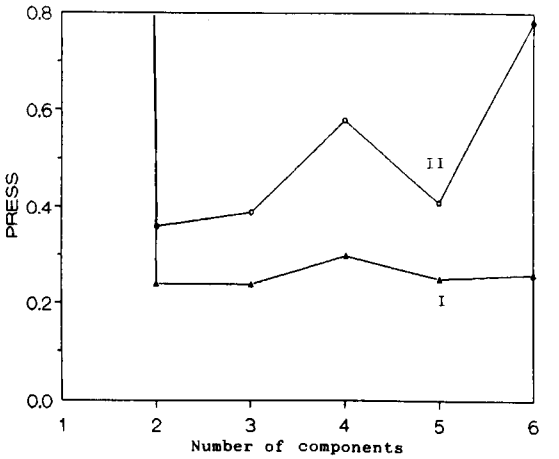

Fig. 6. Plot of PRESS against the number of components, (I) under conditions I and (II) under conditions II (see Table 2).

Range of absorbance

The absorbance of Ce(IV) indicates the progress of the reaction. Under certain conditions, the initial absorbance is fixed and the final absorbance depends on the reaction time. The effect of absorbance range on PRESS is illustrated in Fig. 7. It can be seen that PRESS decreases with increase in the absorbance range. However, PRESS increases when the range exceeds a certain value because the similarity of the CRS of the two components increases. The opti-

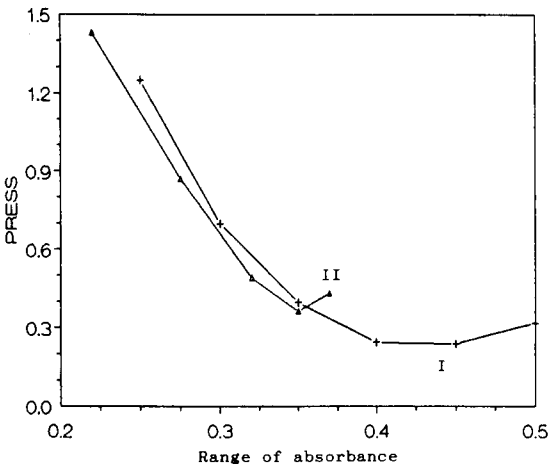

Fig. 7. Plot of PRESS against absorbance range, (I) under conditions I and II under conditions II (see Table 2).

Table 5
Effect of number of absorbance (n_A) on PRESS

Parameter	n_A					
	6	8	10	12	14	16
PRESS (I)	0.403	0.316	0.238	0.272	0.253	0.270
PRESS (II)	0.355	0.372	0.364	0.344	0.433	0.425

mum absorbance range in this paper is shown in Table 4. The initial concentration of Ce(IV) under conditions I is larger than that under conditions II, so the initial absorbance under conditions I is larger.

Number of absorbance

In the same absorbance range, the number of absorbance (n_A) has little effect on the PRESS, as shown in Table 5. The larger n_A is, the more time consuming the computation is; $n_A = 10$ is specified.

Number of smoothing points

When first-order derivatives are obtained by using the Savitzky and Golay method (in this paper, quadratic polynomials are used), it is obvious that the more smoothing points are used, the smoother the first-order derivatives spectrum is, but the more experimental points at both ends are dropped, however. The relationship between the number of smoothing points and PRESS is illustrated in Fig. 8. It can be seen that PRESS decreases with increase in the number of smoothing points. When the number is adequate, PRESS approaches a constant value. In this paper, this number is 15.

Table 6
Prediction result for a simulated sample using the proposed data processing method

C_1 (10^{-8} M)		Error (%)	C_2 (10^{-8} M)		Error (%)
Known	Predicted		Known	Predicted	
9.00	9.03	0.3	1.00	1.01	1.0
8.00	8.00	0.0	2.00	2.00	0.0
6.00	5.97	−0.5	4.00	3.99	−0.3
5.00	4.99	−0.2	4.00	3.99	−0.3
3.00	3.00	0.0	6.00	6.00	0.0
2.00	2.02	1.0	7.00	7.01	0.1
2.00	1.99	−0.5	8.00	7.99	−0.1
1.00	0.98	−2.0	9.00	9.01	0.1

5.3. Error caused by linear interpolation

Linear interpolation is an approximate method for calculating CRS with equal intervals of absorbance. Based on the Eq. 6 and using the parameters in Table 1, a set of simulated data for C_1 and C_2 mixtures were calculated. The result of data processing is shown in Table 6. It can be seen that the error caused by linear interpolation is very low.

5.4. Analysis of mixtures of Ru and Os

By using the seven samples in Table 3 as a standard, some synthetic samples of Ru and Os

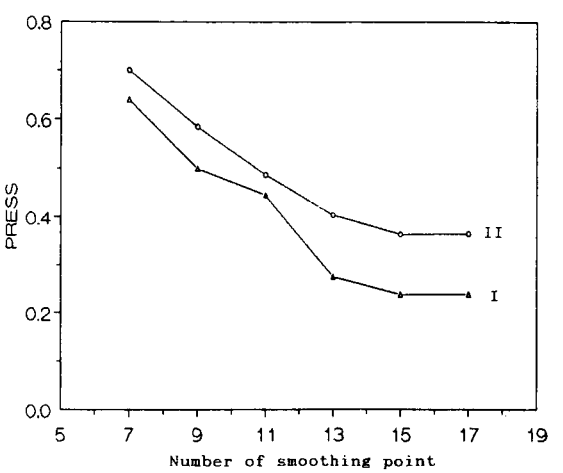

Fig. 8. Plot of PRESS against the number of smoothing points, (I) under conditions and (II) under conditions II (see Table 2).

Table 7
Analysis of mixtures of Ru and Os

Conditions [a]	[Ru] (10^{-8} M)		Error (%)	[Os] (10^{-8} M)		Error (%)
	Added	Found		Added	Found	
I	6.80	6.98	2.6	1.00	0.91	−9.0
	6.00	6.00	0.0	1.67	1.66	−0.4
	5.20	5.28	1.5	2.33	2.38	2.1
	4.00	3.90	−2.5	3.33	3.34	0.2
	2.80	2.78	−0.9	4.33	4.39	1.2
	2.00	2.01	0.5	5.00	4.88	−2.4
	1.20	1.05	12.5	5.67	5.75	1.5
II	6.00	5.99	−0.2	0.133	0.115	−13.5
	5.00	4.83	−3.4	0.333	0.343	4.0
	4.00	4.05	1.2	0.533	0.532	−0.2
	3.33	3.35	0.6	0.667	0.675	1.2
	2.67	2.68	0.4	0.800	0.808	1.0
	1.67	1.66	−0.6	1.00	0.98	−2.3
	0.67	0.70	4.5	1.20	1.14	−0.5

[a] See Table 2.

were analysed under the conditions in Table 2. The results are given in Table 7.

6. Conclusion

The proposed method can be used for the simultaneous determination of two or more components in mixtures in a single run only if the CCKFs of catalysts in certain reaction processes are different. The actual model of CCKF need not be known. It also does not matter whether or not there is blank reaction in the indicator reaction. The method is not limited to whether the catalytic reaction has a fixed order. It does not matter that the reaction order is a non-integer or that it varies during the reaction process.

When PCR is used in kinetic analysis, there is an obvious difference between a pseudo-first-order uncatalysed method (differential reaction rate method) and a catalysed method (discussed in this paper). The former is suitable for determining the concentration of each reactant which interacts with a common reagent while a set of product (or reactant) concentration data at different reaction times are measured. The latter is suitable for determining the concentration of each catalyst which catalyses a common reaction while a set of reaction rate data (CRS) at different reaction process are necessary.

References

[1] D. Perez-Bendito and M. Silva, Kinetic Methods in Analytical Chemistry, Ellis Horwood, Chichester, 1988.
[2] K.B. Yatsimirskii and L.P. Raizman, Zh. Anal. Khim., 18 (1963) 829.
[3] J.B. Worthington and H.L. Pardue, Anal. Chem., 42 (1970) 1157.
[4] A. Moreno, K.M. Silva and D. Perez-Bendito, Anal. Chim. Acta, 159 (1984) 319.
[5] P.A. Rodriguez and H.L. Pardue, Anal. Chem., 41 (1969) 1376.
[6] N. Yonehara, T. Yamane, T. Tomiyasu and H. Sakamoto, Anal. Sci., 5 (1989) 175.
[7] C.P. Fitzpatrick and H.L. Pardue, Anal. Chem., 61 (1989) 2551.
[8] Z.C. Gu, Z.L. Zhu, R.M. Chen, B.L. Lu and C.Q. Han, Analyst, 118 (1993) 1055.
[9] P. Geladi and B.R. Kowalski, Anal. Chim. Acta, 185 (1986) 1.
[10] Z.C. Gu and L. Xu, Chem. J. Chin. Univ., 12 (1991) 748.
[11] A. Savitzky and M.J.E. Golay, Anal. Chem., 36 (1964) 1627.
[12] R.L. Habig, H.L. Pardue and J.B. Worthington, Anal. Chem., 39 (1967) 600.

ELSEVIER

Analytica Chimica Acta 298 (1994) 27–32

ANALYTICA CHIMICA ACTA

Highly sensitive spectrophotometric kinetic determination of vanadium by catalytic effect on the gallocyanine–bromate reaction

Ali A. Ensafi [a,*], A. Kazemzadeh [b]

[a] *College of Chemistry, Isfahan University of Technology, Isfahan, Iran*
[b] *Materials Energy Research Center, Teheran, Iran*

Received 24 November 1993; revised manuscript received 25 April 1994

Abstract

A simple kinetic spectrophotometric method was developed for the determination of traces of vanadium present in petroleum, food and steel. The method is based on the catalytic effect of vanadium on the oxidation of gallocyanine by bromate at a pH of 4.0. The decrease in absorbance of gallocyanine at 620 nm at a fixed time of 4.5 min from initiation of the reaction is proportional to the concentration of V(V) for the range of 0.010–500 $ng \cdot ml^{-1}$. The limit of detection is 0.0005 $ng \cdot ml^{-1}$. The relative standard deviation for ten replicate measurements of 1.00 $ng \cdot ml^{-1}$ of vanadium is 1.7%. The interferences of ions could be eliminated by a simple procedure.

Keywords: Spectrophotometry; Catalytic methods; Vanadium; Gallocyanine; Bromate

1. Introduction

Vanadium is an important microelement in environmental chemistry because of its toxic nature, and therefore the determination of vanadium in environmental and biological samples is of great importance in toxicological research. Small amounts of vanadium are often found to be present either as an impurity or as a dopant in various glass, enamel and other ceramic raw materials, and the determination of vanadium in such materials is essential for quality control and characterization.

Vanadium exists in the +2 to +5 oxidation states with V(V) being the most stable in solution, followed by V(IV). Therefore most of the methods for the selective analysis of vanadium species in solution are based on the spectrophotometric analysis of V(V) and V(IV) after reaction with different complexing agents [1–4].

Atomic emission [5] and atomic absorption spectrometry [6] are used for the determination of total vanadium. However, for the determination of nanogram or lower amounts, these techniques can be applied only after preliminary isolation and preconcentration.

Kinetic methods (with spectrophotometric detection) based on the catalytic effect of vanadium are more sensitive and selective so that it is not necessary to apply preconcentration.

A number of catalytic methods have been proposed, the most sensitive of which are based on the catalytic effect of vanadium(V) on oxidation of organic compounds with an inorganic reactant such as bromate [7–12], peroxydisulphate [13–15], or chlorate [16,17] with photometric detection. An early example was the V(V) catalyzed oxidation of gallic acid with acidified

* Corresponding author.

SSDI 0003-2670(94)00251-G

peroxydisulphate [18,19] which was applied as a standard method to the analysis of waters. However, principal disadvantages of these methods are their low reproducibility, limit of detection ($0.2\ ng \cdot ml^{-1}$) and the long time necessary to complete the determination and interferences from many ions.

This investigation presents a highly sensitive and selective method for the determination of vanadium(V) without preconcentration based on its catalytic effect on the oxidation of gallocyanine (GC) by bromate. The effect of possible interferences is easily removed by a suitable procedure.

2. Experimental

2.1. Reagents

All reagents were of analytical-reagent grade and doubly distilled water was used throughout.

Gallocyanine solution(8.91×10^{-4} M) was prepared by dissolving 0.075 g of gallocyanine (Aldrich) in 10^{-5} M NaOH solution in a 250-ml volumetric flask.

Sodium bromate solution (1.00 M), was prepared by dissolving 37.727 g $NaBrO_3$ (Merck) in water in a 250-ml volumetric flask.

Standard vanadium solution ($1000\ \mu g \cdot ml^{-1}$) was prepared by dissolving 0.2296 g of NH_4VO_3 (Merck) in water in a 100-ml volumetric flask. Working standard solutions were prepared by diluting this stock standard solution.

2.2. Apparatus

A Shimadzu Model 220 spectrophotometer was used to record the absorbance spectra. A Perkin-Elmer Model 35 spectrophotometer with a 1.0-cm glass cuvette was used to measure the absorbance at a fixed wavelength of 620 nm. A thermostat bath (Gallenkamp, Griffin, BGL, 240-V) was used to keep the reaction temperature at 30°C. A stopwatch was used for recording the reaction times

2.3. Recommended procedure

The catalytic reaction was monitored spectrophotometrically by measuring the change in absorbance of the reaction mixture at 620 nm. The fixed time method was used for the first 0.5–4.5 min from initiation of the reaction.

A sample solution of less than 4.0 ml containing less than 0.100 μg of vanadium was poured into a 10-ml volumetric flask, then 1.0 ml of buffer solution (pH 4, citrate) and 3.0 ml of 1.0 M sodium bromate solution were added. The mixture was diluted to ca. 9 ml with water. 0.5 ml of 8.91×10^{-4} M gallocyanine was added and the solution was diluted to the mark with water. The reaction mixture was mixed and immediately an appropriate quantity of the reacting solution was transferred to the spectrophotometric cell and the decrease in absorbance was recorded at 620 nm against water for the first 0.5–4.5 min from initiation of the reaction. The measurement in the absence of added vanadium was repeated to obtain the values for the uncatalyzed reaction and this blank value was subtracted from the previous value. For larger amounts of vanadium (0.100–5.00 μg), 0.80 ml of 8.89×10^{-4} M gallocyanine and 0.10 ml of 1.00 M bromate solution was used. From the net values obtained from standard vanadium solution, a calibration graph of change of absorbance at a fixed time vs. vanadium concentration was constructed.

2.4. Determination of vanadium in petroleum crudes and food

Rice

The sample was dried at 110°C until constant weight was obtained and then ground until a fine powder was obtained. Between 4–6 g of sample were treated with 25 ml of 5 M HNO_3 in a sand bath. More nitric acid was added as necessary until foaming ceased. 10 ml of $HClO_4$ (70%, w/w) were then added and the solution was evaporated to dryness twice under a suitable hood. The residue was dissolved in 25 ml of 0.10 M HCl solution and the mixture was heated to boiling, cooked and the solution filtered (using Whatman No. 40 paper). Vanadium content was determined via the recommended procedure.

Petroleum crudes

All samples were treated with concentrated sulfuric acid (with continuous agitation to avoid foam formation) followed by combustion of carbonaceous ash at 526 ± 30°C. The inorganic residues were digested for 10–15 min with HCl (1:1). After concentration, a few

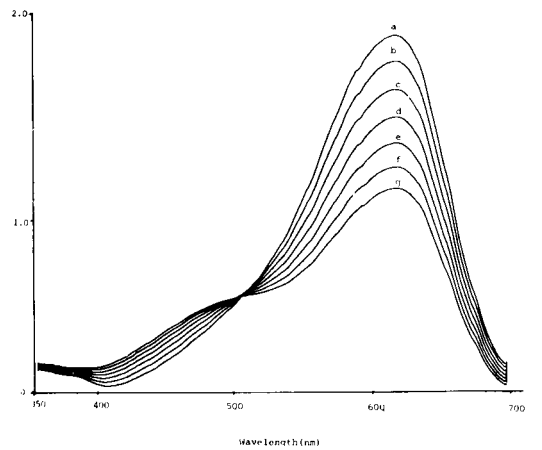

Fig. 1. Variation of GC–BrO_3^- oxidation system with time in the presence of V(V). Conditions: GC, 8.91×10^{-5} M; BrO_3^-, 0.050 M; V(V), 0.010 $\mu g\cdot ml^{-1}$; pH, 4.0; temperature, 30°C. Time: (a) 50 s, (b) 105 s, (c) 205 s, (d) 305 s, (e) 405 s, (f) 505 s, and (g) 605 s from initiation of the reaction.

drops of concentrated HNO_3 and H_2SO_4 were added and the solutions were gently heated until white fumes were formed. The small carbonaceous residues that had not been ignited were destroyed. The solution was finally diluted to 50 ml in a 50-ml volumetric flask and the vanadium content was measured via the recommended procedure.

3. Results and discussion

Gallocyanine is a dye (C.I. No. 51030) and is used as a redox indicator. Its oxidized form is produced by oxidants such as bromate, forming a colourless product in the presence of traces of vanadium. The reaction proceeds very slowly without V(V).

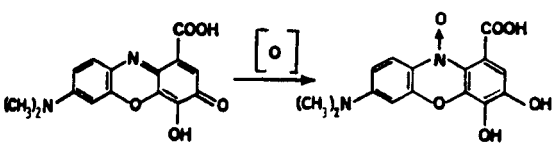

Absorption spectra of gallocyanine(GC)–bromate–V(V) are shown in Fig. 1. The absorbance at 620 nm decreases with time. The rate equation of the catalyzed reaction is:

$$\text{rate} = -d[GC]/dt$$
$$= k[V(V)][GC]^m[BrO_3^-]^n \quad (1)$$

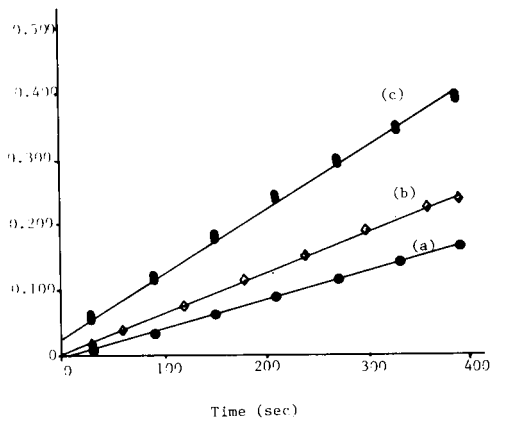

Fig. 2. Effect of absorbance change vs. time in sensitivity. Conditions: pH 4.0; BrO_3^-, 0.26 M; GC, 4.45×10^{-5} M; temperature, 30°C and (a) 0.010, (b) 1.00 and (c) 3.00 $ng\cdot ml^{-1}$ of V(V).

where k is the rate constant. Because $[BrO_3^-] \gg [GC]$, $[BrO_3^-]$ can be considered to be constant and m was found to be 1 (see Fig. 2). By integration of Eq. 1 and by incorporating Beer's law, we obtain the final expression:

$$A = K'[V(V)]t \quad (2)$$

where t is the reaction time.

There are many methods, such as fixed-time, initial rate, rate constant and variable time methods for measuring the catalytic species. Among these, the fixed-time

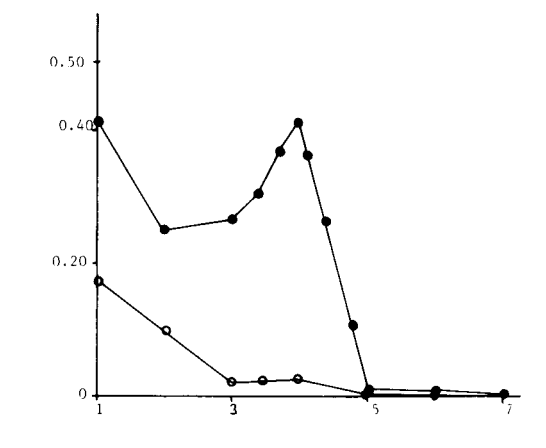

Fig. 3. Effect of pH on the reaction rate with (●) and without (○) V(V). Conditions: GC, 4.45×10^{-5} M; BrO_3^-, 0.10 M; V(V), 0.020 $\mu g\cdot ml^{-1}$; temperature, 30°C and measuring time, 0.5–4.5 min.

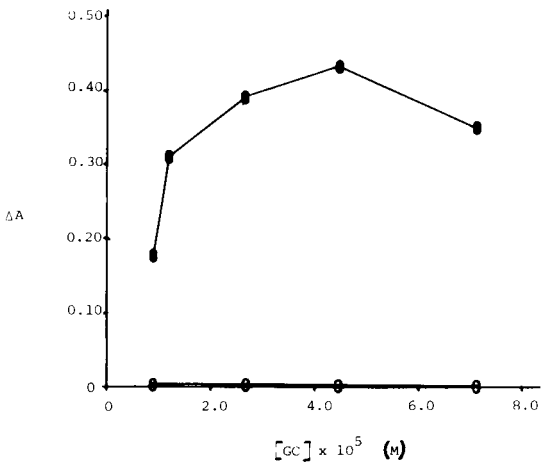

Fig. 4. Effect of GC concentration on the rate of catalyzed (●) and uncatalyzed (○) reaction. Conditions: BrO_3^-, 0.10 M; V(V), 0.020 $\mu g \cdot ml^{-1}$; temperature, 30°C; pH 4 and measuring time, 0.5–4.5 min.

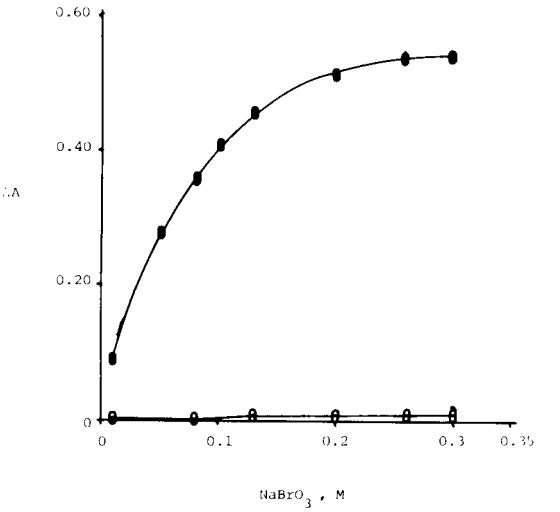

Fig. 5. Effect of bromate concentration on the rate of catalyzed (●) and uncatalyzed (○) reaction. Conditions: GC, 4.45×10^{-5}; V(V), 0.020 $\mu g \cdot ml^{-1}$; temperature, 30°C; pH 4.0 and measuring time, 0.5–4.5 min.

method is the most conventional and simplest, involving the measurement of ΔA at 620 nm. Fig. 2 shows the relationship between A and reaction time for different V(V) concentrations. ΔA increased linearly with time in the range of 0–5 min. This relationship implies that $m = 1$, i.e., the reaction is first order in GC.

3.1. Effect of variables

Fig. 3 shows the effects of pH on the uncatalyzed and catalyzed reactions at 30°C, which were studied with solutions containing no added V(V) (blank) or 0.020 $\mu g \cdot ml^{-1}$ of V(V). The pH was adjusted by adding sulfuric acid or buffer solution. The rate of the catalyzed reaction increased with increasing the pH from 2 to 4.0, whereas the rate of the uncatalyzed reaction is decreased for the overall pH range. A pH of 4.0 was therefore selected.

The effect of gallocyanine concentration on the catalyzed and uncatalyzed reaction for obtaining a con-

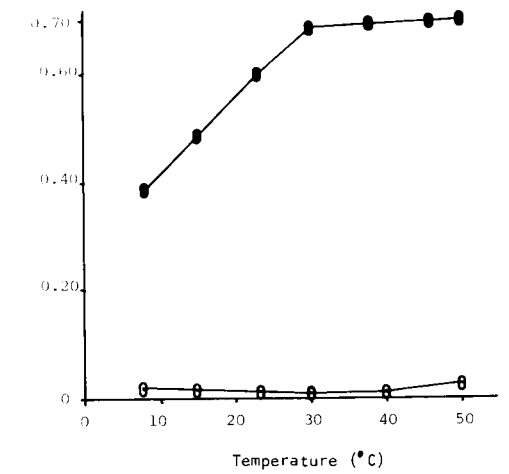

Fig. 6. Effect of temperature on the rate of catalyzed (●) and uncatalyzed (○) reaction. Conditions: GC, 4.45×10^{-5} M; BrO_3^-, 0.30 M; pH 4.0; V(V), 0.020 $\mu g \cdot ml^{-1}$; temperature, 30°C and measuring time, 0.5–4.5 min.

Table 1
Effect of foreign ions on the determination of 0.0010 $\mu g \cdot ml^{-1}$ V(V) at optimum conditions

Species	Tolerance limit ($W_{ion}/W_{V(V)}$)
Sr(II), Ba(III), Ca(II), K^+, Na^+, Th(IV), Co(II), La(III), Cd(II), Zr(IV), $Mg(II)$, NH_4^+, Cl^-, F^-, CN^-, EDTA, CH_3COO^-, ClO_4^-, $S_2O_8^{2-}$, $S_2O_5^{2-}$, NO_3^-, PO_4^{3-}, SO_4^{2-}, ClO_3^-, KHP, BO_3^-, CO_3^{2-}, $C_2O_4^{2-}$, Al(III) [a], Ni(II) [b], Zn(II) [b], Fe(III) [a], Mn(II) [b]	100 000
Rh(III), tartarate, Hg(II) [b], Bi(III) [b], Cd(II) [b]	50 000
Cr(III) [b], Br^-, Ag(I)	500
Cr(III), Al(III), Ce(III), Pb(III)	50
Ce(IV)	2

[a] When 1.0 ml of 1% NaF was added to the solution.
[b] In the presence of 1.0 ml of 0.1% EDTA solution.

Table 2
Determination of vanadium in real samples

Sample	V(V) added ($\mu g \cdot ml^{-1}$)	V(V) found ($\mu g \cdot ml^{-1}$)	Recovery (%)	R.S.D. (%)	V(V) found by standard method ($\mu g \cdot ml^{-1}$)
Fe^{3+}, Ni^{2+}, Mn^{2+}	0.100	0.100	100%	1.2%	–
Cd^{2+}, Mn^{2+}, Ni^{2+}, Co^{2+}	0.100	0.105	105%	1.5%	–
Human serum [c]	–	0.0010	–	1.7%	0.0011 [a]
	0.020	0.021	100%	1.5%	–
Rice [c]	–	–	–	–	0.000 [a]
	0.020	0.021	105%	1.2%	–
Petroleum crude [c]	–	1.300	–	1.3%	1.310 [b]
	5.00	6.310	101%	1.2%	6.300 [b]

[a] Ref. 20
[b] Ref. 21
[c] Absorbance change of the blank has been subtracted from all reported values.

stant and maximum sensitivity was investigated (Fig. 4). The results show that the rate of the catalyzed reaction increased with increasing gallocyanine concentration up to 4.45×10^{-5} M, whereas for the uncatalyzed reaction, the reaction rate was constant. Thus, a gallocyanine concentration of 4.45×10^{-5} M was adopted.

The effect of bromate concentration on the reaction rate was investigated in the range of 0.02–0.70 M of bromate (Fig. 5). The rate of the catalyzed reaction increases with increasing bromate concentration up to 0.25 M, whereas the uncatalyzed reaction rate increased very slowly. A concentration of 0.30 M bromate was therefore adopted.

The effect of reaction temperature was studied in the range of 5–50°C. Fig. 6 shows that at <30°C, the decrease in absorbance increases with temperature, but at higher temperatures it increases slower whereas the rate of the uncatalyzed reaction does not change. This means that after initiation, for the first 0.5 min the rate of the catalyzed reaction (that cannot be used to measure the absorbance changes) was so fast that a large amount of gallocyanine reacted.

The reaction rate decreased slightly with increasing ionic strength of the reaction mixture (using 3.0 M $NaNO_3$).

3.2. Calibration

Calibration graphs were obtained using the fixed-time method. This method was applied to the change in absorbance over an interval of 0.5–4.5 min because its provided the best regression and sensitivity. The oxidation rate of gallocyanine is a linear function of vanadium concentration. This linearity was obtained under the following conditions: With optimum concentrations of bromate and gallocyanine, a temperature of 30°C and a V(V) concentration of 0.010–10 $ng \cdot ml^{-1}$, $\Delta A = 3.195 \times 10^{-4} + 0.153C$ ($n=5$ and $r=0.9999$). With a gallocyanine concentration of 7.13×10^{-5} M and a bromate concentration of 0.010 M and a vanadium concentration of 10–500 $ng \cdot ml^{-1}$, $\Delta A = 0.750 + 7.44 \times 10^{-4}C$ ($n=5$ and $r=0.9995$), where C is the concentration of V(V) in $ng \cdot ml^{-1}$. In both calibration ranges studied, the best correlation coefficients were obtained for changes in absorbance over the first 4.5 min. Higher concentrations of vanadium (>500 $ng \cdot ml^{-1}$) can be studied by the above method using lower concentrations of bromate.

The experimental limit of detection is 0.0005 $ng \cdot ml^{-1}$ V(V). The relative standard deviation for ten replicate measurements of 0.05, 0.50, 1.0, 20.0 and 500.0 $ng \cdot ml^{-1}$ of V(V) was 3.10%, 2.40%, 1.70%, 2.21% and 1.30%, respectively.

3.3. Effect of foreign ions

The effect of more than forty foreign ions on the catalytic determination of 0.0010 $\mu g \cdot ml^{-1}$ of V(V) was examined at the optimum conditions. The results are shown in Table 1, and demonstrate that the catalytic method in combination with the kinetic spectrophotometric detection has high selectivity. The results show that only Al(III), Ce(III) and Cr(III) at levels up to twenty times excess of V(V) have no effect on the

determination of V(V). The interference of higher levels of these ions can be eliminated with 0.1% EDTA or 0.1% NaF solution (Table 1).

3.4. Analysis of samples

The catalytic method was applied to the direct determination of V(V) in petroleum crude, food and steel. The standard addition method (due to unknown ionic strength) is recommended and is compared with the standard method [20,21] (Table 2).

4. Conclusion

Using the proposed method it is possible to determine vanadium at levels as low as 0.50 $pg \cdot ml^{-1}$ without the need for any preconcentration step. Apart from the high sensitivity of the method, addition of EDTA and NaF solution to the sample solutions permits the highly selective determination of vanadium.

References

[1] A.B. Chatterjee, S.P. Bag, A.K. Chakraburtty and P.R. Chakraburtty, Mikrochim. Acta, III (1983) 307.
[2] S. Bhattacharya, S.K. Roy and A.K. Chakraburtty, Anal. Chim. Acta, 257 (1992) 123.
[3] R.S. Chauhan and L.R. Kakkar, Bull. Chem. Soc. Jpn., 65 (1992) 1033.
[4] G. Chakrapuni, D.S.R. Murty, B.K. Balaji and R. Rangaswamy, Talanta, 40 (1993) 541.
[5] H.M. Al-Swaidan, Anal. Lett., 26, (1993), 141.
[6] G. Bagur, D. Gazques, M. Sanchez and A.M. Martin, Anal. Lett., 26, (1993), 125.
[7] T. Yamane, T. Suzuki and T. Mukoyama, Anal. Chim. Acta, 70 (1974) 77.
[8] R. Forteza and V. Cerda, Anal. Chem., 58 (1986) 453.
[9] A.S. Cabeza, J. Medina and F. Bosh, Analyst, 109 (1984) 1559.
[10] M.H. Cordoba, P. Viñas and C.S. Pedreno, Analyst, 110 (1985) 1343.
[11] S. Nakano, E. Kasahara, M. Tanaka and T. Kawoshima, Chem. Lett., (1981) 507.
[12] C.W. Fuller, and J.M. Ottaway, Analyst, 95 (1970) 41.
[13] M.J. Fishman and M.W. Skougstad, Anal. Chem., 36 (1964) 1643.
[14] U. Weigho, Anal. Chem., 55 (1983) 2043.
[15] M. Otto, J. Stach and R. Kirmse, Anal. Chim. Acta, 147 (1983) 277.
[16] H.A. Mottola, CRC Crit. Rev. Anal. Chem., 4 (1975) 229.
[17] P.R. Bontchev, Mikrochim. Acta, (1962) 577.
[18] T. Fukasawa, S. Kawakubo and T. Yamanouchi, Anal. Chim. Acta, 171 (1985) 325.
[19] L. Davbha and J.Arunachalam, Talanta, 40 (1993) 135.
[20] Z. Marczenko, in R.A. Chalmers and M. Masson (Eds.), Separation and Spectrophotometric Determination of Elements, Ellis Horwood, Chichester, 2nd edn., 1986, pp. 623–625.
[21] ASTM Method for Petroleum, American Society for Testing and Materials, Philadelphia, PA, 1975, Method D, pp. 1548–1563.

ELSEVIER

Analytica Chimica Acta 298 (1994) 33–52

ANALYTICA CHIMICA ACTA

Combinatorial problems in the treatment of fuzzy ^{13}C NMR spectral information in the process of computer-aided structure elucidation: Estimation of the carbon atom hybridization and α-environment states [1]

Ivan P. Bangov [a,*], Isabelle Laude [b], Daniel Cabrol-Bass [b]

[a] *Bulgarian Academy of Sciences, Institute of Organic Chemistry, Building 9, Sofia 1113, Bulgaria*
[b] *LARTIC, Université de Nice, Sophia-Antipolis, 06108 Nice Cedex 2, France*

Received 27 January 1994

Abstract

The information derived from various ^{13}C nuclear magnetic resonance spectra has in most cases more fuzzy than crisp character. An approach to treat this information by means of the membership function is discussed. The combinatorial problems emerging from such a treatment are critically considered and a structure generation scheme consisting of multiple depth-first procedures is suggested. It permits to constrain the structure generation process through a non-redundant and flexible employment of the spectral information available.

Keywords: Nuclear magnetic resonance; Combinatorial problems; Computer-aided; Fuzzy theory; Structure elucidation

1. Introduction

The most difficult problem with the development of a computer-aided structure elucidation system originates from the fact that the structural information derived from the different spectra is ambiguous (incomplete, overlapping, alternative). To characterise this type of information, Zadeh [3] has introduced the controversial name *fuzzy*. Further, the ideas of *fuzzy sets* and *fuzzy logic* has been developed by the same author [4]. These notions have been juxtaposed to the ideas of *classical sets* and *classical logic*, both named therein as *crisp*. It has been stressed [5,6] that the spectral information is also fuzzy by its nature. Thus, the structural features provided by the infrared (IR), ^{1}H nuclear magnetic resonance (NMR), and 1D ^{13}C NMR spectra are definitely determined only for small pieces (fragments) of the structure of the query compounds. The constitution of the greatest part remains uncertain and vague and the spectral information can be

* Corresponding author.

[1] This paper is Part 8 of the series Computer-aided structure Generation from a Gross Formula (for Part 7 see [1]) and a continuation of ref. [2].

SSDI 0003-2670(94)00236-F

used solely as a support of a given hypothesis. Although the informational content of the different 2D NMR spectra such as H,H-correlation spectroscopy (H,H-COSY), C,H-COSY [heteronuclear correlation spectroscopy (HETCOR)] and correlation long-range coupling (COLOC) is greater, there is still a great deal of uncertainty in their structural assignment. Even the most powerful but extremely instrumental time and substance intensive technique INADEQUATE often provides ambiguous assignments. Thus, in ref. [7] the information from a series of 2D NMR techniques has been treated as fuzzy. The application of the neural networks approach [8,9] produces also results which may be considered fuzzy. Evidently, the structure elucidation system under development must take into account this character of the employed information.

In a recent paper [2] we have initiated the development of novel approaches to the treatment of fuzzy information by the employment of fuzzy logic and fuzzy graphs. The later notions have been widely discussed by mathematicians [10] but their application to the description of fuzzy chemical structures has not been reported before. The present paper is a continuation of the ideas devised in our previous paper. However, here we focus on combinatorial problems which may be alleviated but not completely solved with the treatment of the fuzzy information. This originates from the fact that we cannot create information where it is absent. The lack of information leads to the creation of numerous different hypotheses which increase enormously the informational entropy. In this particular case of structure elucidation these hypotheses are the different candidate structures. They may be generated by structure generation programs (generators). In many real-world cases such as molecules with more than 10 atoms this makes the problem unmanageable. So long as the generation algorithms are exponential (NP complete) each new piece of crisp information sharply alleviates the combinatorial problem within the generation process. In contrast, fuzzy information is not so effective, but correctly exploited it can also constrain this process. Furthermore, being developed as complementary to a heuristic strategy it can be employed toward perceiving the correct solution. Hereafter we consider the employment of the fuzzy information to the reduction of the redundancy within the structure generation process.

2. Structure generation

Our method for structure generation has been discussed in a series of papers [1,11–15], but for clearer understanding of this new development we shall outline here again its basic ideas. Furthermore, these considerations will be given in the limelight of the fuzzy nature of the information employed.

The starting information for the molecular graph (structure) generation is the empirical (gross) formula. It gives the kinds of atoms and their quantity. We consider the information from the gross formula not ambiguous (crisp). It is assumed that intersecting data from element analysis, mass spectroscopy and ^{13}C NMR can produce such information.

A graph is defined as a mathematical object consisting of two sets: the set V of vertices v_i and the set E of edges $e_{ij} = (v_i, v_j)$:

$$G = (V, E) \tag{1}$$

Each atom from the gross formula except the hydrogen atoms can be considered vertex of the molecular graph. Hence, there is a one-to-one correspondence between the hydrogen depleted molecular formula A and the set of vertices V. The set of edges E can be juxtaposed to the set of bonds B in the molecular structure. Consequently, the molecular graph (chemical structure) can be written as:

$$G^{m} = (A, B) \tag{1'}$$

The generation procedure consists of producing all possible connectivities between the atoms, i.e. all possible sets $E(B)$ without repetitions. This can be represented by the following formal definition:

$$G(S) = \Gamma(V, E, C) \tag{2}$$

where $G(S)$ is the set of generated graphs (structures) and Γ is a generation operator. Γ is not a

simple function but usually an algorithmic procedure. C is a set of constraints under which the generation is carried out. They might be mathematical constraints (generation of topologically distinct structures), chemical constraints (generation of chemically consistent structures) and/or spectroscopic constraints (generation of structures consistent with the spectral information available). Further, our practical implementation of the generation procedure from Eq. 2 will be outlined.

Our method is based on a hierarchical generation scheme: all atoms from the set $A(V)$ except the first are initially partitioned into the following sets [1,13–15]: h, set of heteroatoms; m, set of multiple bond atoms; c, set of carbon atoms having valence greater than 1, and 1, set of the atoms having valences 1. All these atoms may be either single or emanating from different chemical groups or fragments. They are firstly ranked according to their membership in these sets (the order follows the order they are listed above) and within each set according to a factor R [16]:

$$R = R_0 - N_H + q \quad (3)$$

where q is the charge density of the given atom which for free atoms is equal to zero, and for atoms in fragments and chemical groups is different from zero, N_H is the number of hydrogen atoms attached to the given atom, and R_0 is a constant characterising the atom type and hybridization state of the atom. The R_0 values are given in Table 1. The larger R an atom has, the lower level it occupies (the lowest is considered the level where the formation of the structure starts). The partitioning of the atoms according to the R index produces practically an automorphism (equivalent classes) partitioning of the vertices of the molecular graph.

In contrast to the other mathematical representations of chemical structure, all the atoms in our representation are given with their free valences (bonding sites, BSs). Each atom forms one and only one bond with each of the other atoms. In order to reflect this, we denote one BS by an arrow, the other $n-1$ by crosses. Here n is the atom (group) valence, or the degree of the vertex. This is presented in Fig. 1 where the first CH group has all its BSs of the cross type and the other atoms (groups) have one BS of the arrow type, and the other $n-1$ of the cross type. Two cycles of the structure presented in Fig. 1 close at atoms 5 and 8, hence they have 2 BSs of arrow type. The formation of ring systems is discussed bellow. In previous papers we called the arrow BSs, saturating valences (SVs) and the cross BSs, saturation sites (SSs). Consequently, a bond (edge, or arc in our case of directed graphs) is formed between an SV and an SS. Each atom may form SV–SS bonds with the other atoms only, i.e. no

Table 1
Atom codes, valences and initial values R_0 for different types and hybridization states

Atom type and hybridization state	Code	Valence	R_0
C			
sp^3	C	4	4
sp	≡C	2	7
sp^2 (olefinic)	=C	3	11
sp^2 (aromatic)	Ph	3	13
N			
sp^3	N	3	15
sp	≡N	1	18
sp^2 (non-aromatic)	=N	2	20
sp^2 (aromatic)	N:	2	20
O			
sp^3	O	2	23
sp^2 (non-aromatic)	=O	1	25
sp^2 (aromatic)	O:	1	25
F	F	1	32
Cl	Cl	1	33
Br	Br	1	34
I	I	1	35
S			
sp^3	S	2	28
sp^2 (non-aromatic)	=S	1	29
sp^2 (aromatic)	S:	1	29

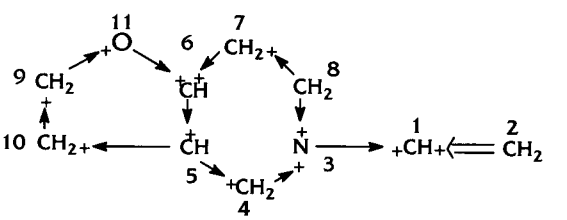

Fig. 1. Directed graph representation of the chemical structure with + and ← type bonding sites forming chemical bonds.

atom can be bonded to itself. The partitioning of the BSs into two sets SVs and SSs leads to generation of directed graphs. In the case of acyclic structure generation they are called directed trees. In a directed tree, each atom, except the first, has one predecessor (an SS of which is to be saturated by the atom SV) and $n-1$ successors (saturating its SSs in our case). The first atom has n successors (all its n BSs are of SS type) and no predecessor (no SV selected for the first atom). So long as the first atom is different from the others, it can be considered the root of the tree [17–19]. Hence, our approach implies the generation of directed rooted trees.

As can be seen from Table 1, we consider the sp^3, sp^2 and sp hybridised atoms as different atom types having different valences. Thus, a double bond is formed between two sp^2, and triple bond between two sp atoms.

The formation of a cycle is carried out after generation of a tree structure, as shown in Fig. 2. The latter is considered the spanning tree of the cyclic structures. The cycle is produced by transforming one by one the unsaturated SSs, left over after the formation of the spanning tree, into an SV (from atom 5 in Fig. 2) and forming closure bonds with the remaining unsaturated SSs (SS from atom 10 is shown in Fig. 2). The number of closure bonds formed for each structure and hence the number of cycles is calculated from the expression:

$$N^{r} = D_{u} - N^{db} - 2N^{tb} \qquad (4)$$

where D_u is degree of unsaturation, N^{db} and N^{tb} are the number of double and triple bonds, respectively.

The hierarchical generation scheme is illustrated in Fig. 2a and its two-dimensional matrix representation in Fig. 2b. Its main advantage is that it allows the treatment of single atoms, fragments and chemical groups in a uniform manner. Thus, as in the case of single atoms, one out of all BSs of a given fragment is transformed into an SV, the other $(n_f - 1)$ being transformed into SSs, where n_f is the fragment (chemical group) valence, i.e., the number of all BSs. The first segment (fragment or chemical group) has all its n_f BSs of SS type and no BS of SV type. Here we shall give new definitions of the notions chemical group and fragment, which better fit our approach.

A chemical group is a substructure consisting of one or several heavy (non-hydrogen) atoms with or without its adjacent hydrogen atoms, where all of the BSs of the heavy atoms are equivalent.

Thus, according to this definition, a non-substituted phenyl ring is considered a chemical group. The same stands for carbonyl, carboxyl, nitrile groups, etc. In contrast, a fragment may be defined as follows.

A fragment is a substructure consisting of more than one heavy (non-hydrogen) atom with or without their adjacent hydrogen atoms, all or some of the BSs of the heavy atoms being non-equivalent.

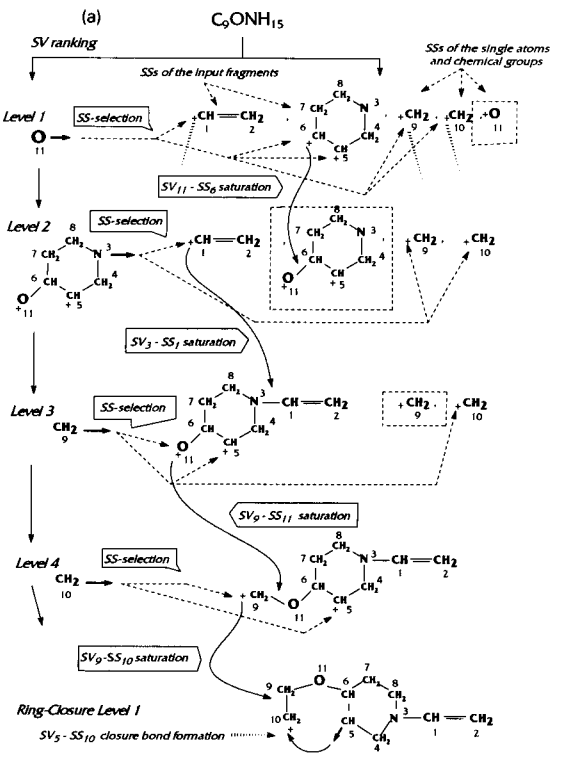

Fig. 2. Hierarchical multi-level structure generation by executing recursively the steps SS selection and SV–SS saturation. (a) Depicture and (b) two-row matrix representation of the generation process.

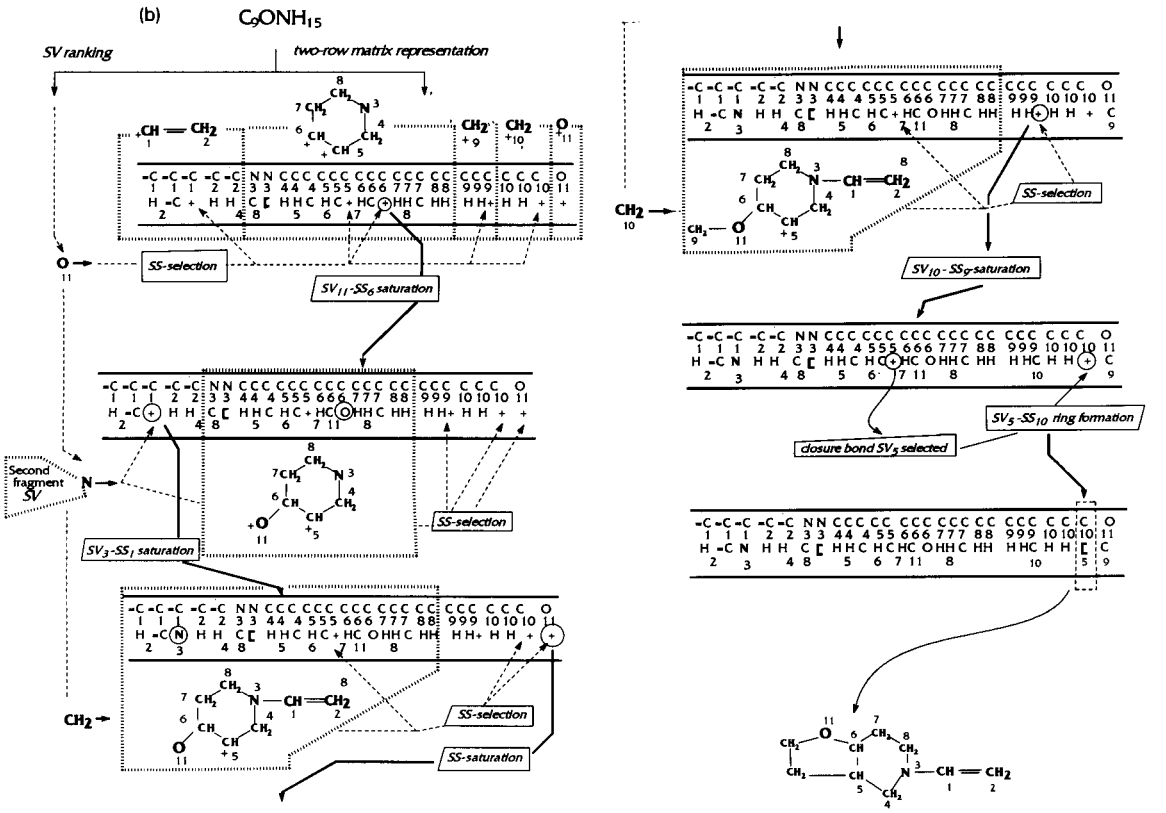

Fig. 2 (continued).

It should be noted that this definition is not formal. It reflects the different ways of treating these objects within the framework of our generation method. Thus, from each chemical group one and only one BS is selected to be transformed into an SV during the whole generation process. In contrast, for every fragment each non-equivalent BS and one and only one from each set of equivalent BSs are selected in turn and transformed into SVs, while the other are transformed into SSs. All the higher level combinations and hence all the structures are generated with this fragment SV, then the program backtracks and a new BS (non-equivalent to the previous SV) is transformed into a new SV of the current fragment. Apparently, in the case of more than one fragment this process consists of nested fragment SV selections leading to a depth-first procedure with backtracking.

The generation process is illustrated by the example presented in Fig. 2a. It starts with a ranking of the selected SVs, according to the rules described above. As we have assumed that the information from the gross formula is crisp, the determination of the *h*-type atoms is not a problem. The information for the C–H adjacent connectivity may also be considered crisp; it can be taken from the C–H direct multiplicities derived from either off-resonance, DEPT, or 2D NMR techniques. Hence, the *1*-type carbon atoms emanating from univalent groups, such as CH_3, HC=O, etc., can be easily determined. More difficult is the problem with the determination of the different *m*-type atoms. Their discrimination from the sp^3 *c*-type carbon atoms is essential because the treatment of double bonds in our method (as described below) is different from the treatment of triple bonds, which in turn is different from

the treatment of single bonds. However, due to the overlapping of the sp^3, sp^2 and sp signal regions the information coming from the chemical shifts is rather fuzzy. Hence, it could be treated in the terms of the possibility theory of Zadeh [3,4]. This treatment will be considered below. The first and the second elements participating in the combinatorial process depicted in Fig. 2a are two fragments. One can see that the whole second fragment is represented by one element SV_3 participating in the generation process. After a full generation of all structure with this SV, new fragment SVs from atoms 5 and 11 will be selected in turn and for each SV all the other higher level combinations will be formed. All SVs from Fig. 2a are ranked according to their R factors as follows: O(11), N(3), CH_2(9), CH_2(10).

Mathematically, the generated structure is represented by the two-row matrix representation given in Fig. 2b. The first-row elements are the BSs given with their numbers (the corresponding atom identifiers are given for clearness). The second-row elements are either "+" elements, which are the free valences, or the numbers of the SV atoms which have already saturated the corresponding SS atoms, or the hydrogen atoms which do not participate in the combinatorial process but are either initially predefined (e.g., by the C–H direct multiplicities of the assigned ^{13}C NMR signals) or simply fill the remaining unsaturated BSs at the highest level where a full complete structure is generated.

The generation approach further consists of the following steps carried out recurrently:

SS selection step. At each level starting from level zero (before the first), an SS selection procedure for the higher level SV–SS saturations is carried out. The program traces all the atom SSs skipping the atom from which the higher level SV emerges and selects a set of SSs for the higher level SV–SS new bond formation leading to the generation of new extensions (substructures). The SS selection procedure is presented in Fig. 2 as dashed lines. Thus, SSs from atoms 1, 5, 6, 9 and 10 have been selected for the first level O(11). SV. The number of extensions which might be generated at a given level are N^l, where N^l is the number of atoms or groups having a valence greater than 1, i.e. atoms or groups providing SSs. Hence, the total number of all extensions (here all kinds of redundant and chemically inconsistent substructures and structures are included) is $\Pi_{l=1}^{h} N^l$ where h is the number of levels.

Evidently, if the numbers N^l selected at this step are decreased the combinatorial process will be highly alleviated. Actually the selection procedure allows most of the constraints to be imposed here. Thus, in order to avoid the generation of topologically equivalent structures (isomorphic graphs), one and only one SS from the atoms of a given equivalent class is selected. However, as will be discussed bellow, in the case of using NMR information within our approach of structure elucidation not the topological (chemical) but magnetical equivalence must be taken into account. If we had crisp information that the higher level SV atom is connected to a given SS atom then only this SS would be selected, and N^l would take the value 1. All this would alleviate sharply the combinatorial problem within the structure generation process. Unfortunately, as discussed above, the different spectroscopic methods do not usually provide such crisp information. By facing the fuzzy character of the spectral information another approach was developed. Following the possibility theory of Zadeh each possible SS may be assigned with the possibility real number in the range 0–1 or 0–100%. This can be carried out in the process of signal assignment. Thus, only the most possible (according to Zadeh theory) SV–SS extensions are taken for the next (higher) level saturation step and hence the structure generation process is highly alleviated.

SV–SS saturation step. The SSs selected at the lower level are saturated at this step. This step produces new bonds forming extensions of the structure under construction.

The process of structure generation is basically a depth-first search over the generation tree with backtracking which consists of nested steps of saturating the successive SS at each level, SS selection for the higher level and a subsequent SV–SS saturation at the higher level. If all the SSs at a given level are saturated then the pro-

gram backtracks to the lower level. This is the main skeleton of the generation procedure, but as we shall see below a heuristic search procedure has been additionally implemented. It carries out a breadth-first check at each level of the depth-first search by an a priori generation of the extensions corresponding to all selected SSs at a given level (hence it is executed just after the SS selection step). One or more of them are confirmed while the other are pruned. Thus, the higher level SV–SS saturation step produces much less extensions, which sharply alleviates the combinatorial problem.

Following this generation scheme we have two extreme cases with respect to the spectral information. The first one is that we can derive crisp spectral information about the SV–SS connectivity at a given level, i.e. only one SS will be selected and saturated at this level. The possibility for the creation of such SV–SS bond is equal to 1 and the possibility for the creation of the other SV–SS bonds equals 0. The other extreme is a complete lack of information. Then all SSs may be assigned with equal possibility values of $1/N^{SS}$, where N^{SS} is the number of SSs at this level. In contrast, the fact that the spectral information is fuzzy makes us to find a way for a priori assessment of the possibility of one or another SV–SS bond creation, i.e. of the assignment of different possibility values to the separate SSs. Further, on the basis of these values some of the SSs are weakly supported and hence are discarded, while only the most supported ones form the current extensions. This is carried out, in our approach, both at the stage of signal assignment (discussed in next section) and at the stage of breadth-first heuristic search during the generation process discussed in detail in refs. [2,20].

3. ^{13}C NMR signal assignment

As discussed in a previous paper [20] we do not favour the intuitive way of thinking with respect to signal assignment inherent to the everyday practice of the spectroscopists: generate a structure and then assign the signals to it. Our signal assignment approach starts at the gross formula input. All the carbon atoms are considered equivalent. Then an arbitrary assignment is carried out: each carbon atom from the molecular formula sequence of atoms is assigned with one ^{13}C NMR signal from the sequence of signals. Here we consider the information from the total number of ^{13}C NMR signals as being crisp. The number of signals from the broad-band proton decoupled (BB) spectrum is compared with the number of carbon atoms in the gross formula. The overlapping signals must be user-recognised and entered as different signals with the same chemical shift and multiplicities values. Thus, each carbon atom adopts two additional attributes: chemical shift and multiplicity. The latter either leaves the carbon atom as it is, in the case of multiplicity 1, or transforms it to CH (multiplicity 2), CH_2 (multiplicity 3) or CH_3 (multiplicity 4) chemical groups. The multiplicity information is considered here also as crisp as it can be exactly derived by employing different NMR techniques, such as off-resonance, DEPT, etc.

As discussed above the carbon atoms having different hybridization states are coded in a different way in our system (see Table 1). Hence, the chemical shifts emerging from the nuclei having an sp^3, sp^2 and sp electron environment must be recognised and the associated carbon atoms transformed into C, =C and ≡C atoms. However, just in this stage the information derived from the chemical shifts is more or less fuzzy. On the other hand, the ranges of the different hybridization states overlap, e.g. the chemical shift range sp^3 C–O (bonded to oxygen) carbon atoms may overlap with the chemical shift range of sp carbon ≡C–C (bonded to sp^3 carbon atom) atoms. On the other hand, the carbon atom nuclei of the same hybridization state may resonate at different regions of the spectrum, depending on the α-environment of the carbon atom, e.g. a vinyl C=C–C (bonded to sp^3 carbon atoms) and a carbonyl C=O carbon atom resonate at different ranges. To take into account all those features each signal is examined at the stage of its input and the system estimates its possibility to be in each of the hybridization/α-environment states listed in Table 2. These possibility values (factors)

Table 2
Input ^{13}C NMR signal hybridization/α-environment attributes

Attribute code	Hybridization state	Carbon atom α-environment connectivity
SP3	sp^3	bonded to any atom
SP3–C	sp^3	bonded to carbon atom only
SP3–O	sp^3	possible bonding to an sp^3 oxygen atom
SP3–N	sp^3	possible bonding to an sp^3 nitrogen atom
SP3–X	sp^3	possible bonding to another sp^3 heteroatom
SP2	sp^2	bonded to any atom
SP2–CC	olefinic sp^2	bonded to carbon atom only
SP2–CC–O	olefinic sp^2	possible bonding to an sp^3 oxygen atom
SP2–CC–N	olefinic sp^2	possible bonding to an sp^3 nitrogen atom
SP2–CC–X	olefinic sp^2	possible bonding to another sp^3 heteroatom
SP2–CO	olefinic sp^2	possible bonding to carbonyl oxygen atom
SP2–COO	sp^2	possible bonding to carboxyl oxygen atom
SP2–ary	aryl sp^2	bonded to carbon atom only
SP2–ary–O	aryl sp^2	possible bonding to an sp^3 oxygen atom
SP2–ary–N	aryl sp^2	possible bonding to an sp^3 nitrogen atom
SP2–ary–X	aryl sp^2	possible bonding to another sp^3 heteroatom
SP1	sp	bonded to any atom
SP–CC	sp	bonded to carbon atom only
SP–CN	sp	possible nitrile bond formation

may be either in the range 0–1 or in the range 0–100% (as it is in our concrete implementation). Further, the user is prompted to select one or more (up to 4) most probable alternative states (Table 2) according to their possibility factors. Thus, each signal can be assigned with one or more hybridization/α-environment attributes. The way of derivation of those possibility factors is discussed in the following section.

The next step is the arbitrary signal assignment of the carbon atoms in the way outlined above. After being assigned each carbon atom adopts two new types of attributes: hybridization attribute presented in Table 3 and α-environment attribute presented in Table 4. They provide new characterisations of the given carbon atom additional to the chemical shift and C–H multiplicity attributes. One can see from Table 3 that these attributes are different from those of the signals. First each signal hybridization/α-environment attribute is split into two carbon atom attributes: hybridization and α-environment. However, in contrast to the common chemical sense, the carbonyl, carboxyl and nitrile groups are considered to have hybridization states different than sp^2. This is so, because the treatment of the two types of attributes in our system is different. While the hybridization attribute of each atom makes the system to construct a specific two-row presentation before starting the generation process (our two-row representations of C=C, C≡C, carbonyl and nitrile groups are discussed below, see Fig.

Table 3
Hybridization attributes of the carbon atoms

Hybridization attribute code	Hybridization state	Atom/group/fragment code	Remark
SP2	sp^2	C=C	olefin-type carbons only
SP1	sp	C≡C	ethyn-type carbons
Ar	sp^2	Ar	aryl-type carbons
CO	sp^2	C=O	carbonyl carbon
COO	sp^2	O–C=O	carboxyl carbon
CN	sp	C≡N	nitrile carbon
SP3	sp^3	–C–	aliphatic carbon

Table 4
α-Environment attributes of the carbon atoms

Hybridization attribute code	α-Environment state	Atom/group/fragment code
C–C	bonded to carbon atoms only	=C–C, –C–C, Ar–C, ≡C–C
C–O	bonded to an sp^3 oxygen atom	=C–O, –C–O, Ar–O, ≡C–O
C–N	bonded to an sp^3 nitrogen atom	=C–N, –C–N, Ar–N, ≡C–N
C–X	bonded to any sp^3 heteroatom	
Any	bonded to any atom	

12), the α-environment attribute acts during the real process of structure generation within the SS selection procedure. According to this scheme each carbon atom can be assigned with one to four alternative hybridization attributes and each state with one to four α-environment attributes. These alternatives reflect the fuzziness of the spectral information. A depth-first procedure with backtracking is developed, which produces for each carbon atom the different alternative hybridization states. Thus, if, say, a signal of 160 ppm is entered, the program may treat the carbon atom first as a carbonyl atom building the corresponding representation, and the second time as an ethene =C–O sp^2 carbon atom bonded to oxygen, forming a new representation. In the first case the carbonyl carbon atom SV traces all the atoms by forming different subfragments containing the carbonyl group. In the second case the olefin carbon atom will form a olefin fragment with another =C atom (the formation of olefin fragments is described below). The C–O α-environment attribute, however, implies that one BSs of this atom must be bonded to an oxygen atom, i.e., if this atom is an SV donating atom of an olefin fragment, the SS selection procedure will select SSs from any of the non-equivalent oxygen atoms only. If it is only an SS donating =C atom, it will be selected by an oxygen atom SV. It should be mentioned here that if two or more SSs are selected from equivalent heteroatoms, generation of duplicated structures results. Hence, the SS selection procedure must select only one SS from any set of equivalent heteroatoms or from any set of magnetically equivalent carbon atoms (having the same chemical shifts). Thus, the number N^l of selected SSs at these levels is highly reduced and the combinatorial problem alleviated. In case of additional nitrogen atoms in the gross formula and the higher level SV carbon atom being assigned with an additional C–N α-environment attribute, then the SS selection procedure will select SSs from both oxygen and nitrogen non-equivalent atoms. In contrast, if a C–C α-environment attribute is assigned, then the SS selection procedure will select SSs emerging from carbon atoms only but not from heteroatoms. In the case of a heteroatom SV, the SS selection procedure selects SSs only from carbon atoms having the corresponding α-environment attribute. Thus, only SSs from carbon atoms having a C–O α-environment attribute will be selected for a SV emerging from an oxygen atom. Consequently, on the one hand the combinatorial problem may be complicated in the case of more hybridization attribute alternatives being selected, but it is alleviated in the process of SS selection with the selection of specific α-environment attributes. The shaper the hybridization and α-environment attribute information the less alternatives are required, which is conductive to less combinations and hence less candidate structures to be generated, and vice versa the fuzzier this informations, the more hybridization and α-environment attribute alternatives should be selected and the combinatorial problem becomes more severe. In any case, however, this approach is more flexible and rather less redundant than the brute-force generation of all possible structures with a further discrimination of the most unlikely ones from the spectral point of view.

4. Determination of the hybridization and α-environment attributes

Usual chemical shift tables [21–23] defined fixed ranges for different carbon types. These tables are very useful when used by skilled specialists, and indeed they have been specifically designed for the usage. Simpler tables have also been set up for students [24]. But the ranges defined in these tables have a limited practical usefulness for the construction of our program for two reasons: first, the ranges are overlapping in many regions of the chemical shift scale and second, the limits of each range are crisp. Thus it is impossible to assess automatically the degree of support of each carbon type from a ^{13}C chemical shift value by using these tables. To overcome this limitation, instead of using such crisp chemical shift ranges we make use of fuzzy sets S_k, which are defined by the associated membership functions (MF) $m_k(\delta)$. For each carbon atom numbered i and assigned to a ^{13}C signal of multi-

plicity M and chemical shift δ_i, giving a pair $\langle M, \delta_i \rangle$, the value of the membership function $m_k(\delta_i)$ is an estimate of the degree of support of the hypothesis that this atom is indeed a member of the fuzzy set S_k, i.e., possesses the corresponding type. By multiplicity considering the M of each signal as reliable, the MFs can be worked out separately for each M value. The MFs are built up by comparing the distribution curves (histograms) of chemical shifts observed for each case (hybridization state and α-environments) in a collection of spectra. In chemical shift regions where the distribution curves of mutually exclusive sets do not overlap, the MFs receive the value 1 for the observed set and zero for the other sets. Within overlapping regions, the relative degree of support of each set is estimated as the ratio of the number of observed cases in each set in the considered region. In regions plainly outside of the observed values for a given set, the corresponding MFs receive the value 0. To model the membership function of the transitions between the regions (inside a unique set, overlapping between several sets and outside this set) a sigmoid function:

$$m_k(\delta) = P_k + \frac{H_k}{1 + \exp[-a_k(\delta - b_k)]}$$

is used.

For each fussy set S_k and each transition region, the parameter are determined empirically to fit the overlapping of the observed distributions curves. P represents the MF's value before the transition region, H_k the height of the change in MF's value in the transition region, b the value of the chemical shift at 50% of the transition and a the "slope" of the transition. If necessary, the functions are normalised at each point so that $\Sigma_k m_k(\delta) \leqslant 1$, $\forall\delta$. Additionally, the value $1 - \Sigma_k m_k(\delta)$ is assigned as the support of the "undefined" case. Normally this value should be close to zero for all atoms because a value significantly different from zero means that a pair $\langle M, \delta_i \rangle$ characterising a signal falls outside the observed histograms. This might arise in the case of very

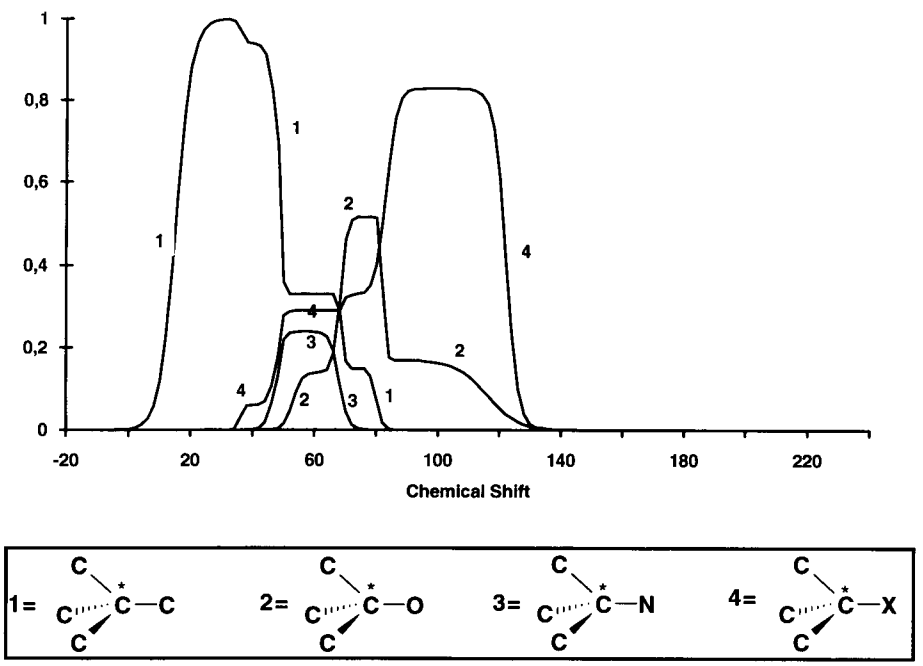

Fig. 3. Membership function curves for different α-environments with multiplicity 1 and sp^3 hybridization state (general case HCNOX).

unusual structures but more likely in the case of errors in the input of a chemical shift or in the multiplicity assignment.

Following this method in our previous paper [2] we have worked out a series of eight MF sets of parameters of the determination of the hybridization of each carbon corresponding to the following cases: $M = 1$, sp^3 (⟩C⟨); $M = 1$, sp^2 (⟩C=); M=1, sp (–C≡ or =C=); $M = 2$, sp^3 (⟩CH–); $M = 2$, sp^2 (=CH–); $M = 2$, sp (=CH), $M = 3$, sp^3 ($-CH_2-$); $M = 3$, sp^2 ($=CH_2$). The case of $M = 4$ is considered non-ambiguous (sp^3, CH_3-). The parameters used to draw the membership functions reported in this paper have been determined without making any distinctions based on the gross formula of the molecule and α-environment of the carbon atoms. However, it was observed that the overlapping between the different distribution curves is noticeably reduced if one considers separately the case of hydrocarbons (noted HC) and of compounds containing only oxygen as heteroatom (noted HCO) from the general case (noted HCNOX). Now, the gross formula is the starting point of our structure generator, therefore in the present work, we have built two additional series of eight MF sets of hybridization determination corresponding to the above mentioned chemical compositions.

Once a hybridization state is assumed for a particular carbon atom it is possible to estimate the relative degree of support of the different α-environments using the same method. The parameters of the corresponding MFs are calculated separately for each multiplicity (1–4), hybridization state (sp^3, sp^2, sp) and chemical composition (HCNOX, HCO) leading to a series of 16 MF value sets. Figs. 3–10 show the series for the general case HCNOX. The curves obtained for the compounds containing only oxygen as heteroatom are of course much simpler and ex-

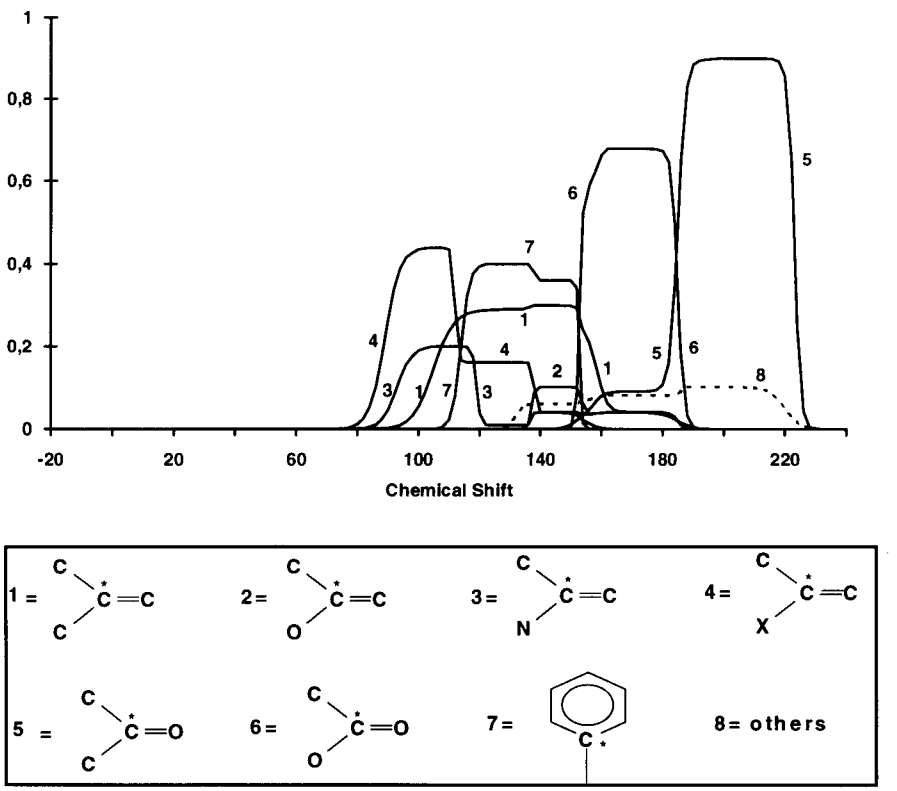

Fig. 4. Membership function curves for different α-environments with multiplicity 1 and sp^2 hybridization state (general case HCNOX).

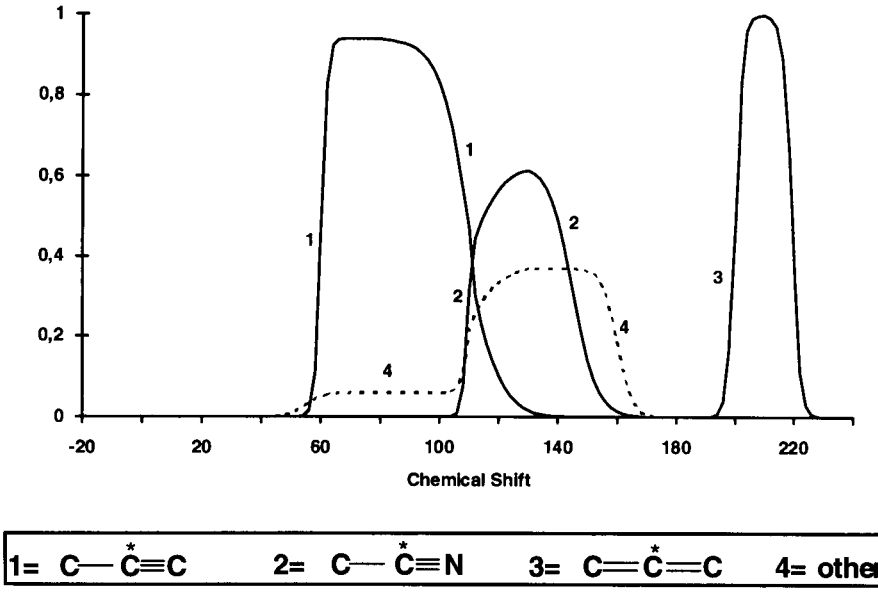

Fig. 5. Membership function curves for different α-environments with multiplicity 1 and *sp* hybridization state (general case HCNOX).

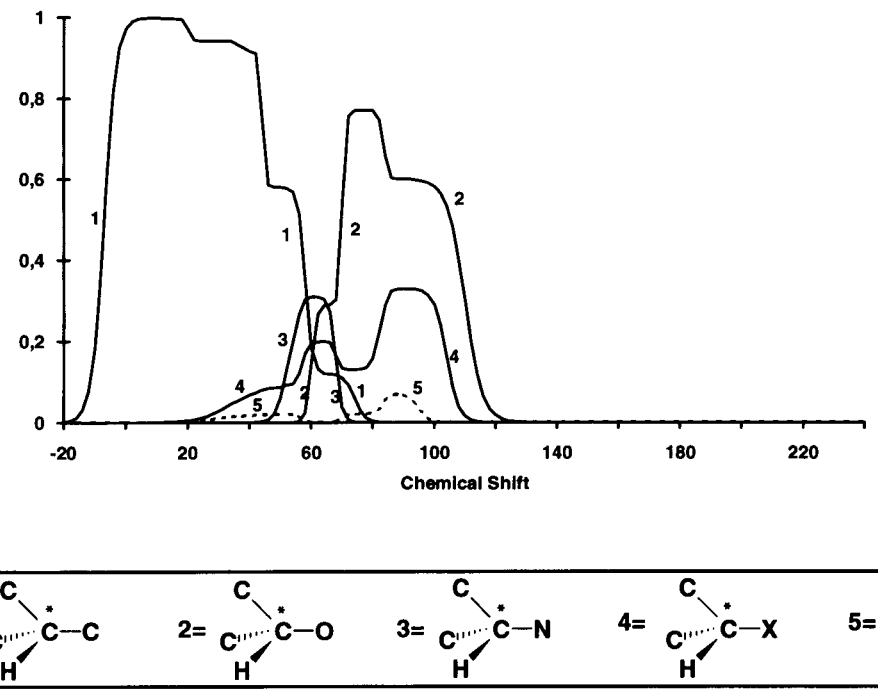

Fig. 6. Membership function curves for different α-environments with multiplicity 2 and sp^3 hybridization state (general case HCNOX).

hibit better separations. The parameters which define these curves are based on the distribution of each hybridization and α-environment state within a collection of compiled spectra employed for their determination. Therefore they are dependent on the size and the composition of this collection. An in-house collection of 8899 carbon atoms assigned to NMR signals from 1300 different compounds has been used to this end. The work is currently being extended to a much larger collection of spectra recently made available to us. On the other hand, Dubois and Carabédian [25] have shown that a sample of 2000 spectra exhibits chemical shift distribution which is very similar to that of a population eight times larger. Consequently, although the curves presented in Figs. 3–10 could be refined by the analysis we are currently pursuing, they should be considered as rather good approximations which provide useful tools to fight against the combinatorial explosion during the initial stages of the structure generation process.

The parameters for calculating MFs for the different hybridization states a α-environments have been incorporated in the ASEC13 (automated structure elucidation based on ^{13}C NMR information) system. For each NMR signal its chemical shift and multiplicity are used in order to calculate the values of the different MFs. The final decision to select one or several possible hybridization and α-environment states for each carbon atom is left to the user. In order to alleviate the burden of making successive multiple selections, the values of all the MFs corresponding to all allowed pairs (hybridization states, α-environments) are displayed in one single ma-

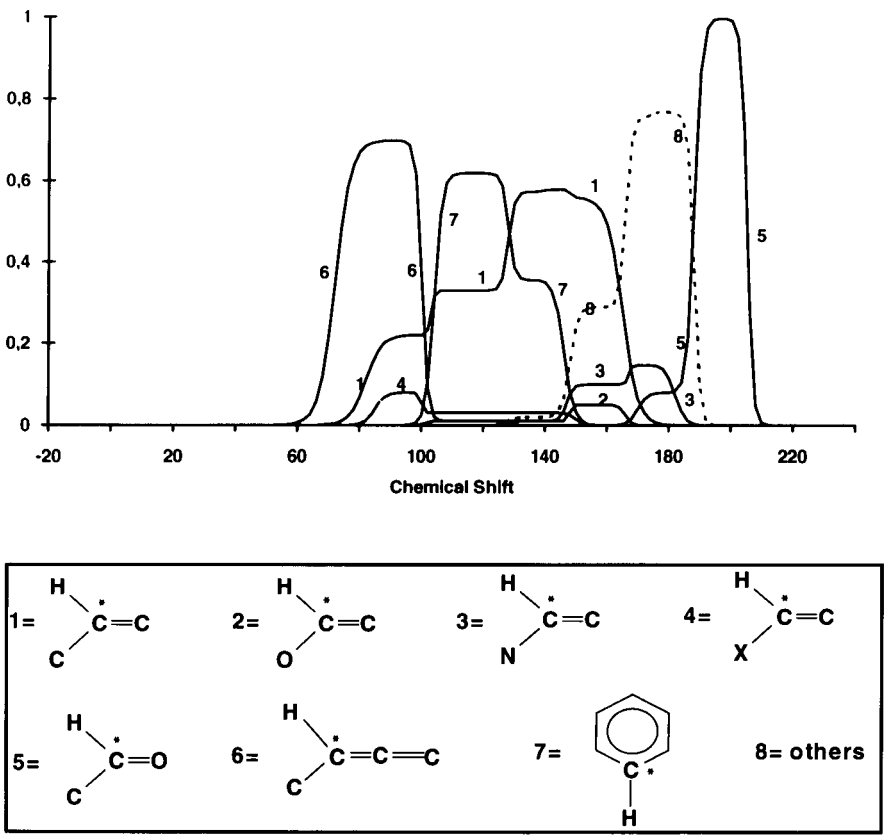

Fig. 7. Membership function curves for different α-environments with multiplicity 2 and sp^2 hybridization state (general case HCNOX).

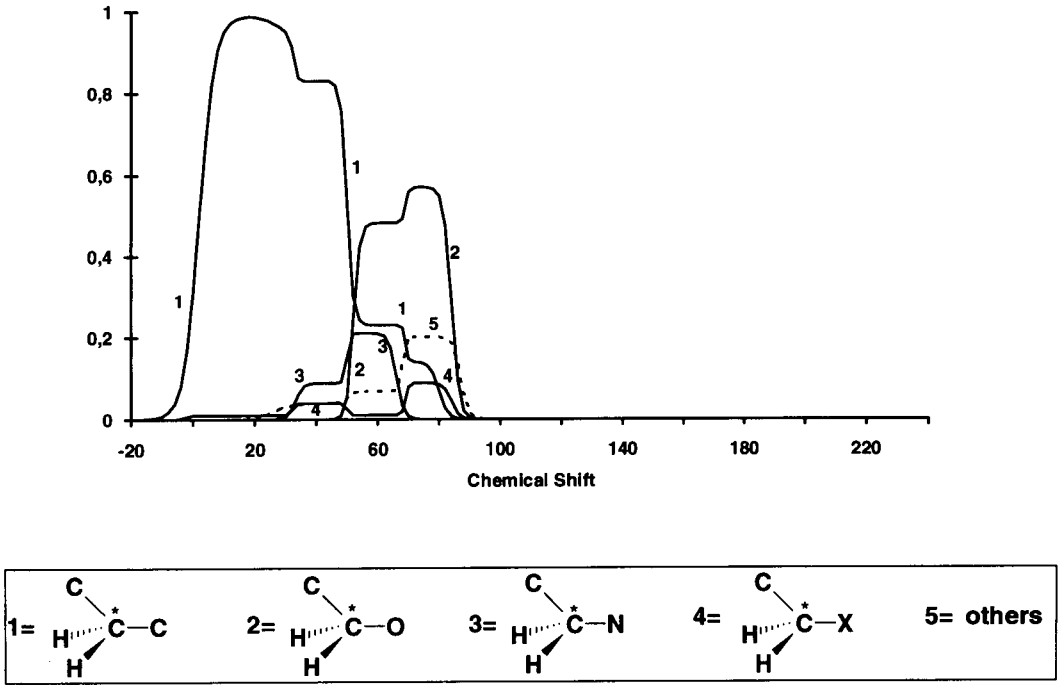

Fig. 8. Membership function curves for different α-environments with multiplicity 3 and sp^3 hybridization state (general case HCNOX).

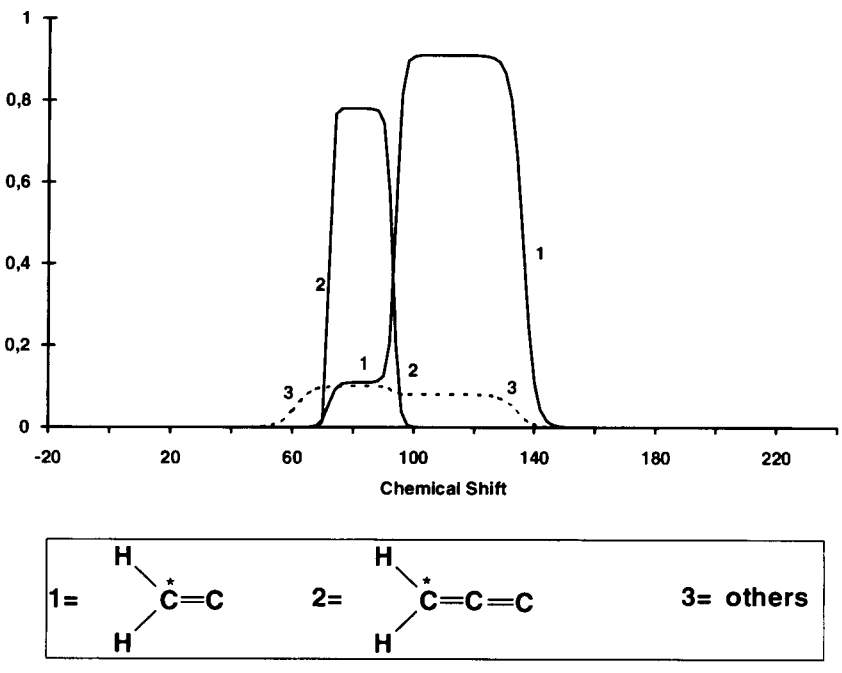

Fig. 9. Membership function curves for different α-environments with multiplicity 3 and sp^2 hybridization state (general case HCNOX).

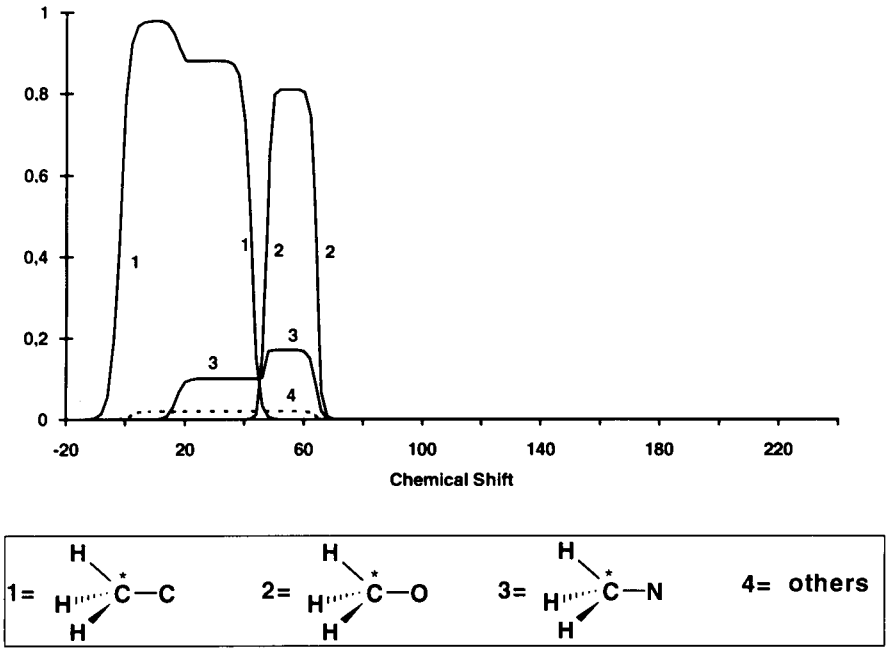

Fig. 10. Membership function curves for different α-environments with multiplicity 4 and sp^3 hybridization state (general case HCNOX).

trix. The value corresponding to a particular pair is calculated by the product of the two separate MFs. The selection screen window from the program work is shown in Fig. 11. The information about the hybridization partitioning of the current signal is given at the upper part of the window. The separate hybridization α-environment states are given in the window and they are disposed to selection. The question mark (?) (non-determined state) implies that this selection corresponds to states different from those given in the window, but complying to the given hybridization (this is the difference between the full hybridization and the sum of hybridization α-environment states corresponding to this hybridization). The user is prompted to select one or more hybridization α-environment states.

5. Mathematical representation and generation of multiple bonds

The multiple bond chemical groups and fragments possess several features which make them distinct from the other units participating in the combinatorial process. A double bond may be represented and generated as a two-membered cycle, and a triple bond as two fused two-membered cycles (see Fig. 12a). Thus during the generation process they may be generated together with the larger-size cyclic structures. This approach is more appropriate in the cases of structure enumeration but for our case of treatment of the ^{13}C NMR information available, we favour the representations given in Fig. 12b where, as discussed above, the sp^2 and sp hybridised atoms are considered for different atom types =C and ≡C. Hence, following our definitions given above while the ethene- and enthyne-type multiple bonds are considered fragments the carbonyl, carboxyl and nitrilemultiple bonds are considered chemical groups. From Fig. 12b it is seen that whereas the latter have equivalent SSs emanating from the only carbon from the only carbon atom, the former may have non-equivalent SSs, both chemically non-equivalent due to different C–H multiplicity attributes (which automatically transform the carbon atoms into =C atoms, =CH, or

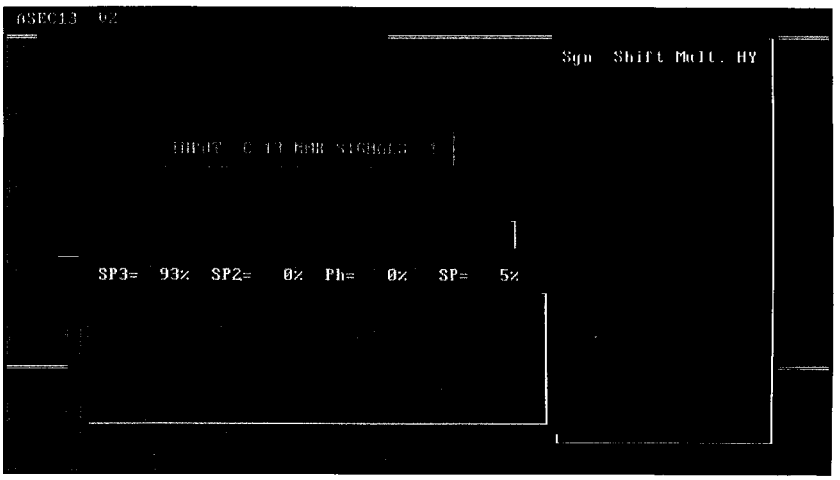

Fig. 11. Screen-window for selection of the hybridization/α-environment signal attributes.

$=CH_2$ groups) and magnetically non-equivalent due to different chemical shift attributes. Thus, if no ^{13}C NMR information was available all multiple bond =C and ≡C atoms are equivalent and we may construct the multiple bond fragments and chemical groups by taking arbitrary one by one those atoms and mutually bonding them. The available ^{13}C NMR information makes them distinguishable, i.e., it predefines that a multiple bond atom of a given chemical shift and multiplicity attribute must be linked to another multiple bond atom which is either an heteroatom (in the case of carbonyl, carboxyl, etc. chemical groups) or another carbon atom with explicitly specified (by the spectrum) chemical shift and multiplicity attribute. The spectrum information for this linkage is in most case fuzzy. Even the most powerful INADEQUATE technique can provide vague or ambiguous information due to the absence or overlapping signal patterns. This requires considering all the possible linkages without repetition. Accordingly, the carbonyl (CO hybridization attribute of the carbon atom), carboxyl (COO hybridization attribute of the carbon atom) and nitrile groups (CN hybridization attribute of the carbon atom) are automatically formed in the way shown in Fig. 12b. Further, the chemical groups are treated by the generator in the same way as the single carbon atoms are treated. In the case when we have only one ethene and/or ethyne fragment they are formed as the two =C (≡C) atoms (or =CH, $=CH_2$, ≡CH groups in the cases of multiplicity different from 1) form a bond and they are treated during the generation process as fragments. However, the presence of more than one multiple-bond fragment of a given type requires the generation of the different linkages between the multiple bond atoms leading to the generation of ethene (ethyne) bonds.

Generally speaking, the generation may be carried out in three ways:

The first is the brute-force generation method where the multiple bonds are generated together with the other bonds within a common combinatorial procedure. This approach produces numerous chemically inconsistent structures such as –C–(=C)–C–, where an sp^2 is attached to two sp^3 carbon atoms.

The second is to assign the signals to the different =C or ≡C atoms, consequently the latter being transformed into =C, =CH, $=CH_2$ or ≡C, ≡CH groups and then to generate all the possible combinations of these atoms and groups resulting in multiple bonds.

The third consists of an initial assignment of the *hybridization attribute* only which indicates that the given atom is either of =C or ≡C original, but the chemical shift and C–H direct multiplicity attributes are not assigned. Consequently, the

=C(≡C) atoms are equivalent and they arbitrarily from C=C(C≡C) fragments. Next step is an exhaustive and non-redundant (without repetitions) generation of all assignments of the chemical shift/C–H multiplicity attributes to the multiple bond atoms.

The latter approach has been favored by us and is developed as a depth-first procedure with backtracking. The generation of different assignments for the case of three double bonds is shown in Fig. 13. The assignment approach is an N^m level hierarchical procedure, where N^m is

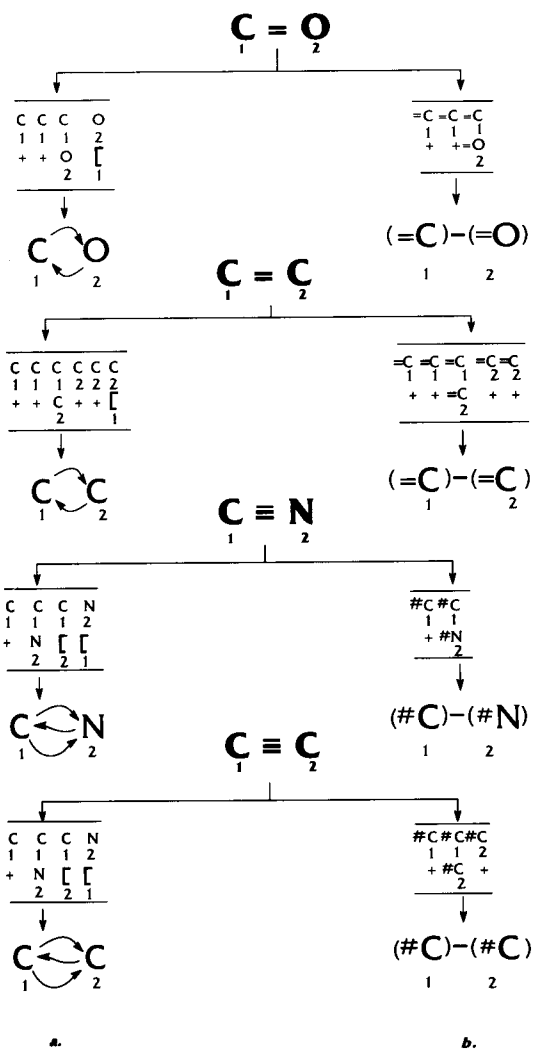

Fig. 12. Two types of representation of multiple-bond fragments and chemical groups.

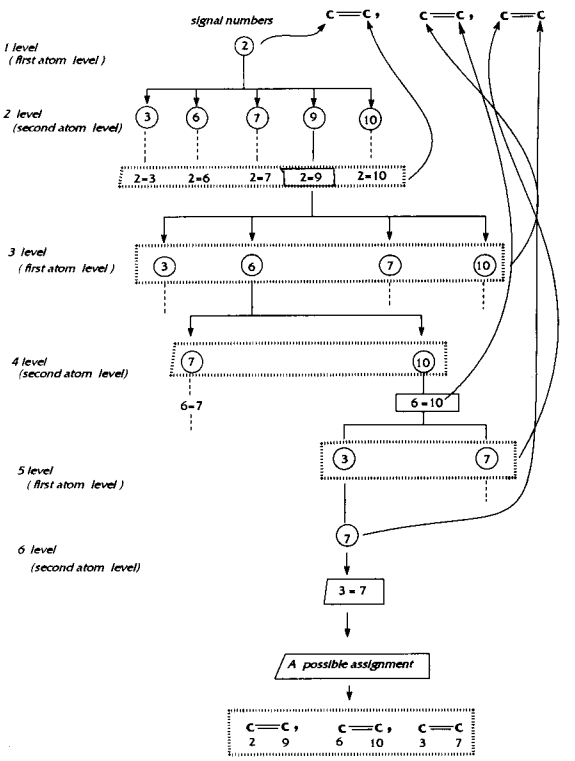

Fig. 13. Formation of multiple-bond fragments.

the number of multiple bond atoms (6 in our case). These levels are partitioned into two groups: first-atom levels and second-atom levels. The first-atom levels are the odd levels (1st, 3rd, 5th in the case of Fig. 13) where the first atoms of each multiple bond fragment is assigned and the second-atom levels are the even number levels (2nd, 4th, 6th in Fig. 13) where the second atoms of each multiple bond are assigned. The assignment procedure is exemplified in Fig. 13 with 6 signals having the sp^2–CC attribute and are provisionally numbered as 2, 3, 6, 7, 9 and 10 (these are the input numbers of those signals).

The assignment procedure consists of the following steps: (i) assignment of the lowest first-atom level; (ii) signal selection for the next second-atom level; (iii) signal assignment at the next second-atom level; (iv) signal selection for the higher first-atom levels; (v) signal assignment at the higher first-atom levels; (vi) signal selection for the higher second-atom levels; (vii) signal

assignment at the higher second-atom levels; The steps (iv)–(vii) are recursively repeated to cover all first and second atoms in all multiple-bond fragments.

Assignment at the lowest first-atom level. The first level implies a sole and arbitrary assignment. Hence, the program automatically assigns the firs signal (2 in the case of Fig. 13) to the first atom of the first multiple bond fragment.

Signal selection for the higher first-atom level. The signals which are to be assigned to the first atoms of the next multiple-bond fragments are selected only under the following constraints: (j) signals which have not been assigned at the lower levels; (jj) signals having multiplicity less than 3. The restriction that signals having multiplicity 3 (forming $=CH_2$ groups) can not be assigned to the first-atom levels is imposed because the first atom of each double-fragment should posses at least one free BS to be transformed into SV.

Signal assignment of the higher first-atom levels. The selected signals at the previous step are assigned to the first atom of the fragment corresponding to the given level. Thus, each first atom of the current fragment obtains new chemical shift and multiplicity attributes.

Signal selection at the second-atom levels. All signals having numbers higher than the signal assigned at the previous first-atom level and not having been assigned are selected at this level.

Signal assignment at the second-atom levels. The selected signals at the previous step are assigned to the second atom of the fragment corresponding to the given level. Thus, each second atom of the current fragment obtains new chemical shift

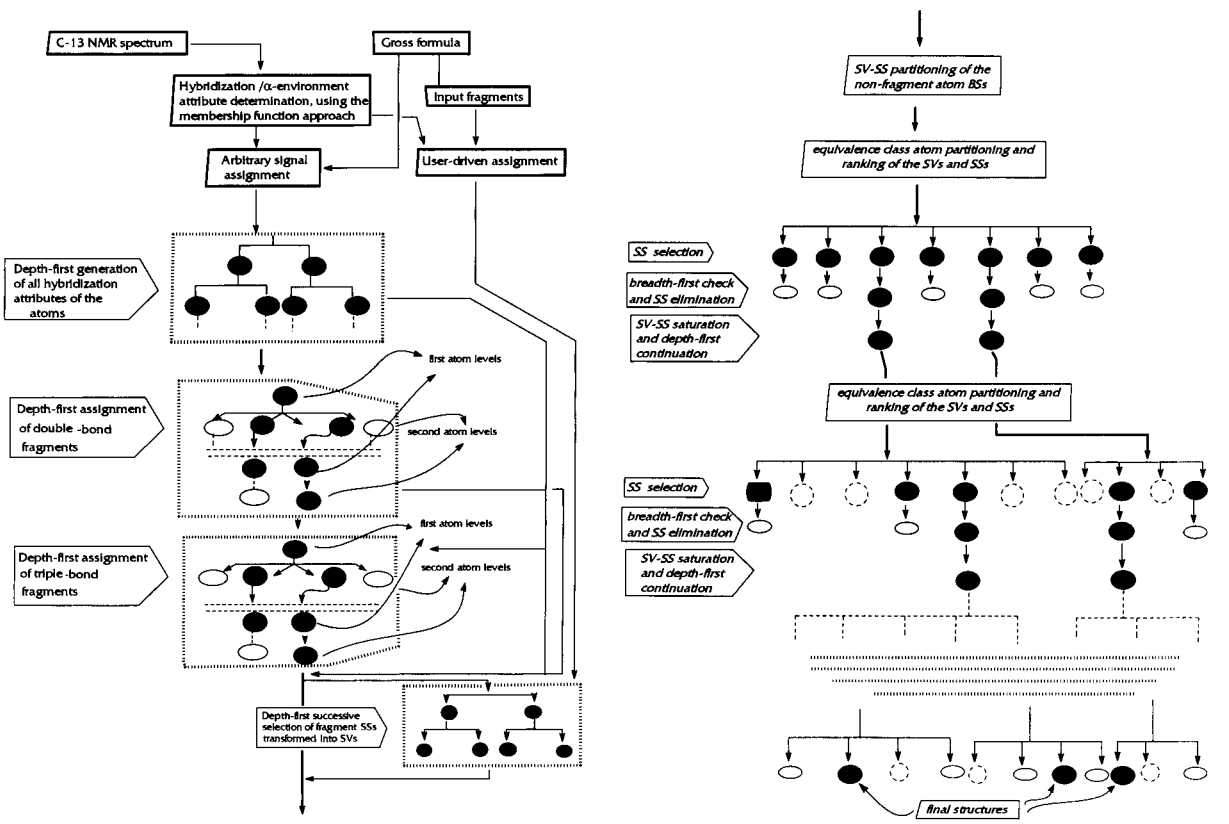

Fig. 14. Depicture of the program's multi-level depth-first with backtracking generation scheme.

and multiplicity attributes. A complete multiple bond fragment is assigned at this level.

The assignment procedure starts from the lowest first-atom level where the first =C atom (having the lowest number) of the first multiple (double in our case) bond fragment is assigned with the first signal. Evidently, this assignment is arbitrary. The only constraints which is imposed is that signals having multiplicity 3 (forming $=CH_2$ groups) cannot be assigned to the first-atom levels. The next, second level is of second-atom type. All the signals with numbers greater than the assigned signal (2 in our case) are subsequently assigned and hence different combinations of double bond fragments are produced. For each such double bond assignment several unassigned signals (9 and 10 in the case of Fig. 13) are selected for the higher first-atom level, and the procedure of selection of higher second-atom level unassigned signals (only signal 9 in our case) is repeated. After all the signals at a given level are exhausted the program backtracks to the lower level.

6. Further alleviation of the combinatorial problem

The general scheme of our approach os structure generation using fuzzy spectral information is given in Fig. 14. It may be separated into several depth-first with backtracking sections: depth-first generation of the specified carbon atom hybridization attributes; depth-first generation alternative double-bond atom assignments (in the case of more than one double bond); depth- first generation of the alternative triple-bond assignments (in the case of more than one triple bond); depth-first tracing of the different fragment BSs to be transformed into SVs (in the case of more than one fragment), and finally depth-first SS selection and SV–SS saturation taking into account the α-environment attribute. Evidently, this is a rather complex generation scheme of nested depth-first with backtracking procedures executed recursively. But even so, it is more constrained than the blind brute-force generating procedure, which produces at the different levels an excessive number of chemical and spectrally irrelevant substructures which must be recognised and pruned afterward.

The generation approach presented in Fig. 14 gives a flexible procedure for complete utilisation of the structural information derived from the spectral data available. If this information is crisper, i.e., less alternatives are given to the program, the generation process is alleviated, and vice versa in cases of fuzzier information, producing more alternatives, the combinatorial problem becomes more complex. In all cases, however, this scheme reflects better the structure information content of the spectral data.

In recent papers [2,20] we have suggested a new approach toward alleviation of complex combinatorial problems by using fuzzy 1D and 2D ^{13}C NMR spectral information. At each current level the problem carries to a breadth-first generation of all higher level SV–SS extensions. The generated substructures are compared with the available spectral information such as the cross peaks from the INADEQUATE spectrum or cross peak from the combined interpretations of HECTOR (C,H-COSY) and H,H-COSY 2D spectra, COLOC, etc. The HECTOR spectrum provides the direct C–H connectivity and the H,H-COSY gives the longer-range (usually through three bonds) couplings between the hydrogen nuclei. So long as the carbon atoms are assigned to the ^{13}C NMR signals in our approach the ^{1}H signal assignment can be automatically obtained from the HETCOR cross peak assignments. Consequently, the following logic has been developed: if two carbon atoms are assigned to two H atoms and the latter are coupled (most likely through three bonds) in the H,H-COSY pattern then the two carbon atoms most likely are adjacent. However, in many cases the H,H-coupling is through more than three bonds. Hence, fuzzy logic instead of the crisp logic was applied by devising several factors having value in the range 0–1 or in the range 0–100% (for more details see [2,20]). The user is prompted to discard the less supported extension at the given level. One or several most supported extension (given in black in Fig. 14) are left for the next level structure construction. In this way whole complete branches of

the generation tree are pruned and the combinatorial problem extremely alleviated. In the most favourable case of having crisp information only one extension at each level is left and the generation process is transformed into construction of one structure. In the case of fuzzy information when more than one alternative extensions are left more structures are generated. Additional possibility factors based on the experiment/calculated (through the empirical additivity rules) ^{13}C chemical shift relationship have been developed giving a complementary estimation of the possibility that a given extension is the correct one.

This approach is applied both to the process of depth-first assignment of multiple bonds (after each second-atom level signal selection all alternative assignments of the second atom, leading to a full assignment of the double bond, are traced and the most probable are left for the next levels of new double-bond assignments) and to the process of generation of SV–SS structural extensions thus sharply reducing the combinatorial redundancy.

Accordingly, two ways of treatment of the fuzzy information are developed. The first one is at the step of hybridization and α-environment attribute assignment, where the most probable hybridization and α-environment attributes for each carbon atom are selected. This leads to an a priori discarding of large sets of extensions at each level SS selection procedure. The second way is at the breadth-first check step, where the generated extensions compete and only the most probable are left for the higher level structure construction.

Acknowledgements

This work and the possibility for one of us (IPB) to stay at the University of Nice have been supported by an EEC grant (program COST), which is gratefully acknowledged.

References

[1] IP. Bangov, J. Chem. Inf. Comput. Sci., 34 (1994) 318.
[2] T. Laidboeur, I. Laude, D. Cabrol-Bass and I.P. Bangov, J. Chem. Inf. Comput. Sci., 34 (1994) 171.
[3] L.A. Zadeh, Inf. Control., 8 (1965) 338.
[4] L.A. Zadeh, J. Fuzzy Sets Sys., 1 (1978) 3.
[5] M. Otto, Chemom. Intell. Lab. Syst., 4 (1988) 101.
[6] M. Otto, J. Anal. Chem., 62 (1990) 797A.
[7] J. Xu, S.K. Strause and B.C. Sanctuary, J. Chem. Inf. Comput. Sci., 33 (1993) 668.
[8] D. Ricard, C. Cachet, D. Cabrol-Bass and T.P. Forrest, J. Chem. Inf. Comput. Sci., 33 (1993) 202.
[9] N. Sbirrazzuoli, C. Cachet, D. Cabrol-Bass and T.P. Forrest, Neural Comput. Appl., (1993) in press.
[10] A. Rosenfeld, in Fuzzy graphs, in L.A. Zadeh, K.-S. Fu, K. Tanakal and M. Shimura (Eds.), Fuzzy Sets and their Applications to Cognitive and Decision Processes, Academic Press, New York, 1974, p. 77.
[11] I.P. Bangov, Commun, Math. Chem. (MATCH), 14 (1983) 235.
[12] I.P. Bangov and K.D. Kanev, J. Math. Chem., 2 (1988) 31.
[13] I.P. Bangov, J. Chem. Inform. Comput. Sci., 30 (1990) 277.
[14] I.P. Bangov, J. Chem. Inf. Comput. Sci., 32 (1992) 167.
[15] I.P. Bangov, Commun. Math. Chem. (MATCH), 27 (1992) 3.
[16] I.P. Bangov, Anal. Chim. Acta, 209 (1988) 29.
[17] N. Trinajstic, S. Nikolic, J.V. Knop, W.R Muller and K. Szimanski, in J.M. Rellor (Ed.), Computational Chemical Graph Theory, Ellis Horwood, London, 1991, Chap. 3, p. 79.
[18] V. Kvasnicka and J. Pospichal, Chemom. Intell. Lab. Syst., 18 (1993) 171.
[19] M.L. Contreras, R. Valdivial and R. Rozas, J. Chem. Inf. Comput. Sci., 32 (1992) 223.
[20] I.P. Bangov, S. Simova, D. Cabrol-Bass and I. Laude, J. Chem. Inf. Comput. Sci., 34 (1994) 546.
[21] W. Bremser, B. Franke and H. Wagner, Chemical Shift Ranges in ^{13}C NMR Spectroscopy, Verlag Chemie, Weinheim–Deerfield Beach–Basle 1982.
[22] E. Pretsch, T. Clerc, J. Seibl and W. Simon, Tables of Spectral Data for Structure Determination of Organic Compounds, Springer Verlag Berlin, 1989.
[23] F.W. Wherli, A.P. Marchand and S. Wehrli, Interpretation of Carbon 13 NMR Spectra, Wiley, Chichester–New York, 1988.
[24] D.W. Brown, J. Chem. Educ., 62 (1985) 209.
[25] J.E. Dubois and M. Carabédian, J. Chem. Inf. Comput. Sci., 31 (1991) 557.

ELSEVIER

Analytica Chimica Acta 298 (1994) 53–64

ANALYTICA CHIMICA ACTA

Analysis of air particulate benzo[*a*]pyrene by a specific enzyme immunoassay: correlation with chemical and atmospheric parameters

A. Roda [a,*], A. Pistillo [a], A. Jus [b], C. Armanino [c], M. Baraldini [d]

[a] *Dipartimento di Scienze Farmaceutiche, Università di Bologna, Bologna, Italy*

[b] *Istituto di Chimica degli Ormoni, CNR, Milan, Italy*

[c] *Istituto di Analisi e Tecnologie Farmaceutiche ed Alimentari, Università di Genova, Genova, Italy*

[d] *Istituto di Scienze Chimiche, Università di Bologna, Bologna, Italy*

Received 31 January 1994; revised manuscript received 17 May 1994

Abstract

A specific and sensitive enzyme immunoassay for benzo[*a*]pyrene (BaP) analysis in air particulate matter has been developed and validated. The low detection limit (1 ng/tube) and the rapidity of the assay permitted extensive study (daily for eighteen months) of BaP concentration in air particulate matter in the city of Bologna. For each assay air was aspirated for 24 h and passed through a cellulose filter which retained the particulate matter and, after a simple extraction step, the BaP was quantitatively analyzed. Pb, Cr, V, Ni and Cd and total particles were also measured from the same filter. Meteorological parameters including temperature, humidity, rain, wind, barometric pressure and cloudiness were recorded. Exhaust gases such as NO_2, CO and SO_2 were also monitored daily. The data were analyzed by a chemometrical approach involving univariate, bivariate and multivariate analysis. The obtained results show a good predictive power of BaP with respect to the presence of metals and gases, and we were also able to identify two sources of BaP, i.e., heating and traffic. Weather conditions in general, and temperature and cloudiness in particular, play a major role in determining BaP levels. During spring and summer, BaP/Pb ratio was drastically reduced as a result of increased solar radiation and temperature, which may be a cause of BaP photodecomposition. The overall results suggest that BaP analysis of air particulate matter is useful in monitoring urban environmental pollution, and that this method could be complementary to conventional ones which identify markers such as gases or heavy metals, resulting in a more complete and detailed monitoring program of urban air pollution.

Keywords: Enzymatic methods; Immunoassay; Air particulate matter; Benzo[*a*]pyrene

1. Introduction

The environmental importance of airborne particulate polycyclic aromatic hydrocarbons (PAH) is well recognized since many of them been proven to be carcinogenic and they are ubiquitous in ambient air [1–3]. Urban residents seem to have a cancer risk higher than those living in rural areas and chronic exposure is generally believed to be of greater significance than short term exposure [4].

In recent years, air particulate PAH have been monitored in many cities and their concentrations vary with seasonal changes, use of domestic heating systems and quantities of vehicle combustion emissions [5–10].

* Corresponding author.

SSDI 0003-2670(94)00235-E

Considerable improvements in chromatographic analytical techniques (gas chromatography (GC) and liquid chromatography (LC)) within the last decade have enhanced our ability to obtain detailed information about the levels of the various components of the complex mixture of PAH in ambient air [11–14]. However, extensive studies and continuous monitoring on a large number of samples are limited by the time required for the analyses.

In a previous study, we reported the development and validation of a quantitative solid-phase enzyme-immunoassay for benzo[*a*]Pyrene (BaP) analysis in water and its application to the determination of BaP levels in tap, river and sea water [15,16]. The method is performed directly on the water sample, and more than 100 samples can be analyzed daily with a detection limit of 1 ng/tube.

The analysis of BaP in air particles is more complex since its distribution in the atmosphere is dependent on many variables. It is believed that most airborne BaP, like other PAH, are primarily associated with organic aerosols produced by incomplete combustion of fossil fuels [17,18].

Thus, the distribution of BaP is governed by air particulate transport by wind currents, fallout through wet and dry precipitation and chemical degradation. Moreover, the effects of atmospheric physics, photochemical degradation, meteorological conditions, and seasonal variation must be carefully evaluated [19].

Thus, a large-scale study is required to correlate the BaP concentration in air particulate matter with the above mentioned parameters, and this can be achieved using the immunoassay for BaP reported in this work.

The above-described method developed for BaP analysis in water [15] was modified and applied to the assay of BaP in air particulate matter collected in the Bologna area.

Total suspended particulate was collected daily (24 h) during the period October 1991–March 1993, and the BaP extracted from the filter was directly analyzed with the BaP specific enzyme-immunoassay.

From the same samples, heavy metals including Pb, V, Ni, Cr, Cd were also measured. NO_2, CO, SO_2 were measured in samples collected in an area close to the BaP particulate sampler.

Atmospheric parameters including temperature, cloudiness, humidity, barometric pressure and wind were also collected and recorded daily. All data were analyzed using a statistical multivariate analysis considering four distinct sets of parameters: BaP, heavy metals, combustion gas and the atmospheric variables.

Table 1
Cross-reactivity with some polycyclic aromatic hydrocarbons in the BaP enzyme immunoassay

Compound	%
Benzo[*a*]pyrene	100
Fluoranthene	10
Pyrene	7
Indeno(1,2,3-*cd*)pyrene	4
Phenanthrene	1
Benzo[*k*]fluoranthene	2
Benzo[*b*]fluoranthene	–
Crysene	–
Acenaphthene	–
Benzo[*e*]pyrene	–
Naphthalene	–
Acenaphthylene	–
Anthracene	–
Benzo[*g,h,i*]perylene	–
Fluorene	–
Dibenzo[*a*]anthracene	–
3,6-Dimethylphenanthrene	–
Methylcolanthrene	–
Perylene	–

2. Experimental

2.1. Reagents

All reagents used were of analytical grade. The PAH (see Table 1), 9,10-dihydrobenzo[*a*]pyren-7(8*H*)-one and trichlorotrifluoroethane were supplied by Aldrich (Milan). Indeno(1,2,3-*c,d*)pyrene, benzo(*k*)fluoranthene and acenaphthylene were supplied by Ultra Scientific Accustandards (New Haven, CT). The other chemicals were purchased from Carlo Erba (Milan). Silica C_{18} and silica NH_2 aminopropyl disposable Bond Elut columns were obtained from Analytichem (Harbor City, CA). Horse radish peroxidase (grade VI) was purchased from Sigma (St. Louis, CA).

2.2. Apparatus

Polystyrene microtiter plates, type Maxisorb F Unframed-microwell module were purchased from

Nunc (Roskilde, Denmark). LC analysis was performed with a Waters liquid chromatograph (MS-600) equipped with a Model 484 absorbance detector (Waters). Conventional microtiter reader was used.

2.3. Sampling sites

The air sampling was carried out in Bologna, a town of some 500,000 inhabitants, located in the north-central part of Italy in the Po Valley (Pianura Padana) close to the central part of the Appennine mountain range. Bologna is a typical medium-sized Italian town with busy traffic and a few sites of industrial emission. Energy for indoor heating, generally used from October to May is derived from natural gas (methane) and heating oils (60% and 40%, respectively). The seasonal variations in temperature, rainfall and wind are typical of a continental climate with cold winters (below 0°C) and hot summers (30–35°C).

2.4. Sampling system

The air sampler was located in an area intermediate between the heart of the city and its outskirts, far from waste incineration or industrial plants; this site represented an average situation as regards air pollution and traffic density. The air was collected at an average sampling rate of 20 l/min. A cellulose acetate filter with a of 0.4–0.5 μm poresize, and a diameter of 50 mm was used. The daily (24 h) collected sample underwent heavy metal and BaP analysis.

2.5. Preanalytical BaP extraction

Two milliliters of trichlorotrifluoroethane were added to a 1 cm diameter portion of the filter and agitated in an ultrasonic bath for 5 min. The eluted BaP solution was dried under a nitrogen stream and reconstituted with 1 ml of 0.1 M phosphate buffer, pH 7.5 containing 3% BSA, and then underwent enzyme-immunoassay.

2.6. Enzyme-immunoassay procedure

This assay includes the use of BaP-specific antibody immobilized on polystyrene microtiter plates as previously described [15]. Briefly, the BaP antiserum, raised in rabbit using a 6-carboxymethyloxime derivative of BaP coupled with bovine serum albumin, was purified by salting out and chromatography, and an appropriate dilution was immobilized by physical absorption. The enzymatic tracer consisted of a conjugate of 9,10-dihydrobenzo[*a*]pyren-7(8*H*)-one-6-(*O*-carboxymethyl)-oxime with horseradish peroxidase (HRP) prepared as previously reported [15]. One-hundred μl of the BaP extract reconstituted with phosphate buffer or 100 μl of appropriate BaP standards (10^{-9}–10^{-5} mol/l) were applied to the microtiter wells containing the immobilized antibody, followed by the addition of 100 μl of the BaP-6-CMO-HRP tracer at a working dilution of 1/10,000, v/v, of the original stock solution.

The immunological reaction was allowed to proceed for 2 h at 37° C, followed by a washing step. The wells were washed 3 times with distilled water and the BaP-6-CMO-HRP bound to the immobilized antibody was measured by adding 200 μl of 0.1 M citrate buffer pH 5 containing 0.003% H_2O_2, 200 mg/100 ml *o*-phenylenediamine, and 45 μl/100 ml Tween 20. After incubation for 15 min, the enzymatic activity was stopped with 50 μl 2 M H_2SO_4 solution and the absorbance read at 490 nm.

2.7. Calculation

Antibody binding was expressed as a B/B_0 (the amount of enzymatic tracer bound relative to the amount bound for zero dose) vs. log dose. The dose-response curve indicated a four parameter function and the best sigmoidal curve was computed by the least squares method. The amount of BaP in the samples was interpolated automatically, and final results were expressed in $\mu g/m^3$ of air.

The specificity of the antiserum was assessed by competition with other structurally related PAHs and expressed as the percentage of cross reactivity at 50% displacement.

2.8. Analysis of metals and gases

Pb, Ni and Cr were evaluated on the same air particulate filters used for BaP analysis (see above) using conventional atomic absorption spectrometry. The filters were treated with HCl and HNO_3 in order to solubilize the metals in ionic form which then underwent analysis following a procedure previously described

Table 2
Measured parameters

Parameter	Unit	Mean	Min.	Max.	S.D.
Benzo[*a*]pyrene (BaP)	ng/m^3	22.7	0.0	174.0	34.1
Particulate	μg/m^3	84.1	10.2	265.3	43.7
Temperature, mean	°C	12.5	−2.6	28.9	8.2
Temperature, min.	°C	8.5	−5.7	23.9	7.5
Temperature, max.	°C	17.4	−0.8	35.6	9.3
Humidity, mean	%	77.5	38.0	100.0	13.1
Humidity, min.	%	63.2	31.0	100.0	18.1
Humidity, max.	%	91.0	46.0	100.0	9.5
Rain	mm	1.8	0.0	51.0	5.7
Wind, mean speed	m/s	2.5	0.1	16.1	1.5
Wind, max. speed	m/s	4.2	1.0	27.3	2.7
Wind, daily total	Km	224.4	14.8	1398.4	128.7
Wind, main direction	grade	207.5	45.0	360.0	99.5
Pressure, mean	millibar	1018.5	990.4	1047.6	9.8
Cloudiness, mean	eighths	4.0	0.0	8.0	2.9
Cloudiness, min.	eighths	2.2	0.0	8.0	3.0
Cloudiness, max.	eighths	5.9	0.0	8.0	2.8
Pb	μg/m^3	0.3	0.1	1.0	0.3
Cr	ng/m^3	13.7	1.4	73.7	11.9
V	ng/m^3	14.9	1.1	72.3	13.3
Ni	ng/m^3	15.8	1.0	65.8	14.6
Cd	ng/m^3	1.4	0.1	6.8	1.2
NO_2	μg/m^3	121.6	53.0	222.0	30.1
CO	μg/m^3	5.1	0.6	22.3	1.8
SO_2	μg/m^3	20.4	1.0	100.0	13.6

[20]. NO_2, CO and SO_2 were collected using conventional air monitoring sensors (Bologna City Environmental Program).

2.9. Meteorological parameters

The list of daily meteorological factors examined, obtained from E.R.S.A (Emilia-Romagna District Meteorological Service), is reported in Table 2 which also shows the other parameters studied.

2.10. Chemometrical analysis

Chemometrical analysis of the data and graphics was done entirely with the latest edition of the computer package Parvus [21], which includes the partial least squares regression methods (PLS) [22] and graphic outputs.

In the PLS technique, a block of X (independent) variables are related to a block of Y (dependent) variables. PLS is an optimal method for determining the predictive relations between two blocks of variables (chemical, environmental, biological, etc.) analyzed on the same samples, when collinearity is present. Collinearity means that data contain redundant information, i.e., that more than one factor causes variations in the data. Several variables are determined, each one in terms of both the information replicated in common and its own noise. Among the block of independent X variables, PLS compresses the information relevant for describing the linear relation with the Y variable in the first few latent variables or PLS components related to the underlying phenomena, and at the same time it removes noise, confining it into the last latent variables. The Parvus version of PLS operates with a full validation procedure [23]. In this study, groups (blocks) of variables of different types were determined, PLS was applied in order to know if, in each block of variables (metereological, metals, gases) a linear relationship with BaP (the Y variable) could be found, and also to predict the BaP value of a sample from its X measured variables. To validate the predictive power of the linear function the leave-more-out method of full cross-validation was used. Results are expressed in terms of the percent of variance in fitting and in prediction. From the PLS equation, which is a linear combination of the original variables, it is possible to quantify the importance of any given variable in building the relation by using the coefficient of that variable in the linear combination divided by its standard deviation.

3. Results and discussion

3.1. Methodological considerations

This method was developed to be specific for BaP; the fact that other PAH exhibited little interference was demonstrated by their low cross-reactivity in the assay (Table 1). Of the PAH assessed, only fluoranthene, pyrene and indeno[1,2,3*cd*]pyrene can show a significant cross-reactivity [15], but they could interfere in the quantitative assay only when present at a concentration 10 times higher than that of BaP.

The antibody used shows a higher specificity with respect to the one previously developed for water analysis [15]. The 6-carboxymethyloxime derivative used

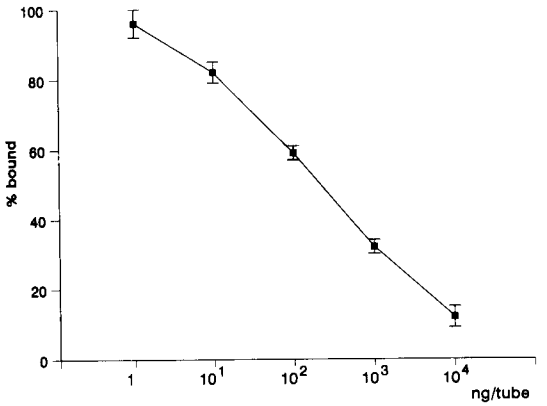

Fig. 1. Dose-response curve for the enzyme immunoassay of BaP in air particulate matter. Each point represents the mean value ± S.D. of five determinations.

for BSA coupling and antibody production is more similar structurally to BaP than the 7-carboxymethyloxime derivative previously reported, in which the A ring is not aromatic.

The extraction of BaP from the filter using TCTFE has been proven to be efficient (98 ± 2%), as documented by a recovery test using ^{3}H labeled BaP absorbed on the filter. After elution with TCTFE the nitrogen dried sample was dissolved in 0.1 M phosphate buffer pH 7.5 containing 3% BSA to facilitate and ensure complete solubilization of BaP. According to the expected BaP concentration and its solubility in the buffer, the amount of BaP recovered from the 10 mm diameter filter can be completely solubilized.

3.2. Assay performance

The enzyme immunoassay permits analysis of quantities as low as 1 ng/tube of BaP as shown by the standard curve reported in Fig. 1. The dynamic range is from 1–10^4 ng/tube of BaP, and with this detection limit it is possible to measure BaP in less than 1 m^3 of air, thus the collected samples must be diluted at least 1/100 before the assay.

The precision of the assay was evaluated within and between 10 consecutive assays; it was shown to be below 2% in the intra-assay study, and below 8% in the inter-assay study. Table 3 shows assay precision in 3 samples, at high (50,200), medium (820) and low (12) concentrations (ng/tube) of BaP.

Since the study was carried out over many months, BaP control samples were always analyzed at the same time as the air particulate BaP samples. The accuracy of the assay had been previously evaluated by comparison with an LC method [15]. A good agreement was found when samples at relatively high BaP concentration were measured independently with the two methods.

3.3. Chemometrical results

The measured variables are listed in Table 2. When any variable values were missing from samples, these were discarded; the statistical analysis was done on the 295 samples without missing values.

The data form a matrix of 295 rows and 25 columns: in each row are the values of the measured parameters (variables) for one sample (objects), the column contains the values of one variable for all the objects.

Some groups of variables are present which differ in determination method and environmental significance: BaP and particulate matter, meteorological parameters, toxic and carcinogenic metals, and exhaust gases. The variable BaP is the target of this study. The relationships between BaP and the other variables or groups of variables were studied in three steps: univariate, bivar-

Table 3
Precision of replicates and sample-to-sample assay of BaP on three different samples

Samples (n = 20)	Intra-assay		Inter-assay	
	Mean (ng/tube)	C.V. (%)	Mean (ng/tube)	C.V. (%)
Low	12	5.5	12	8.1
Medium	802	4.2	806	5.8
High	50,200	3.8	50,800	6.2

C.V. = Coefficient of variation. The BaP samples were collected on a cellulose filter and eluted with TCTFE, as reported in the text.

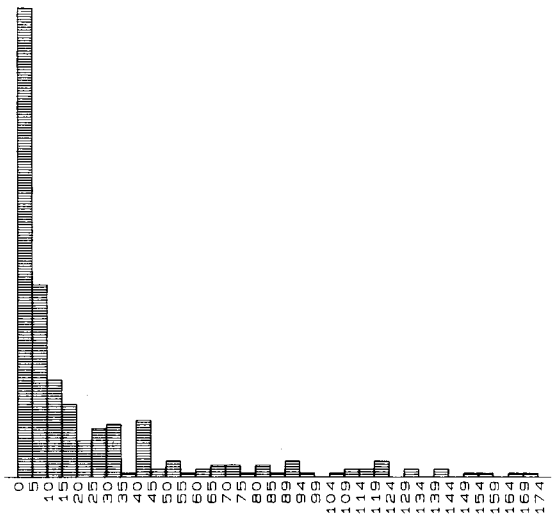

Fig. 2. Frequency distribution of Benzo[*a*]pyrene values.

iate and multivariate, in order to extract as much information as possible from the data.

Univariate analysis

The frequency distribution of BaP values is reported in Fig. 2. It is positively skewed, most samples having BaP concentration ranging from 0 to 10 ng/m^3, but 131 samples had a BaP concentration of >10 ng/m^3.

The frequency distributions of metals also show positive skewness. A logarithmic transformation was applied to BaP and metal values so as to obtain more centrally distributed data, to be subsequently used in correlation and regression studies.

By plotting the BaP concentration of each sample against the progressive sampling index (Fig. 3) a relationship dependent upon season changes in weather becomes evident: the winter samples vary within a wide range of values (from 0.0 to 174.0) while the summer samples vary in the range 0.0–3.0 ng/m^3.

In Fig. 4 the weather dependent relationship of the Pb values is reported: Pb, like the other metals, shows a trend similar to that of BaP, but that of Pb is the least regular.

All the variables were inspected both by histogram and by graphing against the seasonal changes: the most regular weather-dependence is shown by the mean temperature of the sampling days, reported in Fig. 5.

Since it is known that the major source of lead emission is traffic [8] and that vanadium is produced by the burning of heavy oils [24], in order to check whether (and when) the sources of BaP were urban traffic and/or domestic heating, the ratios BaP/Pb and BaP/V were computed and reported (Figs. 6 and 7). In winter and autumn, the ratio BaP/Pb varied within the widest range of values, in spring and summer, on the contrary, the ratio became more constant. If the sample contents in BaP and lead had derived from the same source i.e.,

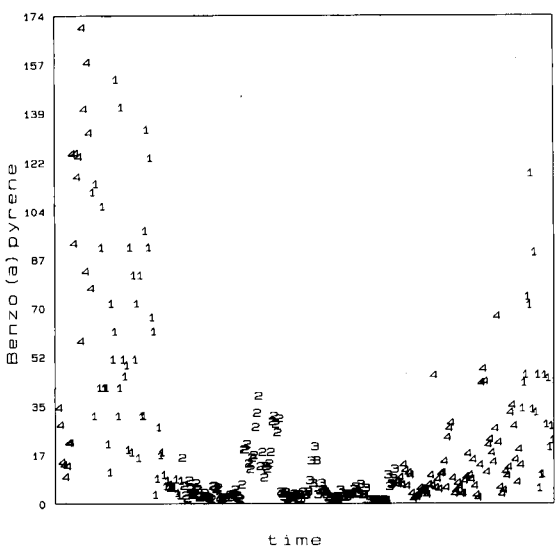

Fig. 3. The values of BaP (ng/m^3) versus the sampling time are reported. The objects are shown by season: 1 = winter, 2 = spring, 3 = summer, 4 = autumn.

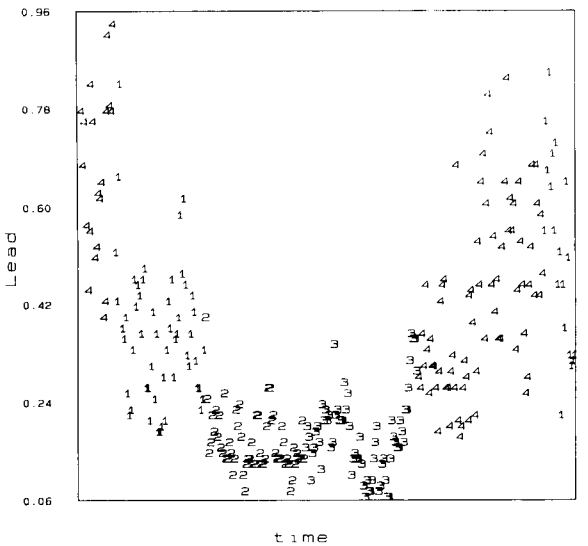

Fig. 4. The values of Pb (μg/m^3) versus the sampling time are reported. The objects are shown by season: 1 = winter, 2 = spring, 3 = summer, 4 = autumn.

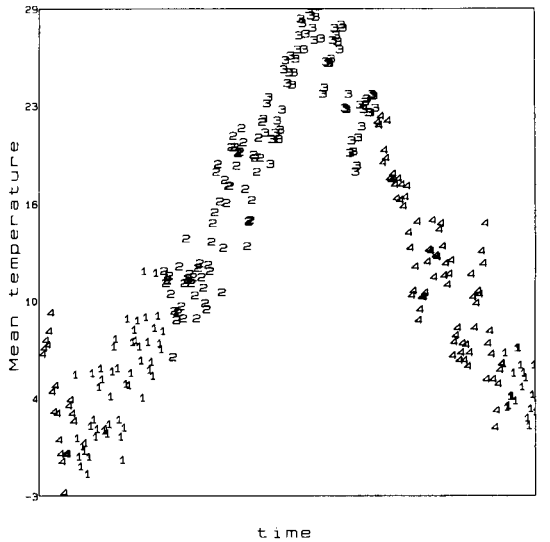

Fig. 5. The mean temperature during the day (°C) versus the sampling time is reported. The objects are shown by season: 1 = winter, 2 = spring, 3 = summer, 4 = autumn.

traffic, their ratio would have been constant through all four seasons. Instead, it seemed that in winter and autumn, one or more additional sources was producing BaP. During the four weeks of May, the BaP concentration in air particulate matter increased to a maximum of 37.0 ng/m^3 (15 May 1992) and then decreased in a near-regular fashion to the mean seasonal values (2.0 ng/m^3): in this period atmospheric pressure was increasing, and reached a maximum of 1026.9 mbar on May 15th after which it decreased at a regular rate until the end of the month. There was no rain during this month: these atmospheric conditions determined a thermic inversion and caused an enrichment of BaP in the particulate matter; Pb and vanadium concentrations had minor increases during the same period.

The ratio between BaP and V varied from 0.1 to 6.9 in winter and autumn, while the ratio BaP/Pb varied from 2.3 to 435.0 in the same season; domestic heating is the main common source of BaP and vanadium in this period. In spite of the position of the sampling site, at a low level in a street where the traffic is heavy, the BaP emitted from domestic heating sources was picked up; thus, in cold weather, two sources of BaP are present, indoor heating and traffic. In the summer, traffic seems to be the principal source.

Bivariate analysis

The Pearson correlation coefficient, r, between each pair of variables was computed; it is a popular numerical summary of the relationship between two measured variables which measures the amount of linear association between them [25,26]. If $r=1$, the maximum value, there is a perfect positive linear association, if $r=0$ there is no linear association, and if $r=-1$, the

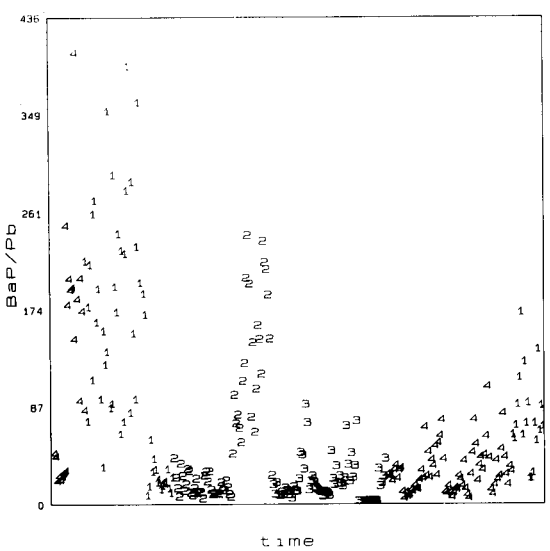

Fig. 6. The ratio BaP/Pb versus the sampling index is reported. The objects are shown by season: 1 = winter, 2 = spring, 3 = summer, 4 = autumn.

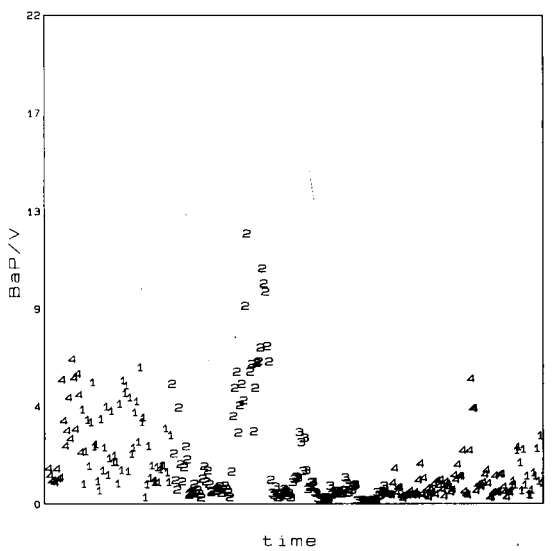

Fig. 7. The ratio BaP/V versus the sampling index is reported. The objects are shown by season: 1 = winter, 2 = spring, 3 = summer, 4 = autumn.

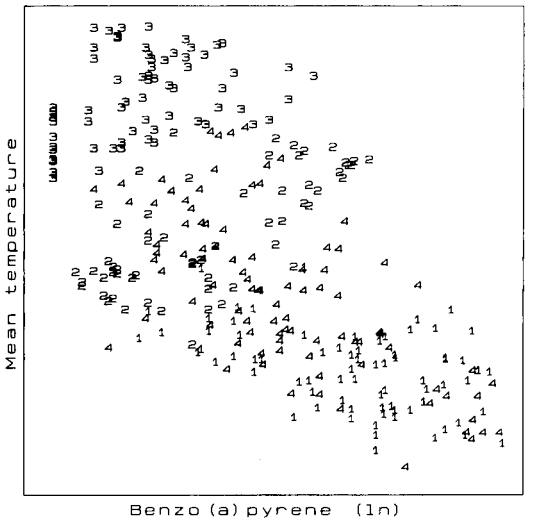

Fig. 8. Scatter plot of ln BaP and mean temperature values. The objects are shown by season: 1 = winter, 2 = spring, 3 = summer, 4 = autumn.

minimum value, there is a perfect negative linear association. All r, with no other information about the data, tell us little about the relationship between the variables. So, to gain a real insight into the data, the bivariate scatter plots were also constructed.

In Fig. 8, the scatter plot of the logarithmic transformation (ln) of the BaP concentrations and mean temperature values is shown: the samples, identified by season (1 = winter, 2 = spring, 3 = summer, 4 = autumn) lie along an almost linear zone with a negative slope, $r = -0.64$, indicating a dependence of BaP on temperature. The scatter plot of BaP (ln) versus Pb concentration (ln) of the samples is shown in Fig. 9. In Fig. 10 a linear dependence between BaP (ln) concentration and CO concentration in the air is seen.

Linear association with BaP

In Tables 4 and 5 the correlation coefficients between BaP and the studied variables are reported. In the Tables, as in the following multivariate correlation study, the logarithmic transformation of BaP and metals was used instead of the original values since, by so doing, higher r values are obtained. The linear association of BaP with the meteorological and chemical variables varies considerably depending upon whether the sampling period is considered in its entirety or as individual seasons. In particular, while r is high and negative for the entire period from November 1991 to January 1993; for humidity, wind direction and barometric pressure, the variables are more linearly associated with BaP in autumn and winter, for temperature and cloudiness, in the spring. The linear association calculated by r disappears in the summer. A very high linear association is calculated with particulate matter in autumn; in contrast, it is not significant in the spring.

During the cold seasons, the metal concentrations have significant (at level 95%) and particularly high correlation coefficients; on the contrary, in spring and

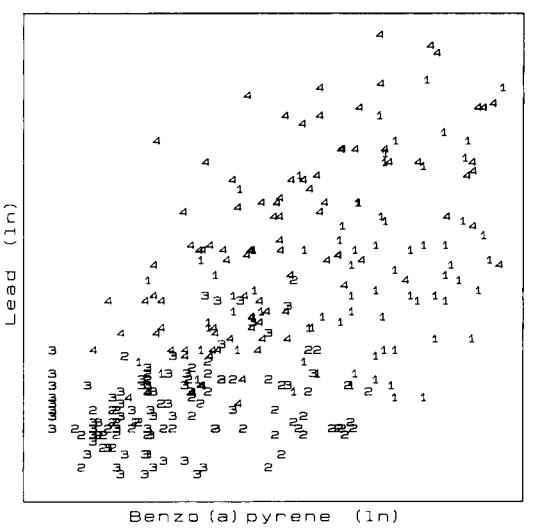

Fig. 9. Scatter plot of ln BaP and ln Pb values. The objects are shown by season: 1 = winter, 2 = spring, 3 = summer, 4 = autumn.

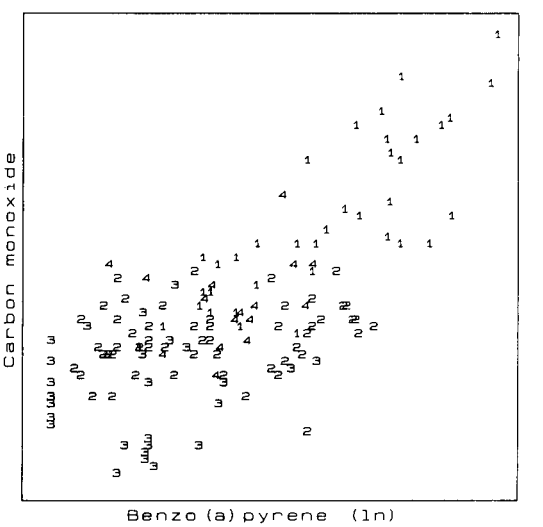

Fig. 10. Scatter plot of ln BaP and CO values. The objects are shown by season: 1 = winter, 2 = spring, 3 = summer, 4 = autumn.

Table 4
Correlation coefficients of benzo[*a*]pyrene with meteorological variables (*T* = temperature, *H* = humidity, *W* = wind, *P* = pressure, *C* = cloudiness) and with air particulate matter. Only correlations significant at 95% confidence level are reported

	Autumn	Winter	Spring	Summer	Nov. 91–Jan. 93
T, medium	–	–	0.67	0.36	−0.64
T, min.	–	–	0.56	0.30	−0.64
T, max.	–	–	0.66	0.34	−0.62
H, medium	0.65	0.70	–	–	0.25
H, min.	0.61	0.60	–	–	0.28
H, max.	0.67	0.67	–	0.26	–
Rain	–	–	–	–	−0.15
W, medium	–	–	–	–	−0.34
W, max.	0.31	–	–	–	−0.24
W, tot.	–	–	–	–	−0.34
W, dir.	0.67	0.50	–	–	0.21
P, medium	0.73	0.68	0.37	–	0.48
C, medium	0.31	0.38	−0.43	−0.28	–
C, min.	–	0.24	–	−0.24	0.16
C, max.	0.45	0.40	−0.49	−0.28	–
Particulate	0.75	0.51	–	0.42	0.53

Table 5
Correlation coefficients of benzo[*a*]pyrene and chemical variables. Only correlations significant at 95% confidence level are reported

	Autumn	Winter	Spring	Summer	Nov. 91–Jan. 93
Pb	0.84	0.64	–	0.34	0.62
Cr	0.77	0.68	−0.31	–	0.49
V	0.82	0.85	–	–	0.58
Ni	0.81	0.85	–	–	0.58
Cd	0.71	0.68	–	–	0.63
NO_2	–	–	0.59	–	0.36
CO	–	0.82	–	–	0.70
SO_2	–	0.64	0.32	–	0.56

Table 6
PLS results: retained variance (%) in fitting and in prediction by the linear relationship between benzo[*a*]pyrene (*Y*) and the block of *X* variables

	A	B	C	D
Meteorological	53–50	58–48	59–52	59–50
Metals	54–53	63–61	65–62	67–64
Gases	54–48	72–60	75–65	90–84

The linear relationship is computed in: dataset A, all samples of the period Nov. 91–Jan. 93; subset B, samples collected on cold days (*T* max. < 15°C); subset C, samples collected on cloudy days (*C* mean > 6); subset D, samples collected on cold and cloudy days

summer *r* values are not significant: this could be explained partly by the increase in traffic density on colder days, and partly by the photodegradation of BaP adsorbed on air particulate matter exposed to sunlight [27].

BaP also has a linear association with CO and SO_2 in the winter and with NO_2 and SO_2 in the spring. Linear association among metals, gases and meteorological parameters: several pairs of metals showed very high correlation ($r > 0.8$), while lower but significant correlations were found in the pairs of meteorological parameters.

Multivariate analysis

Instead of considering variables one or two at a time, a multivariate regression study was carried out to verify the presence of linear relations between BaP and the blocks of other variables determined in the monitoring. The PLS method of regression was used, both to predict the content of BaP and to gather more information about its sources.

The samples from the entire period November 1991–January 1993 and the subsets corresponding to seasons were studied by PLS: the predicted explained variances of these relations were low (ranging from a minimum of 13% for BaP and meteorological variables in summer and to a maximum of 56% for BaP and metals in winter). This would be expected, since in a given season, weather may be quite variable and the abrupt change in seasons on the calendar does not strictly coincide with changes in traffic patterns and domestic heating use. Just as the monitoring data were divided into subsets by season in order to better distinguish linear relations than would be possible for the whole period, the datamatrix was again divided into climatic subsets, using mean temperature and cloudiness as the criteria of subdivision.

PLS was carried out on the new subsets obtained from the original datamatrix. In Table 6, the results of 3 subsets are reported together with the results of the whole period (dataset A):

Cold days: 147 samples collected when the maximum temperature in the day was lower than 15°C (subset B).

Cloudy days: 102 samples collected when the mean cloudiness was greater than six-eighths (subset C).

Cold and cloudy days: 73 samples collected when the maximum temperature was lower than 15°C and

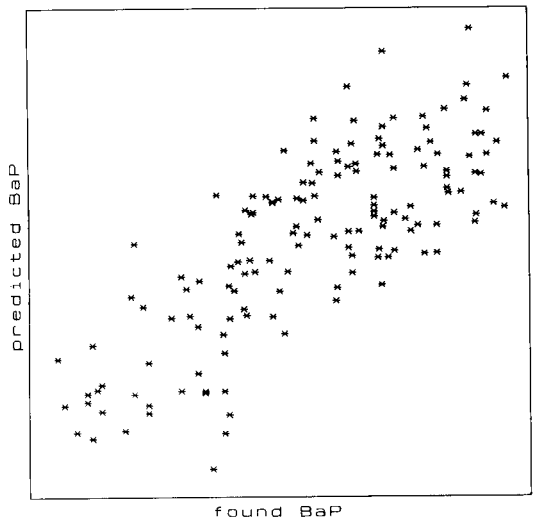

Fig. 11. BaP concentrations on cold sampling days (subset B in Table 6) predicted by the first two PLS components computed from metal block data. The first 2 components explain the 61% predicted variance.

the mean cloudiness was greater than six-eighths (subset D).

The results, summarized in Table 6, will now be briefly discussed in terms of each of the variables in the X block.

3.4. BaP (Y) and meteorological parameters (X)

It is of considerable interest to know whether the BaP content of air particles can be predicted from simple measurements of meteorological parameters. The relation between measured BaP and that predicted from the 15 meteorological variables using a 3 component PLS model, shows 53% variance in fitting and 50% in prediction in data set A; these values are a little higher in subsets B, C and D.

The mean temperature and pressure are the variables of greatest importance in these relations, while humidity, rain and wind variables have minor importance.

Using information determined a posteriori about the weather parameters (contained in the PLS equations), on a given day, BaP could be estimated for that day with a probability of success of about 50%. If the weather conditions could be accurately predicted, using the same equation, BaP content in air particulate matter could be forecast the day before; in this case, with a probability of success of 50% this test could have noteworthy value.

3.5. BaP (Y) and metals (X)

Considering the datamatrix as a whole, a linear relation between BaP and metals was found; in the subsets the relations were better.

In Fig. 11, the relation between measured and predicted (PLS) BaP is shown for subset B: this relation was constructed with the first 2 PLS components, computed from data regarding the 5 metals, and the leave-more-out method (10 groups) of cross-validation was used; 61% of variance is explained. V and Cr are the more important variables in determining the relation on cold days; instead, in days of mean temperature higher than 15°C (subset not reported in the Table) Cd, Ni and Pb are the metals more linearly related with BaP, but the explained variance has only a 37% fit and 34% predicting ability.

When the mean cloudiness during the day was high (subset C), the explained variance increased only a little, and Cr and V remain the most important factors; when, on the contrary, the mean cloudiness during the day was lower than six-eighths (subset not reported in the Table), Cd and Pb are the most important variables and the explained variance is 48% (fit) and 47% (prediction).

In Fig. 12 the linear relation between found and predicted BaP in subset D is shown: it was constructed

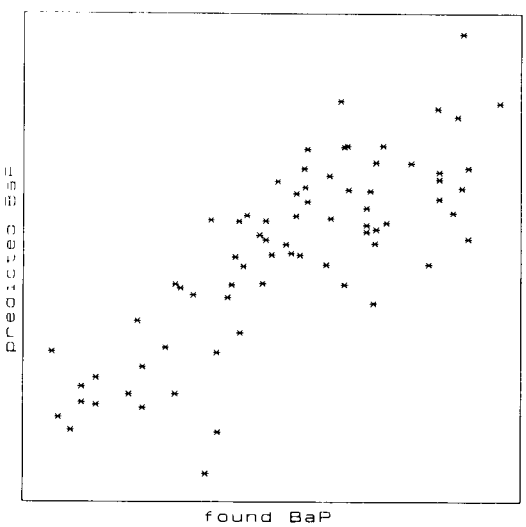

Fig. 12. Benzo[*a*]pyrene concentrations on cold and cloudy days (subset D of Table 6) predicted by the first 2 PLS components computed from metal block data. The first 2 components explain the 64% predicted variance.

using the first 2 PLS components and it explains 64% of the total variance. V and Cr are the most important variables in this relation: when the temperature was lower than 15°C but the sky is clear, the fit and predicted variance were similarly 63% and 60%; V is the first but Ni the second by importance in the PLS relation. Considering days with clear skies and a mean temperature higher than 15°C, a decrease in explained variance was obtained (45% fit, 38% prediction), and Pb, Cd and Ni were the most significant variables, in order of importance.

3.6. *BaP (Y) and gases (X)*

With the block of gases, the PLS shows a significant improvement from subset A to subsets B, C and D, so that when the sky was very cloudy and the temperature low, BaP concentrations in air particulate matter could have been estimated (predicted) by gas determinations, since a good linear relationship was present: three components were used in these relations, and explained variances are listed in Table 6. CO was always the most important variable, and the importance of NO_2 increased when weather conditions worsened.

4. Conclusions

The developed enzyme-immunoassay fulfils the standard requirements for precision and accuracy for a quantitative analysis of BaP in air particulate matter. Its low detection limit permits utilization of very diluted particles in an air sample, practically abolishing aspecificity. Thanks to its rapidity and a simplified preanalytical step, it was possible to carry out this extensive study on BaP concentration in air particulate matter, giving the above-reported data and correlations with the other parameters. The enzyme immunoassay is an analytical tool complementary to multianalyte GC or LC methods, and it could be useful for preliminary screening of environmental pollution.

Studying the BaP concentration in air particulate matter on many samples, we found linear relations with good predictive power between BaP and the metals determined in air particulate matter and between BaP and the monitored gases. We also determined the presence of at least two sources of BaP, domestic heating and traffic, the influence of which change with weather conditions.

Thanks to this immunoassay method, we performed a correlation and regression study on a high number of samples, the results of which add to our knowledge about air pollution in Bologna during the period from the end of 1991 to the beginning of 1993. The results show that BaP in Bologna urban air particulate matter occasionally reached quite high levels, 100–200 ng/m^3, and that these high levels cannot be entirely predicted by those of other pollutants such as heavy metals and exhaust gases. Moreover, thanks to the use of this method, which is an easy analytical tool for continuous monitoring of air BaP concentrations, it may be possible to better control these levels, hopefully reducing them, thus limiting exposure to this potential carcinogen.

References

[1] WHO – International Agency for Research on Cancer, in IARC Monographs on the Evaluation of the Carcinogenic Risk of Chemicals to Man, Vol. 3: Certain Polynuclear Aromatic Hydrocarbons and Heterocyclic Compounds, IARC, Lyon, 1973.
[2] WHO – International Agency for Research on Cancer, in IARC Monographs on the Evaluation of the Carcinogenic Risk of Chemicals to Humans, Vol. 32: Polynuclear Aromatic Hydrocarbons, Part 1, Chemical, Environmental and Experimental Data, IARC, Lyon, 1983.
[3] United States National Academy of Sciences, Particulate Polycyclic Organic Matter, Committee on the Biological Effects of Atmospheric Pollution, National Research Council, National Academy Press, Washington, DC, 1972.
[4] R. Harkov, Sci. Total Environ., 26 (1982) 67.
[5] G. Chatot, R. Dangy-Caye and R. Fontages, Atmos. Environ., 7 (1973) 819.
[6] L. De Maio and M.Corn, Air Pollut. Control Assoc., 16 (1966) 67.
[7] R.J. Gordon, Environ. Sci. Technol., 10 (1976) 370.
[8] H. Gusten and G. Heinrich, in P.W. Jones and P. Leber (Eds.), Polycyclic Aromatic Hydrocarbons in the Lower Atmosphere of Karlsruhe, Polynuclear Aromatic Hydrocarbons, Ann Arbor Sciences, Ann Arbor, MI, 1979, p. 357.
[9] C. Escrivà, M. Morales, A. La Orden, J. Manes and G. Font, Fresenius' J. Anal. Chem., 339 (1991) 743.
[10] F. Valerio, C. Brescianini, M. Pala, A. Lazzarotto, D. Balducci and V. Fontana, Sci. Total Environ., 46 (1985) 121.
[11] M.L. Lee, M. Novotny and K.D. Bartle, Anal. Chem., 11 (1976) 1566.
[12] M.L. Lee, D.L. Vassilaros and D.W. Later, Int. J. Environ. Anal. Chem., 11 (1982) 251.

[13] M.L. Lee, M. Novotny and K.D. Bartle, Analytical Chemistry of Polycyclic Aromatic Compounds, Academic Press, New York, 1981, p. 156.
[14] J. Jaklin and P. Krenmayr, in J. Albaiges and R.W. Frei (Eds.), Fate of Hydrocarbons in the Environment, An Analytical Approach, Gordon and Breach, New York, 1986, p. 73.
[15] A. Roda, M.A. Bacigalupo, A. Jus and A. Minutello, Environ. Sci. Technol., 12 (1991) 1027.
[16] A. Jus, M.A. Bacigalupo, A. Roda and C. Vaccari, Fresenius' J. Anal. Chem, 343 (1992) 55.
[17] P.C. Siebert, C.A. Craig and E.B. Coffey, Preliminary Assesment of the Sources, Control and Population Exposure to Airborne Polycyclic Organic Matter (POM) As Indicated by Benzo[*a*]pyrene (BaP), Final Rep. EPA Contr. No. 68-02-2836, Environmental Protection Agency, 1978.
[18] R.P. Hangebrauck, D.J. von Lehmden and J.E. Meeker, Sources of Polynuclear Hydrocarbons in the Atmosphere, U.S. Dept., HEW, Public Health Service, AP-33, PB 174-706, Washington, DC, 1967.
[19] K.E. Thrane, Atmos. Environ., 22 (1988) 587.
[20] R.J. Thompson, G.B. Morgan and L.J. Purdue, At. Absorp. Newslett., 9 (1970) 53.
[21] M. Forina, R. Leardi, C. Armanino and S. Lanteri, Parvus: an Extendable Package of Programs for Data Exploration, Classification and Correlation, Elsevier Scientific Software, Amsterdam, 1988.
[22] P. Geladi and B. Kowalsky, Anal. Chim. Acta, 185 (1986) 1.
[23] S. Lanteri, Chemom. Intell. Lab. Syst., 15 (1992) 159.
[24] H. Gusten and G. Heinrich, in P.W. Jones and P. Leber (Eds.), Polycyclic Aromatic Hydrocarbons in the Lower Atmosphere of Karlsruhe, Polynuclear Aromatic Hydrocarbons, Ann Arbor Sciences, Ann Arbor, MI, 1979, p. 364.
[25] F. Valerio, C. Brescianini, M. Pala, A. Lanzarotto, D. Balducci and V. Fontana, Sci. Total Environ., 114 (1992) 47.
[26] J.M. Chambers, W.C. Cleveland, B. Kleiner and P.A. Tukey, Graphical Methods for Data Analysis, The Wadsworth Statistic/Probability Series, Wadsworth International Group, Belmont, CA, 1983, p. 76.
[27] F. Valerio and M. Pala, Fresenius' J. Anal. Chem., 330 (1991) 777.

ELSEVIER

Analytica Chimica Acta 298 (1994) 65–73

ANALYTICA CHIMICA ACTA

Computational program for evaluating and optimizing response-surface curves based on central composite designs

A. Gustavo González [a,*], Domingo González-Arjona [b]

[a] *Department of Analytical Chemistry, University of Seville, Seville 41012, Spain*

[b] *Department of Physical Chemistry, University of Seville, Seville 41012, Spain*

Received 21 January 1994; revised manuscript received 27 May 1994

Abstract

A program for optimizing central composite experimental designs, called CCDOPT, has been devised and implemented in QuickBasic. The principal procedures involved are discussed. In order to illustrate how the program works several worked examples have been selected.

Keywords: Optimization methods; Central composite designs

1. Introduction

Response-surface methodology (RSM) appears for the first time in the November 1966 issue of Technometrics [1,2]. Since this year a lot of papers and books have been published within this realm [2–4]. Today, optimization in experimental designs is based on mathematical 'deterministic' or 'black-box' models. Although the first method might be philosophically the most attractive, unfortunately, it often remains inapplicable as there is not always a known law to describe the studied phenomenon [5]. The black-box model involves a model building RSM. The experimental strategy in RSM revolves around the experimental response y, which is a function on several independent variables called factors (z_i). They occupy what is called factor space and a plot of y on this space is the response surface. The region close to the extremum is known as a 'nearly stationary' region [6]. It is substantially a nonlinear zone that can be described adequately by means of nonlinear polynomials as the second order ones. Therefore, by expanding the response function into a second order truncated Taylor's series, the mathematical model is:

$$y = \beta_0 + \sum_{i=1}^{f} \beta_i z_i + \sum_{i=1}^{f} \sum_{j>i}^{f} \beta_{ij} z_i z_j + \sum_{i=1}^{f} \beta_{ii} z_i^2 \qquad (1)$$

f being the dimension of the factor space.

In real processes one is always faced to uncontrollable factors producing an output which varies at random. These uncontrolled factors encompass the background noise or experimental error. Taking into consideration that the background noise is the outcome of summing the uncontrolled factors which follow different distribution laws considered to be mutually independent, it may be assumed that the experimental error is normally distributed according to the central limit theorem. The use of multiple linear regression techniques yields sample regression coefficients b_0, b_i, b_{ij} and b_{ii} which are the estimates of the true coefficients,

* Corresponding author.

SSDI 0003-2670(94)00247-J

β. Thus, the real model equation would be written as

$$y = b_0 + \sum_{i=1}^{f} b_i z_i + \sum_{i=1}^{f}\sum_{j>i}^{f} b_{ij} z_i z_j + \sum_{i=1}^{f} b_{ii} z_i^2 + e(y) \quad (1b)$$

where $e(y)$ is the error associated to the y variable [7] which, as was indicated, is assumed to be normally distributed. Accordingly, the estimated y value is

$$\hat{y} = b_0 + \sum_{i=1}^{f} b_i z_i + \sum_{i=1}^{f}\sum_{j>i}^{f} b_{ij} z_i z_j + \sum_{i=1}^{f} b_{ii} z_i^2 \quad (2)$$

This regression procedure is more straightforward than Yates' algorithm for calculating both main and interaction effects [8]. The aim of optimization is to evaluate the coordinates in the factor space that maximize (or minimize) the objective response-function y. From a chemometric viewpoint, two different methodologies may be applied for attaining the optimum [9]: free-derivative direct search techniques such as simplex algorithm or steepest ascent hill-climbing algorithms and derivative optimization techniques. An advantage of these later techniques is that they find true optima without drawbacks derived from local singular points or fine structures in the function caused by rounding errors, statistical errors, etc. [28].

Two-level factorial designs are insufficient to adjust the response-function to Eq. 1. For this purpose, the factors should take at least three different values, i.e., a three-level factorial design is needed [6]. The number m of coefficients of Eq. 2 is given by

$$m = \frac{(f+1)(f+2)}{2} \quad (3)$$

where f is the number of factors.

A 3^f full factorial design involves a very great number of observations that exceed considerably the number of coefficients to be estimated. A method for alleviating this situation was devised by Box and Wilson in a paper issued in 1951 [9], in which the notion of central composite design (CCD) was presented. The introduction of the "star points" to augment the two-level factorial array was done to allow for an efficient estimate of quadratic terms in the second order model Eq. 2.

The CCD is a special case of designs whose building consists of three portions. (i) A 2^f full factorial design for $f < 5$ or a fractional replicate thereof otherwise, (ii) $2f$ vertices of a cross-polytope or "star points" positioned on the coordinate axes of factorial space $(\pm\alpha,0,\ldots0)$, $(0,\pm\alpha,\ldots0),\ldots(0,0,\ldots\pm\alpha)$ where α is the distance (axial spacing or star arm) from the centre point of the design to a star point, (iii) finally, a number n_0 of extra points at the centre of design $(0,0,\ldots0)$. Therefore, CCD of complete designs requires $N = 2^f + 2f + n_0$ runs.

CCD can readily be transformed into orthogonal designs (OCCD) by an appropriate selection of the star arm [10]

$$\alpha = \sqrt{\frac{\sqrt{(2^f + 2f + n_0)2^f} - 2^f}{2}} \quad (4)$$

Orthogonality eliminates covariances between estimated pure second order coefficients b_{ii}.

Box and Hunter suggested in 1957 [11] another type of CCD called rotatable CCD (RCCD). A design is said to be rotatable if its variance–covariance matrix is invariant to the orthogonal rotation of coordinates. This means that the variance of the predicted values of the responses depends only on the distance from the design centre and not on the direction. The star arm for RCCD is calculated as

$$\alpha = 2^{f/4} \quad (5)$$

The choice of n_0 in RCCD is capital. It was recommended [11] to choose n_0 for which uniform precision is achieved. This property provides approximately a uniform value of the variance of the predicted response, var $y(x)$, inside a sphere of a given radius, i.e., 1.0. However RCCD does not exert control on the variance of the predicted response at a distance that approaches the radius at the perimeter of the design region [2].

Both kinds of CCD are often used in experimental designs. They are commonly applied in pharmaceutical research [5,12], chemical engineering [6], chemical synthesis [13], and especially, instrumental analysis [14–18].

The present paper deals with a computational procedure for optimizing CCD. The program previously evaluates the response function from the experimental data and then performs the searching of the coordinates corresponding to the maximal response within the experimental working range. The optimization

involves eigenanalysis and derivative techniques which leads to very reliable results.

2. Outline of the method

2.1. Coding the variables

Before embarking on calculations, the factor coding is extremely important for the analysis of data [7] and consists of replacing each variable or factor by its unit normal deviate scores. For each factor z_j (j from 1 to f) we have different values (called levels), the lowest of which is $z_j^{\min}$ and the highest of which is $z_j^{\max}$. Each level therefore belongs to the working range ($z_j^{\max}$, $z_j^{\min}$). Then we define the centre of the interval $z_j^0 = (z_j^{\max} + z_j^{\min})/2$ and its radius $r_z = (z_j^{\max} - z_j^{\min})/2$.

The point of coordinates ($z_1^0, z_2^0, \ldots z_f^0$) on the factor space is called the centre of the design. In order to obtain a dimensionless factor space coordinate system, the actual z coordinates are transformed in new coded coordinates, x, according to coding equation

$$x = \frac{z - z^0}{r_z}\alpha \tag{6}$$

In this dimensionless coordinate system, the upper and lower levels for the working range are $+\alpha$ and $-\alpha$ and the centre of the interval is 0. After coding, Eqs. 1–2 may be rewritten as

$$y = \beta_0 + \sum_{i=1}^{f}\beta_i x_i + \sum_{i=1}^{f}\sum_{j>i}^{f}\beta_{ij}x_i x_j + \sum_{i=1}^{f}\beta_{ii}x_i^2 \tag{7}$$

$$\hat{y} = b_0 + \sum_{i=1}^{f} b_i x_i + \sum_{i=1}^{f}\sum_{j>i}^{f} b_{ij}x_i x_j + \sum_{i=1}^{f} b_{ii}x_i^2 \tag{8}$$

Although here y, $\hat{y}$, β and b are referred to the coded coordinate system, we continue with the same notation like that in Eqs. 1-2 to avoid an extra amount of symbols. In the remainder, therefore, these symbols will have significance in the coded factor frame only.

2.2. Performing the fit

The problem of fitting Eq. 7 is quite easy to solve because in matrix form we have

$$\mathbf{y} = \mathbf{X}\boldsymbol{\beta} \tag{9}$$

Where $\mathbf{X}$ is the corresponding data matrix. In this matrix, each column represents the values of the factors in the following order: $1, x_1, x_2, \ldots x_f, x^2_1, x^2_2, \ldots x^2_f, x_1x_2, x_1x_3, \ldots x_1x_f, x_2x_3, x_2x_4, \ldots x_2x_f, \ldots x_{f-1}x_f$. The design matrix $\mathbf{D}$ is within $\mathbf{X}$ (columns $x_1, x_2, \ldots x_f$). The first 2^f rows correspond to a full factorial design where the levels of any factor are 1 or -1. The following $2f$ rows correspond to star points where the levels of any factor may be $\pm\alpha$ or 0. The last n_0 rows correspond to replications at the centre of the design (0,0,...0).

Therefore, the least squares estimate of the coefficients is the column vector

$$\mathbf{B} = (\mathbf{X}^{\mathrm{T}}\mathbf{X})^{-1}\mathbf{X}^{\mathrm{T}}\mathbf{y} \tag{10}$$

The estimation of the residual variance is

$$s^2_{\mathrm{res}} = \frac{\sum(\hat{y}_i - y_i)^2}{N - m} \tag{11}$$

and the coefficient variance–covariance matrix is

$$\mathbf{COV} = (\mathbf{X}^{\mathrm{T}}\mathbf{X})^{-1}s^2_{\mathrm{res}} \tag{12}$$

Once the multiple regression computations have been made, an ANOVA is performed for testing the adequacy of the model [5].

In order to estimate the adequacy of the fit, use is made of the Fisher F test:

$$F = s^2_{\mathrm{fit}}/s^2_{\mathrm{e}}$$

where s^2_{fit} is the lack of fit variance given by

$$s^2_{\mathrm{fit}} = \frac{s^2_{\mathrm{res}}(N-m) - s^2_{\mathrm{e}}(n_0 - 1)}{N - m - n_0 + 1} \tag{13}$$

The pure error variance, s^2_{e}, is calculated from the n_0 central runs.

The model equation is considered to be adequate if F is less than the tabulated value $F(N - m - n_0 + 1, n_0 - 1)$ at a 0.95 confidence level.

The variance of each regression coefficient b_i is easily obtained from the diagonal elements of the variance–covariance matrix [5,6,19]. Once the variance s^2_{bi} is known, the coefficient is tested for significance according to the Student-t test:

$$t = |b_i|/s_{bi}$$

a given coefficient will be significant if t is greater than the tabulated value $t(N - m)$ at a 0.95 confidence level [20–22].

2.3. Finding the optimum

Once the coefficients of the model equation are known, the maximum response surface occurs for those $\mathbf{x}^*$ values for which the partial derivatives are simultaneously zero [23]

$$\frac{\partial y}{\partial x_i}=0 \quad (i=1,2,\ldots f) \tag{14}$$

If such a maximum exists, the column vector $\mathbf{x}^*$ may be calculated from

$$\mathbf{x}^*=\frac{-\mathbf{S}^{-1}\mathbf{s}}{2} \tag{15}$$

where $\mathbf{x}^*$ is the column vector of the optimum coordinates $x^*_1, x^{*2},\ldots x^*_f$, $\mathbf{s}$ is the column vector whose components are the single order coefficients $b_1, b_2,\ldots b_f$, and $\mathbf{S}$ is an $f\times f$ matrix whose diagonal contains the second order coefficients b_{ii} and where any of the diagonal elements ij equals to the half value of the corresponding second order mixed coefficient, $b_{ij}/2$.

The stationary point $\mathbf{x}^*$ would not necessarily be a maximum. It could be a minimum or a saddle point on the fitted response surface. Accordingly, a canonical analysis should be previously performed [19,24]. The canonical analysis consists of noting the signs of the eigenvalues λ_i of the matrix $\mathbf{S}$. This is accomplished by finding the solutions of the fth order polynomial provided by the equation

$$\det(\mathbf{S}-\lambda\mathbf{I})=0 \tag{16}$$

where *det* means the determinant of, and $\mathbf{I}$ is the identity matrix. The signs of λ_i reflect the nature of the stationary point. If all $\lambda_i<0$ such a point is a maximum. If all $\lambda_i>0$ then the stationary point is a minimum. When the λ_i values differ in the sign the stationary point is a minimax or saddle point. The eigenvalues may be easily obtained for computational purposes from the Jacobi's technique [25].

3. Computational details

The method outlined above was implemented in QuickBasic for IBM compatible PC XT or AT. For avoiding slow computations it should be advisable to use at least a 80286 processor. The program, called CCDOPT, has been divided into blocks for a better understanding of its structure. The principal procedures of CCDOPT are discussed below.

The number of factors f (in the range 2–8), the number of replications n_0 and the type of design (orthogonal/rotatable) are typed from keyboard as data inputs. The maximum number of factors is here reduced to 8 according to the limitation when using the QuickBasic dynamic huge arrays, which for exceeding 128 K of memory they must be a power of 2 [26]. The experimental response corresponding to each run is entered from keyboard using the DATAIN procedure. The keyboard inputs are saved in an ASCII file for possible further use.

According to the type of design selected, the axial spacing α is calculated either by Eq. 4 or by Eq. 5.

The encoded data matrix $\mathbf{X}$, whose elements (0, ± 1 or $\pm\alpha$) are arranged as indicated above, is directly generated by the procedure XMATRIX.

Three procedures dealing with matricial computations are used in a program called TRANSMATRIX for obtaining transposed matrices, INVMATRIX, which calculates the inverse of a given matrix, and DMULMATRIX to multiply suitable matrices. The main program calls to these three procedures for evaluating the coefficients of the model equation by multiple linear regression according to Eq. 10. INVMATRIX and DMULMATRIX are also utilized for obtaining the stationary point from Eq. 15.

The procedure EIGENVALUE determines the eigenvalues of the matrix $\mathbf{S}$ cited above by using Jacobi's technique.

The main program produces the following outputs (monitor display or printer):

(i) An ANOVA of the regression model, indicating the sources of variation, and their respective degrees of freedom, sum of squares and variances. The experimental and tabulated values of the Fisher F test are also indicated as well as the correlation coefficient of the fit.

(ii) The values of the slope, intercept and correlation coefficient of the plot of the estimated vs. observed response.

(iii) The estimated regression coefficients and their standard deviations, suggesting from the Student-t test (at a 0.95 confidence level) if it is significant or not significant.

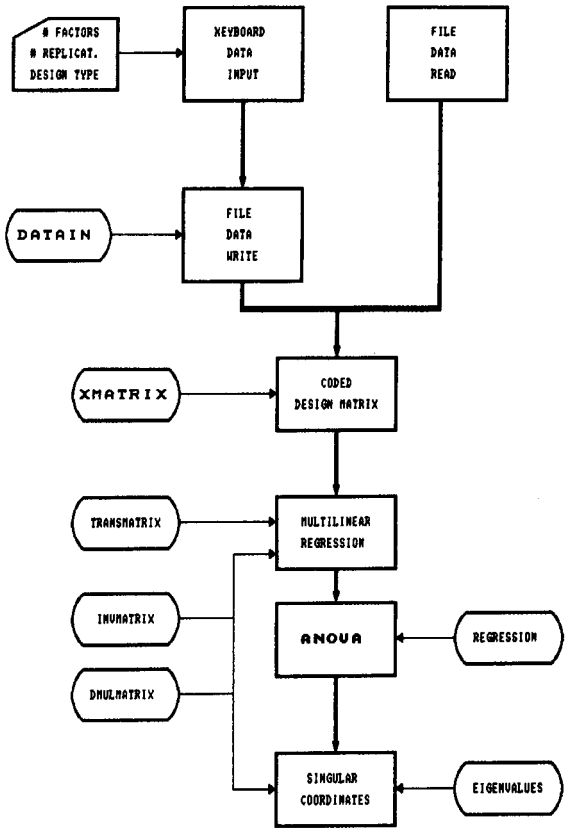

Fig. 1. Flow logic scheme (block diagram) for the program CCDOPT.

(iv) The eigenvalues of matrix **S**, showing if the stationary point is a maximum, a minimum or a minimax.

(v) The coded and uncoded coordinates of the singular point.

For the sake of clearness the flow logic of the program (as block diagram) is depicted in Fig. 1.

Listings of the program are available from the authors upon request.

4. Worked examples

In order to show how the program works and for the sake of illustration we have selected three worked examples, based on the literature.

Example 1. The data for this example were taken from Morgan et al. [8]. In an investigation of the effects of burner height (X1) and lamp current (X2) upon the signal-to-noise (S/N) ratio response in an atomic absorption spectrophotometer, it was decided to use an orthogonal two-factor CCD with five central points. The minimum and maximum values of the factors were: $X1 = 3.2$–10.8 mm and $X2 = 2.93$–13.07 mA. The design matrix and the responses obtained are given in Table 1. The program CCDOPT selecting an orthogonal design, following Ref. [8], produces the following Table of outputs:

Table 1
Design matrix and responses for example 1

Factor levels		Response S/N ratio
$X1$	$X2$	
−1	−1	41
1	−1	71
−1	1	64
1	1	74
−1.267	0	76
1.267	0	91
0	−1.267	44
0	1.267	75
0	0	80
0	0	83
0	0	97
0	0	75
0	0	100

ANOVA of regression model

Source	Deg. freedom	Sum. squares	Variance
Regression	5	3.10115D+003	6.20230D+002
Residual	7	6.07618D+002	8.68026D+001
Replication	4	4.78000D+002	1.19500D+002
Lack of fit	3	1.29618D+002	4.32060D+001
Total	12	3.70877D+003	3.09064D+002

F experimental	F tabulated at 95%	Correlation coeff.
0.36	6.59	0.914422

Computation time (s): 0.77

Model parameters		
Coeffi-cients	Standard dev.	Significance
$b(0)=$	8.73925D+001±4.12767D+000	Significant
$b(1)=$	8.18312D+000±3.46961D+000	Non significant
$b(2)=$	9.05295D+000±3.46961D+000	Significant
$b(1,1)=$	−3.97332D+000±4.10368D+000	Non significant
$b(2,2)=$	−1.89239D+001±4.10368D+000	Significant
$b(1,2)=$	−5.00000D+000±4.65839D+000	Non significant

Searching singular coordinates (Max or Min) Eigenvalues	
No. iterations = 2	
(1):	−3.56636D+000
(2):	−1.93309D+001
There is a maximum	
Coordinates of the singular point	
Coded	
(1)	9.58969D−001
(2)	1.12506D−001
Uncoded	
(1)	9.87615D+000 mm
(2)	8.45020D+000 mA

Allowing for that the involved factors are two, it is possible to obtain a 3D response–surface plot as is observed in Fig. 2. The plot has been drawn by using the SIGMAPLOT 5.0 package. (Other mathematical–statistical packages may be useful as STATGRAPHICS or CSS STATISTICA.)

The maximum S/N ratio appears at the coded values $X1=0.96$ and $X2=0.11$, in excellent agreement with the result obtained by Morgan et al. [8].

Example 2. Villén et al. [15] have applied RCCD to the optimization on the direct analysis of trace amounts components by using a programmed temperature vaporizer (PTV) in the solvent split mode. PVT can be used for internal gas chromatographic concentration of an extract, by prior trapping and at the same time for analyzing trace amounts of organic compounds. Synthetic mixtures of ethyl pentanoate, *trans*-2-hexenal, hexyl acetate, *trans*-2-hexen-1-ol, diethyl succinate, α-terpineol, 2-phenylethyl acetate and 2-phenylethanol, in ethanol–water mixtures (12:88 v/v)

Table 2
Design matrix and responses for examples 2, 3 and 4

Factor levels			Responses		
$X1$	$X2$	$X3$	SAPA	i_d	HAP
−1	−1	−1	34.58	98.60	38
1	−1	−1	103.42	60.45	60
−1	1	−1	31.19	174.50	30
1	1	−1	74.24	124.45	22
−1	−1	1	31.53	109.85	96
1	−1	1	80.75	69.95	150
−1	1	1	38.72	189.00	94
1	1	1	71.69	139.25	116
$-\alpha$ [a]	0	0	11.53	177.55	92
α	0	0	87.52	113.10	12
0	$-\alpha$	0	66.95	63.65	10
0	α	0	42.12	186.20	114
0	0	$-\alpha$	72.37	122.95	8
0	0	α	45.81	118.35	162
0	0	0	50.14	131.45	114
0	0	0	60.39	138.80	116
0	0	0	61.13	135.25	114
0	0	0	56.33	134.20	112
0	0	0	57.97	137.90	110
0	0	0	57.45	131.20	110

[a] The α values for the examples 2, 3 and 4 are 1.682, 1.525 and 1.682, respectively.

were analysed. Three factors were considered: Sample volume ($X1$), flow rate during the splitting period ($X2$) and initial temperature on the PTV ($X3$). The sums of

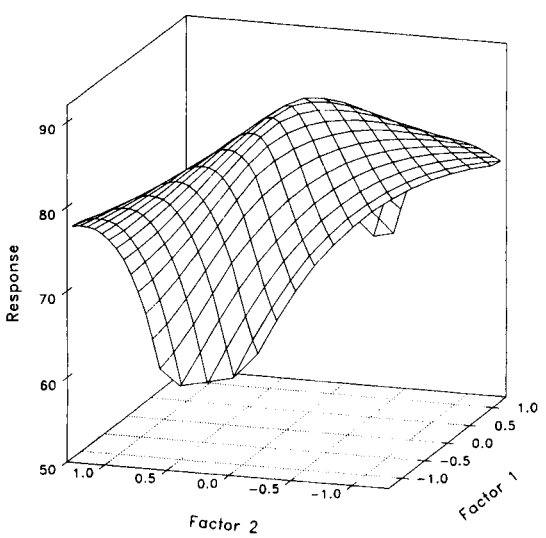

Fig. 2. 3D response-surface for example 1.

absolute peak areas (SAPA) (using a flame ionization detector) on the chromatogram were considered as the response values. The minimum and maximum values for the considered factors were: $X1 = 25$–250 μl, $X2 = 50$–500 ml/min, $X3 = 10$–50°C.

The design matrix and response values are collected in Table 2. The application of CCDOPT selecting a rotatable design gives the following outputs:

ANOVA of regression model

Source	Deg. freedom	Sum. squares	Variance
Regression	9	8.86622D+003	9.85136D+002
Residual	10	2.74557D+002	2.74557D+001
Replication	5	7.68695D+001	1.53739D+001
Lack of fit	5	1.97687D+002	3.95374D+001
Total	19	9.14078D+003	4.81094D+002

F experimental	*F* tabulated at 95%	Correlation coeff.
2.57	5.05	0.984867

Computation time (s): 4.28

Model parameters

Coefficients	Standard dev.	Significance
$b(0)$ =	5.71046D+001 ± 2.13707D+000	Significant
$b(1)$ =	2.35678D+001 ± 1.41781D+000	Significant
$b(2)$ =	−5.57934D+000 ± 1.41781D+000	Significant
$b(3)$ =	−4.78933D+000 ± 1.41781D+000	Significant
$b(1,1)$ =	−1.87010D+000 ± 1.38002D+000	Non significant
$b(2,2)$ =	−9.92304D−002 ± 1.38002D+000	Non significant
$b(3,3)$ =	1.51081D+000 ± 1.38002D+000	Non significant
$b(1,2)$ =	−5.25500D+000 ± 1.85255D+000	Significant
$b(1,3)$ =	−3.71250D+000 ± 1.85255D+000	Non significant
$b(2,3)$ =	3.83750D+000 ± 1.85255D+000	Non significant

Searching singular coordinates (Max or Min)
Eigenvalues

No. iterations = 9

(1):	−3.79452D+000
(2):	4.30323D+000
(3):	−9.67230D−001

Minimax at the effective range

Here the response surface does not present either maximum or minimum, and accordingly, the 'best' experimental conditions may be empirically established. Analyses carried out by injecting 25 μl, with a flow during splitting maximum (500 ml/min) and maintaining the initial PTV temperature at 30°C gives good results [15].

Example 3. The influence of instrumental and chemical factors affecting the differential pulse polarographic measurements of Pb(II) has been studied by López et al. [14]. After a preliminary fractional design (2^{7-2}) for selecting the significant factors among seven possible ones, three factors were chosen.

The potential increment between pulses ($X1$), the pulse amplitude ($X2$) and the pH ($X3$). The response is the peak current (i_d, in nA). The minimum and maximum values of the factors are: $X1 = 2$–8 mV, $X2 = 25$–85 mV, $X3 = 0.74$–2.26.

The design matrix and response values at a constant Pb(II) concentration of 1000 ng cm^{-3} are also indicated in Table 2.

By applying CCDOPT choosing an orthogonal design, the following outputs are obtained:

ANOVA of regression model

Source	Deg. freedom	Sum. squares	Variance
Regression	9	2.53551D+004	2.81724D+003
Residual	10	4.45115D+002	4.45115D+001
Replication	5	5.03550D+001	1.00710D+001
Lack of fit	5	3.94760D+002	7.89520D+001
Total	19	2.58002D+004	1.35791D+003

F experimental	*F* tabulated at 95%	Correlation coeff.
7.84	5.05	0.991336

Computation time (s): 4.29
Model parameters

Coefficients	Standard dev.	Significance
$b(0)$ =	1.35756D+002 ± 2.67748D+000	Significant
$b(1)$ =	−2.18268D+001 ± 1.87573D+000	Significant
$b(2)$ =	3.75646D+001 ± 1.87573D+000	Significant
$b(3)$ =	3.40164D+000 ± 1.87573D+000	Non significant
$b(1,1)$ =	2.28510D+000 ± 2.02878D+000	Non significant
$b(2,2)$ =	−6.48673D+000 ± 2.02878D+000	Significant
$b(3,3)$ =	−8.32495D+000 ± 2.02878D+000	Significant

$b(1,2)=$	−2.71875D+000±2.35880D+000	Non significant
$b(1,3)=$	−1.81250D−001±2.35880D+000	Non significant
$b(2,3)=$	1.06875D+000±2.35880D+000	Non significant

Searching singular coordinates (Max or Min)

Eigenvalues

No. iterations = 8

(1):	2.49360D+000
(2):	−6.54403D+000
(3):	−8.47615D+000

Minimax at the effective range

Now the response-surface also exhibits a saddle point. Similarly to the later example, empirical procedures may be applied for obtaining a 'good enough' response. The most favourable experimental conditions within the corresponding limits are $X1=2$ mV, $X2=85$ mV and $X3=1.5$. It is remarkable that in spite of the prior selection of significant factors, a saddle point was found. Perhaps a previous selection of the proper parameter range would have been more suitable.

Example 4. This example deals with an optimization program in electrothermal atomic absorption spectrometry. The objective of the study is to establish optimal conditions for the atomization of lead in mineralized beef liver [18,27]. The response surface chosen is the height of the absorbance peak (HAP) at 283.3 nm at a fixed lead concentration, expressed in mA. Three factors have been studied: charring temperature ($X1$), charring speed ($X2$) representing the laps of time necessary to pass from the drying temperature of 100°C to the charring temperature and atomization temperature ($X3$) (the atomization ramp is constant and equals to 2 s). The minimum and maximum values of the factors are: $X1=130$–1270°C, $X2=5$–35 s, $X3=1020$–2700°C.

By using CCDOPT selecting a rotatable design, the following outputs are obtained:

ANOVA of regression model

Source	Deg. freedom	Sum. squares	Variance
Regression	9	3.31423D+004	3.68247D+003
Residual	10	1.03777D+004	1.03777D+003
Replication	5	2.93333D+001	5.86667D+000
Lack of fit	5	1.03484D+004	2.06968D+003
Total	19	4.35200D+004	2.29053D+003

F experimental	*F* tabulated at 95%	Correlation coeff.
352.79	5.05	0.872663

Computation time (s): 4.23

Model parameters

Coefficients	Standard dev.	Significance
$b(0)=$	1.12274D+002±1.31387D+001	Significant
$b(1)=$	−3.26250D+000±8.71673D+000	Non significant
$b(2)=$	6.80380D+000±8.71673D+000	Non significant
$b(3)=$	4.13690D+001±8.71673D+000	Significant
$b(1,1)=$	−1.88670D+001±8.48438D+000	Non significant
$b(2,2)=$	−1.53323D+001±8.48438D+000	Non significant
$b(3,3)=$	−7.20258D+000±8.48438D+000	Non significant
$b(1,2)=$	−7.75000D+000±1.13895D+001	Non significant
$b(1,3)=$	7.75000D+000±1.13895D+001	Non significant
$b(2,3)=$	1.25000D+000±1.13895D+001	Non significant

Searching singular coordinates (Max or Min)

Eigenvalues

No. iterations = 10

(1):	−2.22348D+001
(2):	−1.31674D+001
(3):	−5.99965D+000

There is a maximum

Coordinates of the singular point

Coded

(1)	5.19551D−001
(2)	2.19807D−001
(3)	3.17041D+000

Uncoded	
(1)	8.76067D + 002 deg.
(2)	2.19602D + 001 s
(3)	3.44332D + 003 deg.

In this case the maximum in the surface occurs at the uncoded values: $X1 = 876°C$, $X2 = 22$ s and $X3 = 3443°C$. Considering that the optimum value of $X3$ is far away from its maximum working range experimentally available, it would be taken as the maximum value, $X3 = 2700°C$ [27]. Thus, the practical optimum will be: $X1 = 876°C$, $X2 = 22$ s and $X3 = 2700°C$. It is also noticeable that when $X2$ is non significant, any arbitrary value for this factor would be selected. Statistically speaking, after deletion of non significant coefficients, the remainder function is not suitable for optimization purposes.

5. Conclusion

The proposed program suitably performs the optimization of experimental central composite designs and may be of interest in any experimental scientific research.

Acknowledgements

Financial support from the Dirección General de Investigación Científica y Técnica de España through Project PB92-0678 is gratefully acknowledged.

References

[1] W.J. Hill and W.G. Hunter, Technometrics, 8 (1966) 571.
[2] R.H. Myers, A.I. Khuri and W.H. Carter Jr., Technometrics, 31 (1989) 137.
[3] R. Mead and D.J. Pike, Biometrics, 31 (1975) 803.
[4] A.C. Atkinson, Int. Stat. Rev. 56 (1988) 99.
[5] A.G. González, Int. J. Pharm., 97 (1993) 149.
[6] S. Akhnazarova and V. Kafarov, Experimental Optimization in Chemistry and Chemical Engineering, Mir, Moscow, 1982.
[7] P.C. Meier and R.E. Zünd, Statistical Methods in Analytical Chemistry, Wiley, New York, 1993.
[8] E. Morgan, K.W. Burton and P.A. Church, Chem. Int. Lab. Syst., 5 (1989) 283; R.S. Strange, J. Chem. Educ., 67 (1990) 113.
[9] R.G. Brereton, Chemometrics. Application of Mathematics and Statistics to Laboratory Systems, Ellis Horwood, Chichester, 1990.
[10] G.E.P. Box and K.B. Wilson, J. Roy. Stat. Soc. Ser. B., 13 (1951) 1.
[11] G.E.P. Box and J.S. Hunter, Ann. Math. Stat., 28 (1957) 195.
[12] N.A. Armstrong and K.C. James, Understanding Experimental Design and Interpretation in Pharmaceutics, Ellis Horwood, Chichester, 1990.
[13] H. van Ryswyk and G.R. van Hecke, J. Chem. Educ., 68 (1991) 878.
[14] B. López, G. Frutos, P. Sanz and J.P. Martin, Analyst, 118 (1993) 59.
[15] J. Villén, F.J. Señoráns, M. Herraiz, G. Reglero and J. Tabera, J. Chromatogr. Sci., 30 (1992) 261.
[16] R.M. Marcé, M. Calull, J.C. Olucha, F. Borrull, F.X. Rius and J. Zupan, Anal. Chim. Acta, 259 (1992) 237.
[17] J.A. Palasota and S.N. Deming, J. Chem. Educ., 69 (1992) 560.
[18] M. Feinberg and G. Schnitzer, Analusis, 11 (1983) 299.
[19] E. Morgan, Chemometrics. Experimental Designs, Wiley, Chichester, 1991.
[20] Y. Lacroix, Analyse Chimie, Interprétation des Résultats par le Calcul Statistique, Masson et Cie, Paris, 1962.
[21] K. Doerfel, Statistik in der Analitische Chemie, 4th edn., VCH, Weinheim, 1987.
[22] R.J. Tallarida and R.B. Murray, Manual of Pharmacologic Calculations with Computer Programs, Springer, New York, 2nd edn., 1987.
[23] S.N. Deming and S.L. Morgan, Experimental Design: a Chemometric Approach, Elsevier, Amsterdam, 1987.
[24] G.E.P. Box and N.R. Draper, Empirical Model Building and Response Surfaces, Wiley, New York, 1987.
[25] K. Ebert, H. Ederer and T.L. Isenhour, Computer Applications in Chemistry, VCH, Weinheim, 1989.
[26] Microsoft QuickBasic 4.5, User manual, Microsoft Corporation, 1990.
[27] C.J. Ducauze, Chemometrics and Analytical Chemistry, in the II Jornadas Andaluzas sobre Avances en Análisis Químico, Huelva – Sevilla, 26–27 September 1991.
[28] M. Meloun, J. Havel and E. Högfeldt, Computation of Solution Equilibria, Ellis Horwood, Wiley, Chichester, 1988.

ELSEVIER

Analytica Chimica Acta 298 (1994) 75–85

ANALYTICA CHIMICA ACTA

Principles for structure generation of organic isomers from molecular formula

Chang-Yu Hu, Lu Xu *

Applied Spectroscopy Laboratory, Changchun Institute of Applied Chemistry, Academia Sinica, Changchun 130022, Jilin, China

Received 5 April 1994; revised manuscript received 17 May 1994

Abstract

An expert system for the elucidation of the structure of organic compounds (ESESOC) has been developed. The heart of the ESESOC is formed by the structure generator as an integral part, which receives the specific type of information (molecular formula, substructure constraints, etc.) and produces an exhaustive and irredundant list of candidate structures. In this article, the principle of structure generation of organic isomers from molecular formula in the ESESOC system is described. Two types of structure fragments, component and segment, are introduced. The combinatorial algorithms for the composition and partition of integer are applied to decompose the molecular formula into component vectors and segment sets. For the generation of all candidate structures, the bonding adjacency matrix was filled by using a heuristic depth-first method to search the structure generation tree.

Keywords: Expert system; Combinatorial algorithm; Isomers; Structure elucidation

1. Introduction

Exhaustive generation of constitutional isomers of organic compounds is a problem which has fascinated chemists and mathematicians for a long time. It is an important tool involved in structure elucidation [1–13], organic synthesis [14–16], molecular design (QSAR/QSPR) [17–19], and other structure problems [20–24]. Many solutions have been published in the literature. Examples include Stanford's CONGEN [1,2] and GENOA [3] of the DENDRAL system, Munk's ASSEMBLE [4] and COCOA [5] for the CASE system, Sasaki's CHEMICS system [6,7], etc., for structure elucidation. Structural generation must be exhaustive and irredundant. In Stanford's DENDRAL system, a scheme based on the sequential execution of the "partition" and "labeling" steps by taking into account topological symmetry was developed [1,2]. In Munk's CASE system, all possible combinations for connecting the remaining atoms were explored by using a depth-first search algorithm. An elegant mechanism based on filling the connectivity stack [6] in a systematic manner was devised in the CHEMICS system. However, it is extremely time consuming to consider all the permutations for isomorphism check. We believed that some judi-

* Corresponding author.

SSDI 0003-2670(94)00233-C

cious choices must be considered to reduce the number of tested permutations in the practical use for large molecules. However, we do not know how to do it, and Sasaki and coworkers have never explained it. Similar methods were developed by Bohanec and Zupan [8], Faulon [9], etc.

In our laboratory, an interactive program ESESOC (expert system for the elucidation of the structures of organic compounds) has been developed to reduce comprehensive spectroscopic information to its structural implications. The structure generation method used in ESESOC-I [12] is similar to the scheme developed by Munk. In the ESESOC-II system, since we have reported our method for structure generation from a set of structural fragments, in which the abbreviated bonding adjacency matrix (BAM) is filled alternatively by depth-first search strategy [13], some new developments has been achieved, a new element, Si, is added to the system, and the current ESESOC system can be used to process the organic compounds containing eleven elements, viz. C, H, O, N, P, S, Si and halogens.

2. Components and segments

In the ESESOC system, two types of structure fragments are introduced, i.e., component and segment. The component is defined as the element component of the basic structure unit. There is a total of 22 components for the 11 atomic species (Table 1).

The basic structure units with bond attributes and some combinations of them are defined as segments. There are 109 segments selected by trial and error method in the ESESOC-II system (see Table 2), which can be used to form all the organic compounds containing C, H, O, N, P, S, Si, F, Cl, Br and I except some small molecules, such as CH_4, CH_3CH_3, CH_3OH, etc.

Table 1
22 components for 11 atomic elements

1 CH_3	9 NH_2	17 SiH
2 CH_2	10 NH	18 Si
3 CH	11 N	19 F
4 C	12 PH_2	20 Cl
5 OH	13 PH	21 Br
6 O	14 P	22 I
7 SH	15 SiH_3	
8 S	16 SiH_2	

8	0	0	7	1	0	6	2	0	5	3	0
4	4	0	3	5	0	2	6	0	1	7	0
0	8	0	7	0	1	6	1	1	5	2	1
4	3	1	3	4	1	2	5	1	1	6	1
1	7	1	6	0	2	5	1	2	4	2	2
3	3	2	2	4	2	1	5	2	0	6	2
5	0	3	4	1	3	3	2	3	2	3	3
1	4	3	0	5	3	4	0	4	3	1	4
2	2	4	1	3	4	0	4	4	3	0	5
2	1	5	1	2	5	0	3	5	2	0	6
1	1	6	0	2	6	1	0	7	0	1	7
0	0	8									

Scheme 1.

3. Combinatorial problem

3.1. Composition of integer

By a composition of N into K parts, we mean a representation of the form

$$N = \sum_{i=1}^{K} r_i \quad (r_i \geqslant 0)$$

where N, K and r_i are integers and the order of the summands is significant. There are exactly 45 compositions of 8 into 3 parts, as given in Scheme 1.

3.2. Partition of integer

If N is a positive integer, then a representation

$$N = \sum_{i=1}^{K} r_i \quad (r_i \geqslant r_{i+1} \geqslant 0)$$

is called a partition of N, where K and r_i are integers, and the order of the summands is not important. The eleven partitions of 6 are, as given in Scheme 2.

Table 2
109 segments used to form all organic compounds containing C, H, O, N, P, S, Si, F, Cl, Br and I

1	$-CH_2-$	38	O=C=	75	ArS
2	CH_3CH_2-	39	S=C=	76	$-S(\rightarrow O)-$
3	$CH_2=$	40	NH=C=	77	$CH_3S(\rightarrow O)-$
4	$\rangle CH-$	41	$N^{\ominus}=N^{\oplus}=C=$	78	$ArS(\rightarrow O)$
5	$CH_3CH\langle$	42	$C^{\ominus}\equiv N^{\oplus}-$	79	$-S(\rightarrow O)_2-$
6	$(CH_3)_2CH-$	43	HO–	80	$CH_3S(\rightarrow O)_2-$
7	–CH=	44	–O–	81	PH_2-
8	$CH_3CH=$	45	CH_3O-	82	$PH_2(\rightarrow O)-$
9	ArCH [a]	46	ArO	83	–PH–
10	–CH=O	47	NH_2-	84	CH_3-PH-
11	–CH=S	48	–NH–	85	$-PH(\rightarrow O)-$
12	–CH=NH	49	CH_3NH-	86	$CH_3PH(\rightarrow O)-$
13	$N^{\ominus}=N^{\oplus}=CH-$	50	ArNH	87	$\rangle P-$
14	$\rangle C\langle$	51	$\rangle N-$	88	$CH_3P\langle$
15	$CH_3\overset{\vert}{C}-$	52	$CH_3N\langle$	89	$(CH_3)_2P-$
16	$(CH_3)_2C\langle$	53	$(CH_3)_2N-$	90	$\rangle P(\rightarrow O)-$
17	$(CH_3)_3C-$	54	–N=	91	$CH_3P(\rightarrow O)\langle$
18	$\rangle C=$	55	$CH_3N=$	92	$(CH_3)_2P(\rightarrow O)-$
19	$CH_3\overset{\vert}{C}=$	56	O=N–	93	$\rangle P(\rightarrow S)-$
20	$(CH_3)_2C=$	57	S=N–	94	$CH_3P(\rightarrow S)\langle$
21	$\rangle C=O$	58	$(O\leftarrow)S=N-$	95	$(CH_3)_2P(\rightarrow S)-$
22	$\rangle C=S$	59	NH=N–	96	$-SiH_3$
23	$\rangle C=NH$	60	$N^{\ominus}=N^{\oplus}=N-$	97	$-SiH_2-$
24	$\rangle C(=N^{\oplus}=N^{\ominus})$	61	ArN	98	$(CH_3)SiH_2-$
25	$CH_3C(=O)-$	62	$\rangle N(\rightarrow O)-$	99	$-SiH\langle$
26	$CH_3C(=S)-$	63	$CH_3N(\rightarrow O)\langle$	100	$(CH_3)SiH\langle$
27	$CH_3C(=NH)-$	64	$(CH_3)_2N(\rightarrow O)-$	101	$(CH_3)_2SiH-$
28	$CH_3C(=N^{\oplus}=N^{\ominus})-$	65	$-N(\rightarrow O)=$	102	$\rangle Si\langle$
29	ArC– [b]	66	$CH_3N(\rightarrow O)=$	103	$CH_3\overset{\vert}{Si}-$
30	CH_3ArC	67	$O=N(\rightarrow O)-$	104	$(CH_3)_2Si\langle$
31	ArC [c]	68	$S=N(\rightarrow O)-$	105	$(CH_3)_3Si-$
32	–C≡	69	$NH=N(\rightarrow O)-$	106	F–
33	$CH_3-C\equiv$	70	$N^{\ominus}=N^{\oplus}=N(\rightarrow O)-$	107	Cl–
34	CH≡C–	71	ArNO	107	Br–
35	N≡C–	72	HS–	109	I–
36	$N(\rightarrow O)\equiv C-$	73	–S–		
37	=C=	74	CH_3S-		

[a] Aromatic.
[b] Stands for $\rangle\overset{\vert}{Ar}\cdot$.
[c] Stands for $Ar\rangle\overset{\vert}{Ar}\cdot$.

6 = 6
5+1
4+2
4+1+1
3+3
3+2+1
3+1+1+1
2+2+2
2+2+1+1
2+1+1+1+1
1+1+1+1+1+1

Scheme 2.

4. Exhaustive generation of the component vectors from molecular formula

Let n_i ($i = 1, 2, \ldots, 22$) be the number of the ith component in Table 1, then the vector **N** (n_1, n_2, $n_3, \ldots, n_{22}$) is defined as a component vector. The combinatorial algorithms for the composition and partition of integer are applied to decompose the molecular formula into component vectors. Taking $C_6H_8N_2O$ as an example, the component vectors are derived by the following steps:

(1) Distribute the hydrogen atoms over the non-hydrogen atomic species by using the composition algorithm. In the example, there are 8 hydrogen atoms and 3 non-hydrogen atomic species. Constrained by the molecular formula (the part for 2 nitrogen atoms should be less than or equal to 4, and the one for 1 oxygen atom should be less than or equal to 1), 10 out of 45 compositions (listed above) are generated, as shown in Scheme 3.

8	0	0	7	1	0	6	2	0	5	3	0
4	4	0	7	0	1	6	1	1	5	2	1
4	3	1	3	4	1						

Scheme 3.

It means that the molecular formula $C_6H_8N_2O$ is decomposed as $(C_6H_8)(N_2)(O)$, $(C_6H_7)(N_2H)(O)$, $(C_6H_6)(N_2H_2)(O)$, $(C_6H_5)(N_2H_3)(O)$, $(C_6H_4)(N_2H_4)(O)$, $(C_6H_7)(N_2)(OH)$, $(C_6H_6)(N_2H)(OH)$, $(C_6H_5)(N_2H_2)(OH)$, $(C_6H_4)(N_2H_3)(OH)$, $(C_6H_3)(N_2H_4)(OH)$.

(2) Partition the hydrogen atoms for every non-hydrogen atoms. For $(C_6H_6)(N_2H_2)(O)$, the 6 hydrogen atoms are distributed over the 6 carbon atoms and the results are, as shown in Scheme 4.

The 2 hydrogen atoms are distributed over the 2 nitrogen atoms, and the results are

2 = 2 + 0 NH_2 N
1 + 1 NH NH

(3) Considering all combinations, the 14 component vectors generated from $(C_6H_5)(N_2H_2)(O)$ are listed in Table 3. By repeating steps 2 and 3,

Table 3
The 14 component vectors generated from (C_6H_6) (N_2H_2) (O)

Component vector No.	Component																				
	CH_3	CH_2	CH	C	OH	O	SH	S	NH_2	NH	N	PH_2	PH	P	SiH_3	SiH_2	SiH	Si	F	Cl	Br	I
1	2	0	0	4	0	1	0	0	1	0	1	0	0	0	0	0	0	0	0	0	0	0
2	2	0	0	4	0	1	0	0	0	2	0	0	0	0	0	0	0	0	0	0	0	0
3	1	1	1	3	0	1	0	0	1	0	1	0	0	0	0	0	0	0	0	0	0	0
4	1	1	1	3	0	1	0	0	0	2	0	0	0	0	0	0	0	0	0	0	0	0
5	1	0	3	2	0	1	0	0	1	0	1	0	0	0	0	0	0	0	0	0	0	0
6	1	0	3	2	0	1	0	0	0	2	0	0	0	0	0	0	0	0	0	0	0	0
7	0	3	0	3	0	1	0	0	1	0	1	0	0	0	0	0	0	0	0	0	0	0
8	0	3	0	3	0	1	0	0	0	2	0	0	0	0	0	0	0	0	0	0	0	0
9	0	2	2	2	0	1	0	0	1	0	1	0	0	0	0	0	0	0	0	0	0	0
10	0	2	2	2	0	1	0	0	0	2	0	0	0	0	0	0	0	0	0	0	0	0
11	0	1	4	1	0	1	0	0	1	0	1	0	0	0	0	0	0	0	0	0	0	0
12	0	1	4	1	0	1	0	0	0	2	0	0	0	0	0	0	0	0	0	0	0	0
13	0	0	6	0	0	1	0	0	1	0	1	0	0	0	0	0	0	0	0	0	0	0
14	0	0	6	0	0	1	0	0	0	2	0	0	0	0	0	0	0	0	0	0	0	0

6 = 3 + 3 + 0 + 0 + 0 + 0	CH_3	CH_3	C	C	C	C
3 + 2 + 1 + 0 + 0 + 0	CH_3	CH_2	CH	C	C	C
3 + 1 + 1 + 1 + 0 + 0	CH_3	CH	CH	CH	C	C
2 + 2 + 2 + 0 + 0 + 0	CH_2	CH_2	CH_2	C	C	C
2 + 2 + 1 + 1 + 0 + 0	CH_2	CH_2	CH	CH	C	C
2 + 1 + 1 + 1 + 1 + 0	CH_2	CH	CH	CH	CH	C
1 + 1 + 1 + 1 + 1 + 1	CH	CH	CH	CH	CH	CH

Scheme 4.

an exhaustive list of component vectors is obtained.

5. Exhaustive generation of segment vectors from component vector

Let l_i ($i = 1, 2, \ldots, 109$) be the number of the ith segment in Table 2, then the vector **L** ($l_1, l_2, \ldots, l_{109}$) is defined as a segment vector. The segment vectors can be generated exhaustively by the following steps:

(1) Let l_{42}, l_{47}, l_{72}, l_{96}, l_{106}, l_{107}, l_{108}, l_{109} be n_5, n_7, n_9, n_{15}, n_{19}, n_{20}, n_{21}, n_{22}, respectively.

(2) By using the composition algorithm, n_2 is decomposed into l_1, l_2, l_3; n_4 into $l_{14}, l_{15}, \ldots, l_{42}$. All the decompositions are constrained by n_1 (the number of CH_3), n_6, n_8, n_{10} (the number of O, S, NH), etc. Let NCH (the number of component CH) be $(n_3 - l_{34})$; then NCH is decomposed into $l_4, l_5, \ldots, l_{13}$. Let NN (the number of component N) be $(n_9 - 2 * l_{13} - 2 * l_{24} - 2 * l_{28} - l_{35} - l_{36} - 2 * l_{41} - l_{42})$; then NN is decomposed into $l_{51}, l_{52}, \ldots, l_{71}$. By continuing the mentioned process, the numbers of other segments can be obtained.

Taking the last component vector of Table 3 (component vector No. 14 in Table 3) as an example, the partial segment vectors generated from it are listed in Table 4 (only non-zero elements are listed, the values of other elements are zero).

A series of tests, such as bonding attribute consistency (the sum of single, double, triple bonds should be paired), free valence check (the number of monovalent segments should be less than or equal to the total number of trivalent segments plus two times the number of tetravalent segments, plus 2), etc., are performed by examination of the obtained vectors, and the invalid vectors are removed. By examining the segment vectors listed in Table 4, it can be seen that there is only one aromatic segment ArNH ($l_{50} = 1$) in segment vector No. 2, so it is a violation of the $4n + 2$ rules for aromatic compounds, and thus disposed; in segment vector No. 7, there is only one segment $-CH =$ ($l_7 = 1$) containing a double bond, so it cannot be paired, and is thus disposed. Therefore, the segment sets from Table 4 are, as given in Scheme 5.

Table 4
Several segment vectors generated from component vector No. 14 in Table 3

Segment vector No.	Non-zero elements		
1	$l_4 = 6$	$l_{44} = 1$	$l_{48} = 2$
2	$l_4 = 6$	$l_{44} = 1$	$l_{48} = 1, l_{50} = 1$
3	$l_4 = 6$	$l_{44} = 1$	$l_{50} = 2$
4	$l_4 = 6$	$l_{46} = 1$	$l_{48} = 2$
5	$l_4 = 6$	$l_{46} = 1$	$l_{48} = 1, l_{50} = 1$
6	$l_4 = 6$	$l_{46} = 1$	$l_{50} = 2$
7	$l_4 = 5, l_7 = 1$	$l_{44} = 1$	$l_{48} = 2$
8	$l_4 = 5, l_7 = 1$	$l_{44} = 1$	$l_{48} = 1, l_{50} = 1$
9	$l_4 = 5, l_7 = 1$	$l_{44} = 1$	$l_{50} = 2$
10	$l_4 = 5, l_7 = 1$	$l_{46} = 1$	$l_{48} = 2$
11	$l_4 = 5, l_7 = 1$	$l_{46} = 1$	$l_{48} = 1, l_{50} = 1$
12	$l_4 = 5, l_7 = 1$	$l_{46} = 1$	$l_{50} = 2$
13	$l_4 = 4, l_7 = 2$	$l_{44} = 1$	$l_{48} = 2$
14	$l_4 = 4, l_7 = 2$	$l_{44} = 1$	$l_{48} = 1, l_{50} = 1$

Segment set No. 1

ID#	Symbol	Number
4	>CH–	6
44	–O–	1
48	–NH–	2

Segment set No. 2

ID#	Symbol	Number
4	>CH–	4
7	–CH=	2
44	–O–	1
48	–NH–	2

Segment set No. 3

ID#	Symbol	Number
4	>CH–	2
7	–CH=	4
44	–O–	1
48	–NH–	2

Scheme 5.

6. Exhaustive generation of structural isomers from segment set

6.1. Representation

In the ESESOC-II system, a BAM is used to represent the hyper-structures and candidate structures in the process of structure generation. All the bonds of one atom possessing the same bond attributes are represented by one bonding site. The bonds of one atom possessing different bond attributes are divided into separate bonding sites. The bonds of different atoms possessing the same bond attributes will be presented by separate bonding sites. Structure **I** and its BAM are shown in Fig. 1, where the element 0 stands for no bond, 1 for single bond, 2 for double bond, 3 for triple bond and 9 for aromatic bond.

Our BAM possesses the following advantages: (1) the construction of candidate structures from our BAM is very fast because no bond attribute tests are needed; (2) compared with Munk's BAM [5] and Zupan's Matrix E [8] our BAM is normally smaller.

6.2. Generation of the BAM of a hyper-structure

The BAM of a hyper-structure is built up by the following steps: (1) all the segments in the segment set are written in the form of bonding sites and assign a sequential number to each bonding site. If there are m_1 segments of the lowest index number (in Table 2), m_2 of the second lowest, and so on, then the numbers 1, $2,\ldots,$ im_1 must be assigned to the segments of the lowest index number, numbers m_1+1, $m_1+2,\ldots,m_1+m_2$ to segments of second lowest index number, and so on. If there are m_1 bonding sites of segment 1, m_2 of segment 2, and so on, then the numbers $1, 2,\ldots,m_1$ must be assigned to the bonding sites of segment 1, numbers m_1+1, $m_1+2,\ldots,m_1+m_2$ to the bonding sites of second segment, and so on; (2) the generation of the BAM of the hyper-structure starts as a full matrix with elements *b* (see Fig. 2); (3) the forbidden and chemically unreasonable connections are removed, where the removed connections are: (a) connections between the same atom; (b) connections between the different bond attributes; (3) connections leading to small molecules; (d) connections leading to forbidden partial substructures.

As an example, one of the segments generated from the above example is:

segment:	>CH–	–CH=	–CH=O	–CH=NH
number:	1	2	1	2

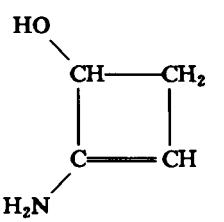

(I)

		1	2	3	4	5	6	7	8
1	HO—	0	0	1	0	0	0	0	0
2	NH_2—	0	0	0	0	0	0	1	0
3	—CH<	1	0	0	1	0	0	1	0
4	—CH_2—	0	0	1	0	1	0	0	0
5	—CH	0	0	0	1	0	0	0	0
6	CH=	0	0	0	0	0	0	0	2
7	>C	0	1	1	0	0	0	0	0
8	C=	0	0	0	0	0	2	0	0

Fig. 1. Structure **I** and its BAM.

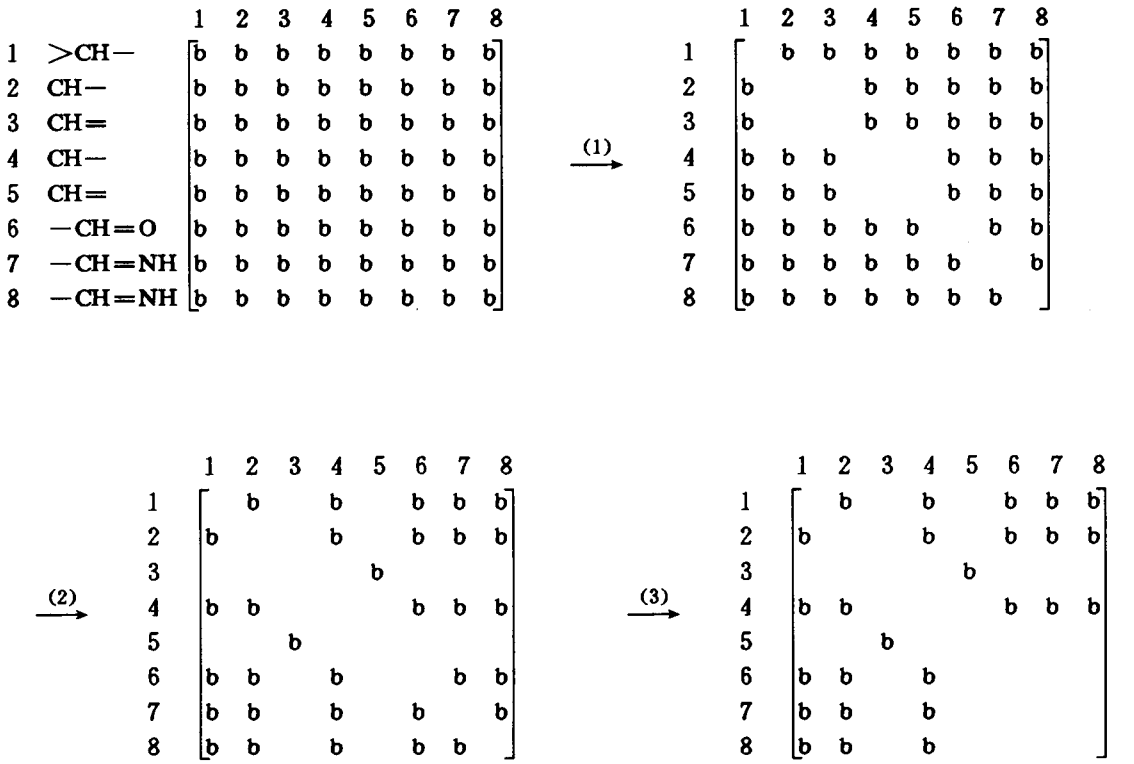

Fig. 2. The the generation process of the BAM of the hyper-structure. (1) Remove the connections between same atom; (2) remove the connections between the different bond attributes; (3) remove the connections to lead to small molecules.

The generation process of the BAM of the hyper-structure is shown in Fig. 2.

6.3. Generation of candidate structures

The process of generation of all candidate structures is equivalent to exploring, in a systematic manner, how the elements of the BAM of the hyper-structure might be filled in. Since the BAM is symmetrical, only the elements of the top half of the BAM of the hyper-structure are processed. The remaining elements of the top half of the BAM of the hyper-structure are numbered by standard ordering (column by column). The numbers are the identifier(ID) of these connections. This standard ordering of the BAM of the hyper-structure obtained from Fig. 2 is shown in Fig. 3.

For the generation of all candidate structures, the BAM must be filled from the first numbered element to the last numbered element, alternatively. This is done by using a heuristic depth-first method to search the structure generation tree.

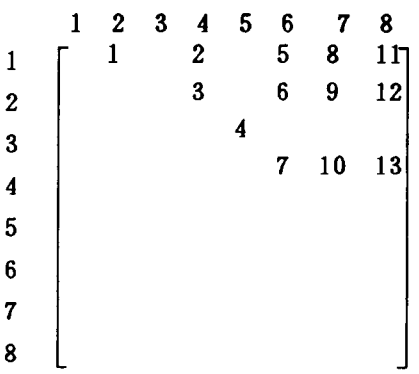

Fig. 3. The standard ordering of the BAM of the hyper-structure.

Taking the BAM illustrated in Fig. 3 as an example, its heuristic depth-first tree expansion is shown in Fig. 4.

6.4. Removing the redundant connections

In this study, a simple approach is suggested to avoid some duplications. We found that if both bonding sites i and j have no symmetry, then connections of i and j have no duplications; if bonding sites i or j have symmetry, then connections of i and j have duplications. So if both i and j are the smallest bonding site number in their symmetry classes, then the connection of i and j is remained, otherwis it is disposed, thus some duplications can be avoided.

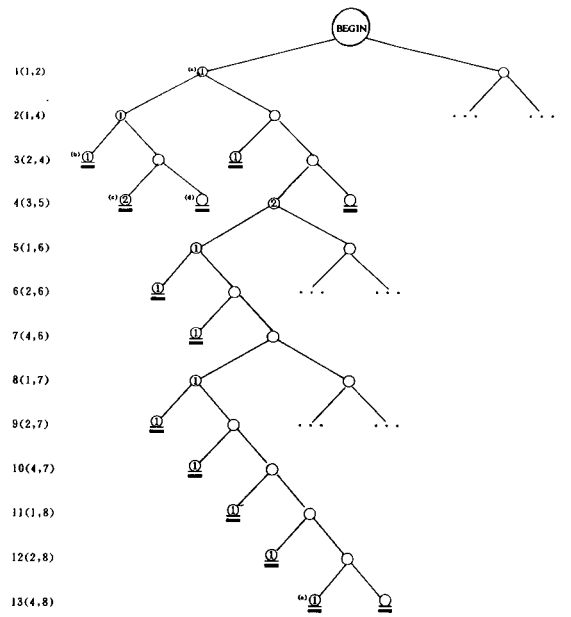

Fig. 4. The depth-first tree expansion (=: stands for terminal descendent node). (a) 1 is filled in the first numbered element of BAM, and a single bond is formed between bonding sites 1 and 2; (b) bonding site 2 has no free valence, so 1 can be filled in the third numbered element, thus this is a terminal descendent node; (c) after 2 is filled in numbered element 4, a 3-number ring is formed, which will lead to a disconnected structure; (d) after 0 is filled in numbered element 4, no double bond can be formed in the following steps; this will lead to a disconnected structure; (e) after 1 is filled in numbered element 13, structure **II** is obtained:

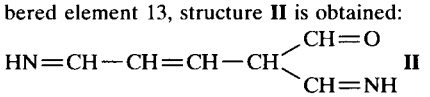

II

After symmetry analysis, the bonds of i and j are added to the BAM. The sequential numbers are assigned to each bonding sites by the following steps:

(1) Choose the first bonding site as current bonding site and give it the sequence number 1.

(2) If there are any attachments to the current bonding site which have not been assigned sequence numbers, then assign the unnumbered attachment the next sequence number of its orbit, and repeat this step; otherwise go to step 3.

(3) If the connected bonding sites are completely numbered, then go to step 4; otherwise the bonding site with sequence number equal to the current bonding site plus one becomes the current bonding site, and go to step 2.

(4) When done, the sequence number is assigned.

After each step of the assignment, if the sequence number of any bonding site is a violation of the original number, then the connection is disposed and removed from hyper-BAM. With those heuristics steps, some duplicates may still be produced, but the duplication factor is quit low (see Table 5). The remaining duplicates can be eliminated by searching the canonical list of structures canonicalized by the algorithm [25], or by checking whether the abbreviated BAM is "maximum" similar to the methods used in the CHEMICS system [6].

6.5. Perception symmetry

An algorithm for the perception of topological symmetry is developed [26], in which two types of new graph invariants, node matrix and bonding matrix, are introduced. This algorithm can be described as follows.

A node library containing various kinds of nodes is built, and the index number of the library is used to discriminate between the different types of non-hydrogen atoms. From the viewpoint of node i, i.e., the immediate neighbours of node i form the first layer the outer neighbours

connecting immediately to the nodes of the first layer form the second layer, and so on. Then a new type layer matrix, node matrix (**NM**), is proposed, whose element nm_{ij} is defined as the sum of the index numbers in the node library for all nodes situated in the jth layer. The bond matrix (**B**) is proposed, whose element b_{ij} is defined as the sum of the codes of the bonds which are a connection between the nodes of the jth layer and the nodes of the $(j-1)$th layer. The weight of a node is calculated by the following function,

$$W[i] = nm_{i1} + \sum_{j=1}^{K} nm_{i(j+1)} \times b_{ij} \times 10^{-j}$$

which specifies the global environments of the nodes and edges.

where $W[i]$ is the weight of the ith node and nm_{ij} and b_{ij} are the elements of the **NM** and **B** matrices, respectively, and K is the number of layers from the viewpoint of node i. The topological symmetry can be detected by iterative calcula-

Table 5
Generated results from ESESOC and partial comparison with the results from DENDRAL

Molecular formulae	Number of isomers from ESESOC [a]	Number of isomers from ESESOC [b]	Duplicate factor	CPU times [c] (s)	Number of isomers from DENDRAL
C_7H_{16}	9	9	$\frac{0}{9} = 0$	< 0.01	
C_8H_{18}	18	18	$\frac{0}{18} = 0$	0.09	
C_9H_{20}	35	35	$\frac{0}{35} = 0$	0.28	
$C_{10}H_{22}$	75	75	$\frac{0}{75} = 0$	0.77	
$C_{11}H_{24}$	161	159	$\frac{2}{161} = 0.012$	2.64	
$C_{12}H_{26}$	362	355	$\frac{7}{362} = 0.019$	8.73	
$C_{13}H_{28}$	822	802	$\frac{20}{822} = 0.024$	28.73	
$C_{14}H_{30}$	1922	1858	$\frac{64}{1922} = 0.033$	94.41	
$C_{15}H_{32}$	4537	4347	$\frac{190}{4537} = 0.042$	311.53	
$C_{16}H_{34}$	10888	10359	$\frac{529}{10888} = 0.048$	989.20	
$C_{10}H_{23}N_1$	1248	1238	$\frac{10}{1248} = 0.013$	25.32	
C_6H_{14}	5	5	$\frac{0}{5} = 0$	< 0.01	5
C_6H_{12}	25	25	$\frac{0}{25} = 0$	0.22	25
C_6H_{10}	77	77	$\frac{0}{77} = 0$	1.40	77
C_6H_8	161	159	$\frac{2}{161} = 0.012$	4.96	159
C_6H_6	229	217	$\frac{12}{229} = 0.052$	10.05	217
C_6H_4	200	185	$\frac{15}{200} = 0.075$	11.92	185
C_6H_2	109	85	$\frac{24}{109} = 0.22$	9.17	85
C_6	33	19	$\frac{14}{33} = 0.42$	3.46	19
$C_3H_{10}N_2O$	106	102 + 3 [d]	$\frac{1}{106} = 0.009$	0.52	102
$C_3H_8N_2O$	563	527 + 31 [d]	$\frac{5}{563} = 0.009$	6.01	527
$C_3H_6N_2O$	1344	1194 + 130 [d]	$\frac{20}{1344} = 0.015$	25.43	1194
$C_3H_4N_2O$	1643	1371 + 231 [d]	$\frac{41}{1643} = 0.025$	46.25	1371
$C_3H_2N_2O$	938	703 + 179 [d]	$\frac{56}{938} = 0.059$	35.59	703
C_3N_2O	146	88 + 37 [d]	$\frac{21}{146} = 0.14$	7.30	88

[a] Isomers from ESESOC after heuristic tree expansion.
[b] Isomers from ESESOC after final duplicate eliminations.
[c] CPU times needed in both (a) and (b).
[d] The isomers containing the functionalities of N (valence = 5).

tion of the weight of the node. This can also be applied to partial assembled structures [26]. It is incorporated into the structure generation algorithm by taking the segment as the node, and the index number of the segment (in Table 2) as node index number.

7. Results and discussion

A new algorithm for the exhaustive and irredundant generation of structural isomers from molecular formula is devised. We think that it is effective. To substantiate the exhaustive character of the algorithm, some empirical formulae are supplied to the structure generator of ESESOC-II to build up all the isomers for the given empirical formulae. The molecular formulae and their numbers of structural isomers are listed in Table 3, and the published results from the DENDRAL algorithm [27] of some empirical formulae are also listed. In Table 3, the numbers of isomers of the molecules not containing N are the same as the results from the DENDRAL system. For the molecules containing N, only the normal valence (3) of N is considered, whereas the functionalities, such as, $\rangle NO-$, $\rangle NO=$, $\rangle C=N^{\oplus}=N^{\ominus}$, etc. (valence = 5), are not included in the DENDRAL system [27], so the number of isomers generated by ESESOC is equal to the number generated by DENDRAL plus the number of isomers containing functionalities of N (valence = 5). Evidently, the results of ESESOC-II are consistent with the published results from the DENDRAL algorithm [27]. The correctness of the structure generation algorithm in the DENDRAL system was rigorously proved [28,29], and the results obtained from the DENDRAL system have been of value in varying the correct implementation of other subsequently developed exhaustive and irredundant algorithms [30]. Therefore, the results of ESESOC-II are exhaustive and irredundant. The CPU times for the generation of the isomers are also listed in Table 3, which include the times for canonicalization and searching the canonical list of structures. This algorithm is programmed in Turbo C and run on a PC/486 computer.

Acknowledgement

The authors acknowledge the financial support of the National Natural Science Foundation of China.

References

[1] R.K. Lindsay, B.G. Buchanan, E.A. Fengenbaum and J. Lederberg, Applications of Artificial Intelligence for Organic Chemistry, the DENDRAL Project, McGraw-Hill, New York, 1980.
[2] L.M. Masinter, N.S. Sridharan, R.E. Carhart and D.H. Smith, J. Am. Chem. Soc., 14 (1974) 7702.
[3] R.E. Carhart, D.H. Smith, N.A.B. Gray, J.G. Nourse and C. Djerami, J. Org. Chem., 46 (1981) 1708.
[4] C.A. Shelley, T.R. Hays, M.E. Munk and R.V. Roman, Anal. Chim. Acta, 103 (1978) 121.
[5] B.D. Christie and M.E. Munk, J. Chem. Inf. Comput. Sci., 28 (1988) 271.
[6] Y. Kudo and S. Sesaki, J. Chem. Inf. Comput. Sci., 16 (1976) 43.
[7] K. Funatsu, N. Miyabayashi and S. Sasaki, J. Chem. Inf. Comput. Sci., 28 (1988) 18.
[8] S. Bohanec and J. Zupan, J. Chem. Inf. Comput. Sci., 31 (1991) 531.
[9] J.L. Faulon, J. Chem. Inf. Comput. Sci., 32 (1992) 338.
[10] L.P. Bangov, Commun. Math. Chem., 14 (1983) 235.
[11] L.P. Bangov, J. Chem. Inf. Comput. Sci., 30 (1990) 277.
[12] C.Y. Hu and L. Xu, Chin. J. Org. Chem., 13 (1993) 129.
[13] C.Y. Hu and L. Xu, Sci. China, (1994) in press.
[14] J.V. Knop, W.R. Miller, Z. Jericevic and N. Trinajetic, J. Chem. Inf. Comput. Sci., 21 (1981) 91.
[15] N. Trinajetic, Z. Jericevic, J.V. Knop, W.R. Miller and K. Szymanski, Pure Appl. Chem., 55 (1983) 379.
[16] J.B. Hendrickson and C.A. Parks, J. Chem. Inf. Comput. Sci., 32 (1992) 323.
[17] V. Kvasnicka and J. Posphichal, J. Chem. Inf. Comput. Sci., 30 (1990) 99.
[18] L.B. Kier, L.H. Hall and J.W. Frazer, J. Chem. Inf. Comput. Sci., 33 (1993) 143.
[19] L.H. Hall, L.B. Kier and J.W. Frazer, J. Chem. Inf. Comput. Sci., 33 (1993) 148.
[20] M.L. Contreras, R. Valdivia and R. Rozas, J. Chem. Inf. Comput. Sci., 32 (1992) 323.
[21] M.L. Contreras, R. Valdivia and R. Rozas, J. Chem. Inf. Comput. Sci., 32 (1992) 483.
[22] K. Szymanski, W.R. Muller, J.V. Knop and N. Trinajetic, J. Chem. Inf. Comput. Sci., 25 (1985) 413.
[23] R.C. Read, R.D. Cameron, C.J. Colbourn and N.C. Wormald, J. Graph Theory, 9 (1985) 551.

[24] S. Zhu and J.P. Zhang, J. Chem. Inf. Comput. Sci., 22 (1982) 34.
[25] C.Y. Hu and L. Xu, J. Chem. Inf. Comput. Sci., (1994) in press.
[26] C.Y. Hu and L. Xu, Anal. Chim Acta, in press.
[27] D.H. Smith, J. Chem. Inf. Comput. Sci., 15 (1975) 203.
[28] H. Brown, L. Hjelmeland, L.M. Masinter, Discrete Math., 7 (1974) 1.
[29] H. Brown, L.M. Masinter, Discrete Math., 8 (1974) 227.
[30] N.A.B. Gray, Computer-Assisted Structure Elucidation, Wiley, New York, 1986.

ELSEVIER

Analytica Chimica Acta 298 (1994) 87–90

ANALYTICA CHIMICA ACTA

Simplex and classical methods for the selection of parameters for the adsorptive stripping voltammetric determination of nitralin. A comparative study

A. San Vicente, A. Arranz, J.M. Moreda, J.F. Arranz *

Departamento de Química Analítica, Facultad de Farmacia, Universidad del País Vasco, Apdo. 450, D.P. 01080-Vitoria, Spain

Received 1 March 1994; revised manuscript received 17 May 1994

Abstract

A method for the determination of the herbicide nitralin by adsorptive stripping voltammetry (AdSV) is proposed. This very sensitive method is based on controlled adsorptive preconcentration of the herbicide on a hanging mercury drop electrode (HMDE). Measurements were taken by differential pulse polarography (DPP) after improving with simplex method accumulation conditions, which was compared with those obtained by the classical methods of variable optimization. Using the simplex method means that the sensitivity is significantly increased compared to the sensitivity obtained by the conventional method (slope ratio 3.79). The time and the experiment number are smaller. Using this method the detection limit reached was 0.13 ng ml^{-1}. Under these conditions the peak current is enhanced 5-fold for 6×10^{-9} M nitralin solution compared to the peak current from the classical method. The response was linear in the range 5×10^{-10} to 1×10^{-6} M, with two different slopes, and the coefficient of variation for a 5×10^{-8} M nitralin solution ($n=10$) was 0.90%.

Keywords: Stripping voltammetry; Herbicides; Simplex method

1. Introduction

Nitralin [4-(methylsulfonyl)-2,6-dinitro-*N*,*N*-dipropylbenzenamine] is a selective herbicide which is used frequently for pre-emergency control of weeds in cotton, groundnut, rape, soya, bean and harvests such as tobacco and tomato.

Among the instrumental methods, AdSV is a technique which has been proven suitable for the quantification of a large variety of organic molecules [1–3], and no reports on the use of this technique for the determination of nitralin have been found in the literature. In AdSV, the amount of analyte accumulated on the electrode surface is a composite of many variables such as the solvent, potential, pH, ionic strength, drop size, stirring speed, scan rate, etc. Besides their effect on the current enhancement, some of the above parameters may influence other properties of the subsequent voltammetric measurement (e.g., reproducibility, peak shape, ...), for this reason the optimization of these parameters is very important. In various situations a compromise should be made to achieve the desired balance between sensitivity and reproducibility. The optimization and selection of experimental parameters and of the dissolution to be measured has been carried out by the modified simplex method [4]. The classical method, which consists of varying the value of the parameter by maintaining the other constant, is lengthy

* Corresponding author.

SSDI 0003-2670(94)00234-D

and does not allow measurement of the influence that each of these has on the others. The modified simplex method allows several different parameters or variables to be varied at the same time and its aim is to force a geometrical figure (simplex) with a number of vertices equal to the number of variables, n, plus one, to move towards a region where the response is optimum.

The modification proposed by Nelder and Mead [5] of the original simplex procedure gives not only a clear indication of when a sufficiently precise stationary optimum has been attained, but also has de advantages of acceleration and adaptation to fit the particular response surface being studied. In addition to the operation of reflection, two new operations are used: expansion and contraction.

The method has been applied successfully to different analytical techniques such as spectrophotometry [6], inductively coupled plasma spectrometry [7], chronoamperometry [8] and AdSV [9].

2. Experimental

2.1. Apparatus

Stripping voltammograms were obtained with a Metrohm compact analyzer for voltammetry and polarography, consisting of a 646-VA processor and a 647-VA stand with an Ag/AgCl (3 M KCl) reference electrode, a platinum auxiliary electrode, a mercury multimode electrode (Metrohm MME) which has a hanging mercury drop electrode (HMDE) and a stirring bar that provided convective transport during the preconcentration. A Metrohm E-605 pH meter was used to measure the pH values.

2.2. Reagents

Stock solutions (1.25×10^{-3} M) of nitralin 99% ($C_{13}H_{19}N_3O_6S$) (MW 345.37) (Lab. Dr. S. Ehrenstorfer) were prepared by dissolution of the appropriate amount of herbicide in acetone. The solution was stored under refrigeration and protected from light.

All other chemicals were of analytical-reagent grade (Merck). Buffer stock solutions of various pH values were prepared by adjusting de pH of a mixture of acetic, phosphoric and boric acid, by the addition of sodium hydroxide solution.

Table 1
Variation intervals for each of the parameters studied

Parameters to be optimized	Variation interval	
Pulse amplitude, ΔE (mV)	−50	−250
Accumulation time, t_{acc} (s)	15	600
Scan rate, V_s (mV/s)	2.5	30.0
Drop size, t_g [a]	1	9
Stirring speed, V_{str} [b]	1	9
Accumulation potential, E_{acc} (mV)	−200	−350
pH	6	10
Ionic strength, μ (M, $NaClO_4$)	0.05	0.50

[a] Drop size: 1–9 correspond to 0.15–0.60 mm^2, respectively.
[b] Stirring speed: 1–9 correspond to 1220–2620 rpm, respectively.

For the preparation of working solutions an appropriate aliquot of the stock solution (1×10^{-7} M) was transferred into a flask with 25 ml of buffer stock solution. All water used purified by the Milli-Q system of Millipore.

2.3. Procedure

The working solution containing 100 ml of herbicide was purged for 10 min with oxygen-free nitrogen.

The preconcentration potential was applied to the electrode for a given time period, while the solution was stirred. After a 15 s rest period, a negative-going scan was initiated, the resulting voltammograms being recorded for different combinations of operational parameters.

3. Optimization methods

3.1. Classical method

This method, called "variable-by-variable" too, was applied to nitralin. For this reason, a variable was modified by maintaining the rest of the variables in their constant values, for the variable parameter to be optimized. Then, and by maintaining in its optimum value that variable, another was modified and via this method all variables were optimized [10].

The intervals chosen to carry out the optimization are given in Table 1 only pH (2–10) and ionic strength (0.00–0.55 M $NaClO_4$) were different.

Table 2
Optimum values for the determination of nitralin by the classical and the simplex method

Parameters	Method classical	Method simplex
Pulse amplitude, mV	−150	−148
Accumulation time, s	150	150
Rest time, s	15	15
Scan rate, mV s^{-1}	20	26
Drop size, mm^2	0.6	0.6
Stirring speed, rpm	2620	1920
Accumulation potential, mV	−300	−345
Potential scan, m	−200 to −800	−200 to −800
pH	8.8	9.9
Ionic strength, M $NaClO_4$	0.00	0.05

The potential applied at the electrodeposition step (−300 mV) and at the beginning of the scan (−200 mV) were not the same, in order to reach more sensitivity.

3.2. Simplex method

A simplex is a geometric figure defined by a number of points equal to one more than the number of dimensions of the space. The method is applicable to any number of dimensions. The parameters to be varied are chosen by initial experiments. Optimization means maximization of response, but it could apply equally well to the process of finding a minimum.

The initial simplex was obtained according to Yabro et all. [11] where $p = 0.8839$ and $q = 0.1768$ for eight variables to be optimized. The intervals chosen to carry out the optimization are given in Table 1. The maximum limits have been established bearing in mind the possibilities of the instrumentation and the reduction characteristics typical of the nitro group.

The advance of the simplex has been allowed in those cases in which the parameters were outside the chosen interval, and whenever the analytical signal obtained was maximum.

4. Results and conclusions

Adsorptive stripping voltammetry has been used for determining nitralin. A spontaneous adsorption process on the HMDE electrode surface, at a specific electroadsorption potential, has been verified. Later a scan is applied towards more negative potentials by means of the impulse technique thereby attaining the reduction of the nitro groups of nitralin.

The optimization of the parameters, both experimental and of the dissolution to be measured, carried out by the classical and the simplex methods was as shown in Table 2. In the classical method, the reduction peak appears at a potential of ca. −425 mV versus Ag/AgCl, and its height varies linearly with the concentration of nitralin in the range 1×10^{-9} M to 1×10^{-6} M. The calibration line was $I_p = -4.37 + 6.18\times10^8 C$, where I_p is expressed in nA and C is the concentration of nitralin in mol l^{-1} (Table 3).

Table 3
Regression data of calibration lines

	Classical	Simplex	
LR	1×10^{-9}–1×10^{-6} M	5×10^{-10}–9×10^{-9} M	1×10^{-8}–1×10^{-6}M
b	6.1757×10^8	23.4484×10^8	19.3462×10^8
a	−4.3706	0.5353	−17.4446
S_b	3.2749×10^6	17.3983×10^6	12.4074×10^6
S_a	1.2189	0.0788	5.6057
S_{yx}	6.4499	0.2950	24.4351
r	0.9994	0.9992	0.9993
n	28	14	19
LD	2.3×10^{-9} M	3.9×10^{-10} M	

LR = linear range; b = slope; a = intercept; S_b = standard deviation of the slope; S_a = standard deviation of the intercept; S_{yx} = error standard deviation; r = correlation coefficient; n = data number; LD = detection limit.

The detection limit ($3S_B$) was estimated as 2.3×10^{-9} M (0.79 ng ml^{-1}) according to the Caulcutt-Boddy criterion [12].

The reproducibility of the method was determined by successive measurements on the 5×10^{-8} M ($n=10$) nitralin solutions, and the coefficient of variation was 1.74%.

By the simplex method, 56 movements were necessary, with a total of 81 vertices, in order to reach the optimum working conditions. The chosen vertex allows to obtain high sensitivity, good reproducibility and the best peak shape.

The reduction peak which appears at a potential of ca. −513 mV versus Ag/AgCl, and the calibration line vary linearly with the concentration of nitralin in two ranges with different slots: 5×10^{-10} M to 9×10^{-9} M and 1×10^{-8} M to 1×10^{-6} M. The straight calibration plots correspond to the equations $i_p=0.53+23.44\times10^8C$ and $i_p=-14.81+19.28\times10^8C$ where i_p is again in nA and C is in mol l^{-1}. The detection limit of 3.9×10^{-10} M (0.13 ng ml^{-1}) has been attained. A coefficient of variation of 0.90% was obtained by successive measurements of 5×10^{-8} M nitralin solution ($n=10$).

The regression data corresponding to calibration lines are shown in Table 3. Comparing these data it may be concluded that the simplex method is advantageous over the classical method because among other reasons it is more sensitive in the two linear ranges (i.e., 3.79 and 3.13 respectively). The detection limit reached (0.13 vs. 0.79 ng ml^{-1}) and the standard deviation (0.29 vs. 6.45) were smaller.

For a selected intermediate value of 5×10^{-8} M ($n=10$) nitralin the reproducibility is better, showing a low coefficient of variation (0.90 vs. 1.74).

Fig. 1 shows the different signals obtained for the reduction peak of a 6×10^{-9} M solution, using the chosen conditions by the classical (A) and the simplex method (B).

Moreover, the amount of time and the number of experiments necessary to obtain the best conditions by the classical method are three times higher than those employed to obtain the best conditions by the simplex method.

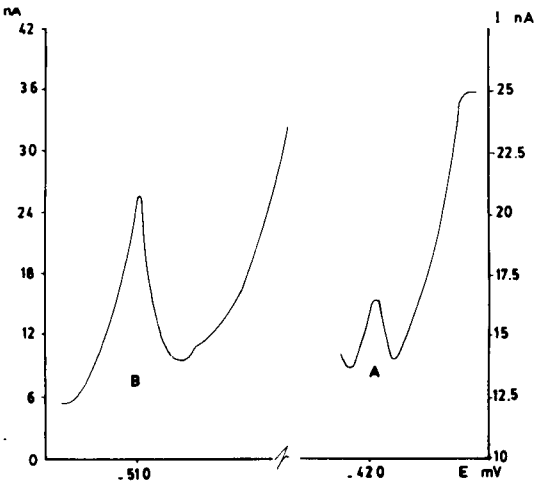

Fig. 1. Analytical signal for a concentration of 6×10^{-9} M nitralin. (A) Classical method: 2.82 nA. (B) Simplex method: 15.00 NA.

Acknowledgements

The authors thank the Education and Universities Department of the Basque Government for the financial support awarded to this project (PGV 8904). They are also grateful to Angel González Pérez for revision of the text.

References

[1] L. Hernández, P. Hernández, E. Lorenzo, C. González and I. González, Fresenius' J. Anal. Chem., 336 (1990) 222.
[2] Z. Gómez de Balugera, J.R. Barrio, A. Goicolea and J.F. Arranz, Electroanalysis, 3 (1991) 423.
[3] M.M. Díaz de Guereñu, J.R. Barrio, A. Arranz and J.F. Arranz, J. Pharm. Biomed. Anal., 10 (1992) 481.
[4] S.L. Morgan and S.N. Deming, Anal. Chem., 46 (1974) 1170.
[5] J.A. Nelder and R. Meat, Comput. J., 7 (1965) 308.
[6] L.R. Maned, B.M. Colvin and A.R. Hanks, J. Environ. Anal. Chem., 61 (1978) 500.
[7] D.J. Caverly and J. Unwin, Analyst, 106 (1981) 1261.
[8] E.G. Cotteril, Analyst, 107 (1982) 1270.
[9] A. San Vicente, J.R. Barrio, A. Goicolea, J.F. Arranz and A. Arranz, Proceedings of Euro Food Chem VI, Hamburg, Sept. 22–21, 1991, pp. 841–846
[10] A. Arranz, A. San Vicente, S.F. dez de Betoño, J.M. Moreda and J.F. Arranz, Fresenius' J. Anal. Chem., submitted for publication.
[11] L.A. Yabro and S.N. Deming, Anal. Chim. Acta, 73 (1973) 391.
[12] R. Caulcutt and R. Boddy, Statistics for Analytical Chemists, Chapman and Hall, London, 1983, p. 201.

ELSEVIER

Analytica Chimica Acta 298 (1994) 91–98

ANALYTICA CHIMICA ACTA

A polarographic, voltammetric and spectroscopic study of 2-mercaptonicotinic acid and its chromium(III) complex

Lorena Armijo, Verónica Arancibia *

Departamento de Química Analítica y Electroquímica, Facultad de Química, Pontificia Universidad Católica de Chile, Santiago, Chile

Received 5 January 1994; revised manuscript received 3 May 1994

Abstract

The redox behaviour of the ligand 2-mercaptonicotinic acid and its chromium(III) complex has been studied in dimethyl sulphoxide. Oxidation of this compound to the corresponding disulphide at +0.90 V vs. SCE is displaced at +0.20 V vs. SCE and −0.05 V vs. SCE upon addition of one and two equivalents of base respectively. The addition of chromium(III) to the ligand, both in its neutral and mono-anionic form, does not produce any change in the spectrum or in the cyclic voltammograms, which indicates that there is very weak or no interaction from chromium. If the proton mercapto group is neutralized, a 1:3 complex is formed and the dimerization does not occur. This complex has been characterized by polarography, cyclic voltammetry, controlled-potential electrolysis, UV–visible spectrometry and magnetic susceptibility measurements. The conditional formation constant was determined by polarographic and spectroscopic methods, giving the values of 2.5×10^{14} and 1.5×10^{14} (25°C), respectively.

Keywords: Polarography; Voltammetry; Chromium complexes; 2-Mercaptonicotinic acid

1. Introduction

Chromium is an essential trace element in man and is involved in the metabolism of glucose. It forms an integral part of the glucose tolerance factor (GTF) which has been defined as a dietary ingredient required for the maintenance of normal glucose tolerance of rats. GTF can be extracted and concentrated from 'brewers' yeast and pork kidney powder and it contains chromium as its active ingredient [1–6].

GTF differs from simple chromium complexes by its much greater stimulation of the effect of insulin on glucose metabolism in epididymal fat tissue. Much smaller amounts of chromium are needed in vivo to improve the impaired glucose tolerance of chromium-deficient rats if the element is given in the form of GTF. Chromium in the form of GTF crosses the placenta of rats easily, in contrast to chromic chloride or acetate, which penetrate only to a very small degree or not at all. These facts suggest that in a normal organism, with a complete diet, part of chromium exists in complexes and that these complexes are responsible for the biological actions of chromium in carbohydrate metabolism [7–11].

Many of the earlier analytical methods were not sensitive enough to detect chromium in biological samples. Since this element was not regularly found, the available evidence led to the conclusion that chromium could not play an essential role in plants or animals. The concentrations of chromium in blood and urine are in the order of several nanograms per gram. However, large variations in published results suggest that con-

* Corresponding author.

SSDI 0003-2670(94)00240-M

tinuous improvement of analytical techniques is taking place [12–16].

The in vivo and in vitro testing of many synthetic complexes of chromium during the past 20 years has detected certain compounds that lack biological activity and a large number with approximately equal activity, but none that are outstanding. The results of in vivo glucose tolerance tests demonstrated that biological activity is restricted to complexes of trivalent chromium [17–19].

Mertz and co-workers [28] proposed in 1974 the first structure of a complex where N-bonded nicotinic acid was coordinated to chromium in an axial form. The N, O or S atoms from the amino acids glycine, glutamic acid or cysteine occupied the equatorial plane. This structure is not yet supported by experimental evidence, and the chemical nature of GTF still remains uncertain [20,21]. Reports indicate that nicotinic acid has a low affinity for binding to chromium [20].

The influence of chromium on glucose tolerance is closely tied to the action of insulin [22,23] and considering the presence of nicotinic acid in GTF, we have decided to study the redox chemistry of 2-mercaptonicotinic acid and of its chromium complexes.

Because of the strong tendency of Cr^{3+} for olation, simple Cr^{3+} compounds are insoluble at the nearly neutral pH of the blood, and complex or chelate formation with ligands capable of competing with OH^- are required to keep Cr^{3+} in solution [24,25]. These competing reactions are difficult to study quantitatively, and to avoid olation this study was carried out with dimetylsulphoxide.

2. Experimental

2.1. Reagents

The reagents for the investigations and syntheses included Cr_2O_3 (Merck), H_2O_2 30% p/v (Merck), $HClO_4$ 70% w/v (Merck), 2-mercaptonicotinic acid (2-MNA) (Aldrich), tetramethylammonium chloride (INC Pharmaceuticals). Tetrabutylammonium hydroxide (TBAOH) (1.0 M in methanol, Aldrich) was used to adjust the acidity of the solution. The supporting electrolyte tetraethylammonium perchlorate (TEAP) was obtained from reaction of a 25% aqueous solution of tetraethylammonium hydroxide (Aldrich) and concentrated perchloric acid and recrystallized from anhydrous ethyl alcohol. The concentration of the supporting electrolyte in the electrochemical experiments was 0.1 M.

Dimethyl sulfoxide (DMSO) (Aldrich, water $<0.005\%$) solvent was used without further purification for all of the experiments High-purity argon was used to deaerate solutions.

$Cr(ClO_4)_3 \cdot 4H_2O$ salt was prepared by a conventional method. Anhydrous salt of Cr(III) was obtained by replacing the water molecules with 1,3-dimethylurea (DMU) to give the hexakis complex $[Cr^{III}(DMU)_6(ClO_4)_3]$. Triethyl orthoformate was used as the dehydrating agent, and 1,3-dimethylurea was obtained from Aldrich.

2.2. Apparatus

A three-electrode potentiostat (Bioanalytical Systems Model CV-1A 230) was used for the cyclic voltammetric and polarographic measurements. Controlled-potential electrolysis was accomplished with a Bioanalytical Systems Model SP-2 potentiostat and PUC coulometer cyclic voltammograms were recorded on a Linear Model 8036 *X–Y* recorder

The working electrode (Beckman) was a platinum inlay electrode with a surface area of 0.23 cm^2. Its surface was polished with alumina before each experiment. The auxiliary electrode was a platinum-coil electrode, which was isolated from the bulk solution by a glass tube with a fine-porosity glass frit at the end; it contained a concentrated solution of supporting electrolyte. The reference electrode was a Ag/AgCl (aqueous tetramethylammonium chloride) electrode which was adjusted to 0.00 V vs. the saturated calomel electrode (SCE). [26] The reference electrode was located inside a Luggin capillary in the cell compartment. For controlled-potential electrolysis, a platinum-mesh working electrode was used.

The UV–visible absorption spectra were recorded with a Hewlett Packard Model 8452 diode-array spectrophotometer. The magnetic susceptibility measurements were made with a Varian Model XL-100 NMR spectrometer by the method of Evans as modified by Rettig (see Ref. [27]).

3. Results and discussion

3.1. Electrochemical behaviour of 2-mercaptonicotinic acid

Fig. 1 shows the cyclic voltammograms of 2-mercaptonicotinic acid (2-MNA) in the presence of one and two equivalents of tetrabutylammonium (TBAOH) in dimethyl sulphoxide (DMSO).

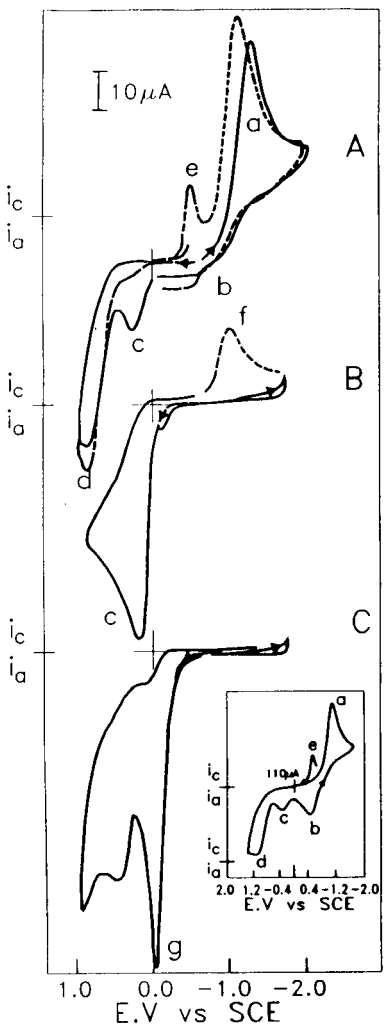

Fig. 1. Cyclic voltammograms in DMSO (0.1 M tetraethylammonium perchlorate, TEAP; scan rate 0.1 V s^{-1}) of solutions: (A) 3.0 mM of 2-mercaptonicotinic acid (2-MNA); inset shows the first cyclic voltammogram when the electrode is preactived by polish with alumina. (B) 3.0 mM 2-MNA and 3.0 mM TBAOH; (C) 3.0 mM 2-MNA and 6.0 mM in TBAOH.

The cyclic voltammogram of 2-MNA exhibits one reduction peak for an initial negative scan at −1.20 V vs. SCE (peak a) and two oxidations at −0.50 V vs. SCE (peak b) and +0.20 V vs. SCE (peak c) coupled to it. An irreversible oxidation peak occurs at +0.90 V vs. SCE (peak d) for an initial positive scan to give a product which is reduced at −0.50 V vs. SCE (peak e) and at −1.06 V vs. SCE (peak f).

On the basis of these results a compound is in solution while b, c, e and f correspond to the generated products on the electrode surface. The study of the peak currents as a function of the square roots of the scan rates indicates that the a, d, e and f peaks are caused by diffusion-controlled processes and that peaks b and c do not show linear dependence with the square root of the scan rate.

When the platinum electrode is preactived by polishing with alumina the anodic peak b increases while peak c decreases (Fig. 1, inset). It was observed that the aprotic solvents deactivate the platinum electrode within a few minutes.

Controlled-potential electrolysis at −1.40 V vs. SCE (E_{peak} = −1.20 V) allowed us to determine that one equivalent of charge per mole of ligand has been transferred in this process. The cyclic voltammograms and the spectra indicate than this process is equivalent to the neutralization of one proton of the carboxylic group (reaction 1)

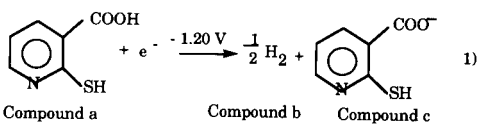

The molecular hydrogen generated in this process is adsorbed on the platinum surface and is oxidized at variable potential. The current decays rapidly in aprotic media (reaction 2)

$$\underset{\text{Compound b}}{H_{2(\text{ads Pt})}} \xrightarrow{-0.50\text{V}} \underset{\text{Compound e}}{2H^+ + 2e^-} \qquad (2)$$

Compound c is present on the electrode surface only and its concentration is variable because the molecular hydrogen oxidation generates protons which produce a decrease of the concentration of c (Fig. 1A). After electrolysis at −1.40 V vs. SCE (E_{peak} = −1.20 V) compound c is produced totally in solution. Controlled-potential electrolysis of these solutions (compound c)

at +0.40 V vs. SCE (E_{peak} = +0.20 V) yields a dimer, when one equivalent of charge is transferred (reaction 3)

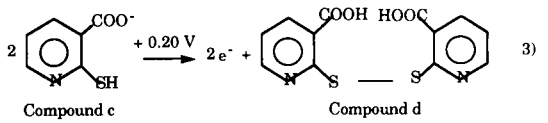

Compound c Compound d

The protons generated in this process are bound to carboxylate groups.

Controlled-potential electrolysis at +1.00 V vs. SCE (Fig. 1A, E_{peak} = +0.90 V) of a solution of the neutral ligand produced the same dimer with one equivalent of charge transferred (reaction 4). The cyclic voltammogram of these solutions are illustrated in Fig. 2A.

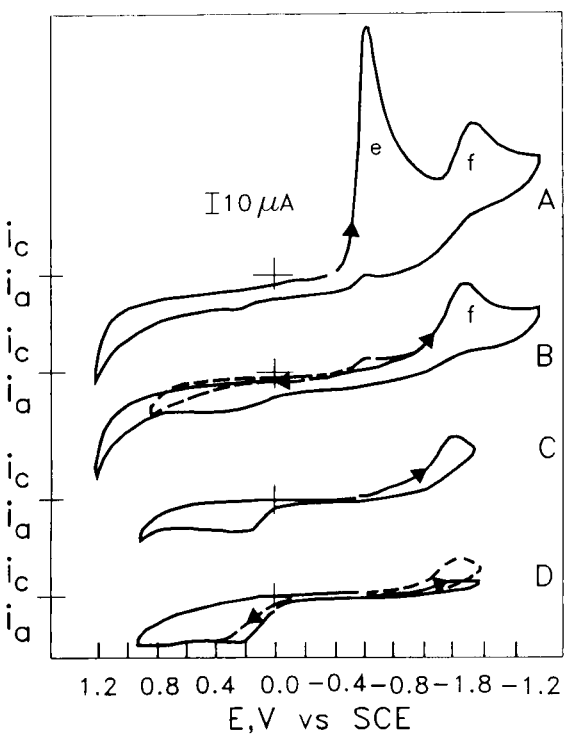

Fig. 2. Cyclic voltammograms in DMSO (0.1 M TEAP; v = 0.1 V s^{-1}) of solutions: (A) 1.0 mM of 2-mercaptonicotinic acid after electrolysis at +1.00 V vs. SCE; (B) the same as A, but after electrolisys at −0.80 V vs. SCE; (C), (D) the same as B, but after electrolisys at −1.30 V vs. SCE., n = 0.5 and n = 1.0, respectively.

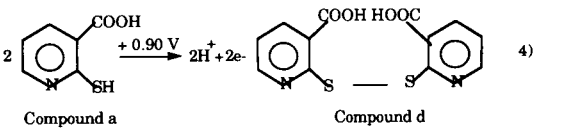

Compound a Compound d

The protons generated in this process remain free because the carboxylic group are protonated. Controlled-potential electrolysis at −0.70 V vs. SCE (E_{peak} = −0.50 V, peak e, Fig. 2A) produces molecular hydrogen liberation (reaction 5). Fig. 2B shows the cyclic voltammogram of this solution.

$$\underset{\text{Compound e}}{H^+ + e^-} \xrightarrow{-0.50V} \underset{\text{Compound b}}{1/2H} \qquad (5)$$

Fig. 2B shows the cyclic voltammograms corresponding to a solution of protonated dimer (compound d). A decrease in the diffusion coefficient and the current intensity is observed.

Controlled-potential electrolysis at −1.26 V vs. SCE of this solution, demonstrates that the cathodic peak at −1.06 V vs. SCE is a two electron process per mole of dimer (reaction 6).

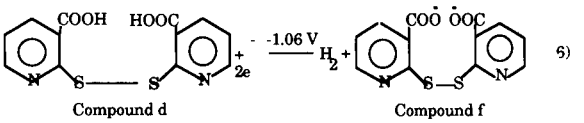

Compound d Compound f

Fig. 2C shows the cyclic voltammograms corresponding to the solution obtained after one equivalent of charge has been transferred and Fig. 2D shows the cyclic voltammograms after two equivalents of charge have been transferred.

The oxidation to the corresponding disulphide occurs at +0.90 V vs. SCE from the protonated ligand (reaction 4) at 0.20 V vs. SCE in the presence of one equivalent of base (reaction 3) and occurs at −0.05 V vs. SCE in the presence of two equivalents of base (reaction 7). As the mercaptonicotinic acid is deprotonated, the reactivity increases and it is easier to oxidize this compound.

In order to prepare this dimer from di-anionic ligand, controlled-potential electrolysis at +0.20 V vs. SCE (E_{peak} = −0.05 V) was realized. As the electrolysis starts the current drops almost immediately to a residual value and the desired compound is not formed. Apparently, the dimer, now anionic, is adsorbed and passivates the electrode.

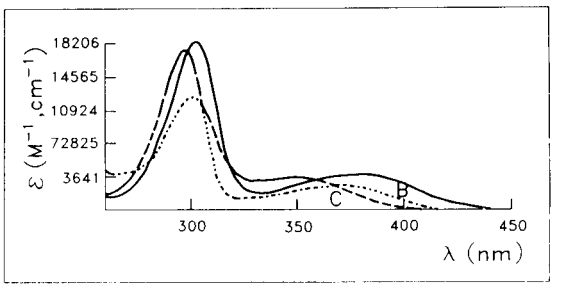

Fig. 3. Absorption spectra in DMSO (0.1 M TEAP) of solutions: (A) 1.0 mM of 2-mercaptonicotinic acid (2-MNA); (B) 1.0 mM 2-MNA and 1.0 mM TBAOH; (C) 1.0 mM 2-MNA and 2.0 mM in TBAOH.

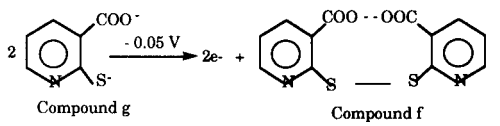

On the other hand, an irreversible anodic peak appears at +0.20 V vs. SCE (Figs. 1C, 3C and 2D) which is attributed to the oxidation of the carboxylate group. The oxidation of this compound becomes even easier because of the proximity of the carboxylate groups which increases the charge density.

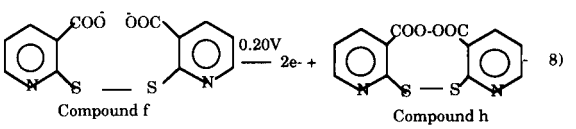

3.2. Spectra of ligand

Fig. 3 shows the UV–visible spectra of solutions of neutral, mono-anionic and di-anionic forms of ligand in DMSO (Fig. 3A, B and C, respectively). The neutral forms exhibit an absorption maximum at 302 nm ($\varepsilon = 18000\ M^{-1}\ cm^{-1}$) corresponding to the pyridine ring, another maximum occurs at 378 nm ($\varepsilon = 3777\ M^{-1}\ cm^{-1}$) and is associated with to the mercapto group. The addition of one equivalent of base produces a small hipsochromic shift with a small decrease in the extinction coefficients: 296 nm ($\varepsilon = 17400\ M^{-1}\ cm^{-1}$) and 370 nm ($\varepsilon = 2488\ M^{-1}\ cm^{-1}$). This is caused by the interaction of the proton that remains between the carboxylate and mercapto group.

The addition of two equivalents of base causes a bathochromic and hipsochromic shift with change in the extinction coefficients: 309 nm ($\varepsilon = 12420\ M^{-1}\ cm^{-1}$) and 350 nm ($\varepsilon = 3521\ M^{-1}\ cm^{-1}$). The transition energy increases because the basal state is stabilized.

The disulphide shows a bathochromic shift: 370 nm ($\varepsilon = 400\ M^{-1}\ cm^{-1}$) with a high decrease of extinction coefficient.

3.3. Electrochemical behaviour of complexes with Cr(III)

The cyclic voltammogram of the DMSO solution that contains 1.0 mM $[Cr^{III}(DMU)_6(ClO_4)_3]$ is illustrated in Fig. 4A. An initial negative scan yields two reduction peaks at −0.81 V vs. SCE and at −1.20 V vs. SCE. Controlled-potential electrolysis at −1.00 V vs. SCE requires 1.0 electron per metal ion and yields a blue green solution (Fig. 4B).

Controlled-potential reduction of this system at −1.40 V vs. SCE was not possible. When the electrolysis starts the current drops almost immediately to the residual value and the electrode now is of chromium.

The following reactions are taking place:

$$Cr(III) + e^- \xrightarrow{-0.81V} Cr(II) \quad (9)$$

$$Cr(II) + 2e^- \underset{-0.08V}{\overset{-1.20V}{\rightleftharpoons}} Cr(0) \quad (10)$$

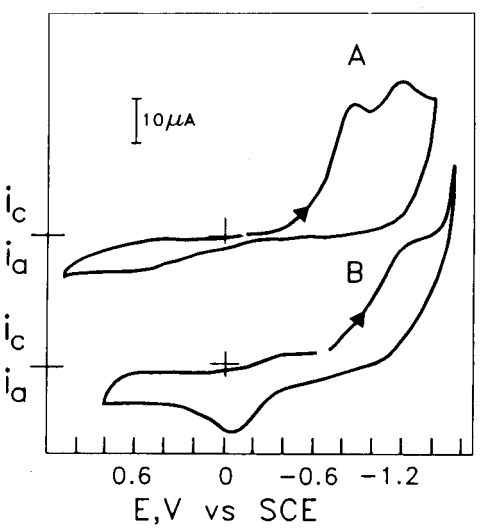

Fig. 4. Cyclic voltammograms in DMSO (0.1 M TEAP; $v = 0.1$ V s^{-1}) of solutions that are: (A) 1.0 mM in $[Cr^{III}(DMU)_6](ClO_4)_3$; (B) the same as A, but after electrolisys at −1.00 V vs. SCE.

Fig. 5 shows the cyclic voltammograms of a solution of 2-mercaptonicotinic acid in the presence of one equivalent of base and in the presence of increasing amounts of Cr(III), so that 1:3; 1:2 and 1:1 metal–ligand stoichiometric ratios are obtained in solution (Fig. 5A, B, C and D, respectively). It can be observed that when the concentration of metallic ion increases the peak current at −0.81 V vs. SCE increases which is due to the reduction of free Cr(III) to Cr(II). The visible spectra of these solutions are equivalent, which indicates that there is no interaction between the metallic ion and the carboxylate group.

Fig. 6 illustrates the effect of the addition of 0.27, 0.33, 0.50 and 1.00 equivalents of chromium(III) (Fig. 6B, C, D and E, respectively) on the voltammetric

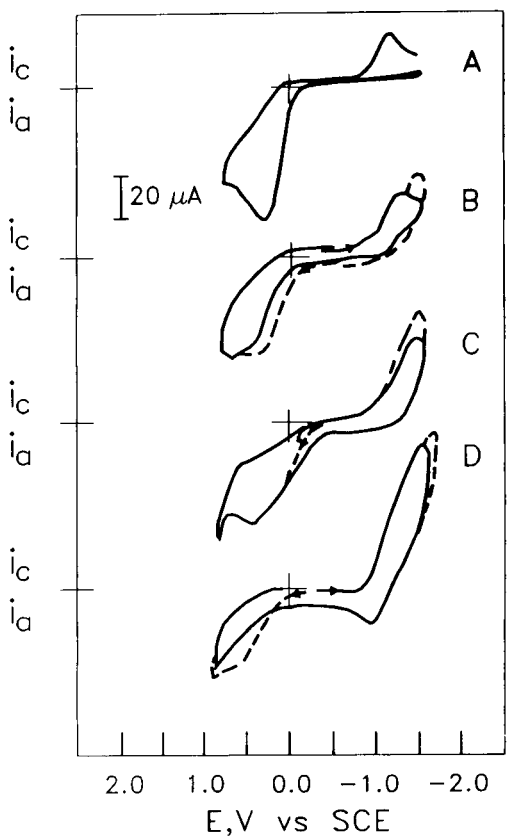

Fig. 5. Cyclic voltammograms in DMSO (0.1 M TEAP; $v = 0.1$ V s^{-1}) of (A) 3.0 mM in 2-mercaptonicotinic acid (2-MNA) and 3.0 mM TBAOH; (B) solution A plus 1.0 mM $[Cr^{III}(DMU)_6](ClO_4)_3$; (C) solution A plus 1.5 mM $[Cr^{III}(DMU)_6](ClO_4)_3$; (D) solution A plus 3.0 mM $[Cr^{III}(DMU)_6](ClO_4)_3$.

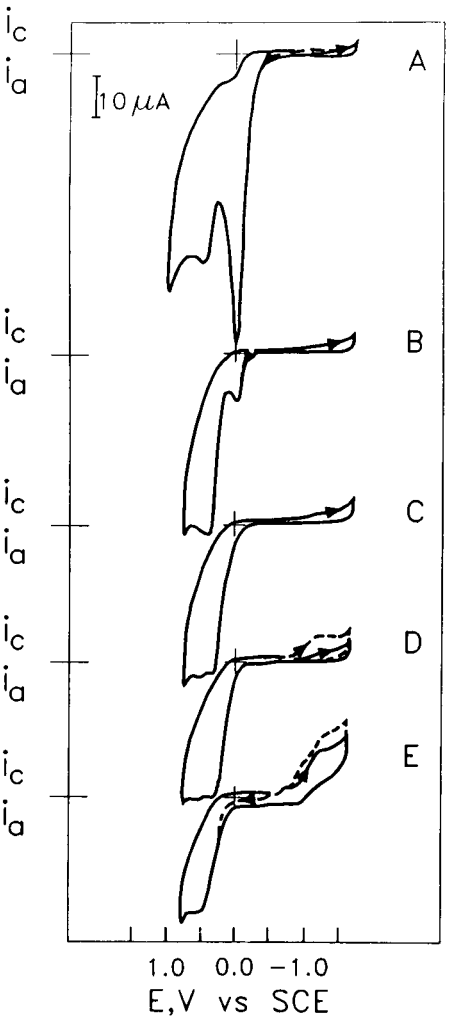

Fig. 6. Cyclic voltammograms in DMSO (0.1 M TEAP; $v = 0.1$ V s^{-1}) of solutions: (A) 3.0 mM in 2-mercaptonicotinic acid (2-MNA) and 6.0 mM in TBAOH; (B) solution A plus 0.8 mM $[Cr^{III}(DMU)_6](ClO_4)_3$; (C) solution A plus 1.0 mM $[Cr^{III}(DMU)_6](ClO_4)_3$; (D) solution A plus 1.5 mM $[Cr^{III}(DMU)_6](ClO_4)_3$; (E) solution A plus 3.0 mM $[Cr^{III}(DMU)_6](ClO_4)_3$.

behaviour of a 3.0 mM solution of the di-anion of the ligand (Fig. 6A). In the presence of 0.27 equivalents of chromium(III) (Fig. 6B) an anodic peak is observed at −0.00 V vs. SCE, which corresponds to the oxidation of the free ligand. In the presence of 0.33 equivalents of chromium(III) (Fig. 6C) this peak at 0.00 V vs. SCE is not observed. It can be concluded that a 1:3 complex is formed. On the other hand the reduction of

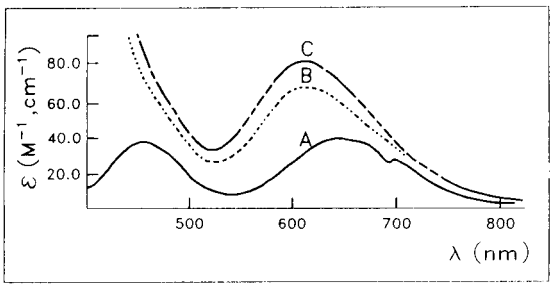

Fig. 7. Visible spectra in DMSO of solutions that are: (A) 3.0 mM in $[Cr^{III}(DMU)_6](ClO_4)_3$; (B) solution A plus 6.0 mM of 2-mercaptonicotinic acid (2-MNA) and 12.0 mM of TBAOH; (C) solution A plus 9.0 mM in 2-MNA and 18.0 mM of TBAOH.

free chromium(III) ($E_{peak} = -0.81$ V vs. SCE) is observed when the stoichiometric ratio is 1:2 and 1:1 (Fig. 6D and E, respectively).

3.4. Spectra of complexes with Cr(III)

Fig. 7 illustrates the visible spectrum of the DMSO complex of free Cr(III), and in the presence of 2 and 3 equivalents of di-anionic ligand (Fig. 7A, B and C, respectively). It can be observed that the solvated metallic ion presents absorption maxima at 460 nm ($^4T_1$, $\varepsilon = 34.0\ M^{-1}\ cm^{-1}$), 645 nm ($^4T_2$, $\varepsilon = 36.0\ M^{-1}\ cm^{-1}$) and a shoulder at 704 nm (^2E, $^2T_1$, $^4A_2$, $\varepsilon = 22.0\ M^{-1}\ cm^{-1}$) (Fig. 7A). The addition of di-anionic ligand causes a hipsochromic shift with a great increase in the extinction coefficients as the concentration of ligand in the solution increases reaching the maximum value at metal to ligand ratio of 1:3 (610 nm, $\varepsilon = 86.4\ M^{-1}\ cm^{-1}$) (Fig. 7C).

The magnetic moments for solutions that contain free metallic ion and in the presence of mono-anionic and di-anionic ligand are 3.8–3.9 MB, as expected for high-spin (d^3) chromium(III) ions.

3.5. Conditional constants determination

In order to determine the stoichiometry and conditional formation constant, spectrophotometric titration was performed at 610 nm. The results of this measurements show that the experimental curve is as linear as the theoretical curve, which indicates the high stability of the complex.

In 0.1 M TEAP supporting electrolyte chromium(III) gave a wave for the reduction of chromium(III) to chromium(II). Upon the addition of 2-mercaptonicotinic acid in the presence of two equivalents of TBAOH to a solution of chromium(III), the chromium reduction wave shifted to more negative potentials, indicating the complex formation. The magnitude of this shift depends upon the stability of the complex formed, the concentration of the complexing agent, and p, the number of moles of the complexing agent reacting with one mole of the metallic ion. In this case if the concentration of free ligand is ten times higher, the complex wave is shifted after the solvent reaction. Analysis of the polarographic data confirmed that the chromium(III) to ligand ratio is 1:3 and that the complex formed had a conditional stability constant of 2.5×10^{14} (25°C).

3.6. Conclusions

The results of this study show that the metallic ion in the complex is bound at the mercapto group, since in the presence of one equivalent of base only carboxylate is deprotonated and no complex is formed. The formation of a chromium(III)–sulphur bond is thermodynamically unfavourable because the Cr(III) ion is a hard acid while the sulphur ligands are soft bases [27]. However the results of this study show that the metallic ion in the complex is bound to the mercapto group, since in the presence of one equivalent of base only carboxylate is deprotonated and no complex is formed.

References

[1] W. Mertz, Physiol. Rev., 49 (1969) 163.
[2] J.F. Potter, P. Levin, R.A. Anderson, J.M. Freiberg, A. Reubin and D. Elahi, Metabolism, 34 (1985) 199.
[3] E. Offenbacher and F.X. Pi-Sunyer, Diabetes, 29 (1980) 919.
[4] W.H. Glinsmann and W. Mertz, Metabolism, 15 (1966) 510.
[5] K. Schwartz and W. Mertz, Arch. Biochem. Biophys., 85 (1959) 292.
[6] K. Schwartz and W. Mertz, Arch. Biochem. Biophys., 72 (1957) 519.
[7] National Diabetes Data Group, Diabetes, 28 (1979) 1039.
[8] E. Boyle, M.D.B. Mondschein and H.D. Harriman, Southern Medical J., 70 (1977) 1449.
[9] L. Sherman, J.A. Glennon, W.J. Brech, G.H. Klomberg and E.S. Gordon, Metabolism, 17 (1968) 439.
[10] C.T. Gurson and G. Saner, Am. J. Clin. Nutr., 24 (1971) 1313.
[11] K.N. Jeejeebhoy, R.C. Chu, E.B. Marliss, G.R. Greenberg and A.K. Bruce-Robertson, Am. J. Clin. Nutr., 30 (1977) 531.

[12] L. Ping and K. Matsumoto, Anal. Chim. Acta, 147 (1983) 205.
[13] M. Simonoff, Y. Llabador, C. Hamon and W.G.N. Simonoff, Anal. Chem., 56 (1984) 454.
[14] J.M. Harnley, K.Y. Patterson and C. Veillon, Anal. Chem., 55 (1983) 1417.
[15] K.W. Pratt and W.F. Kock, Anal. Chem., 58 (1986) 124.
[16] W.F. Davidson and W. Secrest, Anal. Chem., 44 (1972) 1808.
[17] Y. Jiacan, D. Guangzhi, G. Jiyou, Y. Baoxhen, C. Shuqing, C. Shunyang and C. Zerong, Huaxi Yike Daxue Xuebaon, 19 (1988) 167. (C.A., 109 (1988) 142370p).
[18] K. Govindaraju, K. Ramasami and D. Ramaswamy, J. Inorg. Biochem., 35 (1989) 127. (C.A., 110 (1989) 166263c).
[19] K. Govindaraju, K. Ramasami and D. Ramaswamy, J. Inorg. Biochem., 35 (1989) 137. (C.A., 110 (1989) 166264d).
[20] L.E. Gerdom, Diss. Abs. Int., 44 (1984) 3772-B.
[21] E. Gonzalez-Vergara, Diss. Abs. Int., 43 (1983) 3973-B.
[22] G.D. Christian, E.C. Knoblock, W.C. Purdy and W. Mertz, Biochim. Biophys. Acta, 66 (1963) 420.
[23] G.D. Christian, E.C. Knoblock and W.C. Purdy, Biochim. Biophys. Acta, 66 (1963) 415.
[24] R. Colton, Coord. Chem. Rev., 90 (1988) 1.
[25] F.A. Cotton, Química Inorgánica Avanzada, Limusa-Wiley, Mexico, 1969.
[26] D.T. Sawyer and J. Roberts, Experimental Electrochemistry for Chemists, Wiley Interscience, New York, 1974, p. 212.
[27] R.G. Pearson, J. Chem. Educ., 45 (1968) 581.
[28] W. Mertz, E.W. Toepfer, E.E. Roginski and M.M. Polansky, Fed. Proc., Fed. Am. Soc. Exp. Biol., 33 (1974) 2275.
E.W. Toepfer, W. Mertz, M.M. Polansky, E.E. Roginsky and W.R. Wolf, J. Agric. Food Chem., 25 (1977) 162.

ELSEVIER

Analytica Chimica Acta 298 (1994) 99–103

ANALYTICA CHIMICA ACTA

Simultaneous determination of cadmium and lead in indium metal and indium salts by differential pulse anodic stripping voltammetry without preliminary separation

J. Opydo

Institute of Chemistry, Technical University of Poznań, 60-965 Poznań, Poland

Received 17 December 1993; revised manuscript received 20 May 1994

Abstract

This paper presents a method for the determination of trace levels of cadmium and lead in indium metal and indium salts, using differential pulse anodic stripping voltammetry at the hanging mercury drop electrode. The electrochemical activity of indium, which usually interferes in the determination of cadmium and lead, is inhibited by the addition of Sulforokanol L-3 (oxyethylated lauryl alcohol sodium sulphate salt). The base electrolyte was 0.2 M citrate buffer at pH 3.7. This electrolyte in the presence of 0.1% Sulforokanol L-3 makes possible the determination of 5×10^{-9} M Cd(II) and 5×10^{-9} M Pb(II) in the presence of 0.05 M In(III), i.e., 9.8×10^{-6}% Cd and 1.8×10^{-5}% Pb in indium. The accuracy and precision of the described method were satisfactory (the relative standard deviation was 4.9–10.6% for Cd and 3.3–6.9% for Pb).

Keywords: Stripping voltammetry; Electrochemical masking; Cadmium; Indium; Lead

1. Introduction

In anodic stripping voltammetry problems occur when In(III), Cd(II) and Pb(II) ions have to be determined simultaneously because of their similar reduction potentials. A proper choice of supporting electrolyte allows the determination of two of them (e.g., Cd–Pb and In–Pb) provided that they occur in comparable amounts; a large excess of one of the ions causes coincidence of voltammetric peaks. Thus, when trying to determine part of these ions in the presence of excess amounts of others, it is necessary to perform their extraction separation or to use the effect of "electrochemical masking".

Previous investigations have shown that the degree of damping of the electrochemical activity of depolarizers increases with ionic potential [1,2]. Taking into account ionic potentials of Pb(II), Cd(II) and In(III) equal to 1.59, 2.02 and 3.26, respectively (after the acceptance of ionic radius according to Ref. [3]), it may be expected that the process of electroreduction will be inhibited more strongly in indium than in lead and cadmium.

There are many publications that report on damping of electrochemical activity of In, Cd and Pb. The influence of cationic surfactants on the anodic stripping peaks of many ions in various supporting electrolytes was investigated in [4], the influence of polyethylene glycols in tartrate solution was reported in [5], whereas the influence of Sulforokanol L-3 and alkylbenzenesulphonate on the anodic stripping peaks of lead and indium in various supporting electrolytes was studied in [6] and the influence of sodium dodecyl sulphate, sodium dodecyl sulphonate and sodium stearinate on

SSDI 0003-2670(94)00253-I

the peaks of many ions in various electrolytes was described in [2,7]. In a HCl–EDTA electrolyte containing phemerol, Cd was determined in the presence of excess amounts of indium [8]. All these studies, however, indicating a possibility to determine Cd and Pb in the presence of excess amounts of indium, do not permit a selective determination of Cd and Pb in indium matrices.

The aim of the present study was to develop a method for a simultaneous determination of Cd and Pb in indium and indium salts by differential pulse anodic stripping voltammetry (DPASV), after inhibiting the indium electrochemical activity by using Sulforokanol L-3. The supporting electrolyte was 0.2 M citrate buffer at pH 3.7. The choice of the supporting electrolyte and surfactant is partially based on earlier investigations [4–7] and partially on the present studies dealing with the influence of Sulforokanol L-3 (SR) on the anodic stripping peaks of Cd(II) in 0.5 M sodium sulphate solution, 0.2 M citrate buffer (pH 2.7, 3.7, 4.6 and 7.3) and 0.5 M tartrate buffer at pH 4.4.

2. Experimental

2.1. Apparatus

Anodic stripping voltammograms were obtained with a PA-4 polarographic analyzer, Laboratorni Pristroje (Czech republic). Electrochemical measurements were made in a 3-electrode system: a hanging mercury drop electrode (HMDE), produced by Laboratorni Pristroje, a saturated calomel electrode (SCE) and a Pt wire electrode. The differential pulse amplitude was 50 mV and the scan-rate was 10 mV s^{-1}.

2.2. Reagents

Sulforokanol L-3 was obtained from Rokita (Poland), spectroscopic indium wire from Johnson Matthey, indium A.R. and indium nitrate from POCh and indium chloride from Merck. The supporting solutions were prepared from the analytical-reagent grade chemicals: sodium sulphate, sodium citrate, citric acid, sodium tartrate and sodium hydrogen tartrate. Standard solutions of Cd(II), Pb(II) and In(III) were prepared by dissolving the metals in nitric acid. Solutions with concentrations below 1 mM were prepared just before use. Water was doubly distilled in a quartz still.

2.3. Determination of cadmium and lead in metallic indium

Weigh out about 0.1 g of indium, dissolve it in 2–3 ml of concentrated nitric acid, evaporate the excess of acid. Dissolve the remaining moist salts in a small amount of water and add 20 ml of 0.25 M citrate solution and 1.25 ml of 2% Sulforokanol L-3 solution. Adjust the pH to 3.7 ± 0.1, transfer the solution to a 25-ml standard flask and make up to the mark with water.

Transfer 20 ml of the solution into the voltammetric cell and pass purified nitrogen through it for 15 min. Start the stirrer and electrolyse for 2–15 min at -0.90 V vs. SCE (depending on the expected metals content). Record the stripping voltammogram of Cd and Pb from -0.90 to -0.10 V. Estimate the concentrations of metals by the standard additions method.

2.4. Determination of cadmium and lead in indium salts

Weigh an amount of salt equivalent to about 0.1 g of indium, dissolve it in 20 ml of 0.25 M citrate solution, add 1.25 ml 2% Sulforokanol L-3, and adjust the pH to 3.7 ± 0.1. Determine cadmium and lead as above.

3. Results and disscussion

The influence of SR on the anodic stripping peaks of Pb(II) and In(III) in various supporting electrolytes is described in the Ref. [6] containing a developed method for the determination of Pb in indium and indium salts. The investigations presented in this paper show a small inhibition of Pb electroreduction in 0.5 M Na_2SO_4, 0.2 M citrate solution (pH 3.7 and 7.3) and in 0.5 M tartrate solution at pH 4.4, whereas the indium peaks are suppressed for 100% in all applied supporting electrolytes, except for 0.5 M Na_2SO_4.

The influence of SR on the anodic stripping peaks of Cd(II) in different supporting electrolytes is presented in Fig. 1. The results obtained are presented as dependences of the relative peak heights (i/i_o) on the concentration of SR (c), where i is the peak height of a metal ion in the presence of a surfactant and i_o is the

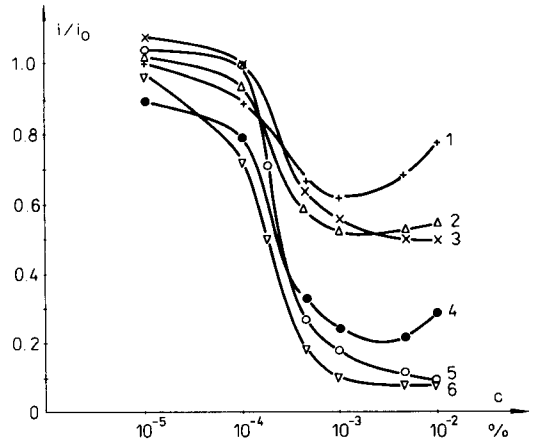

Fig. 1. Effect of Sulforokanol L-3 (SR) on the relative peak height of Cd(II) in (1) 0.5 M Na_2SO_4, (2) 0.2 M citrate buffer at pH 2.7, (3) 0.2 M citrate buffer at pH 3.7, (4) 0.2 M citrate buffer at pH 4.6, (5) 0.2 M citrate buffer at pH 7.3 and (6) 0.5 M tartrate buffer at pH 4.4. Concentration of Cd, 1 μM; deposition potential, −0.90 V vs. SCE; deposition time, 2 min.

peak height of a metal ion in the absence of a surfactant.

A very large (ca. 80%) decrease in the peak height of cadmium is observed already at nearly 10^{-3}% SR in tartrate solution as well as in citrate solution at pH 4.6 and 7.3. For this reason it is impossible to adapt tartrate solution, which was used in Ref. [6], for further studies. Considering determination of cadmium, the most advantageous would be the application of sodium sulphate solution, though in this supporting electrolyte the peak of indium is also not damped. Therefore, the most favourable seems to be the application of citrate solution at pH 2.7 and 3.7. In these electrolytes the peak of Cd(II) is damped in about 50%. In subsequent investigations, citrate buffer at pH 3.7 was used as a relatively well-know electrolyte from earlier studies.

Dependences in Fig. 1 show a fairly significant influence of the supporting electrolyte on the degree of the Cd electroreduction inhibition. The dependences obtained in citrate buffers could suggest that the degree of electrode process damping depends on the solution pH. On the other hand, however, the Cd peak damping in tartrate solution at pH 4.4 is comparable to that in citrate solution at pH 7.3, but it is the smallest in the solution of Na_2SO_4.

This problem is partially explained by results reported in Ref. [7]. The influence of supporting electrolyte does not depend either on the complex forms arising in the solution or on a complex stability. It is know that the inhibitory action of surfactants is related to a decrease of the electrode process constant rate [9–11]. For that reason electrochemically irreversible processes (i.e., controlled by a slow rate of charge transfer) should be significantly more susceptible to the action of surfactants than reversible processes. In Ref. [7] the directional coefficients (γ) as a criterion of electrode process reversibility were determined in the function $\log(i_g - i)i^{-1}$ vs. E, where i_g is a limiting current, i is the current at any point of the wave, and E is potential. The coefficients γ for Cd are: 35 in 0.5 M Na_2SO_4, 34 in 0.2 M citrate solution at pH 3.7, 62 in citrate solution at pH 4.6, 61 in citrate solution at pH 7.3 and 62 in 0.5 M tartrate solution at pH 4.4 (in citrate solution at pH 2.7, $\gamma = 32$). From these data it follows that electroreduction processes of Cd in citrate buffers at pH 4.6 and 7.3 and in tartrate buffer are controlled by a slow rate of charge transfer. Damping of Cd peaks by SR and other surfactants in these solutions is also the strongest.

Voltammetric characteristics of cadmium are presented in Fig. 2. In citrate solution at pH 3.7, cadmium forms the anodic stripping peak at the potential of −0.60 V. Curve a shows the dependence of the Cd peak height on the deposition potential (i_p vs. E_{dep}). The introduction of SR causes a decrease in the Cd peak height (curve a'). The strongest damping (ca.

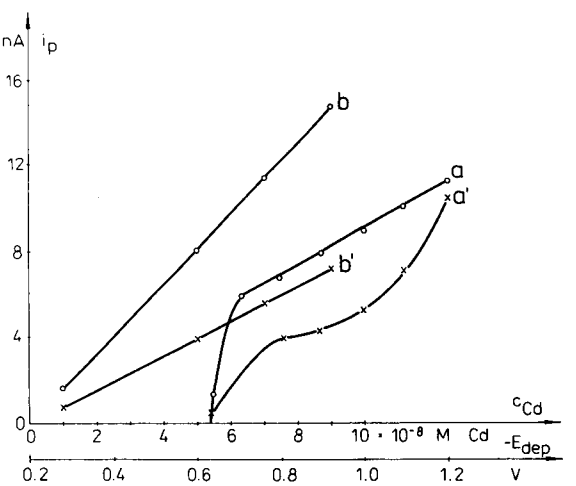

Fig. 2. Dependence of the peak current for cadmium on the deposition potential (a, a') and on the cadmium concentration (b, b'). Concentration of cadmium: (a, a') 5×10^{-8} M. Background electrolyte, (a, b) 0.2 M citrate buffer at pH 3.7; (a', b') as for (a) and (b) +0.1% Sulforokanol L-3. Deposition potential (b, b'), −0.90 V; deposition time 2 min.

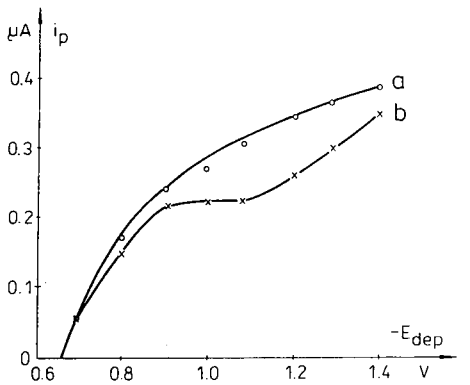

Fig. 3. Dependence of the peak current for indium on the deposition potential in the absence (a) and presence 1×10^{-5}% Sulforokanol L-3 (b). Concentration of indium, 1 μM. Background electrolyte, 0.2 M citrate solution at pH 3.7. Deposition time, 2 min.

50%) occurs in the potential range −0.8 to −1.0 V, after which it decreases with E_{dep} moving in a more negative direction. Such a strong damping of the Cd peak within this range of potentials is probably connected with the maximum adsorption potential, which ranges from −0.9 to −1.0 V for anionic surfactants [2]. Curves b and b′ show dependences of the Cd peak height on cadmium concentration. A linear dependence was found within the concentration range 5×10^{-9} to 1×10^{-6} M.

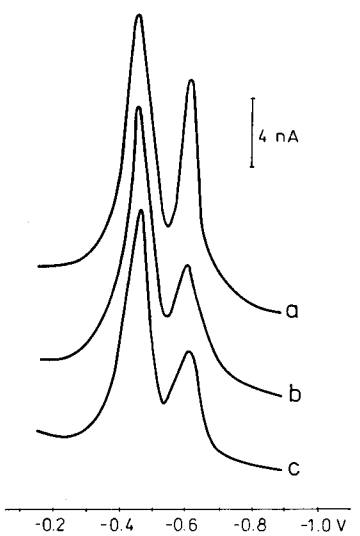

Fig. 4. Peaks for cadmium (5×10^{-8} M) and lead (5×10^{-8} M) in the presence of Sulforokanol L-3 and indium in 0.2 M citrate solution at pH 3.7. Concentration of indium: (a, b) 0; (c) 0.05 M. Concentration of Sulforokanol: (a) 0; (b, c) 0.1%. Deposition potential, −0.90 V; deposition time, 3 min.

Indium in citrate solution at pH 3.7 forms a peak at the potential of −0.58 V. Fig. 3 shows the dependences of i_p vs. E_{dep} for 1×10^{-6} M In in the absence (curve a) and in the presence of 1×10^{-5}% SR (curve b). A stronger inhibition of indium electroreduction by SR is observed when the deposition potential is below −1.1 V. When the potential moves in a more negative direction, it causes quite a rapid disappearance of inhibition. It follows from the analysis of curves a and b that the deposition potential used in further studies should be chosen. From the point of view of cadmium determination the most advantageous would be $E_{dep}=-1.2$ V. However, in view of a smaller inhibition of indium electroreduction at this potential, the potential of −0.9 V was chosen as optimum for the further part of the studies.

Complete damping of the indium electrochemical activity was obtained for 0.05 M In in the presence of 0.1% SR. A further increase of indium and SR concentrations does not result in complete inhibition. This at the same time is a medium making possible the determination of trace amounts of Cd(II) and Pb(II) (Fig. 4). Complete suppression of the indium peak at 0.05 M indium concentration makes possible the determination of Cd and Pb in the indium matrices. The determination of 5×10^{-9} M Cd and 5×10^{-9} M Pb in the indium matrix at 0.05 M concentration corresponds to 9.8×10^{-6}% Cd and 1.8×10^{-5}% Pb in indium.

The developed method was statistically evaluated by estimating the precision and recovery of cadmium and lead determined in the presence of 0.05 M indium and 0.1% SR. The results are summarized in Table 1. The recovery of added metals was very good and the precision of their determination was satisfactory.

Following the described procedure the concentrations of Cd and Pb were determined in the indium metal and indium salts with different degrees of purity. The results were compared with data obtained with the use of the atomic absorption spectrophotometric method (Table 2). The accuracy and precision of the proposed method is also satisfactory (the relative standard deviation ranged within 4.9–10.6% for Cd and 3.3–6.9% for Pb).

Experiments show that a 10^2–10^3-fold molar excess of Zn(II), Cu(II), Sb(III), Sn(IV) and Bi(III) has no effect on the determination of 5×10^{-9} M Cd and 5×10^{-9} M Pb.

Table 1
Recovery and precision of the determination of cadmium and lead in the presence of 0.05 M indium and 0.1 % Sulforokanol L-3[a]

Metal	Found (nM)	Added (nM)	Total found (nM)	S.D. (nM)	R.S.D. (%)
Cd	17	20	28.0	2.9	10.3
		50	66.5	6.1	9.2
		100	120.0	5.9	4.9
Pb	30	30	60.3	2.0	3.3
		60	89.0	3.3	3.7
		100	132.0	5.0	3.8

[a]Results are means of seven measurements.

Table 2
Cadmium and lead content of indium matrices

Indium matrix	Grade	Sample weight (g)	Cadium			Lead		
			Found DPASV ($\mu g\,g^{-1}$)	S.D. ($\mu g\,g^{-1}$)	Found AAS ($\mu g\,g^{-1}$)	Found DPASV ($\mu g\,g^{-1}$)	S.D. ($\mu g\,g^{-1}$)	Found AAS ($\mu g\,g^{-1}$)
In	A.R.	0.1	2.8	0.23	2.6	30.7	1.6	30.9
$InCl_3$	A.R.	0.2	1.7	0.18	1.5	5.8	0.4	5.7
$In(NO_3)_3 \cdot 4.5H_2O$	Reagent	0.3	2.2	0.14	2.4	16.9	0.7	16.6

This work was supported by the Technical University of Poznań, Grant No. 31-430/93/BW.

References

[1] Z. Lukaszewski, A. Ciszewski, M.K. Pawlak and J. Opydo, Euroanalysis IV, Fourth European Conference on Analytical Chemistry, Helsinki/Espoo, 23–28 August 1981, Book of Abstracts, M. Kivimäki and L. Nünistö, Abstract No. 203.
[2] J. Opydo, Doctoral Thesis, Technical University of Poznań, 1982.
[3] Yu.Yu. Lur'e, Spravochnik po analiticheskoi khimii, Izdat. Khimiya, Leningrad, Moscow, 1963, p. 382.
[4] A. Ciszewski and Z. Łukaszewski, Anal. Chim. Acta, 146 (1983) 51.
[5] M.K. Pawlak, Doctoral Thesis, Technical University of Poznań, 1977.
[6] J. Opydo, Anal. Chim. Acta, 262 (1992) 117.
[7] J. Opydo, Talanta, 39 (1992) 229.
[8] W. Christmann, Z. Łukaszewski and R. Neeb, Fresenius' Z. Anal. Chem., 302 (1980) 32.
[9] J. Lipkowski and Z. Galus, J. Electroanal. Chem., 98 (1979) 91.
[10] G. Pyzik and J. Lipkowski, J. Electroanal. Chem., 123 (1981), 351.
[11] R. Guidelli, M.L. Foresti and M.R. Moncelli, J. Electroanal. Chem., 113 (1980) 171.

ELSEVIER

Analytica Chimica Acta 298 (1994) 105–112

ANALYTICA CHIMICA ACTA

Binding characteristics of avidin and surface immobilized octylbiotin: implications for the development of dynamically modified optical fiber sensors

Yunlong Wang, Donald R. Bobbitt *

Department of Chemistry and Biochemistry, University of Arkansas, Fayetteville, AR 72701, USA

Received 2 March 1994; revised manuscript received 26 May 1994

Abstract

Specific sensing ligands can be immobilized onto C_{18} derivatized optical fibers by a dynamic modification protocol as part of a general strategy for producing optical fiber sensors. To investigate the influence of the hydrophobic surface and accessibility of the sensing ligand on the binding characteristics of the ligand and target analyte, an optical fiber sensor for fluorescently labeled avidin has been developed. Biotin's hydrophobicity is enhanced through the attachment of a C_8 moiety which allows it to be associated with the C_{18} modified optical fiber surface through a hydrophobic interaction. Measurement of both the time dependence and K_{assoc} for the binding of FITC–avidin to the surface immobilized biotin show that the hydrophobic immobilization process decreases the binding strength relative to that observed in homogeneous solution. When compared to previous studies in which a lipid-derivatized biotin was associated in an LB film, the association constant is reduced by 2–3 orders-of-magnitude. These results, in combination with the lipid-derivatized biotin/LB film studies suggest that spacers can be used to enhance the accessibility of the biotin moiety thereby leading to improved binding characteristics. This result has important implications for the design and development of dynamically modified, optical fiber sensors.

Keywords: Sensors; Avidin; Octylbiotin; Sensing ligands

1. Introduction

The incorporation of optical fibers as key components in remote sensing protocols is an area of active investigation due to the fact that optical fibers possess specific characteristics which suggest their use in these types of measurement situations [1,2]. These characteristics include the ability to deliver and collect light from remote locations, the ruggedness of the sensing system, the minimal interference expected in the measurement of a light signal as opposed to electrical transduction, and the small diameter of the fiber. This last property suggests that sensing systems based on optical fibers can be substantially miniaturized resulting in minimal impact on the system under study. For example, a submicrometer optical fiber sensor has been developed which is capable of providing pH measurements in a single cell from a rat embryo [3].

Although optical fibers can provide an excellent mode for the transfer of an analytical signal from a remote location, in an environment containing several closely related species, spectral discrimination alone is frequently inadequate to select among the various species. Thus, to improve the selectivity of the sensor, or

* Corresponding author.

SSDI 0003-2670(94)00261-J

to impart additional capability to the measurement system, specific sensing reagents have been associated with the optical fiber surface. Tromberg et al. [4] and Vo-Dinh et al. [5] have reported the successful attachment of a specific antibody to an optical fiber to produce an immunosensor of exceptional selectivity. Both anti-immunoglobin G [4] (selective for immunoglobin G) and anti-benzo[a]pyrene [5] (selective for benzo[a]-pyrene) have been covalently attached to either a support matrix [4] which was then mechanically fastened to the fiber surface, or to the fiber surface itself directly [4,5]. Although the selectivity of these sensing systems is excellent, they are not easily amenable to regeneration and this may limit their application.

As an approach towards the development of a regenerable optical fiber based sensor, Bright et al. [6] have demonstrated the successful attachment of anti-human serum albumin antibody fragments to a quartz matrix which was then mechanically fastened to the distal end of an optical fiber. The sensor was regenerated over 50 times by using chaotropic agents to disrupt the antibody–antigen complex, and the sensor was shown to provide good analytical figures-of-merit. Interestingly, the immobilized antibody fragments were about 40% less selective when compared to the binding characteristics of the native antibody. The authors suggest that surface immobilization may alter the binding characteristics of the antibody fragment. Recently, this approach has been improved as it has been shown that the stability of the surface immobilized antibody fragments can be enhanced by attaching the fragments to a fluoropolymer modified surface in place of the quartz substrata [7]. Ultimately, the success of this approach is governed by the binding characteristics of the sensing ligand–analyte couple and it is conceivable that in situations where this binding interaction is very strong, the complex may not be amenable to disassociation without causing damage to the sensing ligand or surface.

Selectivity can also be achieved in an optical fiber sensing system by coupling an enzyme to the fiber surface to take advantage of its specificity towards a particular substrate. For example, using a photoinitiated polymerization procedure, penicillinase was immobilized in a polyacrylamide matrix covalently linked to the optical fiber surface [8]. Ultimately, diffusion of the substrate into the matrix limits the performance of the sensor. Alternately, a novel approach has been recently described in which a covalently linked biotin surface on an optical fiber was used to associate the protein avidin. A biotinylated enzyme could then be coupled to the optical fiber through the binding of the biotin moiety on the enzyme to the avidin on the fiber [9]. Although the response time of this sensor was excellent (<2 min), the limit-of-detection was only 0.1 mM for various organic esters.

It is clear from the above discussion that the development of general strategies for the immobilization of sensing ligands onto optical fibers is an important factor in the development of this technology. A general approach for the renewable immobilization of sensing reagent with the surface of an optical fiber has recently been developed [10,11] based upon a dynamic modification protocol. In this approach, the surface at the sensing tip of an optical fiber is rendered hydrophobic through the covalent attachment of a C_{18} moiety. A desired ligand can then be associated with the modified fiber surface through either its inherent or designed hydrophobicity. For example, the introduction of a C_8 group at the N-3 position of riboflavin was found to impart sufficient hydrophobicity to the modified riboflavin such that it would adhere to a C_{18} modified optical fiber surface in aqueous solution. The binding of riboflavin binding protein (RBP) to the hydrophobically immobilized riboflavin led to a decrease in the intrinsic fluorescence of the dynamically associated riboflavin and the extent of fluorescence quenching could be related to the concentration of RBP. The regeneration of the sensing surface was achieved by washing off the riboflavin–RBP complex from the optical fiber with methanol, and the surface was then renewed by immersing the optical fiber tip in a solution of 3-octylriboflavin. In such manner, the sensing surface was renewed repetitively [10] demonstrating excellent reproducibility from one modification step to the next. The approach is general and the mild conditions used to associate the specific reagent with the sensing tip helps ensure the chemical, or biochemical activity of the reagent.

From these earlier studies it was observed that RBP exhibited different binding properties with 3-octylriboflavin associated with an optical fiber, as opposed to bulk solution studies of the modified riboflavin. This difference has implications for the use of the dynamic modification procedure to immobilize biological ligands that require complex structural elements to be

maintained in order for the association to proceed. In order to understand this question better, an optical fiber sensor for avidin has been developed which is based on dynamically associated octylbiotin. The unusually strong and fast non-covalent interaction of avidin with biotin makes the complex immune to extreme conditions of pH and other denaturing reagents [12,13]. Thus, this is an excellent test of the dynamic modification approach as the intact complex is difficult to disrupt. Since the binding properties of avidin and biotin have been well characterized, the knowledge gained from these studies can be used to direct investigations designed to utilize the dynamic modification process to associate complex biological entities on optical fiber surfaces.

2. Experimental

2.1. Materials

The optical fiber used for these studies had a 1000 μm core diameter and a protective jacket composed of nylon (Ensign-Bickford Optics, Avon, CT, type HCNM1000T). For hydrophobic modification of the optical fiber surface, chlorodimethyloctadecylsilane, chlorotrimethylsilane and methanol were purchased from Aldrich (Milwaukee, WI) and used without further purification. Toluene and methylene chloride were also obtained from Aldrich and were distilled under nitrogen prior to use. For the modification of biotin and assessment of its interaction with avidin, *N*-hydroxysuccinimide biotin (NHS-Biotin) and ImmunoPure FITC Conjugated Avidin ($F/P = 3.0$) were purchased from Pierce (Rockford, IL). Octylamine, diethyl ether, dimethylformide (DMF), isopropanol, dimethyl sulfoxide (DMSO) and HEPES (4-(2-hydroxyethyl)-1-piperazine-ethanesulfonic acid) were obtained from Aldrich and used as received. Water was deionized through a Fisher Science Ultrapure Cartridge (Barnstead Still and Sterilizer, Boston, MA, Model BD-1) prior to use. The nitrogen used as a blanket for the synthetic procedures was oxygen free and further purified by passing sequentially through a 30 × 5 cm diam. column containing anhydrous calcium chloride and then a 30 × 5 cm diam. silica gel column prior to use.

2.2. Instrumentation

The optical configuration used to measure the fluorescence from the dynamically modified optical fiber sensor has been described in detail previously [10]. Modifications made to improve the detection system over the previous report included the use of a boxcar sampling system for data collection and signal averaging, and a cooled photomultiplier tube to reduce the intrinsic noise level. 488.0 nm excitation light from an air-cooled argon ion laser was modulated using an acousto-optic modulator (AOM) (Interactive Radiation, Northvale, NJ, Model EFL-DO80A04) driven by an AOM driver (Model D080A010). The modulation frequency for the AOM was determined by a pulse generator (Hewlett-Packard, Colorado Springs, CO, Model 8011A). The first order beam from the AOM was used as the excitation source for fluorescence. Light detection was accomplished using a photomultiplier tube (PMT) cooled by a PMT cooler (Products for Research, Danvers, MA, Model TE104RF). The signal from the PMT was then sent to a boxcar sampling system (Stanford Research Systems, Palo Alto, CA, Model SR280 with Model SR250 gated integrator and averager). The time-dependent signal was sampled and averaged by the boxcar, digitized and then sent to a laboratory computer for storage.

2.3. Synthetic procedures

Preparation of C_{18} modified optical fiber

The optical fiber surface was prepared by successive polishing with 60, 9, 1 and 0.3 μm lapping film. The surface was then activated by refluxing the optical fiber in 2 M HCl for 2 h. This was accomplished by suspending a bundle of polished fibers in a 1000-ml round bottom flask containing 500 ml of the acid. The fibers were then washed thoroughly with distilled water and dried at 120°C overnight. The activated fibers were then placed in a 25-ml round bottom flask containing 20 ml of toluene and 0.5 g of chlorodimethyloctadecylsilane. The mixture was stirred and refluxed for 4 h, and then the reflux was continued in an ultrasonic bath for 24 additional hours. The solution mixture was removed and 20 ml of toluene containing 5 ml of chlorotrimethylsilane was added for end-capping. Ultrasonic agitation was continued for 12 h. All synthetic steps proceeded in an enclosed anhydrous system under the

protection of nitrogen. After modification, the fibers were placed in a Soxhlet extractor and washed in turn by methanol, methylene chloride and hexane.

Preparation of octylbiotin

50 μl of octylamine were added to a 5-ml vial containing 20 mg of NHS-Biotin dissolved in 1 ml of DMF. The mixture was stirred at room temperature for 24 h and then transferred to a 10-ml flask containing 1 ml of 0.25 M Na_2CO_3 to salt out the product. The precipitate was separated and washed three times with diethyl ether, and then thoroughly with water. The product was dried in vacuum at room temperature for 12 h and stored at 5°C. Characterization of the purified product was accomplished by ^{1}H NMR. {Data for octylbiotin: white solid, m.p. 185–187°C. ^{1}H NMR (90 MHz, $(CD_3)_2SO$) δ 0.9 (t, 3 H, $-CH_3$), δ 1.3 (m, 18 H, $-(CH_2)_3-$, $-(CH_2)_6-$), δ 2.1 (t, 2 H, $-CH_2CO-$), δ 2.7 (m, 3 H, $-(CH_2)S(CH)<$), δ 3.0 (m, 2 H, $>CHNHCO-$), δ 6.4 (d, 3 H, –CONH–). Data for NHS-Biotin, white solid, m.p. 170–172°C. ^{1}H NMR (90 MHz, $(CD_3)_2SO$) δ 1.6 (m, 6 H, $-(CH_2)_3-$), δ 2.1 (t, 2 H, $-CH_2COO-$), δ 2.6 (m, 3 H, $-(CH_2S(CH)<$), δ 2.8 (t, 4 H, $-CH_2CON-$), δ 3.0 (m, 2 H, $>CHNHCO-$), δ 6.4 (d, 2 H, –CONH–)}. The purified product exhibited a melting point of 185–186°C. For comparison, the NHS-Biotin starting material has a melting point of 170–172°C, while biotin has a m.p. of 232–233°C. The product was insoluble in water but readily soluble in isopropanol.

Avidin–biotin interaction studies

The dynamically modified avidin sensor was prepared by immersing the tip of a C_{18} modified optical fiber in 5 ml of 0.2 M octylbiotin (dissolved in isopropanol) for 5 min. The dynamically modified fiber was then rinsed with 10 mM HEPES buffer containing 0.15 M NaCl and dried with a stream of warm air. The tip of the octylbiotin modified optical fiber was then immersed in a 20 μl sample of avidin for incubation. After incubation, the fiber was rinsed with HEPES buffer to remove any non-specifically bound avidin, and then placed into 10 μl of HEPES buffer for fluorescence measurements. When the measurement was complete, the octylbiotin–avidin complex was removed from the fiber surface using sequential washes of first DMSO, and then methanol. The optical fiber surface was then renewed, as described above, prior to the next measurement cycle. The blank for each measurement was obtained using the same fiber as originally used for the fluorescence measurement, after first washing off the octylbiotin–avidin complex. Each measurement, including the blank was repeated a minimum of two times.

3. Results and discussion

As demonstrated previously [10], the dynamic modification approach has shown potential as a general method for immobilizing specific sensing ligands onto the surface of an optical fiber. However, as discussed, differences were noted in the binding between riboflavin binding protein and surface associated octylriboflavin which were not observed for nonimmobilized riboflavin. The association of riboflavin and RBP is not well characterized and no studies have been reported concerning the binding of a surface immobilized, hydrophobic riboflavin derivative to RBP. To better define the origin of the observed differences and assess their importance with respect to dynamic immobilization via a hydrophobic interaction, the association of biotin and avidin was used as a model system. Biotin, an important coenzyme in biological systems has been studied extensively and one of its well-known properties is its strong binding to avidin, a protein of 67 kDa found in egg-whites [14]. The avidin–biotin complex possesses an association constant, K_{assoc} which has been determined to be on the order of 10^{15} M^{-1}. Langmuir-Blodgett (LB) films doped with phospholipid-derivatized biotin have been studied in detail with respect to the binding of avidin to the immobilized biotin [15,16]. These films possess chemical and physical characteristics which are similar to the optical fiber bound hydrophobic surfaces used in the dynamic modification protocol. Thus, this interaction provides an ideal system which can be used to evaluate the potential of the dynamic modification technique in applications where complex structural elements direct the biological association and these elements must be preserved in order to maintain biological activity [17].

Biotin's hydrophobicity was enhanced through the elongation of the $-(CH_2)_4$–COOH moiety to $-(CH_2)_4$–$CONH(CH_2)_7CH_3$, as described in the Experimental section. The synthetic route utilized the succinamide derivative of the carboxylic acid function-

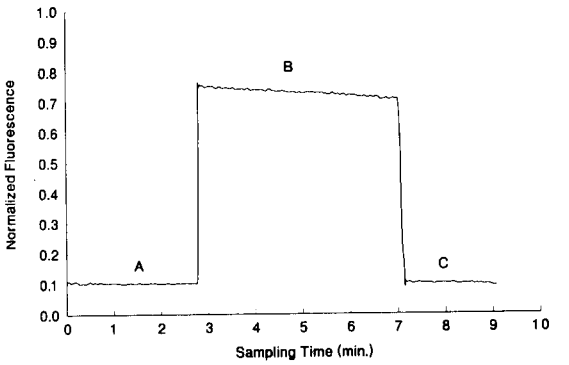

Fig. 1. Fluorescence signal obtained using a hydrophobically immobilized, octylbiotin-modified optical fiber. The octylbiotin-modified optical fiber was incubated in 20 μl of a 7.5×10^{-8} M solution of FITC–avidin for 15 min. The fiber was then rinsed with buffer and the fluorescence measured. Detection was carried out in a 10 μl sample of 10 mM HEPES saline buffer: excitation, 488 nm; fluorescence observed at 527 nm. The octylbiotin–avidin complex was then removed from the fiber surface by DMSO, followed by a methanol rinse prior to re-modification with octylbiotin.

ality due to the favourable leaving properties of this moiety. The reaction is quite facile resulting in a high yield of octylbiotin. ^{1}H NMR spectroscopic analysis of both the NHS-Biotin starting material and the octylbiotin product showed that the reaction and isolation procedures developed for the preparation of octylbiotin were effective yielding pure product. A strong ^{1}H resonance for $-(CH_2)_6-$ at $\delta=1.3$ ppm was observed for octylbiotin and the ratio of the peak area for this resonance relative to the area of ^{1}H resonances for the other functional groups was used as a reference for evaluating the purity of the product (see above). Octylbiotin would not dissolve in water or diethyl ether, it was only sparingly soluble in methanol but was readily soluble in DMF, isopropanol and DMSO.

Fig. 1 shows the fluorescence signal observed after the incubation of an octylbiotin-modified fiber in 20 μl of a 7.5×10^{-8} M solution of FITC-labeled avidin for 15 min, vida infra. Since there are three FITC labels per avidin, the effective concentration of fluorophore is actually 2.3×10^{-7} M. After the incubation period, the optical fiber was rinsed to remove nonspecifically absorbed avidin and then immersed in 10 μl of fresh buffer for the fluorescence measurements. The resulting fluorescence signal is given in region B and clearly shows the excellent signal-to-noise ratio (SNR) obtained with the optical fiber sensor. With continuous photoexcitation of the fiber the measured fluorescence was observed to decrease slowly with time and this was assumed to be due to photodegradation of the fluorescent label on the avidin. Support for this comes from a study in which the excitation light was blocked for several minutes while the fiber remained in the measurement buffer. Once excitation was re-established, the fluorescence observed was identical to that measured prior to the blockage of the excitation source. This suggests that photodegradation of the fluorophore and not dissociation of the biotin–avidin complex is responsible for the time-dependent reduction in the signal intensity.

The inflection points in Fig. 1 represent periods during which signal measurement was suspended as the surface characteristics were changed. Upon the completion of the fluorescence measurements, the biotin–avidin complex was removed from the optical fiber by immersion in isopropanol. It should be noted that the signal measured prior to incubation in labeled avidin (region A), and the signal obtained upon removal of the avidin–biotin complex (region C) is identical. This supports the idea that the surface sensing characteristics can be renewed, as needed without carryover. To determine the reproducibility of this approach, the established modification, measurement and wash steps were repeated 15 times using the same optical fiber surface, and the relative standard deviation in the fluorescence signal over the course of the 15 cycles was 4%. For this determination, the first 20 data points (10 s measurement period) were averaged together to provide a value for the maximum signal per modification trial. The good experimental precision suggests that the amount of biotin that can be associated with the optical fiber surface is determined by the surface characteristics (i.e., density of the hydrophobic layer) and is a constant from one measurement to the next.

The specificity of the dynamic modification procedure was tested by immersing both a bare fiber and a C_{18} modified fiber, respectively, in a solution of octylbiotin, and these fibers were then rinsed with buffer and incubated in a 7.5×10^{-7} M solution of FITC-labeled avidin. The fluorescent intensity observed for the bare fiber was equivalent to that of a blank measurement obtained using a bare fiber incubated directly with fluorescently labeled avidin. In comparison, the biotin modified C_{18} fiber had a stable fluorescent intensity which was 18 times larger than this blank. This

indicates that there is no association between the bare fiber and the octylbiotin, or between the bare fiber and avidin, while the hydrophobic interaction between the C_{18}-modified fiber and octylbiotin made the octylbiotin associate strongly with the fiber surface. The procedure was repeated for both bare and C_{18} modified optical fibers using nonhydrophobic (i.e., native) biotin. After incubation with fluorescently labeled avidin and rinsing, neither fiber provided a signal which could be differentiated from the blank. This lends support to the idea that the sensing ligand is associated through a hydrophobic interaction and not through a surface adsorption process. Finally, direct incubation of a C_{18} modified optical fiber and FITC–avidin gave a very small signal which was approximately 5% larger than the blank signal. This represents the degree of nonspecific association occurring between FITC–avidin and the C_{18} surface.

In the development of chromatographic detection schemes utilizing immobilized enzymes, researchers have identified the conformational mobility of the enzyme as the limiting parameter [18]. When the conformational mobility of the enzyme is reduced, for example, as a consequence of attachment through a covalent linkage to the support, the biological activity is usually severely affected. Pidgeon et al. [19] have used an immobilized artificial membrane-solid phase (IAM-SP) layer to associate trypsin with a silica-based support [20]. The IAM-SP approach utilizes a synthetic lipid environment to associate an enzyme through its inherent hydrophobicity. It was determined that trypsin, immobilized though this noncovalent interaction maintained hydrolytic activity towards a number of substrates. The use of a lipid environment to immobilize a biologically active entity is similar in principle to the dynamic modification protocol. The success reported for the IAM-SP method lends support to the premise that hydrophobic immobilization has potential as a general means for associating specific sensing ligands with optical fibers while at the same time maintaining the biological activity of the ligand. However, in order to apply this concept fully, more knowledge is needed concerning the effect of the hydrophobic surface on the binding process.

To address the effect of the hydrophobic immobilization procedure on the binding of octylbiotin to avidin, both the time dependence and the strength of the binding were determined. The time dependence of the binding behaviour of avidin to hydrophobically immobilized octylbiotin was studied using a standard solution of FITC-labeled avidin (7.5×10^{-7} M) in which a biotin modified fiber was incubated for varying periods of time. The results from these experiments are given in Fig. 2 which shows a plot of the fluorescent intensity measured with a biotin modified optical fiber as a function of the time of incubation in the FITC-avidin solution. To mitigate the influence of photodegradation on the data, the fluorescence was measured for approximately 1 min and only the first 20 data points were averaged to provide a measure of the signal for that incubation trial. The solid circles are the experimentally determined values, while the solid line is the best fit to the data and it is given to emphasize the point where the response saturates. It is clear that for this fiber and avidin concentration, the biotin on the fiber surface becomes saturated at incubation times exceeding approximately 15 min. This time domain is similar to that reported previously for a biotin–enzyme conjugate [21], and is identical to that observed for a dipalmitoyl-derivative of biotin immobilized in a hydrophobic LB film [16]. In Ref. [16], the accessibility of the surface immobilized biotin relative to the binding region in avidin was cited as the parameter defining the binding kinetics. It is likely that similar considerations govern the binding of avidin to hydrophobically immobilized octylbiotin. In comparison to the above results, the binding of biotin and avidin in homogeneous solutions is extremely fast [22] ($t_{0.5} \ll 2$ s; 10 nM Avidin) with a second order rate constant of 7×10^{7} M^{-1} s^{-1}.

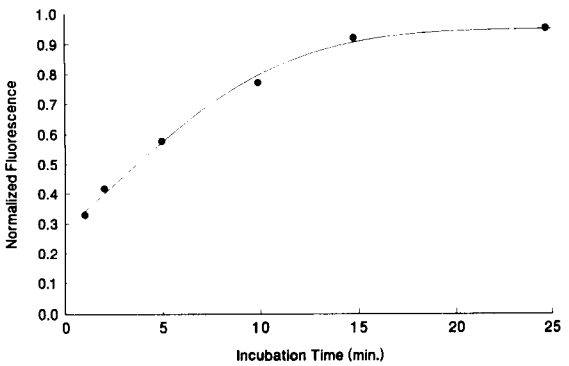

Fig. 2. Observed fluorescence measured as a function of incubation time. An octylbiotin modified fiber was incubated in a 7.5×10^{-7} M of FITC-labeled avidin for various time intervals. Measurement conditions given in Fig. 1.

To more fully define the binding characteristics of avidin and hydrophobically immobilized biotin, the association constant, K_{assoc} for the binding process was determined. For these experiments, octylbiotin modified fibers were incubated for a constant time period (15 min) in FITC–avidin solutions of varying concentration which spanned a range in avidin concentration of approximately two orders-of-magnitude. Since there are a fixed number of surface biotin sites, the binding of FITC–avidin to the surface can be thought of as a competition for these sites. Such processes are encountered, for example, when considering adsorption onto an adsorbent consisting of distinct surface sites and they are approximately modeled by the Langmuir isotherm at low concentration [23].

Using the Langmuir model, the fractional coverage of the surface sites by solute is given by θ, which is defined below in Eq. 1 [23]

$$\theta = K_{assoc}[\text{avidin}]/(1 + K_{assoc}[\text{avidin}]) \quad (1)$$

The observed fluorescence will be a function of the number of surface sites bound to labeled analyte. Thus, the measured fluorescence will track the extent of surface coverage and a plot of fluorescence intensity versus [FITC–avidin] will allow one to estimate K_{assoc} using Eq. 1. Fig. 3 shows the fluorescence intensity measured as a function of [FITC–avidin] in the incubation solution. The solid circles are experimentally determined values, while the line was determined using Eq. 1 and a nonlinear least squares fit to the experimentally determined data. From the fit, a value for K_{assoc} of 1.1 (± 0.4) $\times 10^7$ M^{-1} was obtained.

Inherent in the Langmuir model is the assumption that all sites provide an equivalent probability for a binding event to occur, and that this probability remains constant as the surface becomes saturated. The deviation from the model observed in Fig. 3 at high avidin concentrations is evidence that this assumption is no longer valid under these conditions. Therefore, the fit at low [avidin] was used for the determination of K_{assoc} where the Langmuir model is expected to hold. Another important consideration concerns the affect of biotin surface coverage on the binding of avidin. In Ref. [16] it was found that when a LB film was prepared using a phospholipid-derivatized biotin, the surface coverage of biotin controlled the amount of avidin that would bind as long as the surface coverage was less than 5% of saturation. For surface coverages of 5%, or greater,

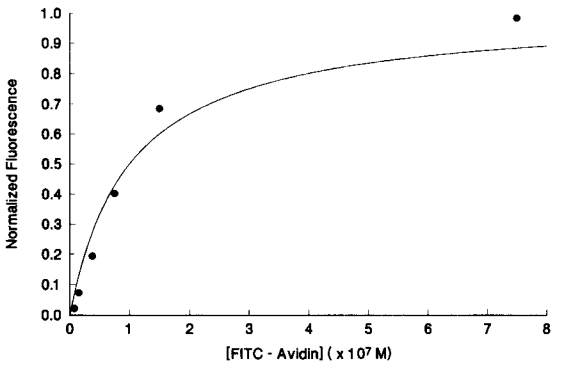

Fig. 3. Observed fluorescence measured as a function of [FITC–avidin]. The solid circles are experimentally determined values, while the solid line represents the best fit of the data to Eq. 1. Measurement conditions given in Fig. 1.

it was found that avidin binding was independent of the amount of biotin on the surface. It is assumed that this is due to the large size difference between avidin and biotin and it is expected that similar considerations would hold for the dynamically modified optical fiber system.

The K_{assoc} determined for hydrophobically immobilized octylbiotin can be compared to a value of 9×10^9 M^{-1} observed for avidin binding to a dipalmitoyl-derivative of biotin associated in an LB film [16]. This report cites accessibility of the surface associated biotin as a key factor in the observed binding characteristics. From tabulations of bond lengths and angles these authors estimate that the dipalmitoyl biotin derivative is slightly longer (ca. 2–5 Å) than the hydrophobic tail of the LB surface ($CH_3(CH_2)_{18}COOH$) in which it is immobilized. Therefore, by inspection, it is clear that the C_8 biotin derivative used for the studies reported herein is not protruding far, if at all from the C_{18} surface on the fiber and this may contribute strongly to the nonaccessibility of the biotin. Further, in Ref. [16] it was found that when the biotin moiety was extended away from the hydrophobic LB film surface by a spacer placed between the hydrophobic tail and the hapten, the observed K_{assoc} increased by 1 to 2 orders-of-magnitude, and the time domain for binding equilibrium to occur decreased by a factor of approximately 5. This improvement is significant and clearly shows that such considerations as surface accessibility are important and must be considered in designing ways to improve the hydrophobic modification protocol.

4. Conclusions

These studies have shown that the dynamic modification process, as applied to the production of optical fiber sensors, is compatible with complex biological molecules and associations. The well defined structural requirements that govern the binding of avidin to biotin are maintained for surface immobilized octylbiotin and these results suggest that a similar process will work for other complex associations. For the dynamically modified avidin sensor, the binding characteristics, in terms of the time domain necessary to achieve saturation of surface sites has been established. These characteristics are similar to previous reports involving biotin immobilized in LB films. Although the strength of the binding between dynamically associated octylbiotin and avidin, as determined by K_{assoc} is substantially reduced relative to that measured in homogeneous solution for avidin and biotin, the response is similar to that observed using a hydrophobic LB film to immobilize a lipid–biotin derivative. One result of note from the LB film studies [16] was that the binding was enhanced by the use of a spacer to position the biotin moiety away from the hydrophobic region of the LB film surface. By extension of this concept, spacer arms may also improve the hydrophobic immobilization protocol and work is in progress designed to evaluate this idea more fully.

Acknowledgements

This work was supported, in part by grant No. EHR-9108762 from the National Science Foundation and grant No. 1 R03 RR04236-01 from the National Institutes of Health. D.R.B. also acknowledges the support of the Camille and Henry Dreyfus Foundation through a teacher-scholar fellowship.

References

[1] W.R. Seitz, CRC Crit. Rev. Anal. Chem., 19 (1988) 135.
[2] O.S. Wolfbeis, Fiber Optic Chemical Sensors and Biosensors, Vol. I, II, CRC Press, Boca Raton, FL, 1991.
[3] T. Weihong, Y.S. Zhong, S. Smith, D. Birnbaum and R. Kopelman, Science, 258 (1992) 778.
[4] B.J. Tromberg, M.J. Sepaniak, T. Vo-Dinh and G.D. Griffin, Anal. Chem., 59 (1987) 1226.
[5] T. Vo-Dinh, B.J. Tromberg, G.D. Griffin, K.R. Ambrose, M.J. Sepaniak and E.M. Gardenhire, Appl. Spectrosc., 41 (1987) 735.
[6] F.V. Bright, T.A. Betts and K.S. Litwiler, Anal. Chem., 62 (1990) 1065.
[7] F.V. Bright, K.S. Litwiler, T.G. Vargo and J.A. Gardella, Jr., Anal. Chim. Acta, 262 (1992) 323.
[8] T.J. Kulp, I. Camins, S.M. Angel, C. Munkholm and D.R. Walt, Anal. Chem., 59 (1987) 2849.
[9] S. Luo and D.R. Walt, Anal. Chem., 61 (1989) 1069.
[10] F.K. Ogasawara, Y. Wang and D.R. Bobbitt, Anal. Chem., 64 (1992) 1637.
[11] D.R. Bobbitt, F.K. Ogasawara, Y. Wang and K. Ng, Proc. SPIE-Int. Soc. Opt. Eng., 1648 (1992) 227.
[12] E.A. Bayer and M. Wilchek, Methods Biochem. Anal., 26 (1980) 1.
[13] J.M. Becker and M. Wilchek, Biochim. Biophys. Acta, 264 (1972) 165.
[14] M. Wilchek and E.A. Bayer, Methods Enzymol., 110 (1990) 184.
[15] S. Zhao and W.M. Reichert, in P. Stroeve and A.C. Balazs (Eds.), Macromolecular Assemblies in Polymeric Systems, ACS Symposia Series 493, American Chemical Society, Washington, DC, 1992, p. 122.
[16] S. Zhao and W.M. Reichert, Langmuir, 8 (1992) 2785.
[17] P.C. Weber, D.H. Ohlendorf, J.J. Wendoloski and F.R. Salemme, Science, 243 (1989) 85.
[18] T. Alebic-Kolbah and I.W. Wainer, Am. Lab., 10 (1993) 52R.
[19] C. Pidgeon, C. Marcus and F.M. Alvarez, in T.O. Baldwin and J.W. Kelly (Eds.), Applications of Enzyme Biotechnology, Plenum Press, New York, 1992, p. 201.
[20] W.-K. Chui and I.W. Wainer, Anal. Biochem., 201 (1992) 237.
[21] S. Daunert, L.G. Bachas and M.E. Meyerhoff, Anal. Chim. Acta, 208 (1988) 43.
[22] N.M. Green, Biochem. J., 89 (1963) 585.
[23] A.W. Adamson, Physical Chemistry of Surfaces, Wiley, New York, 2nd edn., 1967, Chap. 8.

ELSEVIER

Analytica Chimica Acta 298 (1994) 113–119

ANALYTICA CHIMICA ACTA

Use of a biosensor consisting of an immobilized NADH oxidase column and a hydrogen peroxide electrode for the determination of serum lactate dehydrogenase activity

Masayoshi Tabata [a,*], Fumiyo Koushima [a], Masayuki Totani [b]

[a] *College of Medical Technology, Kyoto University, Sakyo-ku, Kyoto 606, Japan*
[b] *National Institute of Health and Nutrition, Shinjuku-ku, Tokyo 162, Japan*

Received 4 March 1994; revised manuscript received 13 May 1994

Abstract

A sensitive flow system for electrochemical determination of the reduced coenzyme NADH was developed using immobilized NADH oxidase from *Bacillus licheniformis*. The immobilized enzyme was packed into a 20 mm × 2 mm I.D. mini-column, and the sample volume used was only 5 μl per assay, with an assay time of approximately 20 s and a detection limit of 100 pmol NADH. The flow system using a biosensor consisting of an immobilized NADH oxidase column and a hydrogen peroxide electrode was applied to the determination of lactate dehydrogenase (LDH) activity in human serum, which was obtained by measuring the NADH produced in the LDH reaction for 3 min at 37°C. The use of an immobilized NADH oxidase column avoided interference by NADH peroxidase in the NADH oxidase preparation. The present method gave a linear response up to 3120 I.U. l^{-1} LDH with satisfactory reproducibility and accuracy. The serum LDH activity correlated satisfactorily with that obtained by a well-established spectrophotometric method. The immobilized enzyme reactor unit showed good operational stability over a 2-month period, during which it was repeatedly used for over 1600 analyses.

Keywords: Enzymatic methods; Flow system; Hydrogen peroxide electrode; Immobilized enzymes; Lactate dehydrogenase; NADH oxidase; Serum

1. Introduction

Lactate dehydrogenase (LDH) is one of the valuable enzymes in serum used in the early diagnosis of myocardial infarction and hepatitis. Therefore, the activity of LDH should be determined rapidly and in a small volume of serum sample. The most widely used means of determining LDH activity in serum are spectrophotometric measurements that follow the rate of oxidation of NADH [1] or the rate of reduction of NAD^+ [2] in the LDH reaction at 340 nm. The reduction in the pyruvate concentration as the dinitrophenylhydrazone [3] and the coupling of NAD^+ reduction to the reduction of a tetrazolium salt, for example 2-*p*-iodophenyl-3-*p*-nitro-phenol-5-phenyl tetrazolium chloride (INT),

* Corresponding author.

SSDI 0003-2670(94)00231-A

with phenazine methosulfate or diaphorase serving as an intermediate electron carrier [4] have been measured by colorimetric methods. Direct measurement of the rate of oxidation of NADH or reduction of NAD^+ at 340 nm and the dinitrophenylhydrazine method, were not very sensitive. The tetrazolium salt methods were inaccurate, because they involved many problems in the reduction of the tetrazolium salt. Fluorimetric [5,6], chemiluminometric [7] and enzyme electrode [8] methods for measuring serum LDH activity have also been reported. However, the former two required expensive instruments, and the latter was insufficiently sensitive.

We took an interest in measuring NADH with a hydrogen peroxide electrode, and developed a sensitive and accurate method for determining serum LDH activity, which did not require a blank correction. The method developed required 5.0 μl of serum, with an assay time of approximately 3 min, using a simple flow system involving an immobilized NADH oxidase (NOX) column and a hydrogen peroxide electrode with a flow-through cell. The NOX preparation used contained not only high NOX activity but also low NADH peroxidase activity. However, the use of an immobilized NOX column removed the effect of NADH peroxidase.

The reaction mixture incubated at 37°C for 3 min for the LDH reaction was introduced into the NOX column to produce hydrogen peroxide from NADH according to the NOX reaction:

$$\text{lactate} + NAD^+ \xrightarrow{\text{LDH}} \text{pyruvate} + NADH + H^+$$

$$NADH + H^+ + O_2 \xrightarrow{\text{NOX}} NAD^+ + H_2O_2$$

The reaction mixture containing the produced hydrogen peroxide was introduced into the hydrogen peroxide electrode, and the hydrogen peroxide concentration was determined by measuring the slope of the initial linear portion of the response curves obtained with the hydrogen peroxide electrode.

The new method is described here, and the potential of applying the NOX column to the determination of a wide variety of dehydrogenases and analytes of biological interest is discussed.

2. Experimental

Apparatus

The equipment (Fig. 1) included a peristaltic biominipump AC-2120 (ATTO Corporation, Tokyo), a hydrogen peroxide electrode OX-01 with a flow-through cell (Kyoto Daiichi Kagaku) and a recorder 056-1001 (Hitachi, Tokyo).

Materials

NOX (from *Bacillus licheniformis*, 2.3 U mg^{-1} solid, 36 μg protein mg^{-1} solid) was obtained from Marukin Shoyu, Kyoto. NOX has been found to have a molecular weight of 240 000 and to exist as a tetramer with a subunit molecular weight of 60 000. The enzyme contained 1 mol of FAD per subunit. The NOX was very stable, showed high catalytic activity, and did not contain detectable amounts of other oxidases and catalases [9]. NAD^+ and NADH used were from Kohjin, Tokyo. All other chemicals were commercially available and of analytical-reagent grade. Porous alkylamino glass (80–120 mesh, 500 Å pore size, 0.17 meq. functional amino group g^{-1}) was obtained from Pierce, Rockford, IL.

Reagents

LDH activity was determined using a NOX column and 50 mM sodium pyrophosphate buffer, pH 8.8, containing 60 mM lithium lactate, 0.6

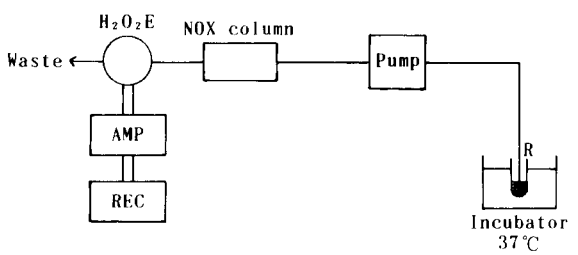

Fig. 1. Flow system for the determination of serum LDH activity using a biosensor consisting of an immobilized NOX column and a hydrogen peroxide electrode. R = reaction mixture containing 5.0 μl sample and 500 μl pyrophosphate buffer (50 mM, pH 8.8) with 60 mM lactate, 0.6 mM NAD^+ and 0.69 μM FAD. Pump = peristaltic pump. NOX column = 20 mm × 2.0 mm. H_2O_2E = hydrogen peroxide electrode. AMP = amperometer. REC = recorder. The flow-rate used was 1.4 ml min^{-1}. The feed rate of the chart paper was 120 mm min^{-1}.

mM NAD^+ and 0.69 μM flavin adenine dinucleotide (FAD).

Preparation of immobilized enzymes

NOX was immobilized onto porous alkylamino glass beads with glutaraldehyde through Schiff's base formation according to the method of Weetall [10]. To 1.5 ml of the NOX preparation (30 mg ml^{-1}) were added 100 mg of glutaraldehyde-treated glass beads. The protein concentration of the enzyme solution was determined by measuring the absorbance at 280 nm before and after the immobilization reaction. The coupling yield was calculated as the percent disappearance of the amount of protein initially added to the reaction mixture [11], and was found to be 69%.

Analytical procedure

An NOX column was prepared by packing a mini-column, 20 mm × 2.0 mm I.D., with NOX glass beads according to the method described previously [11]. The column contained ca. 102 mg wet weight of glass beads, which held 0.27 mg of NOX. A schematic diagram of the flow system is shown in Fig. 1. PTFE tubing (0.5 mm I.D.) was used throughout the flow system.

LDH activity was assayed as follows. Pyrophosphate buffer (0.5 ml, 50 mM, pH 8.8) containing 60 mmol of lactate, 0.6 mmol of NAD^+, and 0.69 μmol of FAD per liter was pre-incubated at 37°C for 5 min. The LDH reaction was started by adding 5.0 μl of serum. After the reaction mixture was incubated for 3 min at 37°C, it was introduced into a flow-through cell equipped with a hydrogen peroxide electrode through the NOX column at a flow-rate of 1.4 ml min^{-1}. The potential of the hydrogen peroxide electrode was fixed at 0.6 V, and the current measured with an ammeter. The current response curve obtained with the hydrogen peroxide electrode was registered with a recorder at a fast feed rate of chart paper, 120 mm min^{-1}. In order to determine the LDH activity with high detection sensitivity in a small amount of reaction mixture, the slope, i.e. the change in current for 5 s, of the initial linear portion of the response on the recorder was measured. For comparison, the LDH activity in serum was also determined by the ultraviolet spectrophotometric method using pyruvate as the substrate on a Hitachi Model 726 automatic analyzer.

3. Results

Effect of FAD concentration on the NOX reaction

The time course of the soluble NOX-catalyzed oxidation of NADH in the presence and absence of added FAD is shown in Fig. 2. The catalytic reaction rate in the presence of added FAD (25 μM) was about 10 times faster than that in the absence of added FAD, which was very low. The rate in the NOX column reactor was also low in the absence of added FAD. Therefore 0.69 μM FAD was incorporated in the buffer passing through the NOX column. These results are in

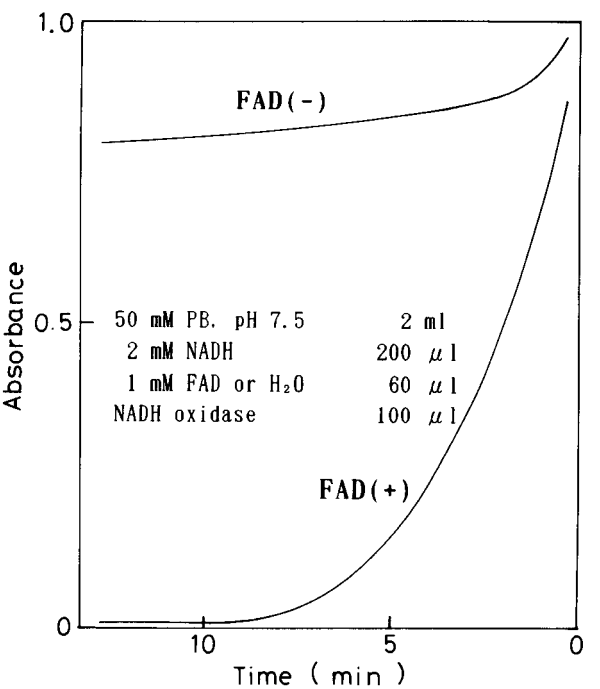

Fig. 2. Time course of NOX-catalyzed NADH oxidation. The decreased absorbance at 340 nm was recorded during the incubation of NOX with NADH alone or NADH plus FAD in a total volume of 2.36 ml at 30°C. The direction of recording is from right to left. PB = potassium phosphate buffer. The concentration of the NOX preparation was 1.0 mg ml^{-1}.

agreement with those obtained using NOX from *Bacillus megaterium* [12] and *Thermus aquatious* [13], but not from *Brevibacterium ammoniagenes*, which gave high activity even in the absence of added FAD but involved great difficulties in purification [14].

pH optimum of immobilized NOX

The pH optima of soluble and immobilized NOX were studied in the pH range 6.5–10.5. The pH profile for immobilized NOX was almost the same as that for soluble NOX. No significant difference in the responses was found over the pH range 6.5–10.5, suggesting that the immobilized NOX had a very broad pH optimum. This result would be applicable to link NOX to an NAD^+-dependent dehydrogenase which had a definite pH optimum. In the present method pH 8.8 was selected for the optimal reaction of LDH.

Recovery of hydrogen peroxide in the NOX reaction

For the soluble enzyme, 50 μl of NOX solution in the range 0.66 to 4.0 mg ml^{-1} were added to 3.0 ml of 50 mM potassium phosphate buffer, pH 7.0, containing 25 μM FAD and 0.10 mM NADH. After all the NADH in the reaction mixture was converted to NAD^+ at 30°C by the NOX reaction, the hydrogen peroxide produced was measured with the hydrogen peroxide electrode. The amount of hydrogen peroxide produced by the NOX reaction was compared with the amount produced in a similar reaction mixture, but containing 0.10 mM hydrogen peroxide instead of 0.10 mM NADH. The recovery of hydrogen peroxide produced by the NOX column (20 mm × 2.0 mm I.D.) was also examined in the system shown in Fig. 1. The results obtained are summarized in Table 1. In the experiments involving NADH, the recovery decreased as the reaction time of soluble NOX became longer, however, the NOX column showed good recovery. The amount of hydrogen peroxide in the solution containing no NADH did not decrease even after 32 min. These results showed that the NOX preparation had NADH peroxidase activity. NADH peroxidase could not be removed from the NOX preparation by chromatography.

Table 1
Recovery of hydrogen peroxide in the NOX reaction

NOX preparation (μg)	NADH [a] (mM)	H_2O_2 [a] (mM)	Reaction time [b] (min)	Recovery (%)
33		0.10	32	100
33	0.10		32	49
66	0.10		18	63
100	0.10		12	69
400	0.10		3	80
400		0.10	3	100
Column [c]	0.10		1 s [d]	97

[a] The final concentration in the reaction mixture.
[b] The reaction time required for all the NADH (0.10 mM) in the reaction mixture to be converted to NAD^+.
[c] 20 mm × 2.0 mm.
[d] The time (in seconds) required to pass through the NOX column.

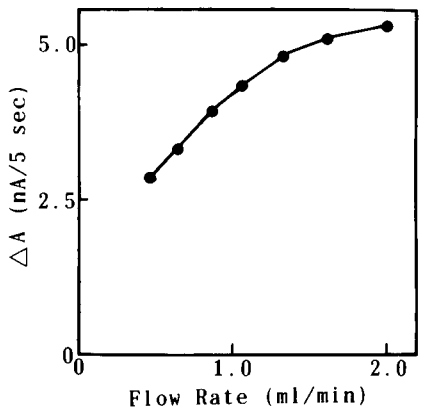

Fig. 3. The effect upon the response of the flow-rate through the biosensor consisting of an NOX column and a hydrogen peroxide electrode. The final concentration of NADH was 85 μM.

Effect of flow-rate on response

Fig. 3 shows the effect of the flow-rate of the reaction mixture on the change in current. This change gradually increased with flow-rate, but it did not reach a plateau even at 2.0 ml min^{-1}. This high flow-rate shortened the initial linear portion of the response curve and lowered the reproducibility, because the volume of the reaction mixture used was small (505 μl). From this consideration, 1.4 ml min^{-1} has been selected as the optimum flow-rate.

Time course of LDH reaction

The time course of the LDH reaction using human serum with an LDH activity of 1231 I.U. l^{-1} was examined. LDH activity was measured by determining the change in current for 5 s after a 1-, 2-, 3-, 4-, or 5-min incubation at 37°C of reaction mixtures containing the substrate and serum. The LDH activity increased linearly with incubation period up to 5 min. All subsequent data were obtained from a 3-min incubation.

Sample volume

The optimal sample volume for the determination of serum LDH activity was examined by using serum with a LDH activity of 1231 I.U. l^{-1} in the range 3–10 μl. The change in current over 5 s increased linearly with sample volume up to 10 μl. Since smaller serum volumes lowered the reproducibility of the response, 5 μl was selected as the optimal sample volume.

3.1. Evaluation of analytical data

Determination of NADH and NADPH

A flow system (Fig. 1) involving the NOX column reactor and the hydrogen peroxide electrode was used to determine NADH and NADPH. A wide range of proportionality was found between sample concentration up to 1.8 mM for NADH or 20 mM for NADPH, measuring the change in current for the first 5 s (Fig. 4). The NOX column converted almost all the NADH to NAD^+. The substrate selectivity of the NOX column for NADH was approximately 11 times larger than that for NADPH in the presence of added FAD, as shown in Fig. 4. Although not shown in the figure, the linearity reached 10 mM for NADH and 110 mM for NADPH under the standard conditions.

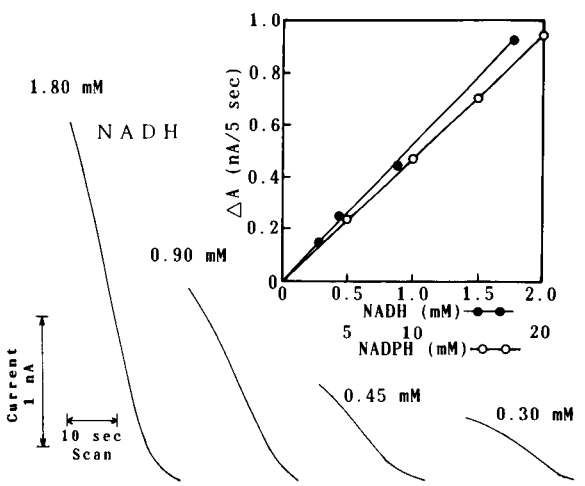

Fig. 4. Determination of NADH and NADPH using a flow system with a biosensor consisting of an immobilized NOX column and a hydrogen peroxide electrode. Tracings of the chart records for standard NADH solutions and plots (inset) for calibration curves for (•) NADH and (○) NADPH are shown. NADH and NADPH are shown as the concentration in the sample.

Table 2
Precision of the LDH activity determination

Sample	Concentration (I.U. l^{-1})	Coefficient of variation (%)	
		Within-day	Day-to-day
Serum 1	94.0 ± 4.70 [a]	5.0	
	95.0 ± 6.27		6.6
Serum 2	1121 ± 32.5	2.9	
	1119 ± 44.8		4.0

[a] Mean ± standard deviation ($n = 10$).

Linearity of LDH activity

A calibration graph obtained by first diluting human serum containing 3120 I.U. l^{-1} LDH with physiological saline is linear up to at least 3120 I.U. l^{-1} LDH activity, and has the equation

$$\Delta A = 540[\text{LDH activity (I.U. } l^{-1})]$$

where ΔA is the A charge $\times 10^{-9}$ per 5 s.

Precision

Two specimens of pooled human sera with low and high LDH activities were repeatedly analyzed over a 10-day period. As shown in Table 2, the present method gave satisfactory results for within-run and day-to-day precision.

Detection limit

Using standard NADH and NADPH solutions, the lower limit of detection (3 × baseline noise) was found to be 0.1 nmol for NADH and 1.2 nmol for NADPH per 5 μl sample.

Operational stability

The NOX column had retained 85% of its original activity after about 1600 runs over 2 months. When the column was stored at 4°C, no loss of activity occurred even after 5 months.

Comparison with a standard method

Comparison measurements of LDH activity in serum were carried out with serum samples from hospitalized patients in Kyoto University Hospital. The results obtained using the present method (y) compared well with the routine laboratory data obtained by the ultraviolet spectrophotometric method (x) using pyruvate as the substrate up to at least 1000 I.U. l^{-1} (lactate → pyruvate): $y = 0.419x - 9.320$, $r = 0.991$, $n = 44$, where r is the correlation coefficient. Because the rate of conversion of lactate to pyruvate by the LDH reaction was approximately half as fast as it of pyruvate to lactate, the present method using lactate as the substrate showed approximately half the activity (I.U. l^{-1}) of the ultraviolet method using pyruvate as the substrate.

4. Discussion

Because pyruvate at high concentration inhibits the LDH reaction, the method using the pyruvate-to-lactate reaction is inaccurate at elevated levels of LDH due to exhaustion of the pyruvate substrate with consequent loss of zero-order reaction conditions. The LDH activity was also determined by measuring the pyruvate, lactate, or NADH produced by the LDH reaction in a flow system involving a hydrogen peroxide electrode and the respective immobilized oxidases for the products, namely pyruvate oxidase, lactate oxidase, or NOX. When pyruvate oxidase or lactate oxidase was employed for such an assay, samples of serum containing a considerable concentration of endogenous pyruvate or lactate, always required a blank correction, which doubled the number of runs per sample. However, when endogenous lactate or pyruvate in serum was removed by using an immobilized lactate or pyruvate oxidase/catalase column as a pre-column prior to the action of LDH in the flow-injection analysis system, the blank correction was not necessary [7]. Since endogenous NADH was not detected in serum, the present method did not need a blank correction or any pre-column, which simplified the procedure and the system.

Two particular techniques were used to increase the sensitivity and shorten the assay time in the present method. One was the use of an immobilized NOX column (20 mm × 2.0 mm) which was independent of the presence of NADH peroxidase in the NOX preparation, and produced as much hydrogen peroxide as possible in about 1 s. The other was that LDH activity was estimated from the change in current over 5 s of the initial linear portion of the response curve.

As shown in Table 1, the recoveries of hydrogen peroxide decreased considerably as the time required for all the NADH in the reaction mixture to be oxidized to NAD by soluble NOX became longer. However, the NOX column showed a very high recovery. We postulate that in the soluble form, the following reaction of NADH peroxidase contained in the NOX preparation might proceed more easily in the reaction mixture because NADH peroxidase, NADH and hydrogen peroxide were present together in the reaction mixture for a long time, while in the immobilized NOX column, the NADH peroxidase reaction could hardly proceed in the column because almost all of NADH was converted to NAD in the column in about 1 s.

$$NADH + H^+ + H_2O_2 \xrightarrow{\text{NADH peroxidase}} NAD^+ + 2H_2O$$

Thus, when NOX was used, the immobilized NOX in column form was more applicable to determine the hydrogen peroxide produced from NADH than soluble NOX. The determination of peak area or peak height to measure serum LDH activity needed a large volume of serum sample and lengthened the assay time. However, the present method which estimated LDH activity from the change in current for 5 s over the initial linear portion of the response curve as shown in Fig. 4 lessened the volume of the reaction mix-

ture, namely serum sample, and shortened the assay time.

Since the present method is a simple analytical system with a very short assay period, it can be further applied to any compound or any reaction that gives rise to NADH. For example, we found that creatine kinase activity and 3-hydroxybutyrate could be determined by placing an additional co-immobilized hexokinase/glucose-6-phosphate dehydrogenase column for creatine kinase activity and an additional immobilized 3-hydroxybutyrate dehydrogenase column for 3-hydroxybutyrate just before the NOX column, respectively.

Acknowledgement

The authors thank Marukin Shoyu Co. Ltd. for the generous supply of the NOX preparation, and Kyoto Medical Science Laboratory for the cooperation of this work.

This work was supported by a Grant from the Human Health Science Foundation, Japan.

References

[1] F. Wroblewski and S. LuDue, Proc. Soc. Exp. Bio. Med., 90 (1955) 210.
[2] W.E.C. Wacker and D.D. Vlner, New Engl. J. Med., 255 (1956) 449.
[3] P.G. Cabaud and F. Wroblewski, Am. J. Clin. Pathol., 30 (1958) 234.
[4] A.L. Babson and G.E. Phillips, Clin. Chim. Acta, 12 (1965) 210.
[5] S. Udenfriend (Ed.), Fluorescence Assày in Biology and Medicine, Academic Press, New York, 1962.
[6] L. Brooks and H.G. Olken, Clin. Chem., 11 (1965) 748.
[7] M. Tabata, M. Totani and T. Murachi, Anal. Biochem., 193 (1991) 112.
[8] K. Miki, T. Ikeda, S. Todoriki and M. Senda, Anal. Sci., 5 (1989) 269.
[9] T. Sugimori, Y. Tsukada and Y. Tatsuki, Japanese Patent No. 63-251082, 1988.
[10] H.H. Weetall (Ed.), Immobilized Enzymes, Antibodies and Peptides, Marcel Dekker, New York, 1975.
[11] J. Endo, M. Tabata, S. Okada and T. Murachi, Clin. Chim. Acta, 95 (1979) 411.
[12] Y. Saeki, M. Nozaki and K. Matsumoto, J. Biochem., 98 (1985) 1433.
[13] C.J. McNeil, J.A. Spoors, D. Cocco, J.M. Cooper and J.V. Bannister, Anal. Chem., 61 (1989) 25.
[14] T. Murachi, M. Totani, M. Ikemoto and M. Tabata, J. Biotechnol., 14 (1990) 33.

ELSEVIER

Analytica Chimica Acta 298 (1994) 121–128

ANALYTICA CHIMICA ACTA

Determination of hydrogen peroxide in sea water by flow-injection analysis with chemiluminescence detection

David Price [a], Paul J. Worsfold [a,*], R. Fauzi C. Mantoura [b]

[a] *Department of Environmental Sciences, University of Plymouth, Plymouth PL4 8AA, UK*

[b] *Plymouth Marine Laboratory, Prospect Place, West Hoe, Plymouth PL1 3DH, UK*

Received 18 April 1994; revised manuscript received 25 May 1994

Abstract

Hydrogen peroxide (H_2O_2) plays a key role in many marine chemical processes, e.g., redox reactions involving transition metals and organic compounds. A rapid, flow-injection procedure with chemiluminescence detection for the determination of H_2O_2 in sea water is reported. It is based on the H_2O_2 induced oxidation of an alkaline solution of luminol in the presence of a catalyst (cobalt(II)). The sample throughput was 120 h^{-1} with small sample volumes (100 μl) and low detection limits (10 nM in Milli-Q water; 5 nM in sea water, $S/N=3$). The working linear range, which is suitable for the determination of ambient levels of H_2O_2 in sea water was 5–500 nM. A portable, automated version of the monitor has been successfully deployed onboard ship in the western Mediterranean and a typical depth profile for H_2O_2 is presented.

Keywords: Flow injection; Chemiluminescence; Hydrogen peroxide; Sea water; Waters

1. Introduction

Hydrogen peroxide is ubiquitous in the hydrosphere and is an important species in many marine chemical processes. It is believed to play a vital role in redox reactions in sea water, e.g., the "photo-Fenton reaction" involving iron(II), organic matter and hydroxyl radicals [1] and is particularly influential in the top 10 metres where it can be present at concentrations of up to 1000 nM [2]. Elevated levels of H_2O_2 are indicative of highly photochemically active sea water [3] and its measurement has been used to trace areas of reactive water [4]. Hydrogen peroxide is primarily produced photochemically via free-radical reactions between dissolved organic chromophores and oxygen [5] but minor (<5%) sources include biological production from certain species of phytoplankton [6] and wet/dry deposition of photochemically produced H_2O_2 in the atmosphere [7]. Decomposition has been found to occur by both biological [8] and photochemical [9] pathways. Hydrogen peroxide is a reactive, and therefore transient, species in sea water which implies that analysis must be carried out immediately after sample collection.

Various laboratory based analytical techniques have been reported for the quantification of H_2O_2 in synthetic solution [10] but only two of these have been used at sea. Johnson et al. [11] used the reaction of *N*-ethyl-*N*-(sulphopropyl)aniline and 4-aminoantipyrene with H_2O_2 to form a coloured condensation product ($\lambda_{max}=569$ nm) using a reagent-injection flow-injection (FI) manifold. The detection limit for this method was 12 nM (3 S.D.). A fluorimetric horseradish peroxidase-scopoletin method was originally used for

* Corresponding author.

SSDI 0003-2670(94)00250-P

atmospheric detection of H_2O_2 [12] but has since been used at sea [3,7,13,14]. In this reaction, catalysed by horseradish peroxidase, H_2O_2 is quantified by its quenching of the fluorescence of scopoletin. The method reported a working range of 0–200 nM (detection limit not specified) but higher concentrations can be determined by dilution with sea water of known H_2O_2 concentration [3]. A continuous-flow system based on this reaction has since been developed [7]. A similar limit of detection (4–5 nM; 3 S.D. of blank) was achieved with a laboratory-based fluorimetric method for sea water samples [15]. Hydrogen peroxide was quantified by dimerisation of (*p*-hydroxyphenyl)acetic acid in the presence of peroxidase. This batch method used a single mixed reagent that produced a stable product at sea which did not require immediate measurement.

Flow injection with on-line preconcentration and chemiluminescence (CL) detection has been used successfully for the shipboard determination of four metal ion species (cobalt [16], manganese [17], iron [18] and copper [19]). Low cost, high sensitivity and excellent portability make the FI–CL approach ideal for rapid shipboard determinations. The best known liquid phase CL reaction involves the oxidation of luminol (5-amino-2,3-dihydro-1,4-phthalazinedione) by H_2O_2 in the presence of a catalyst. The reaction is optimal at pH 10–11 and is catalysed by a variety of metal ions and haem-containing enzymes; cobalt(II) is the most efficient inorganic catalyst. When the components are mixed blue light ($\lambda_{max}=440$ nm) is emitted with a maximum CL intensity reached 2 s after mixing.

This paper reports an FI method with CL detection for the direct determination of H_2O_2 in sea water at the nM level. Results from shipboard trials of the automated monitor in the western Mediterranean are also presented.

2. Experimental

2.1. Reagents and standards

All solutions were prepared from ultra-pure Milli-Q water (Millipore). Luminol, cobalt(II) nitrate hexahydrate and 30% v/v H_2O_2 were analytical grade and supplied by Fluka (Gillingham). All other chemicals were reagent grade and supplied by Merck (Poole).

The reagent stocks and working solutions were prepared in 0.1 M sodium carbonate and the pH adjusted by addition of 2 M HCl. Stock solutions of luminol (10^{-3} M) and cobalt(II) (10^{-2} M) in high density polythene containers (stable for 2 months) were used to prepare working solutions by serial dilution and kept refrigerated (4°C) to minimise decomposition. Dilute luminol solutions were most active approximately 24 h after preparation and therefore freshly prepared the day before use.

Aliquots of freshly prepared stock solutions of H_2O_2 were acidified with 2 M HCl and titrated with standard potassium permanganate. The stock solutions were then diluted with Milli-Q water to accurately known concentrations. Storage of a 0.1 M stock solution of H_2O_2 at 4°C showed little decomposition ($<2\%$) over a period of a month.

2.2. Instrumentation and procedures

The FI manifold (Fig. 1) was optimised for rapid determinations due to the instability of the analyte. PTFE tubing (0.8 mm i.d.) was used throughout except for the peristaltic pump tubes which were silicone. The sample (100 μl) was introduced into the luminol carrier stream by a Universal Valve Switching Module (Anachem) with a PTFE rotary injection valve (Rheodyne 7010), merged with the cobalt(II) stream and transported to the detector. The light detector was a low noise, end window PMT (Thorn EMI 9789QA). An internal amplifier (Thorn EMI C634) was connected to the PMT and both were housed in a light tight container. The PMT was supplied with 1.1 kV from a Thorn EMI PM28B power supply and the amplifier was independently powered by a 15 V supply (BBH Products, Farnell).

The two streams, after merging at a perspex T-piece within the detector housing, passed into a coiled glass flow-cell (240 μl) situated immediately in front of the PMT window. The resulting signal was recorded as a voltage on a strip chart recorder (Kipp and Zonen, BD111). The analytical system (peristaltic pumps and injection valve) was controlled by an in-house designed custom-made 8052 micro-controller. The controller could operate independently or via a user interface to a portable computer.

All instrumentation was housed in a wooden container ($100\times50\times60$ cm) to allow transportation and

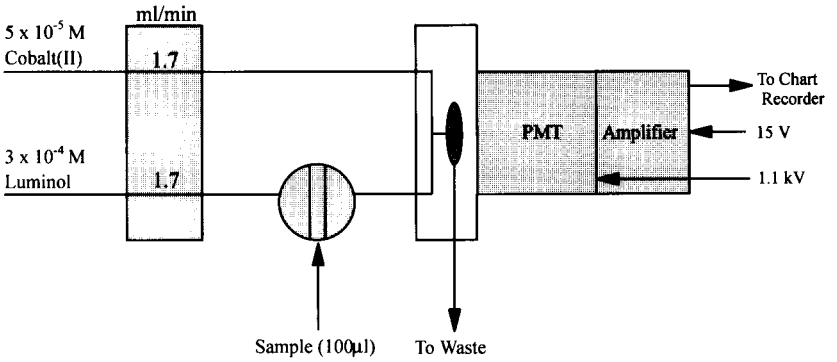

Fig. 1. Flow-injection manifold for the chemiluminescence based determination of H_2O_2 in sea water. The distance from the injection valve to the point of merging was 20 cm and the distance from the point of merging to the flow cell was 2.0 cm.

fixing to shipboard benches. The individual components were held in place by bungee ties while at sea.

3. Results and discussion

3.1. Background chemiluminescence

A continuous background CL emission is generated as a result of mixing of the two reagent streams. This is typically of the order of 50–150 mV and is largely due to the presence of H_2O_2 in purified waters such as Milli-Q. An elevated background such as this would seriously degrade the limit of detection and therefore make the technique unsuitable for the determination of H_2O_2 in sea water. Previous methods for low level H_2O_2 determinations have used catalase to provide H_2O_2 free blanks [7,15] but the catalase remains active in solution and is therefore unsuitable for preparing reagents. In this work H_2O_2 was scavenged from all water used to prepare reagents by passing it through a gravity-fed column of MnO_2 chemically bound to Amberlite XAD-7 polymeric beads. This material was prepared by heating 0.5 M potassium permanganate (500 ml) to 70–80°C, adding the beads (100–200 ml) and maintaining the temperature for 15 min. After cooling, the coated beads were washed and packed into a gravity fed column (80 mm height, 10 mm diameter). The procedure was adapted from a reported method for scavenging radionuclides from sea water [20]. Hydrogen peroxide was removed according to the following reaction:

$$MnO_2 + H_2O_2 + 2H^+ = Mn^{2+} + O_2 + 2H_2O$$

This approach is preferable to using a column of solid MnO_2 because it maintains good flow characteristics and is effective for at least 30 days of regular use. All reagent solutions were therefore prepared using H_2O_2 scavenged Milli-Q water to reduce the continuous background CL signal. Preliminary experiments showed that this procedure routinely reduced the background CL emission to 1–5 mV, which was sufficient for the determination of H_2O_2 in sea water at the nM level. Reagent solutions were degassed with helium before use to prevent the entrainment of air bubbles within the manifold. Background electronic noise was minimised to 0.5–5 mV (peak-to-peak) using a low-noise PMT.

3.2. Optimisation

Optimisation was carried out using a modified simplex algorithm (written in house). The key variables for maximising the sensitivity of CL emission were considered to be the flow rate of the luminol and cobalt(II) streams (these were kept equal to achieve good mixing at the T-piece), the pH of both streams (these were kept equal to provide a homogeneous pH), the sample volume, the voltage applied to the PMT and the luminol and cobalt(II) concentrations. The starting point for the simplex was taken from a previously reported manifold for H_2O_2 determination in synthetic media [21]. The ranges, step sizes, starting conditions and optimum conditions for H_2O_2 determinations are shown in Table 1. These conditions were valid for H_2O_2 concentrations up to 1000 nM in both Milli-Q and sea water and were typically reached after 15–20 iterations

Table 1
Results from simplex optimisation of the FI–CL method for H_2O_2 in sea water showing the range, step size, starting conditions and optimum conditions of each variable

Variable	Unit	Range	Step size	Starting conditions	Optimum conditions
Flow rate	ml min^{-1}	0.8–2.0	0.1	1.3	1.7
pH	–	9.0–12.0	0.2	10.0	10.8
Sample vol.	ml	0.03–0.40	Variable	0.03	0.10
PMT voltage	kV	0.9–1.2	0.05	1.1	1.1
[Luminol]	M	10^{-8}–10^{-4}	Variable	1×10^{-8}	3×10^{-5}
[Cobalt(II)]	M	10^{-8}–10^{-2}	Variable	1×10^{-6}	5×10^{-4}

Table 2
Calibration data for H_2O_2 solutions prepared in Milli-Q water and sea water

$[H_2O_2]$ (nM)	Milli-Q water		Sea water	
	CL Emission (mV)	R.S.D.; $n=5$ (%)	CL emission (mV)	R.S.D.; $n=5$ (%)
0	16	4.7	24	3.5
5	17	3.2	30	2.1
10	21	2.6	37	1.6
25	25	2.1	42	1.9
50	40	2.1	80	1.9
75	55	1.8	125	1.9
100	67	2.0	175	0.3
250	215	1.0	455	0.3
500	450	0.1	910	0.1

The correlation coeficients (r^2) for Milli-Q water and sea water are 0.993 and 0.998 respectively.

of the simplex. All subsequent experiments used these optimum conditions unless otherwise stated.

3.3. Sea water calibration

Surface sea water was collected from the English Channel (approximately 15 km south of Plymouth at the Eddystone Rocks), filtered, transferred to a high density polythene container and stored in the dark.

A potential difficulty with this approach to H_2O_2 detection in sea water is the fact that sea water is buffered at ~pH 8.2 but the analytical method is optimal at pH 10.8. At such a high pH precipitation of calcium and magnesium cations as their hydroxides normally occurs but was not experienced within the FI manifold due to the high flow rates used and the dispersion of the sea water sample. A protocol of daily flushing with 0.5 M HCl was however established as a precautionary measure.

The working linear range of the optimised manifold was 5 to 500 nM, which is suitable for the determination of ambient levels of H_2O_2 in sea water. Calibration data are shown in Table 2 and represented graphically in Fig. 2. The limits of detection ($S/N=3$) were 5 and

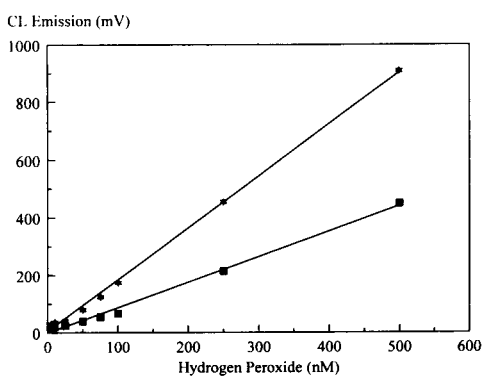

Fig. 2. Hydrogen peroxide calibrations in Milli-Q water and sea water. ■ = Milli-Q; ★ = sea water.

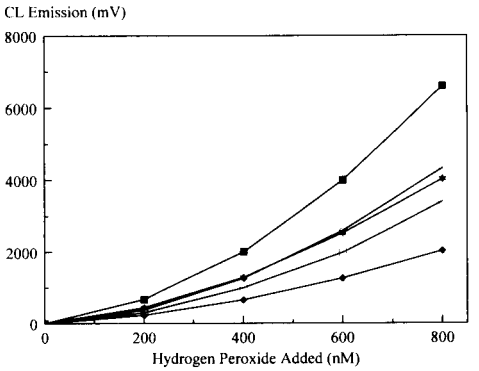

Fig. 3. CL emission of H_2O_2 spiked estuarine samples (Tamar) and spiked Milli-Q water. Salinity (expressed as ‰) was measured using an Autolab Precision Salinometer (Model 601 Mk. III). ■ = 34.1‰; ◇ = 30.7‰; □ = 26.1‰; ◆ = 0‰; ★ = Milli-Q water.

10 nM for sea water and Milli-Q respectively. Repeatability was in the range of 0.1–4.7% for replicate sample injections ($n=5$) and the reproducibility for the complete experimental procedure (including sample manipulation) was 3.8% for the analysis of replicate samples of 100 nM H_2O_2 ($n=5$). Higher H_2O_2 levels, e.g., those found in rainwater [7], can be quantified by sample dilution or by re-optimisation of the experimental conditions.

3.4. Matrix effects

Samples were taken from various locations in the Tamar estuary, ranging from the river end-member (i.e., 0‰ salinity) to the sea water end-member (34.1‰ salinity), and spiked with 200–800 nM H_2O_2. The CL emission from each of these treated samples and similarly treated Milli-Q water is shown in Fig. 3. These experiments were carried out using elevated reagent concentrations (to prevent reagent depletion at higher H_2O_2 concentrations) and the responses are therefore non-linear.

The sea water end-member gave a higher CL emission than Milli-Q water whilst the river water end-member gave a lower emission. River water is characterised by a significantly higher concentration of organic matter, lower pH and lower salinity than sea water. The reduced CL emission in river water can be explained by the rapid partial removal of the added H_2O_2 spike on reaction with the organic matter. The enhanced emission for the sea water matrix is more difficult to explain. Fig. 4 clearly shows that the effect is not due to changes in NaCl concentration. Additional experiments showed that sample pH had no effect on the CL emission over the pH range 3.0–10.0 due to buffering within the FI manifold. Trace metals in the matrix also had no effect because their concentrations in natural waters are at least one thousand times lower than the concentration of the Co(II) catalyst used. In order to eliminate potential matrix effects during shipboard operation, e.g., in close proximity to an estuarine plume, a standard additions procedure was used throughout.

3.5. Shipboard measurements

Hydrogen peroxide was determined at sea using the optimised manifold deployed onboard RRS Discovery in the western Mediterranean for 4 weeks in July 1993. Sea water samples were transferred from 10 l Niskin/Go-Flo bottles attached to a 12 bottle rosette into separate 50 ml amber glass bottles. Each sample was drawn directly into the manifold using PTFE tubing and the analysis of 12 samples, including standard additions, took 45 min. The practical limit of detection for the standard addition procedure onboard ship was 10 nM and the reproducibility ($n=4$) for a 42.3 nM surface sea water sample was 1.3%. Over 40 depth profiles were obtained during the period of the cruise from different oceanographical environments. All profiles exhibited a surface maximum followed by a sharp, near exponential decline in concentration with depth, impli-

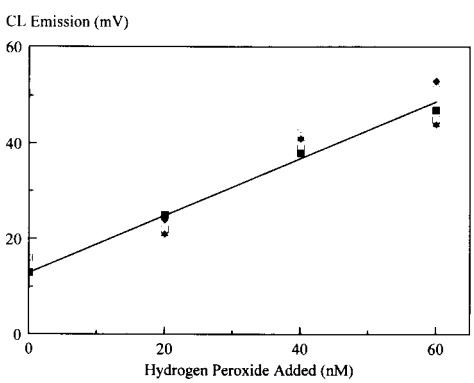

Fig. 4. Effect of sodium chloride concentration (expressed as ‰) on CL emission of H_2O_2 induced oxidation of luminol. ■ = 0‰; ◇ = 10‰; ★ = 20‰; ◆ = 30‰; □ = 40‰.

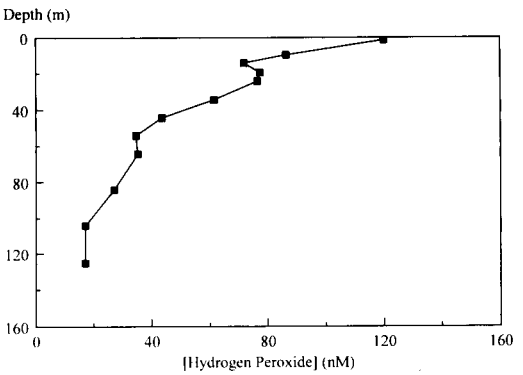

Fig. 5. Depth profile at Station MA1/9 (40°56.25'N, 6°2.77'E). Cast was made at 12.52 h local time on 18th July 1993.

cating a surface source of H_2O_2. The extent of photochemical production of H_2O_2 is dependent on a number of physico-chemical parameters, e.g., latitude, time of day and year, spectral characteristics of the light, albedo (e.g., cloud cover), availability of organic chromophores, partial pressure of oxygen, light attenuation in the water column, amount of wet deposition and physical mixing processes. Therefore, the combined effect of these parameters at the time and place of sampling determines the nature of the depth profile. The FI–CL H_2O_2 profiles from the Mediterranean are in good agreement with previously reported field results [3,7,13,14,22].

Fig. 5 shows the profile from Station MA1/9, an oligotrophic station off the south of France and Table 3 shows the relevant hydrographic data. The increase

Table 3
Hydrographic and H_2O_2 data for Station MA1/9 (40°56.25'N, 6°2.77'E)

Depth (m)	Temperature (°C)	Salinity (‰)	Oxygen (μM)	H_2O_2 (nM)
1.26	23.42	37.72	206.5	120
9.51	21.83	37.72	226.3	86.3
14.03	21.36	37.65	219.8	71.7
19.27	21.07	37.76	225.5	77.3
24.17	20.79	37.93	222.3	76.4
34.43	20.30	37.99	229.2	61.3
44.19	16.17	37.74	262.9	43.5
53.99	15.43	37.93	264.5	34.5
64.15	13.94	37.95	255.0	35.2
84.22	13.26	38.11	237.2	26.9
104.01	13.19	38.22	222.8	17.0
125.30	13.19	38.28	210.7	17.0

Cast was made at 12.52 pm local time on 18th July 1993.

Table 4
Comparison of solid state and PMT detectors for the determination of H_2O_2 over the range 600–3000 nM

H_2O_2 (nM)	Solid state detector (mV)	PMT (mV)
3000	65	>11800 (off scale)
2000	38	10140
1000	13	4050
900	12	3310
800	10	2960
700	9	2460
600	7	1900
Mean R.S.D. ($n=5$)	3.1%	1.0%
Background signal (mV)	80–120	1–5
Background noise (mV)	3–5	0.5–5

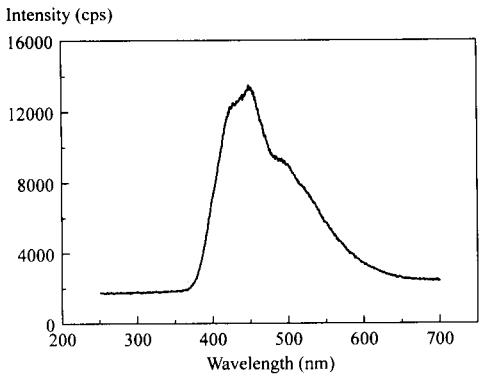

Fig. 6. CL emission spectrum for the H_2O_2 induced oxidation of luminol in alkaline solution obtained using a 578×385 pixels CCD (Instruments S.A.).

in H_2O_2 concentration at 20–30 m depth is attributed to sub-surface mixing processes and correlates well with temperature and salinity profiles (which suggest entrainment of surface water at this depth).

PMT based CL detection has been shown to be suitable for the shipboard monitoring of H_2O_2. For more remote deployments however a solid-state (photodiode) based detector offers a number of potential advantages including lower cost, lower power requirements, increased ruggedness and greater stability. Therefore, the performance of a solid-state CL detector designed in-house (Camspec, Cambridge) was compared with that of the PMT based detector described above. The results given in Table 4 show that the sensitivity of the solid-state detector is significantly lower than the PMT detector. This is partially due to incompatibility of the spectral response characteristics of the photodiode ($\lambda_{max} \sim 700$ nm) as compared with the maximum emission wavelength of the luminol reaction ($\lambda_{max} = 440$ nm; see Fig. 6). The solid state detector is therefore unsuitable for determining H_2O_2 in sea water but nonetheless has the required sensitivity for monitoring other environmental matrices, e.g., rainwater.

4. Conclusions

The FI–CL method described above is ideally suited to the shipboard determination of H_2O_2 in sea water over the range 5–500 nM. The instrumentation was sufficiently rugged to be transported by road and sea and was operational within 1 h of unpacking. The sample throughput was 120 h^{-1}, the reproducibility was 3.8% and there was minimal down time during the four week deployment at sea. Reagent consumption for a typical 10 h working day was <1 l for each FI stream. The major benefit of this approach is the real time acquisition of ambient H_2O_2 concentrations in sea water. This is particularly important for such a reactive and transient species as H_2O_2.

Acknowledgements

One of us (DP) would like to thank the Natural Environment Research Council and Plymouth Marine Laboratory (PML) for financial support under the CASE scheme. The authors are grateful to all crew and officers of the RRS Discovery for their shipboard expertise, to Nick Blundell and Adrian Hopkins for their assistance with the automation of the monitor and to Tim Fileman for his invaluable help at PML.

References

[1] R.G. Zepp, B.C. Faust and J. Hoigné, Environ. Sci. Technol., 26 (1992) 313.
[2] R.G. Zika, in N.V. Blough and R.G. Zepp (Eds.), Effects of Solar Ultra-violet Radiation on Biogeochemical Dynamics in Aquatic Environments, Woods Hole Oceanogr. Inst. Tech. Rep. WHOI-90-09, 1990.
[3] C.A. Moore, C.T. Farmer and R.G. Zika, J. Geophys. Res., 98-C2 (1993) 2289.
[4] R.G. Zika, P.J. Milne and O.C. Zafiriou, J. Geophys. Res., 98-C2 (1993) 2223.
[5] W.J. Cooper, R.G. Zika, R.G. Petasne and J.M.C. Plane, Environ. Sci. Technol., 22 (1988) 1156.
[6] S.E. Stevens, Jr., C.O.P. Patterson and J. Myers, J. Phycol., 9 (1973) 427.
[7] W.J. Cooper, E.S. Saltzman and R.G. Zika, J. Geophys. Res., 92-C3 (1987) 2970.
[8] W.J. Cooper and R.G. Zepp, Can. J. Fish. Aquat. Sci., 47 (1990) 888.
[9] J.W. Moffet and O.C. Zafiriou, J. Geophys. Res., 98-C2 (1993) 2307.
[10] D. Price, P.J. Worsfold and R.F.C. Mantoura, Trends Anal. Chem., 11 (1992) 379.
[11] K.S. Johnson, C.M. Sakamoto-Arnold, S.W. Willason and C.L. Beehler, Anal. Chim. Acta, 201 (1987) 83.

[12] R.G. Zika and E.S. Saltzman, Geophys. Res. Lett., 9 (1982) 231.
[13] R.G. Zika, E.S. Saltzman and W.J. Cooper, Mar. Chem., 17 (1985) 265.
[14] R.G. Zika, J.W. Moffet, R.G. Petasne, W.J. Cooper and E.S. Saltzman, Geochim. Cosmochim. Acta, 49 (1985) 1173.
[15] W.L. Miller and D.R. Kester, Anal. Chem., 60 (1988) 2711.
[16] C.M. Sakamoto-Arnold and K.S. Johnson, Anal. Chem., 59 (1987) 1789.
[17] T.P. Chapin, K.S. Johnson and K.H. Coale, Anal. Chim. Acta, 249 (1991) 469.
[18] V.A. Elrod, K.S. Johnson and K.H. Coale, Anal. Chem., 63 (1991) 893.
[19] K.H. Coale, K.S. Johnson, P.M. Stout and C.M. Sakamoto, Anal. Chim. Acta, 266 (1992) 345.
[20] R.M. Gershey and D.R. Green in J.C. Guary, P. Guegueniet and R.J. Pentreath (Eds.), Radionucleides: a Tool for Oceanography, Elsevier, Amsterdam, 1988.
[21] A. Nabi and P.J. Worsfold, J. Chem. Soc. Pak., 9 (1987) 575.
[22] K.S. Johnson, S.W. Willason, D.A. Wiesenburg, S.E. Lohrenz and R.A. Arnone, Deep-Sea Res., 36 (1989) 241.

ELSEVIER

Analytica Chimica Acta 298 (1994) 129–133

ANALYTICA CHIMICA ACTA

Determination of 3-hydroxybutyrate in serum by flow-injection analysis using a co-immobilized 3-hydroxybutyrate dehydrogenase/NADH oxidase reactor and a chemiluminometer

Nobutoshi Kiba *, Hidekazu Koemado, Junko Inagaki, Motohisa Furusawa

Department of Applied Chemistry and Biotechnology, Faculty of Engineering, Yamanashi University, Kofu 400, Japan

Received 17 January 1994; revised manuscript received 25 April 1994

Abstract

A flow-injection system with a co-immobilized enzyme reactor is described for the determination of 3-hydroxybutyrate. 3-Hydroxybutyrate dehydrogenase and NADH oxidase were immobilized on aminated poly(vinyl alcohol) beads and packed into a stainless-steel column (5 cm × 4 mm i.d.). Serum was diluted 10-fold with borate buffer (pH 9.4) and ultrafiltered. Filtrate (20 μl) was injected into the carrier stream. The hydrogen peroxide produced was detected chemiluminometrically via a luminol–hexacyanoferrate(III) reaction. The calibration graph was linear for 2×10^{-7} M–5×10^{-4} M; the detection limit was 8×10^{-8} M and the sample throughput was 30 h^{-1} without carryover.

Keywords: Chemiluminescence; Flow injection; Co-immobilized enzymes reactor; 3-Hydroxybutyrate

1. Introduction

The measurement of 3-hydroxybutyrate (HB) is of clinical importance in the diagnosis and management of a metabolic derangement of carbohydrate metabolism such as diabetes and alcoholic ketosis. Several enzymatic methods have been developed for the determination of HB based on the conversion of 3-hydroxybutyrate to acetoacetate with concomitant reduction of nicotineamide adenine dinucleotide (NAD^+) to reduced nicotineamide adenine dinucleotide (NADH) with 3-hydroxybutyrate dehydrogenase (EC 1.1.1.30, HBDH) [1–7]. Although methods for the autoanalyser have been standardized [4–6], a small diagnostic laboratory does not always have access to such sophisticated instrumentations for the determination of HB. In this situation an immobilized HBDH electrode in batch system has been developed for the rapid and simple determination of HB in undiluted whole blood and serum [8]. The method is suitable for bedside use because of its short response time (30 s) and appropriate reproducibility. By using the immobilized enzyme in a continuous-flow system manual handling is minimized and the reproducibility is enhanced. The object of this study is to develop a sensitive and reproducible flow-injection method for the determination of HB in serum with chemiluminescence detection. HBDH reversibly catalyzes the following reaction:

$$CH_3CH(OH)CH_2COO^- + NAD^+ = CH_3COCH_2COO^- + NADH + H^+$$

As the equilibrium of the reaction is far in favour of HB ($K = 1\times10^{-9}$) [2], it has to be shifted towards

* Corresponding author.

SSDI 0003-2670(94)00252-H

the NADH formation for sensitive determination of HB. This can be accomplished by increasing the NAD^+ concentration (15 mM) and the pH (pH 9.5) [3]. HBDH was immobilized onto poly(vinyl alcohol) beads and used in a flow-injection (FI) system for the fluorimetric determination of HB in serum under the conditions at pH 9.3 and 4 mM NAD^+ [9].

NADH oxidase (NAOD) catalyzes the reaction in which NADH is oxidized with the production of hydrogen peroxide using molecular oxygen as an electron acceptor according to the reaction [10,11];

$$NADH + H^+ + O_2 = NAD^+ + H_2O_2$$

NAOD from *Brevibacterium ammoniagenes* [12] has been immobilized onto alkylamine glass beads and used as a reactor in the chemiluminometric FI system for the determination of NADH, though no detailed conditions have been reported [12]. The NAOD was also co-immobilized with hexokinase and D-glucose-6-phosphate dehydrogenase and used as a reactor in FI system for the determination of magnesium ion in human serum [12]. In this work, NAOD from *Bacillus megaterium* and HBDH were covalently co-immobilized with glutaraldehyde onto aminated poly(vinyl alcohol) beads.

This paper describes a FI system for the determination of HB with a co-immobilized HBDH/NAOD reactor. In the reactor, NAOD acts as a trapping enzyme, that is, the NADH produced by the HBDH reaction is removed by the NAOD reaction with concomitant formation of hydrogen peroxide. The hydrogen peroxide formed in the reactor was detected by measuring the chemiluminescence emitted when mixed with luminol and potassium ferricyanide. The FI method was applied to the determination of HB in human serum.

2. Experimental

2.1. Materials

HBDH (D-3-hydroxybutyrate: NAD^+ oxidoreductase, from *Pseudomonas sp.*, grade III, 120 U mg^{-1}) and NAOD (EC number not assigned, from *Bacillus megaterium*, 50 U mg^{-1}) were obtained from Toyobo (Osaka) and Asahi Kasei (Tokyo), respectively. Activity for each enzyme was measured spectrophotometrically at 340 nm with HB or NADH as substrate at pH 9.0 at 30°C. NAD^+ (free acid, 96%) was from Kohjin (Tokyo). Poly(vinyl alcohol) beads (GS-520, 13 μm diameter) were from Showa Denko (Tokyo). D,L-3-Hydroxybutyrate sodium salt (D,L-HB salt), flavine adenine dinucleotide (FAD) disodium salt, luminol, potassium ferricyanide and tris(hydroxylmethyl)aminomethane (Tris) were from Nacalai Tesque (Kyoto). All other chemicals were of analytical-reagent grade.

Borate buffer (pH 9.4) consisting of 0.1 M boric acid–0.1 M KCl–0.1 M sodium carbonate was prepared. A stock solution (10 mM) was made by dissolving D,L-HB salt in water. D-Isomer concentration is assumed to be half of D,L-HB salt. A potassium ferricyanide stock solution (200 mM) was prepared and diluted ten-fold with water before use. NAD^+ solution [3 mM NAD^+ in 0.02 M phosphate buffer (pH 6.8)] and luminol solution [3 mM luminol in carbonate buffer (pH 10.5) consisting of 0.4 M sodium hydrogen carbonate–0.4 M sodium carbonate] were prepared daily.

The method for the amination of the beads was similar to that described previously [13]. The aminated beads were packed into a stainless-steel column (5 cm × 4 mm i.d.) by slurry-packing method. Glutaraldehyde (2%) in 0.1 M phosphate buffer (pH 7.0) was pumped through the column for 2 h at 0.3 ml min^{-1} and then the column was washed with deaerated water for 30 min at 0.5 ml min^{-1}. For preparing the co-immobilized HBDH/NAOD reactor, enzymes solution [HBDH 5 mg (600 U) and NAOD 5 mg (250 U) in 10 ml of 0.1 M phosphate buffer (pH 7.0)] was circulated through the column at 0.2 ml min^{-1} for 6 h at 15°C. The time course of immobilization process was monitored by a spectrophotometer (Jasco UVIDEC-100-VI) with a flow-through cell at 383 nm. NAOD was immobilized with a 87% yield.

2.2. Apparatus and procedure

The arrangement of the FI module used in this study is shown in Fig. 1. The borate buffer (pH 9.4) and the NAD^+ solution were each pumped by Hitachi L-6000 LC pumps at a flow-rate of 0.3 ml min^{-1} and mixed before a Sanuki SVI-6M2 injector with a 20 μl loop. The chemiluminescence was measured with a Soma S-3400 luminometer with a flow-through cell (100 μl), connected to a SIC SC77 signal cleaner and TOA FBR-

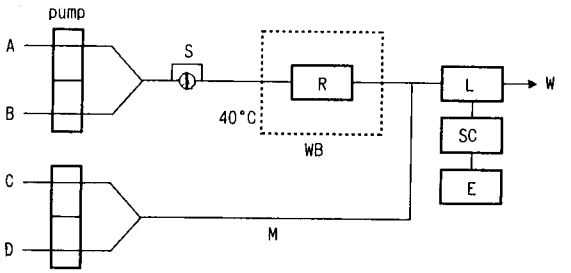

Fig. 1. Manifold for the chemiluminometric determination of HB in serum with a co-immobilized HBDH/NAOD reactor. A = 0.1 M borate buffer (pH 9.4) (0.3 ml min^{-1}), B = 3.0 mM NAD^+ in 0.01 M phosphate buffer (pH 6.8) (0.3 ml min^{-1}), C = 3 mM luminol in 0.4 M carbonate buffer (pH 10.5) (0.5 ml min^{-1}), D = 20 mM potassium ferricyanide solution (0.5 ml min^{-1}), S = injector with a loop, R = co-immobilized HBDH/NAOD reactor, maintained at 40°C, W = water bath, M = mixing coil (5 m × 0.5 mm i.d.), L = luminescence detector, SC = signal cleaner, E = recorder, W = waste.

251A recorder. The reactor was maintained at 40°C. The reactor was stored at ca. 5°C in 3.0 mM NAD^+ in 0.02 M phosphate buffer (pH 6.8) when not in use.

Serum (5 μl) was diluted 10-fold with the borate buffer (pH 9.4) and filtered on an ultrafiltration membrane (Advantec Q0100, nominal molecular weight cut-off 10,000). The filtrate (20 μl) was injected via a sample injector. The time taken to prepare the sample solution was about 1 min.

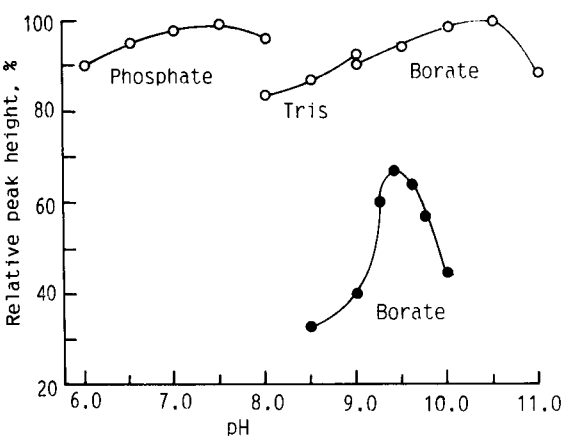

Fig. 2. Effect of pH on the activity of the co-immobilized HBDH/NAOD for NADH and HB. Phosphate = phosphate buffer consisting of M/30 potassium dihydrogen phosphate–M/30 disodium hydrogen phosphate, Tris = tris buffer consisting of 0.1 M tris(hydroxymethyl)aminomethane–0.1 M hydrochloric acid, Borate = borate buffer consisting of 0.1 M boric acid–0.1 M KCl–0.1 M sodium carbonate. ○ = 5 μM NADH, ● = 5 μM HB.

The present method was compared with the manual method [7]. Serum (0.75 ml) was added into 0.6 M ice-cold perchloric acid (1.5 ml) and the suspension was centrifuged. The supernatant (0.3 ml) and 15 mM NAD^+ in 1.5 M Tris solution (0.7 ml) were added into a cuvette which was placed into a 37°C water bath. The initial absorbance was read at 340 nm against distilled water and then 10 μl of HBDH solution (2 mg in 10 ml of 0.1 M phosphate buffer (pH 7.0) was added and read after 30 min.

3. Results and discussion

3.1. Properties of co-immobilized HBDH/NAOD reactor

To test the activities of the reactor, the system shown in Fig. 1 was used and measurements were made to study the effect of pH using M/30 phosphate buffer, 0.1 M tris buffer or 0.1 M borate buffer between pH 6.0 and 11.0. Fig. 2 shows the effect of pH on peak-height for NADH and HB. The peak-height for NADH was essentially independent of pH. The optimum pH for HB was 9.4.

The effects of temperature on the peak-height for NADH and HB were examined over the range 20–50°C (Fig. 3). The activity for NADH was almost constant up to 40°C and a slow decrease in activity was observed above 40°C. The peak-height for HB was maximum at about 40°C.

Fig. 4 shows the effects of NAD^+ concentration on the peak-height for NADH and HB. The decrease in peak-height for NADH commenced at above 5×10^{-4} M NAD^+. At higher NAD^+ concentrations the equilibrium of the above reaction is shifted to the left. On the other hand, the optimum NAD^+ concentration for HB was 1.5 mM. At lower NAD^+ concentrations the equilibrium of the first reaction is in favour of HB and at higher ones the second reaction is hindered. Compared with the immobilized HBDH [9], optimum NAD^+ concentration is 2.5 mM lower. The solution of 3.0 mM NAD^+ was used in the system.

The peak-height and peak-shape were dependent on the flow-rates of the solutions. The lower flow-rates were preferable for the enzyme reactions (conversion efficiencies), but the peak broadening at lower rates was undesirable for analytical sensitivity (peak-

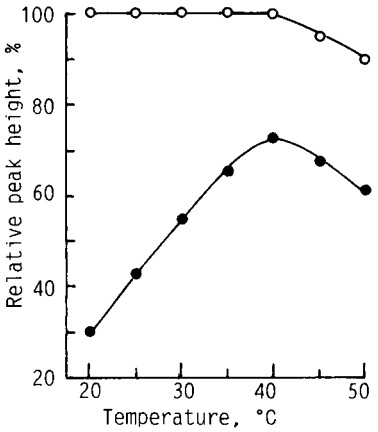

Fig. 3. Effect of temperature on the activity of the co-immobilized HBDH/NAOD for NADH and HB. ○=5 μM NADH, ●=5 μM HB.

height). Maximum peak-height was obtained at a flow-rate of 0.3 ml min^{-1}, while greater peak area was obtained at lower flow-rates. The peak-height decreased linearly as the flow-rate of carrier stream increased from 0.4 to 1.0 ml min^{-1}. The peak-height at 0.4 ml min^{-1} was about 1.6 times that at 1.0 ml min^{-1}. A total flow-rate of 0.6 ml min^{-1} was selected, as a compromise between sensitivity and sample throughput; at this flow-rate, the sample throughput was 30 h^{-1}. At a flow-rate of 0.3 ml min^{-1} the peak-height was 1.2 times that at 0.6 ml min^{-1}, but the sample throughput was 10 h^{-1}. Generally a rapid test would enjoy greater clinical utility than a slow one and a more rapid return of biochemical information to the clinician results in earlier diagnosis with an earlier institution of appropriate therapy.

Under the conditions in Fig. 1, the conversion efficiencies of the reactor for NADH and HB were 58% and 42%, respectively. The effectiveness for HB is about half that in the immobilized HBDH reactor [9]. Under the same conditions the presence of up to twice the molar amounts of acetoacetate did not interfere with the measurement of HB. The presence of equimolar amounts of reducing substances such as L-ascorbic acid, uric acid and glutathione depressed the peak-height for HB (10 μM) by 95%, 96% and 75%, respectively.

Though FAD is an activator for soluble NAOD [10], in the presence of even 200 μM FAD the oxidation of NADH was not accelerated because NAOD may be fully active under the conditions shown in Fig. 1. At higher FAD concentrations the peak-heights decreased because FAD (absorption coefficient at 450 nm is 1×10^4) absorbs the chemiluminescent light of luminol (maximum intensity wavelength is ca. 420 nm).

The operational stability of the reactor was evaluated over a period of 6 weeks. The reactor was used for 5 h per day (150 injections of 5 μM HB) and then washed with 0.1 M phosphate buffer (pH 7.0) and stored at 6°C in a refrigerator when not in use. The activities for HB and NADH decreased slowly to 86% and 93% of the initial values, respectively, after 6 weeks (6300 injections). FAD did not show any stabilizing effect on NAOD, when added to its stock solution. The co-immobilized enzymes were lyophilized and stored at −15°C in the presence of sucrose (500 mg per g of the co-immobilized enzymes). The enzymes retained 80% of the original activity for HB after 6 months.

3.2. Calibration

Under the conditions in Fig. 1, the plot of peak-height against HB concentration was linear from 0.2 μM to 500 μM. The least-squares calibration equation for HB was $y = 0.809x + 6.336$, where y is the common logarithm of peak-height (cm) and x is the common logarithm of HB concentration (M), with a linear correlation coefficient of $r = 0.999$ (11 data points). Below a concentration of 0.2 μM the concave graph was obtained and above a concentration of 500 μM the graph curved convexly. The coefficient of variation (C.V.%) for 9 replicated injections of 5.0 μM HB was 0.75%.

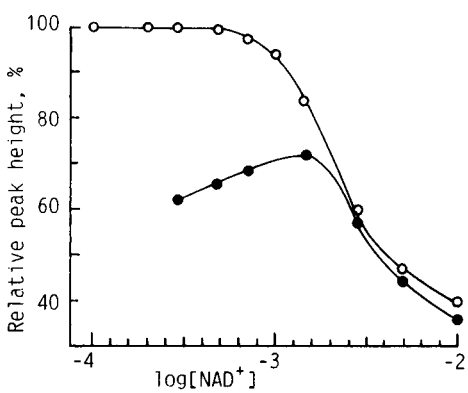

Fig. 4. Effect of NAD^+ concentration on the peak-height. ○=5 μM NADH, ●=5 μM HB.

Table 1
Recovery of 3-hydroxybutyrate added to pooled serum [a]

Added, μM	Recovered [b]	Recovery, %
20.0	19.6 (1.2)	98.0
60.0	59.5 (0.97)	99.2
180	183 (0.84)	102
500	498 (0.82)	99.6
1500	1545 (0.78)	103
3000	3060 (0.77)	102

[a] Values corrected for HB (23.7 μM) already present in serum.
[b] All values are means (μM) with C.V. (%) in parentheses ($n=6$).

The limit of detection (signal-to-noise ratio = 3) was 0.08 μM (0.2 ng in a 20 μl injection) with a C.V. of 5.6%.

3.3. Application

The flow-injection system shown in Fig. 1 was applied to the determination of HB in serum. The HB is normally present in blood at a concentration of 50 μM, though the values fluctuate considerably during 24 h [14,15].

Precision and reproducibility

Pooled human serum was repeatedly analysed during 4 weeks. The reactor was used for analyses of 180 samples per day and standards were measured at 90-sample intervals, in order to correct the variation of the coversion efficiency. The system gave satisfactorily precise and reproducible results; for serum containing 34.8 μM HB, the within-day coefficient of variation (C.V.) was 1.3% and the day-to-day C.V. was 2.7%.

Recovery

Table 1 shows the recovery of known concentrations of HB added to pooled human serum. Recoveries obtained by the present method were 98–103%.

Comparison with other methods

The above method (y) for pooled human serum measurements ($n=25$, 19 μM–2.96 mM) was compared with the manual method (x) [7]. The calculated linear regression and correlation coefficient were $y=1.021x-0.009$ and $r=0.996$.

4. Conclusion

The flow-injection system with co-immobilized HBDH/NAOD reactor and chemiluminometer is useful for sensitive and reliable measurements of HB. Compared with the fluorimetric FI method with the immobilized HBDH [9], the NAD^+ concentration is about half and the sensitivity is five times higher. The high sensitivity of luminescence allows drawbacks of low conversion efficiency for HB to be overcome. The co-immobilized HBDH/NAOD reactor is stable enough to permit the measurement of more than 6000 samples.

References

[1] D.H. Williamson. J. Mllanby and H.A. Krebs, Biochem. J., 82 (1962) 90.
[2] H.A. Krebs, J. Mellanby and D.H. Williamson, Biochem. J., 82 (1962) 96.
[3] A. Brashear and G.A. Cook, Anal. Biochem., 131 (1983) 478.
[4] D.D. Koch and D.H. Feldbruegge, Clin. Chem., 33 (1987) 1761.
[5] N.F. Nuwayhid, G.F. Johnson and R.D. Feld, Clin. Chem., 34 (1988) 1790.
[6] N.F. Nuwayhid, G.F. Johnson and R.D. Feld, Clin. Chem., 35 (1989) 1526.
[7] P.A. Ruell and G.C. Gass, Ann. Clin. Biochem., 28 (1991) 183.
[8] C.J. McNeil, J.A. Spoors and J.M. Cooper, K.G.M.M. Alberti and W.H. Mullen, Anal. Chim. Acta, 237 (1990) 99.
[9] N. Kiba, H. Koemado and M. Furusawa, Talanta, 41 (1994) in press.
[10] Y. Saeki, M. Nozaki and K. Matsumoto, J. Biochem., 98 (1985) 1433.
[11] C.J. McNeil, J.A. Spoors, D. Cocco, J.M. Cooper and J.V. Bannister, Anal. Chem., 61 (1989) 25.
[12] T. Murachi M. Totani, M. Ikemoto and M. Tabata, J. Biotechnol., 14 (1990) 33.
[13] N. Kiba, Y. Inoue and M. Furusawa, Anal. Chim. Acta, 243 (1991) 183.
[14] D. Gonzalez-Robledo, M. Silva and D. Perez-Bendito, Anal. Chim. Acta, 217 (1989) 239.
[15] K.E. Wildenhoff, Acta Med. Scand., 191(1972) 303.

ELSEVIER

Analytica Chimica Acta 298 (1994) 135–139

ANALYTICA CHIMICA ACTA

Fluorescence quenching method for the determination of atmospheric ozone using 2′,7′-dichlorofluorescein

Gong Guoquan *, Zhu Qingzhi, Wang Huaigong

Department of Chemistry, Lanzhou University, Lanzhou 730000, China

Received 8 February 1994; revised manuscript received 16 May 1994

Abstract

A highly sensitive and selective fluorescence quenching method has been developed for the rapid determination of atmospheric ozone with 2′,7′-dichlorofluorescein as fluorogenic reagent ($\lambda_{ex} = 505$ nm, $\lambda_{em} = 520$ nm) at pH 4.0–6.0. Ozone is collected in a solution of potassium bromide giving bromine (Br_2), which is estimated by the fluorescence quenching method using 2′,7′-dichlorofluorescein. Bromine may be used for calibration because the relationship between this compound and ozone has been determined. The calibration graph is linear over the range 0.01–0.50 μg per 25 ml ozone. The detection limit is 0.01 μg per 25 ml ozone. Nitrogen oxide does not interfere with the method. The method has been applied successfully to the determination of atmospheric ozone.

Keywords: Fluorimetry; Bromine; 2′,7′-Dichlorofluorescein; Ozone; Quenching

1. Introduction

Ozone has increasing applications in a variety of industries and is used, for instance, in various chemical syntheses, and as a bleaching agent for textiles. However, it is a toxic gas with a threshold limit value (TLV) of only 0.2 mg m^{-3} (0.1 ppm, v/v) in air [1], and it could represent a considerable hazard in an industrial atmosphere. A sensitive method is required for the determination of atmospheric ozone at levels below the threshold limit value.

Spectrofluorimetry has been widely applied to determine many anions and cations. However, the determination of ozone by the fluorescence quenching method has not been reported previously. At present the most widely used procedure is the potassium iodide method [2–6], but this has the disadvantages of insufficient sensitivity and being affected by nitrogen oxide. Amos [7] has reported the determination of ozone by spectrofluorimetry using 2-diphenylacetyl-1,3-indandione-1-hydrazone as a fluorogenic reagent, but the reaction takes a long time and the sensitivity is low. Ikeura and Tasoh [8] used the reaction of ozone with *p*-acetamidophenol to develop a fluorimetric method, but the operation is troublesome. We have therefore used 2′,7′-dichlorofluorescein as fluorogenic reagent and developed a fluorescence quenching method for the determination of trace ozone. Ozone is collected in a solution of potassium bromide giving bromine

* Corresponding author.

SSDI 0003-2670(94)00243-F

(Br_2), which reacts with 2′,7′-dichlorofluorescein to produce a non-fluorescent substance and to cause a decrease in the fluorescence quenching intensity of the system. Nitrogen oxide does not interfere with this method. The method offers several distinct advantages over other fluorimetric methods [7–10] for ozone: higher sensitivity, wider pH range, greater accuracy, reproducibility, and ease of operation and it is more rapid. This method has been applied to the determination of atmospheric ozone with satisfactory results.

2. Experimental

2.1. Apparatus

An RF-540 spectrofluorimeter (Shimadzu, Kyoto) equipped with a plotter unit and a 1 × 1 cm quartz cell was used for recording the spectra and making fluorescence measurements; an SPM-10A digital pH meter (Xiao shan, China) and a DB-6H gas sample collector (Qingdao, China) were used.

2.2. Reagents

All chemicals were of analytical-reagent grade. Deionized, distilled water was used throughout.

Potassium bromide solution: dissolve 2.0 g potassium bromide in water and dilute to 100 ml.

Potassium bromate solution, 0.0167 M: dissolve 0.2789 g potassium bromate in water and dilute to 100 ml.

Potassium bromate–potassium bromide solution: dissolve 1.0 g potassium bromide in water, add 10.0 ml of 0.0167 M potassium bromate solution, 5.0 ml of 0.5 M H_2SO_4 solution and dilute to volume in a 100-ml standard flask with water.

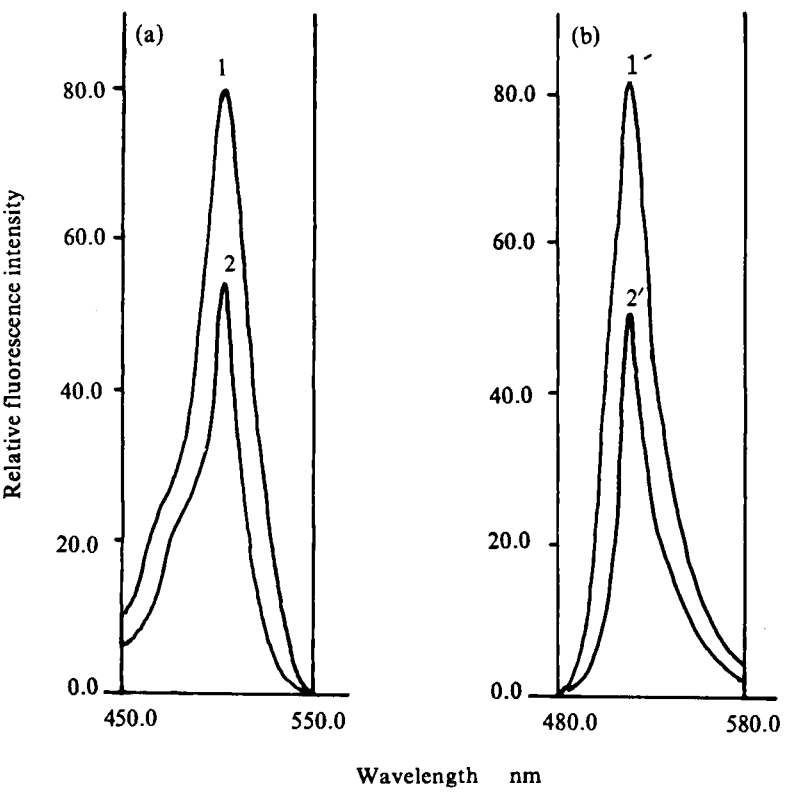

Fig. 1. (a) Excitation and (b) emission spectra of the 2′,7′-dichlorofluorescein system (1,1′) and 2′,7′-dichlorofluorescein–Br_2 system (2,2′).

This solution corresponded to 240 μg ml^{-1} ozone solution. It was diluted to 0.5 μg ml^{-1} with water as working solution.

Dilute sulphuric acid: a 0.5 M solution was used.

Buffer solution: a pH 5.2 buffer solution was prepared by mixing 5.0 ml of 0.03 M sodium phosphate dibasic with 160.0 ml of 0.03 M potassium phosphate monobasic.

Absorbing solution: mix 40.0 ml of the potassium bromide solution (2%) with 10.0 ml of buffer solution (pH = 5.2) in a 50 ml flask.

2′,7′-Dichlorofluorescein solution: a stock solution (2×10^{-5} M) was prepared by dissolving 4.0 mg 2′,7′-dichlorofluorescein (Shanghai, China) in water and diluting to volume in a 500-ml standard flask. The stock solution was diluted to 2×10^{-6} M as working solution.

2.3. Analytical procedure

Ozone was absorbed in two absorbers in series each containing 10.0 ml of absorbing solution. When the sampling was completed, 2.0 ml of the absorbing solution were pipetted into a 25-ml standard flask, and 1.6 ml of 2×10^{-6} M 2′,7′-dichlorofluorescein solution and 2.0 ml of buffer solution were added. The solution was diluted to volume with water and mixed. The fluorescence intensity was measured at 520 nm (with excitation at 505 nm) against a reagent blank. The concentration of ozone in the absorbing solution was calculated from the fluorescence–concentration curve described below.

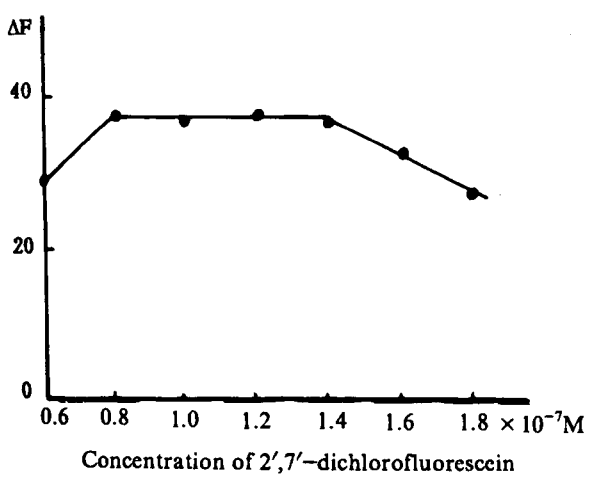

Fig. 2. Influence of 2′,7′-dichlorofluorescein concentration on the fluorescence quenching of the system.

3. Results and discussion

3.1. Spectral characteristics

As shown in Fig. 1, the excitation and emission spectra of the 2′,7′-dichlorofluorescein and 2′,7′-dichlorofluorescein–Br_2 systems are similar. The excitation and emission wavelength are 505 nm and 520 nm, respectively. The fluorescence intensity of the blank decreased when Br_2 was added.

3.2. Optimum conditions for fluorescence quenching

The experimental results indicated that a maximum and constant fluorescence quenching was reached when the 2′,7′-dichlorofluorescein concentration was in the range 8×10^{-8}–1.4×10^{-7} M. The fluorescence quenching decreased for values outside this range (Fig. 2). In this work, a 2′,7′-dichlorofluorescein concentration of 1.2×10^{-7} M was chosen.

The effect of pH on the fluorescence quenching of the system was examined. The maximum fluorescence quenching occurred in the pH range 4.0–6.0 (Fig. 3). A pH of 5.2 is recommended for use, and an addition of 2.0 ml buffer solution per 25 ml of final solution was chosen. The effect of temperature on the reaction was also investigated. The optimum fluorescence quenching was reached rapidly at room temperature, and remained-unaltered for up to 8 h. Raising the temperature did not increase or decrease the fluorescence quenching. Room temperature is therefore recommended.

3.3. Interferences

The tolerance limits of some ions and gaseous oxidants for the determination of 0.25 μg ozone by the procedure described were studied, and the

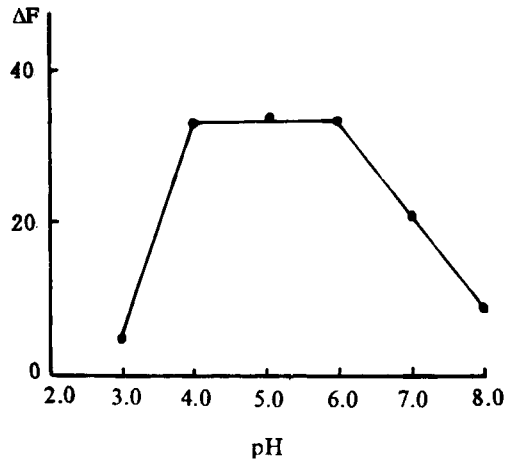

Fig. 3. Effect of pH on the fluorescence quenching of the system.

results are given in Table 1. The relative error is less than ±5%. From Table 1, it can be seen that nitrogen oxide and sulfur trioxide do not interfere with the determination, even when present in large excess. However, chlorine seriously interferes with the determination of ozone.

3.4. Calibration

Since ozone reacts with bromide to form bromine, the relationship between fluorescence quenching and concentration of bromine was investigated by adding a known amount of bromine to the analytical solution. A linear relationship was observed in the range 0.03–1.7 μg 25 ml^{-1} bromine. Bromide ion did not increase or decrease the blank fluorescence. Various concentrations of ozone in air were determined by the analytical procedure and simultaneously analyzed using the neutral potassium iodide procedure [6], and the amount of ozone found with the neutral potassium iodide procedure was used as standard. In this way we established the quantitative relationship between ozone and bromine via fluorescence quenching. We found that 1.0 μg ozone corresponded to 3.3 μg bromine, 1.0 mol of ozone generated 1.0 mol of bromine, so to speak, $O_3 \equiv Br_2$. If we make a conversion between bromine and ozone, the linearity of ozone is in the range 0.01–0.5 μg 25 ml^{-1}. The regression line and correlation coefficient found by the least-squares method is: $\Delta F = 136.4C + 0.12$, $r = 0.9996$ (the unit of C is μg 25 ml^{-1}), where ΔF is the fluorescence quenching and C the ozone concentration.

Table 1
Tolerance of foreign ions in the determination of 0.25 μg ozone

Ions addes	Tolerance ratio (w/w)
NO_3^-, SO_4^{2-}, F^-, Cl^-, HCO_3^-, Na^+, K^+	10000
SCN^-, Ca^{2+}, Mg^{2+}	5000
Cr^{6+}, Mn^{2+}, Ni^{2+}	2000
NO_2^-, Zn^{2+}	1000
Se^{4+}	500
Al^{3+}	400 [a]
Cu^{2+}	200
Fe^{3+}	100 [a]
NO_2	1000
NO	2000
SO_3	500
Cl_2	0.5

[a] In the presence of citrate.

3.5. Collection of ozone

Two-liter samples of ozone atmosphere of various concentrations were collected at 0.2 l min^{-1}

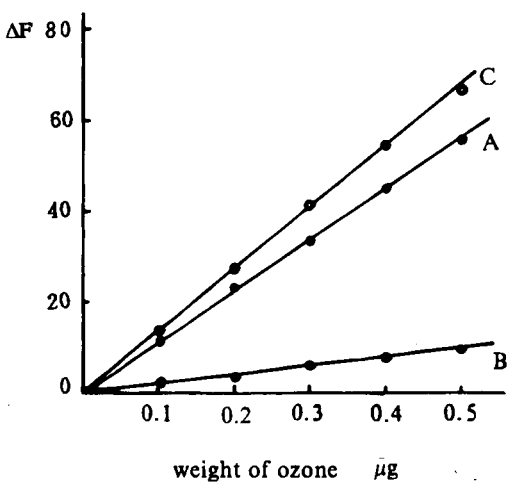

Fig. 4. Relationship between fluorescence quenching value and the weight of ozone in a 2-l sample. (A) Sample collected in the first absorber of two absorbers in series; (B) sample collected in the second of two absorbers in series; (C) sample collected in two absorbers in series.

as described in section 2.3. The fluorescence quenching values were plotted against the weight of ozone in the sample. Straight lines, graph A for the first absorption solution and graph B for the second, were obtained. The combined fluorescence quenching values of both absorbers were plotted against the weight of ozone in the sample, and thus graph C was obtained (Fig. 4). In this way, we found that the collection efficiency was only 83% when only one absorber was used. Therefore, two absorbers in series are recommended.

3.6. Determination of ozone

Twenty ml of absorbing solution were used during a 10-min sampling period and 2 l samples of ozone atmosphere were collected at 0.2 l min^{-1}. After ozone was absorbed, appropriate amounts of the absorbing solution were taken for the determination of ozone according to the analytical procedure described. The results are given in Table 2 and were compared with those obtained by the neutral potassium iodide method [6].

Table 2
Determination of atmospheric ozone

Sample No.	Amount of ozone found (mg m^{-3})	
	This method [a]	Potassium iodide method [b]
1	0.275	0.292
2	0.838	0.874

[a] Averages of six determination.
[b] Averages of three determination.

4. Conclusion

The proposed method is a highly sensitive and selective fluorescence quenching method for the determination of ozone. The procedure is simple, rapid and the results are reproducible.

Acknowledgement

This project was supported by the National Natural Science Foundation of China (Gansu).

References

[1] Ministry of Labour, Safety, Health and Welfare, New Series No. 8, Dusts and Fumes in Factory Atmospheres, 3rd edn., H.M. Stationery Office, London, 1966.
[2] B.E. Saltzman and N. Gilbert, Anal. Chem., 31 (1959) 1914.
[3] G. Bergshoeff, R.W. Lanting, J.M.G. Prop and H.F.R. Regnders, Anal. Chem., 52 (1986) 541.
[4] R.N. Dietz, J. Prozansky and J.D. Smith, Anal. Chem., 45 (1973) 402.
[5] R.W. Lanting, Atmos. Environ., 13 (1979) 553.
[6] I.C. Cohen, A.F. Smith and R. Wood, Analyst, 93 (1968) 507.
[7] D. Amos, Anal. Chem., 42 (1970) 842.
[8] Ikeura and Tasoh, Taiki Osen Gakaishi, 24 (1989) 160.
[9] E.A. Peeregud and E.T. Stepanenko, Zh. Analit. Khim., 15 (1960) 96.
[10] Ikeura and Tasoh, Kankyo Gijutsu, 19 (1990) 232.

PRINCIPAL COMPONENTS

By **D.L. Massart** and **P.J. Lewi**

This attractively packaged set, comprising 4 videos, a manual and a software package, is an introduction to the use of principal components analysis (PCA) and related methods in chemometrics. Emphasis has been placed on the use of PCA to display graphically the structure of data sets or to extract graphically information from such a set (display methods). However, links are provided to several other important methods, such as evolving factor analysis, principal component regression and partial least squares.

In order to induce students to learn PCA, and convince them of the usefulness of the methods, several real-life examples have been included. These examples have been chosen to illustrate the generality of the data analysis approach. The data pertain to food, industrial and environmental analysis, animal experimentation, medicinal chemistry, virology and epidemiology. In the software section an additional example concerned with food analysis has been added. Section 3 of the manual contains a complete list of figures. This allows the user to look at some of the figures in a more leisurely fashion or to re-read text which has been heard when viewing the videos. Some of the visuals and some of the texts (occasionally shortened) have been included in this section.

Two types of software augment this series. The first is a tutorial version of a commercial software package called SPECTRAMAP, which has been modified for didactical use. SPECTRAMAP is a performant software for methods derived from PCA that gives excellent display quality.

The other type of software is a listing of a MATLAB® program. In order to understand completely a mathematical algorithm or method, the authors recommend the user to program it himself, using MATLAB®. In this way the user can also obtain all the intermediate results, thereby understanding what happens with a data set when analyzed by PCA. This section also contains an additional data set with which the user can experiment with the software. Some hints are given in to teachers and self-learners on how to use the material to optimize results.

Contents: VIDEOS:

Part A: Principal components as display method.

Part B: Display variables and relationships between variables and objects.

Part C: Singular value decomposition; Eigenvalues; Evolving factor analysis; Software and exercises.

Part D: The display of latent variables in tabulated data.

A 25-minute demonstration video, containing a representative selection from all four video tapes is available at cost price.

ELSEVIER

An imprint of Elsevier Science

MANUAL:

1. Introduction.
2. Proposed didactical concepts.
3. List of Visuals.
4. Software Section.

4A. SPECTRAMAP (P.J. Lewi, J. Van Hoof, M. Nijs).

4B. A MATLAB program for principal components analysis (M. Massart).

©1994 Complete set VHS PAL
Price: Dfl. 1750.00 (US$1000.00)
ISBN 0-444-81622-4
Complete set VHS NTSC
Price: Dfl. 1750.00 (US$1000.00)
ISBN 0-444-81655-0
Manual
Price: Dfl. 65.00 (US$37.00)
ISBN 0-444-81653-4
Demonstration copy
VHS PAL Video
Price: Dfl. 50.00 (US$28.50)
ISBN 0-444-81980-0
Demonstration copy
VHS NTSC Video
Price: Dfl. 50.00 (US$28.50)
ISBN 0-444-81979-7

Additional copies of the manual may be ordered separately.

ORDER INFORMATION
ELSEVIER SCIENCE B.V.
P.O. Box 330
1000 AH Amsterdam
The Netherlands
Fax: +31 (20) 5862 845

For USA and Canada
P.O. Box 945
Madison Square Station
New York, NY 10159-0945
Fax: +1 (212) 633 3680

US$ prices are valid only for the USA & Canada and are subject to exchange rate fluctuations; in all other countries the Dutch guilder price (Dfl.) is definitive. Customers in the European Union should add the appropriate VAT rate applicable in their country to the price(s). Books are sent postfree if prepaid.

Trace Element Analysis in Biological Specimens

Edited by **R.F.M. Herber** and **M. Stoeppler**

Techniques and Instrumentation in Analytical Chemistry Volume 15

The major theme of this book is analytical approaches to trace metal and speciation analysis in biological specimens. The emphasis is on the reliable determination of a number of toxicologically and environmentally important metals. It is essentially a handbook based on the practical experience of each individual author. The scope ranges from sampling and sample preparation to the application of various modern and well-documented methods, including quality assessment and control and statistical treatment of data. Practical advice on avoiding sample contamination is included.

In the first part, the reader is offered an introduction into the basic principles and methods. Quality control and all approaches to achieve reliable data are treated as well.

The chapters of the second part provide detailed information on the analysis of thirteen trace metals in the most important biological specimens.

The book will serve as a valuable aid for practical analysis in biomedical laboratories and for researchers involved with trace metal and species analysis in clinical, biochemical and environmental research.

Contents:

© 1994 590 pages Hardbound
Price: Dfl. 475.00 (US$ 271.50)
ISBN 0-444-89867-0

ELSEVIER SCIENCE

ORDER INFORMATION
ELSEVIER SCIENCE B.V.
P.O. Box 330
1000 AH Amsterdam
The Netherlands
Fax: (+31-20) 5862 845

For USA and Canada
P.O. Box 945
Madison Square Station
New York, NY 10159-0945
Fax: (212) 633 3680

US$ prices are valid only for the USA & Canada and are subject to exchange rate fluctuations; in all other countries the Dutch guilder price (Dfl.) is definitive. Customers in the European Union should add the appropriate VAT rate applicable in their country to the price(s). Books are sent postfree if prepaid.

PUBLICATION SCHEDULE FOR 1995

	O'94	N'94	D'94	J	F	M	A	M	J	J	A	S
Anal. Chim. Acta	296/2 296/3 297/1–2	297/3 298/1 298/2	298/3 299/1 299/2	299/3 300/1–3 301/1–3	302/1 302/2–3 303/3							
Vib. Spec.		8/1		8/2		8/3		9/1		9/2		9/3

INFORMATION FOR AUTHORS

Detailed "Instructions to Authors" for *Analytica Chimica Acta* was published in Volume 289, No. 3, pp. 381–384. Free reprints of the "Instructions to Authors" of *Analytica Chimica Acta* and *Vibrational Spectroscopy* are available from the Editors or from: Elsevier Science B.V., P.O. Box 330, 1000 AH Amsterdam, The Netherlands. Telefax: (+31-20) 5862 459.

Manuscripts. The language of the journal is English. English linguistic improvement is provided as part of the normal editorial processing. Authors should submit three copies of the manuscript in clear double-spaced typing on one side of the paper only. *Vibrational Spectroscopy* also accepts papers in English only.

Rapid publication letters. *Letters* are short papers that describe innovative research. Criteria for letters are novelty, quality, significance, urgency and brevity. Submission data: max. of 2 printed pages (incl. Figs., Tables, Abstr., Refs.); short abstract (e.g., 3 lines); *no* proofs will be sent to the authors; submission on floppy disc; *no* revision will be possible.

Abstract. All papers, reviews and letters begin with an Abstract (50–250 words) which should comprise a factual account of the contents of the paper, with emphasis on new information.

Figures. Figures should be suitable for direct reproduction and as rich in contrast as possible. One original (or sharp glossy print) and two photostat (or other) copies are required. Attention should be given to line thickness, lettering (which should be kept to a minimum) and spacing on axes of graphs, to ensure suitability for reduction in size on printing. Axes of a graph should be clearly labelled, along the axes, outside the graph itself.

All figures should be numbered with Arabic numerals, and require descriptive legends which should be typed on a separate sheet of paper. Simple straight-line graphs are not acceptable, because they can readily be described in the text by means of an equation or a sentence. Claims of linearity should be supported by regression data that include slope, intercept, standard deviations of the slope and intercept, standard error and the number of data points; correlation coefficients are optional.

Photographs should be glossy prints and be as rich in contrast as possible; colour photographs cannot be accepted. Line diagrams are generally preferred to photographs of equipment. Computer outputs for reproduction as figures must be good quality on blank paper, and should preferably be submitted as glossy prints.

Nomenclature, abbreviations and symbols. In general, the recommendations of IUPAC should be followed, and attention should be given to the recommendations of the Analytical Chemistry Division in the journal *Pure and Applied Chemistry* (see also *IUPAC Compendium of Analytical Nomenclature, Definitive Rules*, 1987).

References. The references should be collected at the end of the paper, numbered in the order of their appearance in the text (*not* alphabetically) and typed on a separate sheet.

Reprints. Fifty reprints will be supplied free of charge. Additional reprints (minimum 100) can be ordered. An order form containing price quotations will be sent to the authors together with the proofs of their article.

Papers dealing with vibrational spectroscopy should be sent to: Dr J.G. Grasselli, 150 Greentree Road, Chagrin Falls, OH 44022, U.S.A. Telefax: (+1-216) 2473360 (Americas, Canada, Australia and New Zealand) or Dr J.H. van der Maas, Department of Analytical Molecular Spectrometry, Faculty of Chemistry, University of Utrecht, P.O. Box 80083, 3508 TB Utrecht, The Netherlands. Telefax: (+31-30) 518219 (all other countries).

0003-2670/94/$07.00

Time-of-Flight Mass Spectrometry and its Applications

Edited by **E.W. Schlag**, Institut für Physicalische und Theoretische Chemie, Universität München, Germany

Previously published as a special issue of the journal
International Journal of Mass Spectrometry and Ion Processes, Volume 131 (1994)

The present set of contributions attempts to give a survey of current applications from many of the active groups in the field. A variety of new applications are considered which are no doubt just the beginning of large new areas of application.

Contents: Laser assisted reflectron time-of-flight mass spectrometry (B.A. Mamyrin). How to specify the ion optical system of a time-of-flight mass spectrometer (T. Bergmann, T.P. Martin). The application of ion optics in time-of-flight mass spectrometry (D. Ioanoviciu). Design considerations in energy resolved time-of-flight mass spectrometry (A.E. Giannakopulos *et al.*). Laser ion sources for time-of-flight mass spectrometry (U. Boesl *et al.*). Photoemission electron impact ionization in time-of-flight mass spectrometry: an examination of experimental consequences (S.M. Colby, J.P. Reilly). High-resolution mass spectrometry in a linear time-of-flight mass spectrometer (J.M. Grundwürmer *et al.*). The design and performance of an ion trap storage-reflectron time-of-flight mass spectrometer (B.M. Chien *et al.*). Pulse amplitude analysis: a new dimension in single ion time-of-flight mass spectrometry (P.V. Bondarenko *et al.*). Mass analyzed threshold ionization: structural information for a mass spectrum and mass information for ionic spectroscopy (P.M. Johnson, L. Zhu). Decay energetics of molecular clusters studied by multiphoton mass spectrometry and pulsed field threshold ionization (H.J. Neusser, H. Krause). Using reflectron time-of-flight mass spectrometer techniques to investigate cluster dynamics and bonding (S. Wei, A.W. Castleman, Jr.). The one dimensional photofragment translational spectroscopic technique: intramolecular clocking of energy redistribution for molecules falling apart (H.J. Hwang *et al.*). Quantitative determination of kinetic energy releases from metastable decomposition of sputtered organic ions using a time-of-flight mass spectrometer with a single-stage ion mirror (D.F. Barofsky *et al.*). Kinetic energy analysis in time-of-flight mass spectrometry: application of time of flight methods to clusters and pyrolysis studies in supersonic expansions (J.S. Riley, T. Baer). Photodissociation of magnesium ion-molecule complexes in a refectron time-of-flight mass spectrometer (C.S. Yeh *et al.*. Resonance-enhanced two-photon ionization time-of-flight spectroscopy of cold perfluorinated polyethers and their external and internal van der Waals dimers (D.S. Anex *et al.*). Time-of-flight mass spectrometry of DNA laser-ablated from frozen aqueous solutions: applications to the Human Genome Project (P. Williams). Factors affecting the resolution in matrix-assisted laser desorption-ionization mass spectrometry (A. Ingendoh *et al.*). Sequencing of peptides in time-of-flight spectrometer: evaluation of post-source decay following matrix-assisted laser desorption-ionization (MALDI) (P. Kaufmann *et al.*). Energy-isochronous time-of-flight analyzers (H. Wollnik). Author index. Subject index.

©1994 422 pages Paperback
Price: Dfl. 215.00 (US$122.75)
ISBN 0-444-81875-8

ELSEVIER
An imprint of Elsevier Science

ORDER INFORMATION
ELSEVIER SCIENCE B.V.
P.O. Box 330
1000 AH Amsterdam
The Netherlands
Fax: +31 (20) 5862 845
For USA and Canada
P.O. Box 945
Madison Square Station
New York, NY 10159-0945
Fax: +1 (212) 633 3680

US$ prices are valid only for the USA & Canada and are subject to exchange rate fluctuations; in all other countries the Dutch guilder price (Dfl.) is definitive. Customers in the European Union should add the appropriate VAT rate applicable in their country to the price(s). Books are sent postfree if prepaid.